PCCP

PAPER

Cite this: *Phys. Chem. Chem. Phys.*, 2015, **17**, 27428

Serpentine diffusion trajectories and the Ouzo effect in partially miscible ternary liquid mixtures†

Rajamani Krishna

This work investigates the transient equilibration process when partially miscible ternary liquid mixtures of two different compositions are brought into contact with each other. Diffusional coupling effects are shown to become increasingly significant as the mixture compositions approach the meta-stable regions of the phase equilibrium diagrams. The proper modelling of coupled diffusion phenomena requires the use of a Fick diffusivity matrix [*D*], with inclusion of non-zero off-diagonal elements. The primary objective of this article is to develop a simple, robust, procedure for the estimation of the matrix [*D*], using the Maxwell–Stefan (M–S) formulation as a convenient starting point. In the developed simplified approach, the Fick diffusivity matrix [*D*] is expressed as the product of a scalar diffusivity and the matrix of thermodynamic correction factors [Γ]. By detailed examination of experimental data for the matrix [*D*] in a wide variety of ternary mixtures, it is deduced that the major contribution of diffusional coupling arises from the contributions of non-ideal solution thermodynamics, quantified by the matrix of thermodynamic correction factors [Γ]. An important consequence of strong thermodynamic coupling is that equilibration trajectories are serpentine in shape and may exhibit incursions into meta-stable zones opening up the possibility of spontaneous emulsification and the Ouzo effect. If diffusional coupling effects are ignored, the equilibration trajectory is linear in composition space. For a wide variety of partially miscible ternary mixtures, it is demonstrated that the corresponding linear equilibration trajectories do not anticipate the possibility of emulsification.

Received 31st July 2015,
Accepted 21st September 2015

DOI: 10.1039/c5cp04520g

www.rsc.org/pccp

1. Introduction

The aniseed-based alcoholic beverage Ouzo consists of a three component mixture of ethanol ($\approx$45 vol%), water (55 vol%) and an essential oil called trans-anethol ($\approx$0.1%).[1] The addition of five volumes of water to one volume of Ouzo causes the drink to appear milky white.[1] Vitale and Katz[2] have coined the generic term "Ouzo effect" to describe such a process of creating meta-stable liquid–liquid dispersions. Since no input of mechanical energy is involved, this offers an energy-efficient method of producing nanospheres and nanoparticles.[3]

Essential to the formation of meta-stable dispersions is the requirement that the composition trajectories during equilibration enter the meta-stable region in the liquid–liquid phase equilibrium diagram. As an illustration, Fig. 1 presents a schematic of the liquid/liquid phase equilibrium for a ternary liquid mixture consisting of glycerol, acetone, and water. The binodal and spinodal curves converge at the plait point. The region between the spinodal and binodal envelopes is meta-stable.

Consider the equilibration of two mixtures of compositions L and R, as indicated in the ternary composition diagram. In the paper by Ruschak and Miller,[4] the necessary conditions for spontaneous emulsification are derived in terms of diffusion equilibration composition trajectories that must necessarily enter the meta-stable regions. Ruschak and Miller[4] adopted the Fickian formulation in which the diffusion flux of each species i, J_i, with respect to the molar average mixture velocity, is considered to be linearly dependent on its own composition gradient

$$J_i = -c_t D_i \frac{dx_i}{dz}; \quad i = 1, 2, 3 \tag{1}$$

Additionally, they assumed that the component diffusivities in the ternary mixture are equal to one another, *i.e.* $D_1 = D_2 = D_3 = D$. Only two of the eqn (1) are independent because the mole fraction gradients sum to zero

$$\frac{dx_1}{dz} + \frac{dx_2}{dz} + \frac{dx_3}{dz} = 0 \tag{2}$$

and the diffusion fluxes also sum to zero

$$J_1 + J_2 + J_3 = 0 \tag{3}$$

Van't Hoff Institute for Molecular Sciences, University of Amsterdam, Science Park 904, 1098 XH Amsterdam, The Netherlands. E-mail: r.krishna@contact.uva.nl; Fax: +31 20 525 5604; Tel: +31 20 627 0990

† Electronic supplementary information (ESI) available: (a) Detailed derivations of flux expressions, and discussions on phase stability, (b) interpolation procedures for the estimation of M-S diffusivities D_{ij} from data for the infinite dilution diffusivities, (c) detailed analysis of the published experimental and MD data for diffusivities in binary and ternary mixtures, and (d) transient equilibration trajectories in 34 different ternary mixtures in order to demonstrate forays into the meta-stable regions. See DOI: 10.1039/c5cp04520g.

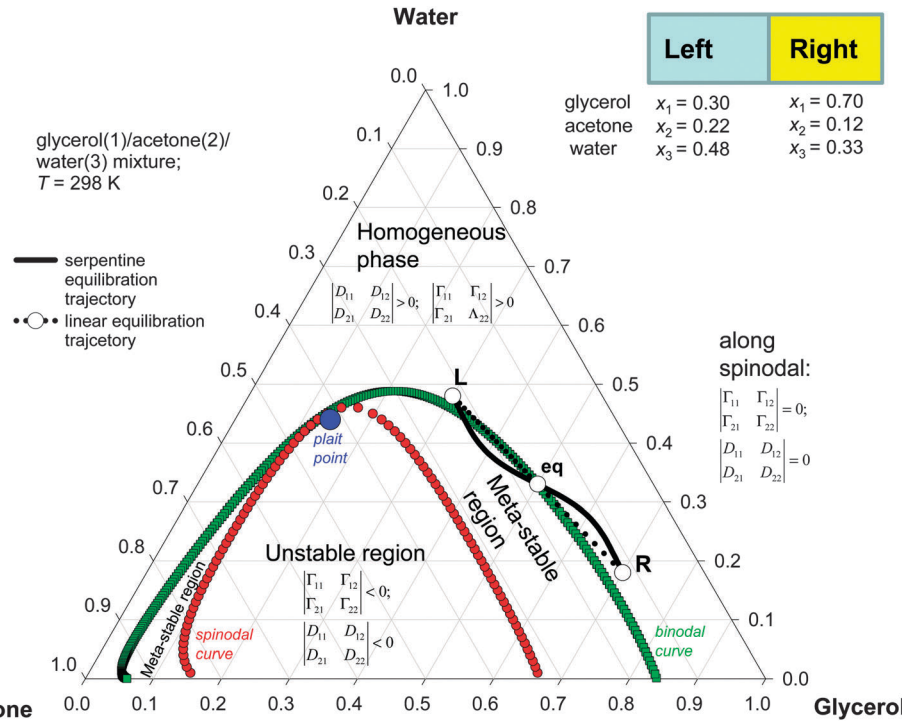

Fig. 1 Trajectories followed during equilibration of homogenous mixtures of two different compositions for the system glycerol(1)/acetone(2)/water(3); the equilibrium composition $x_{1,eq.} = 0.5$, $x_{2,eq.} = 0.17$ and $x_{3,eq.} = 0.33$. The continuous solid black line is the trajectory calculated using eqn (24) and (25), taking $D_{1,self} = 0.01$, $D_{2,self} = 3.2$, $D_{3,self} = 0.5 \times 10^{-9}$ m^2 s^{-1}. Further simulation details are provided in the ESI.†

The transient equilibration of mixtures with different initial mole fractions in adjacent compartments (Left: x_{iL}; Right: x_{iR}) is described by the familiar solution for inter-diffusion between two semi-infinite slabs[5,6]

$$x_i = \frac{1}{2}(x_{iL} + x_{iR}) + \frac{1}{2}\mathrm{erf}\left[-\frac{z}{\sqrt{4Dt}}\right](x_{iL} - x_{iR}); \quad i = 1, 2, 3 \quad (4)$$

For the specific choice of the initial compositions (Left: x_{iL}; Right: x_{iR}), eqn (4) yields the linear equilibration trajectory, depicted by the dotted line in Fig. 1, that is at a tangent to the binodal curve, consequently, no emulsification is feasible in this case.

A large body of experimental data[7–13] for transient equilibration trajectories in ternary mixtures of metal alloys, glasses, ceramics, and liquids indicate that the ternary diffusion process in condensed phases is strongly coupled, *i.e.* the flux of any constituent species may be engendered by the driving forces of all constituents in the mixture. Within the Fickian framework, coupling effects are accounted for by defining a matrix of Fick diffusivities $[D]$ including non-zero off-diagonal elements[12,14]

$$\begin{pmatrix} J_1 \\ J_2 \end{pmatrix} = -c_t \begin{bmatrix} D_{11} & D_{12} \\ D_{21} & D_{22} \end{bmatrix} \frac{\mathrm{d}\begin{pmatrix} x_1 \\ x_2 \end{pmatrix}}{\mathrm{d}z} \quad (5)$$

The elements of the Fickian matrix $[D]$ are accessible from measurement techniques such as Taylor dispersion,[15–17] or holographic laser-interferometry.[18]

With this information on the Fick matrix $[D]$, the transient equilibration trajectory is determined by solving the coupled two-dimensional matrix equation

$$\begin{pmatrix} x_1 \\ x_2 \end{pmatrix} = \frac{1}{2}\begin{pmatrix} x_{1L} + x_{1,R} \\ x_{2L} + x_{2,R} \end{pmatrix} + \frac{1}{2}\mathrm{erf}\left[-\frac{z}{\sqrt{4t}}\begin{bmatrix} D_{11} & D_{12} \\ D_{21} & D_{22} \end{bmatrix}^{-1/2}\right]\begin{pmatrix} x_{1R} - x_{1L} \\ x_{2R} - x_{2L} \end{pmatrix} \quad (6)$$

The Sylvester theorem, detailed in Appendix A of Taylor and Krishna,[14] is required for the explicit calculation of the composition trajectories described by eqn (6).

The primary objective of the present article is to develop a simple, robust procedure for the estimation of the elements of the Fick matrix $[D]$ in partially miscible ternary liquid mixtures. The secondary objective is to investigate the transient equilibration characteristics of a wide variety of liquid mixtures, 34 in total, in order to demonstrate that curvilinear trajectories are almost invariably encountered. For the glycerol/acetone/water mixture, for example, it will be shown that the equilibration process follows the serpentine path, shown by the continuous solid line in Fig. 1, that forays into the meta-stable region indicating that spontaneous emulsification is feasible.

The ESI† accompanying this publication provides (a) detailed derivations of flux expressions, and discussions on phase stability, (b) discussion on interpolation procedures for the estimation of M–S diffusivities $Đ_{ij}$ from the data for the infinite dilution diffusivities, (c) detailed analysis of the

published experimental and MD data for diffusivities in binary and ternary mixtures and (d) transient equilibration trajectories in 34 partially miscible ternary mixtures.

2. Phase stability and its influence on diffusional coupling

For the interpretation and estimation of the Fick matrix $[D]$, it is convenient to adopt the fundamental Maxwell–Stefan (M–S) diffusion formulation that employs chemical potential gradients as driving forces[12,14]

$$-\frac{x_i}{RT}\frac{\mathrm{d}\mu_i}{\mathrm{d}z}=\sum_{\substack{j=1\\ j\neq i}}^{n}\frac{x_jJ_i-x_iJ_j}{c_t\mathcal{D}_{ij}};\quad i=1,2,\ldots n \tag{7}$$

It is helpful to express the left member of eqn (7) in terms of the mole fraction gradients by introducing a $(n-1)\times(n-1)$ matrix of thermodynamic factors $[\Gamma]$:

$$\begin{aligned}&\frac{x_i}{RT}\frac{\mathrm{d}\mu_i}{\mathrm{d}z}=\sum_{j=1}^{n-1}\Gamma_{ij}\frac{\mathrm{d}x_j}{\mathrm{d}z};\\ &\Gamma_{ij}=\delta_{ij}+x_i\frac{\partial\ln\gamma_i}{\partial x_j};\quad i,j=1,2\ldots n-1\end{aligned} \tag{8}$$

For partially miscible liquid mixtures, the elements of $[\Gamma]$ can be calculated from UNIQUAC or NRTL models describing phase equilibrium thermodynamics.[14,19]

It is convenient to define a $(n-1)\times(n-1)$ matrix of inverse diffusivities $[B]$ whose elements are given by

$$\begin{aligned}&B_{ii}=\frac{x_i}{\mathcal{D}_{\mathrm{in}}}+\sum_{\substack{k=1\\ k\neq i}}^{n}\frac{x_k}{\mathcal{D}_{ik}};\\ &B_{ij(i\neq j)}=-x_i\left(\frac{1}{\mathcal{D}_{ij}}-\frac{1}{\mathcal{D}_{in}}\right);\quad i,j=1,2\ldots n-1\end{aligned} \tag{9}$$

Combining eqn (7)–(9), eqn (7) can be recast into $(n-1)$ dimensional matrix notation

$$(J)=-c_t[B]^{-1}[\Gamma]\frac{\mathrm{d}(x)}{\mathrm{d}z}=-c_t[\Lambda][\Gamma]\frac{\mathrm{d}(x)}{\mathrm{d}z} \tag{10}$$

with the definition

$$[\Lambda]=[B]^{-1} \tag{11}$$

Molecular dynamics (MD) simulations provide direct access to the individual elements of $[\Lambda]$.[20,21]

Comparing eqn (5) and (10), the following explicit expression for the Fickian matrix is obtained

$$[D]=[B]^{-1}[\Gamma]=[\Lambda][\Gamma] \tag{12}$$

Specifically, for a ternary mixture, $n=3$, the following expression can be derived

$$\begin{aligned}&\begin{bmatrix}D_{11}&D_{12}\\ D_{21}&D_{22}\end{bmatrix}\\ &=\frac{\begin{bmatrix}\mathcal{D}_{13}(x_1\mathcal{D}_{23}+(1-x_1)\mathcal{D}_{12})&x_1\mathcal{D}_{23}(\mathcal{D}_{13}-\mathcal{D}_{12})\\ x_2\mathcal{D}_{13}(\mathcal{D}_{23}-\mathcal{D}_{12})&\mathcal{D}_{23}(x_2\mathcal{D}_{13}+(1-x_2)\mathcal{D}_{12})\end{bmatrix}}{x_1\mathcal{D}_{23}+x_2\mathcal{D}_{13}+x_3\mathcal{D}_{12}}\\ &\times\begin{bmatrix}\Gamma_{11}&\Gamma_{12}\\ \Gamma_{21}&\Gamma_{22}\end{bmatrix}\end{aligned} \tag{13}$$

The important and persuasive advantage of the M–S formulation is that the elements of the Fickian matrix $[D]$ can be estimated from the data for the M–S diffusivities of the constituent binary pairs, $\mathcal{D}_{ij}$, along with information on phase equilibrium thermodynamics.

Eqn (13) highlights two different sources of "coupling" that contribute to significant off-diagonal contributions of the Fickian matrix $[D]$: (a) differences in the M–S diffusivities of the binary pairs, $\mathcal{D}_{ij}$, and (b) thermodynamic coupling, quantified by the off-diagonal elements of $[\Gamma]$.

Consider phase stability in ternary liquid mixtures that may undergo phase separation yielding two liquid phases that are in equilibrium with each other. In the homogeneous single phase region, the second law of thermodynamics dictates that the rate of entropy production must be positive definite

$$\sigma=-\frac{1}{T}\sum_{i=1}^{n}\frac{\mathrm{d}\mu_i}{\mathrm{d}z}J_i=-\frac{1}{T}\sum_{i=1}^{n-1}\frac{\mathrm{d}(\mu_i-\mu_n)}{\mathrm{d}z}J_i\geq 0 \tag{14}$$

In order to obey this constraint, the determinants of both $[\Gamma]$ and $[D]$ must be positive definite,[12] *i.e.*

$$|\Gamma|>0;\ |D|>0;\ (\Gamma_{12}\Gamma_{21})/(\Gamma_{11}\Gamma_{22})<1;\ (D_{12}D_{21})/(D_{11}D_{22})<1;\quad \text{phase stability} \tag{15}$$

The ratio $(\Gamma_{12}\Gamma_{21})/(\Gamma_{11}\Gamma_{22})$ may be considered as a quantification of the extent of thermodynamic coupling. By the same token, the ratio $(D_{12}D_{21})/(D_{11}D_{22})$, composed of the elements of the Fick diffusivity matrix $[D]$, may be regarded as a quantification of the extent of diffusional coupling. Fig. 2 presents a plot of the ratio $(D_{12}D_{21})/(D_{11}D_{22})$ as function of the corresponding value of the ratio $(\Gamma_{12}\Gamma_{21})/(\Gamma_{11}\Gamma_{22})$ for three different mixtures. For all three mixtures, diffusional coupling effects are strongly correlated with the corresponding thermodynamic coupling factors. Diffusional coupling effects for the completely miscible acetone/benzene/methanol mixtures are found to be significantly lower than that for the two partially miscible glycerol/acetone/water, and water/chloroform/acetic–acid mixtures. Similar plots for other ternary mixtures (see Fig. S34, S37, and S47 of ESI†) provide further verification of the small magnitude of diffusional coupling in completely miscible ternary mixtures. Furthermore, the ratio $(\Gamma_{12}\Gamma_{21})/(\Gamma_{11}\Gamma_{22})$ reaches an asymptotic value of unity along the spinodal curve, that defines the limit of phase stability

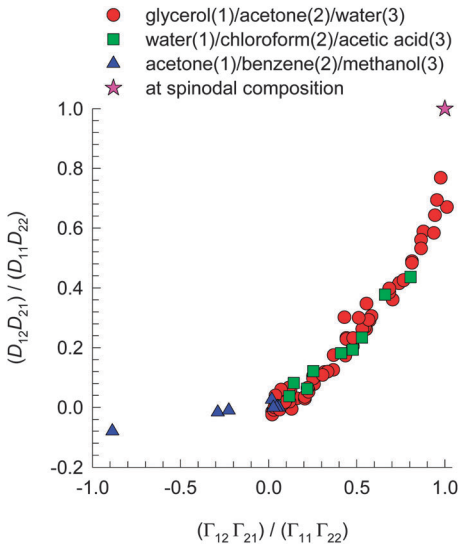

Fig. 2 The ratio $(D_{12}D_{21})/(D_{11}D_{22})$ of the elements of the Fick diffusivity matrix $[D]$, as experimentally determined for acetone(1)/benzene(2)/methanol(3),[27] glycerol(2)/acetone(2)/water(3),[15–17] and water(1)/chloroform(2)/acetic-acid(3)[28,29] mixtures, plotted as a function of the corresponding value of the ratio $(\Gamma_{12}\Gamma_{21})/(\Gamma_{11}\Gamma_{22})$.

$$|\Gamma| = 0;\ |D| = 0;\ (\Gamma_{12}\Gamma_{21})/(\Gamma_{11}\Gamma_{22}) = 1;\ (D_{12}D_{21})/(D_{11}D_{22}) = 1;\ \text{spinodal curve} \tag{16}$$

3. Factoring out thermodynamic influences in ternary mixtures

For binary liquid mixtures, the factoring out of thermodynamic influences leads to well-behaved composition dependencies of the M–S pair diffusivity $Đ_{ij}$; this has been demonstrated for a wide variety of binary liquid mixtures.[12,14,22] The "factoring out" strategy can also be extended to ternary liquid mixtures. Towards this end, eqn (12) is used to determine the square-root of the determinant of the Fick diffusivity matrix:

$$|D|^{1/2} = |\Lambda|^{1/2}|\Gamma|^{1/2} \tag{17}$$

With eqn (13) as a starting point, the following explicit expression can be derived

$$|\Lambda|^{1/2} = \sqrt{\frac{Đ_{12}Đ_{13}Đ_{23}}{x_1Đ_{23} + x_2Đ_{13} + x_3Đ_{12}}} \tag{18}$$

The right hand side of eqn (18) can be estimated from the infinite dilution M–S diffusivities at the extremes of the composition ranges, as suggested in earlier studies[20–21,23,24]

$$Đ_{ij} = \left(Đ_{ij}^{x_i\to 1}\right)^{x_i}\left(Đ_{ij}^{x_j\to 1}\right)^{x_j}\left(Đ_{ij}^{x_k\to 1}\right)^{x_k} \tag{19}$$

For the estimation of $Đ_{ij}^{x_k\to 1}$, the i–j pair diffusivity when both i and j are present in infinitely dilute concentrations, Wesselingh and Bollen[23] have suggested the following formula

$$Đ_{ij}^{x_k\to 1} = \sqrt{\left(Đ_{ik}^{x_k\to 1}Đ_{jk}^{x_k\to 1}\right)} \tag{20}$$

Fig. 3 presents the comparison of the MD simulation values of $|\Lambda|^{1/2}$ for methane/ethane/n-hexane, methane/ethane/propane, methane/propane/n-hexane, ethane/propane/n-butane, and propane/n-butane/n-pentane mixtures as a function of the mole fraction of the first component, x_1; the MD simulation methodology and details are provided in the ESI.† The values of $|\Lambda|^{1/2}$ exhibit a simple dependence on x_1, with a small degree of scatter.

We now compare the values of $|\Lambda|^{1/2}$ with the estimations using a combination of eqn (19) and (20). The estimation procedure will be illustrated for ternary methane(1)/ethane(2)/n-hexane(3) mixtures. From the MD simulation data for the three binary mixtures methane(1)/ethane(2), methane(1)/n-hexane(3), and ethane(2)/n-hexane(3), we can determine the M–S diffusivities (units: 10^{-8} m^2 s^{-1}) at the limiting compositions; the values are:

$$\begin{aligned} &Đ_{12}^{x_1\to 1} = 5.3; \quad Đ_{12}^{x_2\to 1} = 2.58; \quad Đ_{13}^{x_1\to 1} = 3; \\ &Đ_{13}^{x_3\to 1} = 1.05; \quad Đ_{23}^{x_2\to 1} = 1.09; \quad Đ_{23}^{x_3\to 1} = 0.84 \end{aligned} \tag{21}$$

From the Wesselingh-Bollen interpolation eqn (20), we calculate

$$\begin{aligned} Đ_{12}^{x_3\to 1} &= \sqrt{\left(Đ_{13}^{x_3\to 1}Đ_{23}^{x_3\to 1}\right)} = 0.94; \\ Đ_{13}^{x_2\to 1} &= \sqrt{\left(Đ_{12}^{x_2\to 1}Đ_{23}^{x_2\to 1}\right)} = 1.677; \\ Đ_{23}^{x_1\to 1} &= \sqrt{\left(Đ_{12}^{x_1\to 1}Đ_{13}^{x_1\to 1}\right)} = 3.99 \end{aligned} \tag{22}$$

From the nine infinite dilution values determined above, the value of $|\Lambda|^{1/2}$ can be estimated for any composition x_1, x_2, x_3, and can be calculated from eqn (18).

The crosses in Fig. 3 are calculations using eqn (18), along the interpolation formulae (19), and (20); there is good agreement between the MD simulated $|\Lambda|^{1/2}$ and the estimated values.

The quantity $|\Lambda|^{1/2}$ may be interpreted as an "averaged" M–S diffusivity in the ternary liquid mixture. Indeed, for the special case in which all the pair diffusivities are identical to one another, *i.e.* $Đ_{12} = Đ_{13} = Đ_{23} = Đ$, results in $|\Lambda|^{1/2} = Đ$.

The infinite dilution M–S diffusivities are relatable to the self-diffusivities,[20]

$$\begin{aligned} &Đ_{12}^{x_1\to 1} = D_{2,\text{self}}^{x_1\to 1}; \quad Đ_{12}^{x_2\to 1} = D_{1,\text{self}}^{x_2\to 1}; \\ &Đ_{13}^{x_1\to 1} = D_{3,\text{self}}^{x_1\to 1}; \quad Đ_{13}^{x_3\to 1} = D_{1,\text{self}}^{x_3\to 1}; \\ &Đ_{23}^{x_2\to 1} = D_{3,\text{self}}^{x_2\to 1}; \quad Đ_{23}^{x_3\to 1} = D_{2,\text{self}}^{x_3\to 1}; \end{aligned} \tag{23}$$

An alternative estimation procedure for $|\Lambda|^{1/2}$ in terms of the self-diffusivities in the ternary mixture is

$$|\Lambda|^{1/2} = \left(D_{1,\text{self}}\right)^{x_1}\left(D_{2,\text{self}}\right)^{x_2}\left(D_{3,\text{self}}\right)^{x_3} \tag{24}$$

Fig. S19 (ESI†) provides validity of the accuracy of eqn (24) for the estimation of $|\Lambda|^{1/2}$.

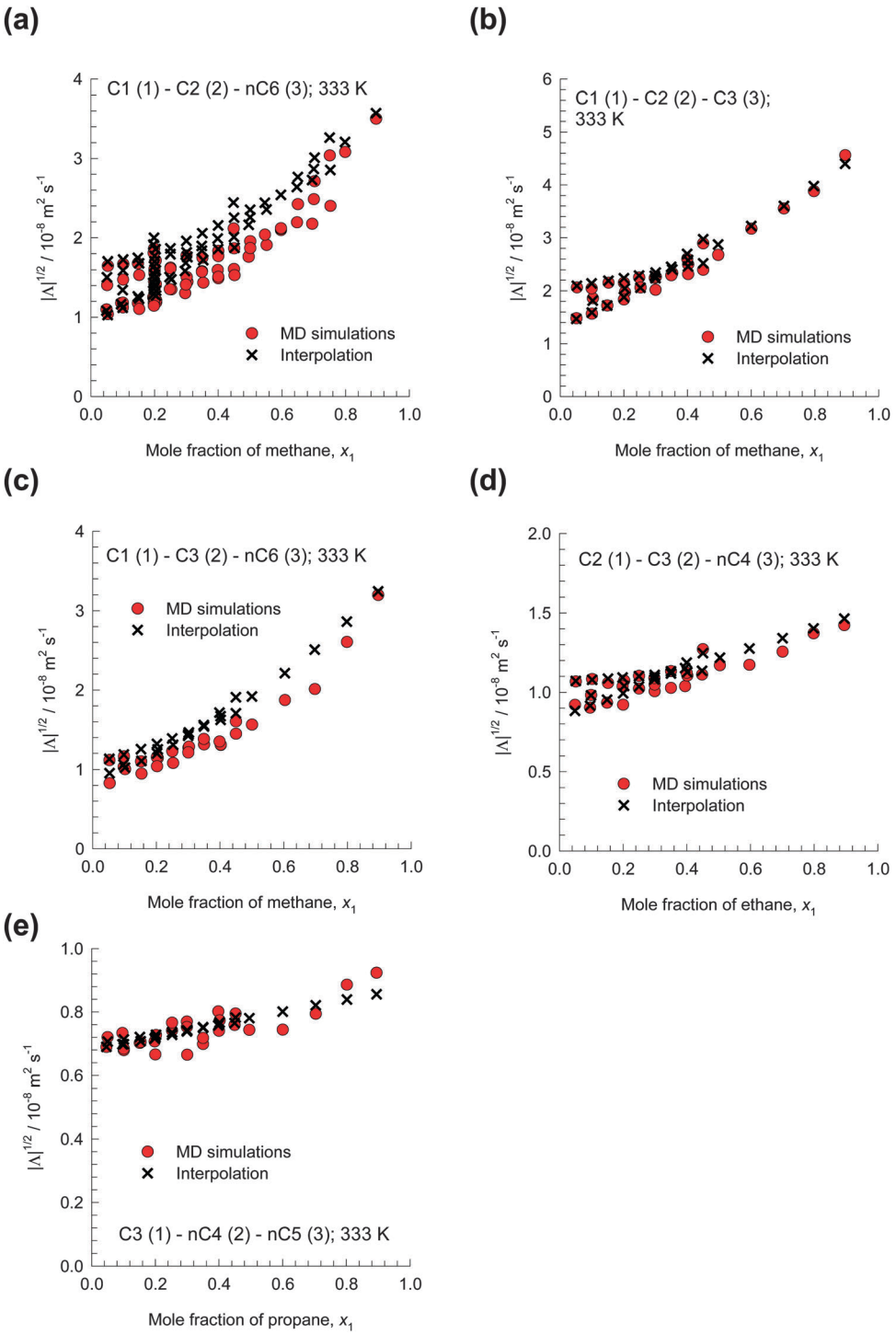

Fig. 3 MD simulated values[20] (shown by red circles) of $|\Lambda|^{1/2}$ for (a) methane(1)/ethane(2)/*n*-hexane(3), (b) methane(1)/ethane(2)/propane (3), (c) methane(1)/propane(2)/*n*-hexane (3), (d) ethane(1)/propane(2)/*n*-butane(3), and (e) propane(1)/*n*-butane(2)/*n*-pentane (3). The crosses represent calculations using eqn (18)–(20). Further calculation details are provided in the ESI.†

Experimental data for Fick diffusivities in completely miscible ternary mixtures are now investigated. Fig. 4 presents the experimental data for $|D|^{1/2}/|\Gamma|^{1/2}$ for acetone/benzene/carbon-tetrachloride,[25] methanol/1-propanol/iso-butanol,[26] methanol/1-butanol/1-propanol,[18] acetone/water/1-propanol,[18] acetone/1-butanol/1-propanol,[18] and 1-propanol/1-chlorobutane/n-heptane[18] mixtures as a function of the mole fraction of the first component, x_1. For all six mixtures, the composition dependence of $|\Lambda|^{1/2}$ is mild because of the factoring out of the thermodynamic influences. The crosses represent calculations using eqn (18),

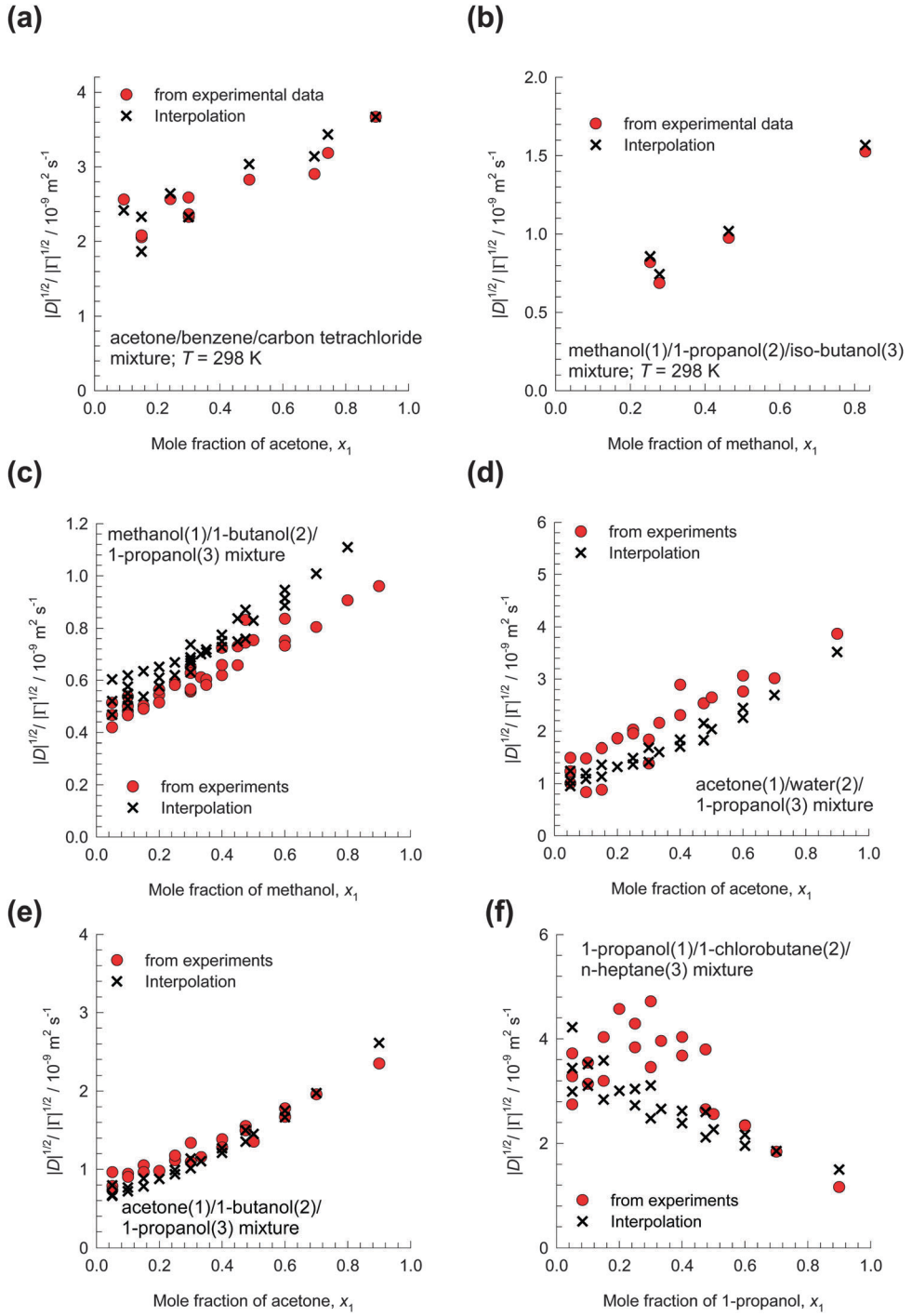

Fig. 4 Experimental data for $|D|^{1/2}/|\Gamma|^{1/2}$ for (a) acetone/benzene/carbon-tetrachloride,[25] (b) methanol/1-propanol/iso-butanol,[26] (c) methanol/1-butanol/1-propanol,[18] (d) acetone/water/1-propanol,[18] (e) acetone/1-butanol/1-propanol,[18] and (f) 1-propanol/1-chlorobutane/*n*-heptane[18] mixtures as a function of the mole fraction of the first component, x_1. The crosses represent calculations using eqn (18), along the interpolation formulae (19) and (20). The input parameters $\mathcal{D}_{ij}^{x_i\to 1}$, and $\mathcal{D}_{ij}^{x_j\to 1}$ for each of the six mixtures are provided in the ESI.†

along the interpolation formulae (19) and (20). The required input parameters $\mathcal{D}_{ij}^{x_i\to 1}$ and $\mathcal{D}_{ij}^{x_j\to 1}$ were determined from the experimental data for the constituent binary pairs. For all mixtures, the estimations using eqn (18) are in reasonably good agreement with experimental data.

Focusing attention on partially miscible mixtures, Fig. 5 presents the experimental data for $|D|^{1/2}/|\Gamma|^{1/2}$ for glycerol/acetone/water and water/chloroform/acetic–acid mixtures. Factoring-out the thermodynamic influences leads to scalar diffusivities, $|\Lambda|^{1/2}$, that are in reasonable agreement with estimations using the interpolation eqn (24).

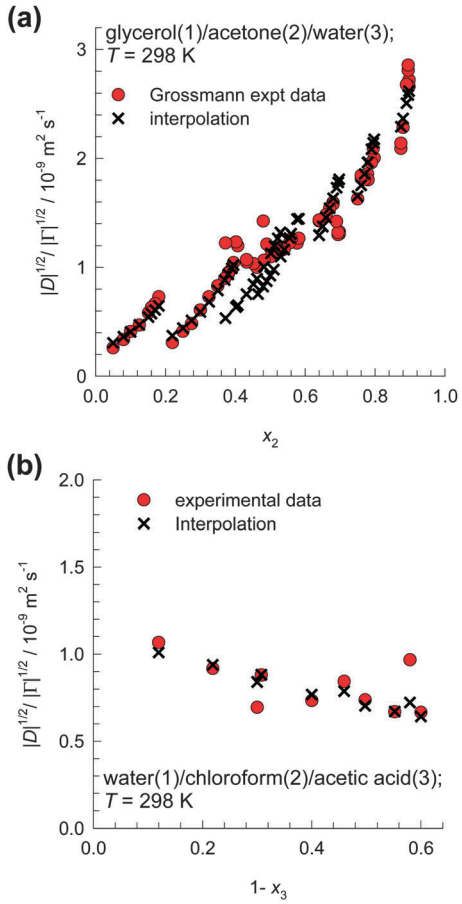

Fig. 5 (a) Experimental data[15–17] for $|D|^{1/2}/|\Gamma|^{1/2}$ for glycerol(1)/acetone(2)/water(3)mixtures as a function of the mole fraction of acetone, x_2. (b) Experimental data[28,29] for $|D|^{1/2}/|\Gamma|^{1/2}$ for water(1)/chloroform(3)/acetic-acid(3) mixtures as a function of $(1 - x_3)$. For both mixtures, the crosses represent calculations using the eqn (24). The input parameters, along with further simulation details are provided in the ESI.†

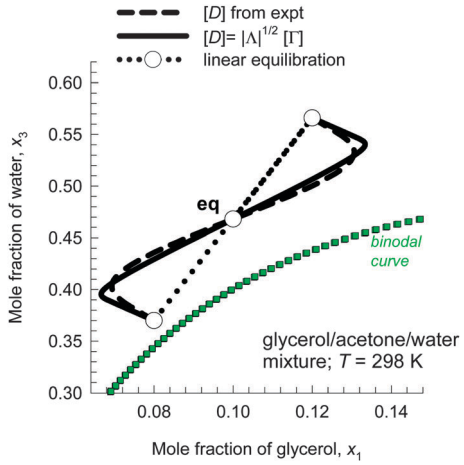

Fig. 6 Equilibration trajectories in glycerol(1)/acetone(2)/water(3) mixtures at 298 K for the equilibrium composition x_1 = 0.1, x_2 = 0.432, x_3 = 0.468. The input parameters, along with further simulation details are provided in the ESI.†

Having established that thermodynamic influences are the major contributors to diffusional coupling, the following estimation of the Fickian matrix is suggested

$$[D] = |\Lambda|^{1/2}[\Gamma] \qquad (25)$$

The parity plots in Fig. S30, S33, S36, S43, S44, S45, S46, S49, S50, S51, S52, S66, and S72 of the ESI† confirm that this simplified procedure is of reasonably good accuracy for the estimation of $[D]$.

4. Equilibration trajectories in partially miscible ternary mixtures

Fig. 6 presents the transient equilibration trajectories, calculated using eqn (6), when glycerol/acetone/water mixtures of two different compositions are brought into contact. At the equilibrated composition, $x_{1,eq.}$ = 0.1, $x_{2,eq.}$ = 0.432 and $x_{3,eq.}$ = 0.468, Grossmann and Winkelmann[15–17] report the Fick diffusivity matrix as $[D] = \begin{bmatrix} 0.4901 & 0.2267 \\ 0.4585 & 0.3991 \end{bmatrix} \times 10^{-9}$ m^2 s^{-1}. The dashed line in Fig. 6 represents the trajectories calculated using the experimentally determined value of the Fickian matrix $[D]$. The continuous solid lines use eqn (25) for the estimation of Fick diffusivities; in this case the value of scalar diffusivity $|\Lambda|^{1/2}$, estimated from eqn (24), is 7.54 × 10^{-9} m^2 s^{-1}. The matrix of thermodynamic factors at the equilibrated composition is calculated to be $[\Gamma] = \begin{bmatrix} 1.44 & 0.533 \\ 0.958 & 0.41 \end{bmatrix}$. The serpentine trajectories, signifying the occurrence of uphill diffusion,[12] are essentially captured by the simplified eqn (25). The conclusion to be drawn is that such curvilinear trajectories are primarily caused by thermodynamic influences. It is important to stress that the magnitude of the scalar diffusivity, $|\Lambda|^{1/2}$, has no influence on the equilibration trajectory in composition space, but does influence the time required for equilibration. If diffusional coupling effects are completely ignored, and the matrix $[D]$ is assumed to be diagonal as is postulated in the classical Ruschak–Miller analysis,[4] the equilibration trajectory is linear in composition space; this is indicated by the dotted line in Fig. 6.

Having established the reliability of the use of simplified eqn (25) for the estimation of the Fickian matrix $[D]$, the equilibration trajectories in thirty-four different partially miscible liquid mixtures were investigated. Fig. 7 provides a sample of the obtained results for six of the investigated mixtures: water/DMSO/THF, water/acetone/phenol, water/trichloroacetic-acid/antipyrine, water/acetic acid/dichloromethane, water/caprolactam/toluene, and [omim][Cl]/ethanol/*tert*-amyl ethyl ether. In every case, the straight-line equilibration trajectory (indicated by dotted lines) lies entirely within the homogeneous, single-phase region; *i.e.* no emulsification is possible. By contrast, the equilibration trajectory calculated using eqn (25) follows serpentine paths that foray into the meta-stable regions, this suggests the possibility of spontaneous emulsification for each mixture under the chosen conditions. Analogous results are

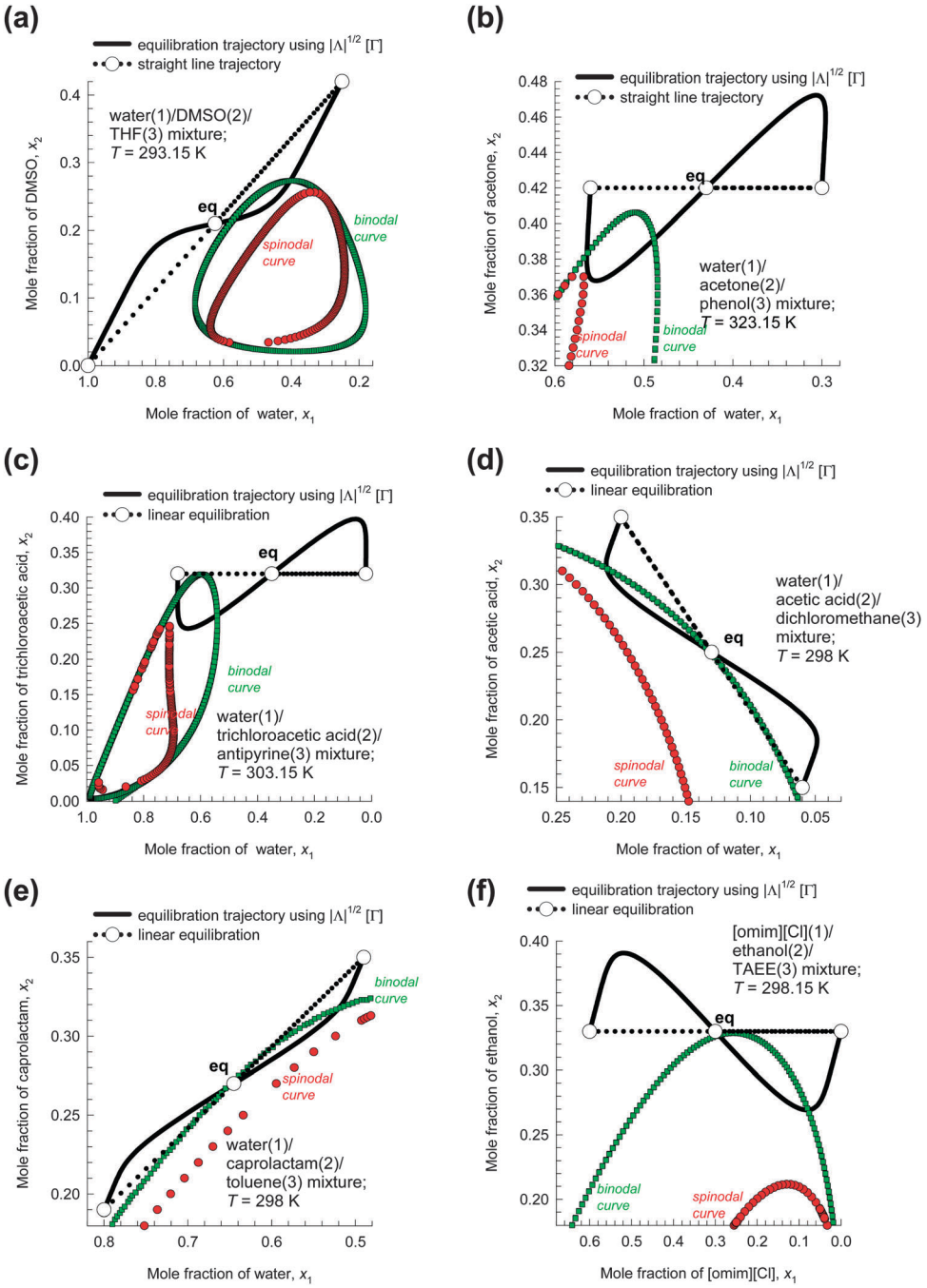

Fig. 7 Trajectories followed during equilibration of homogenous mixtures of different compositions for (a) water/DMSO/THF, (b) water/acetone/phenol, (c), water/trichloroacetic-acid/antipyrine, (d) water/acetic acid/dichloromethane, (e) water/caprolactam/toluene, and (f) [omim][Cl]/ethanol/TAEE mixtures. Further simulation details, and input data, are provided in the ESI.†

obtained for transient equilibration trajectories in all other mixtures; see Fig. S76–S111 of the ESI.†

5. Conclusions

The following major conclusions can be drawn from the investigations reported in this work.

(1) In ternary liquid mixtures, diffusional coupling effects are primarily caused by the influence of non-ideal solution thermodynamics. Diffusional coupling effects are of significantly lesser importance in completely miscible liquid mixtures, than in partially miscible mixtures.

(2) In partially miscible liquid mixtures, diffusional coupling effects become increasingly significant as the spinodal compositions are approached.

(3) Eqn (25) provides a simple, robust, procedure for estimation of the Fick diffusivity matrix. Use of eqn (25) captures the essential features such as uphill diffusion,

and serpentine composition trajectories during transient equilibration.

(4) Serpentine trajectories anticipate the possibility of emulsification even when the corresponding linear equilibration trajectory forbids such an eventuality.

Notation

$[B]$	Matrix defined by eqn (9), m^{-2} s
c_t	Total molar concentration of the mixture, mol m^{-3}
$Đ_{ij}$	M–S exchange coefficient, m^2 s^{-1}
$[D]$	Fick diffusivity matrix, m^2 s^{-1}
$\lvert D\rvert^{1/2}$	Square-root of the determinant of $[D]$, m^2 s^{-1}
$D_{i,\mathrm{self}}$	Self-diffusivity of species i, m^2 s^{-1}
J_i	Molar diffusion flux of species i, mol m^{-2} s^{-1}
n	Number of components in the mixture, dimensionless
R	Gas constant, 8.314 J mol^{-1} K^{-1}
t	Time, s
T	Absolute temperature, K
x_i	Mole fraction of component i in the bulk fluid phase, dimensionless
z	Direction coordinate, m

Greek letters

δ_{ij}	Kronecker delta, dimensionless
γ_i	Activity coefficient of component i, dimensionless
Γ_{ij}	Thermodynamic factors, dimensionless
$[\Gamma]$	Matrix of thermodynamic factors, dimensionless
$\lvert\Gamma\rvert^{1/2}$	Square-root of the determinant of $[\Gamma]$, dimensionless
$[\Lambda]$	Matrix defined by eqn (9) and (11), m^2 s^{-1}
$\lvert\Lambda\rvert^{1/2}$	Square-root of the determinant of $[\Lambda]$, m^2 s^{-1}
μ_i	Molar chemical potential, J mol^{-1}
σ	Rate of entropy production, J m^{-3} s^{-1} K^{-1}

Acknowledgements

Dr J. M. van Baten provided the code for calculation of the binodal curve, and this contribution is gratefully acknowledged.

References

1 N. L. Sitnikova, R. Sprik, G. Wegdam and E. Eiser, *Langmuir*, 2005, **21**, 7083–7089.
2 S. A. Vitale and J. L. Katz, *Langmuir*, 2003, **19**, 4105–4110.
3 F. Ganachaud and J. L. Katz, *ChemPhysChem*, 2005, **6**, 209–216.
4 K. J. Ruschak and C. A. Miller, *Ind. Eng. Chem. Fundam.*, 1972, **11**, 534–540.
5 J. Crank, *The Mathematics of Diffusion*, Clarendon Press, Oxford, 2nd edn, 1975.
6 M. E. Glicksman, *Diffusion in Solids: Field Theory, Solid-state Principles, and Applications*, John Wiley, New York, 2000.
7 L. S. Darken, *Trans. AIME*, 1949, **180**, 430–438.
8 J. S. Kirkaldy, *Can. J. Phys.*, 1957, **35**, 435–4440.
9 D. Vielzeuf and A. Saúl, *Contrib. Mineral. Petrol.*, 2011, **161**, 683–702.
10 A. K. Varshneya and A. R. Cooper, *J. Am. Ceram. Soc.*, 1972, **55**, 312–317.
11 R. Krishna, C. Y. Low, D. M. T. Newsham, C. G. Olivera-Fuentes and G. L. Standart, *Chem. Eng. Sci.*, 1985, **40**, 893–903.
12 R. Krishna, *Chem. Soc. Rev.*, 2015, **44**, 2812–2836.
13 M. Haeberl and E. Blass, *Chem. Eng. Res. Des., Trans. IChemE.*, 1999, **77**, 647–655.
14 R. Taylor and R. Krishna, *Multicomponent mass transfer*, John Wiley, New York, 1993.
15 T. Grossmann and J. Winkelmann, *J. Chem. Eng. Data*, 2005, **50**, 1396–1403.
16 T. Grossmann and J. Winkelmann, *J. Chem. Eng. Data*, 2007, **52**, 336–340.
17 T. Grossmann and J. Winkelmann, *J. Chem. Eng. Data*, 2007, **52**, 341–344.
18 S. Rehfeldt and J. Stichlmair, *Fluid Phase Equilib.*, 2010, **290**, 1–14.
19 R. Krishna, C. Y. Low, D. M. T. Newsham, C. G. Olivera Fuentes and A. Paybarah, *Fluid Phase Equilib.*, 1989, **45**, 115–120.
20 R. Krishna and J. M. van Baten, *Ind. Eng. Chem. Res.*, 2005, **44**, 6939–6947.
21 X. Liu, A. Bardow and T. J. H. Vlugt, *Ind. Eng. Chem. Res.*, 2011, **50**, 4776–4782.
22 R. Krishna and J. A. Wesselingh, *Chem. Eng. Sci.*, 1997, **52**, 861–911.
23 J. A. Wesselingh and A. M. Bollen, *Chem. Eng. Res. Des.*, 1997, **75**, 590–602.
24 H. A. Kooijman and R. Taylor, *Ind. Eng. Chem. Res.*, 1991, **30**, 1217–1222.
25 H. T. Cullinan and H. L. Toor, *J. Phys. Chem.*, 1965, **69**, 3941–3949.
26 F. O. Shuck and H. L. Toor, *J. Phys. Chem.*, 1963, **67**, 540–545.
27 A. Alimadadian and C. P. Colver, *Can. J. Chem. Eng.*, 1976, **54**, 208–213.
28 V. Vitagliano, R. Sartorio, S. Scala and D. Spaduzzi, *J. Solution Chem.*, 1978, **7**, 605–621.
29 D. Buzatu, F. D. Buzatu, L. Paduano and R. Sartorio, *J. Solution Chem.*, 2007, **36**, 1373–1384.

Electronic Supplementary Information (ESI) to accompany:

Serpentine Diffusion Trajectories and the Ouzo Effect in Partially Miscible Ternary Liquid Mixtures

Rajamani Krishna*

Van 't Hoff Institute for Molecular Sciences, University of Amsterdam, Science Park 904,

1098 XH Amsterdam, The Netherlands

*email: r.krishna@contact.uva.nl

Table of Contents

1. Diffusion in *n*-component fluid mixtures: Fick, Maxwell-Stefan, and Onsager formalisms

In his classic paper published in 1945 entitled *Theories and Problems of Liquid Diffusion*, Onsager[1] wrote *The theory of liquid diffusion is relatively undeveloped… It is a striking symptom of the common ignorance in this field that not one of the phenomenological schemes which arc fit to describe the general case of diffusion is widely known*. In the Onsager formalism for *n*-component mixtures, the diffusion fluxes J_i are postulated as being linearly dependent on the driving forces that are taken to be the chemical potential gradients, $\frac{d\mu_i}{dz}$. The fluxes J_i

$$J_i \equiv c_i(u_i - u); \quad i = 1,2,..n \tag{1}$$

are defined with respect to the chosen molar average reference velocity frame u

$$u = x_1 u_1 + x_2 u_2 + \cdots x_n u_n \tag{2}$$

The molar fluxes N_i in the laboratory fixed reference frame are related to the diffusion fluxes J_i by

$$N_i \equiv \quad c_i u_i = J_i + x_i N_t; \quad N_t = \sum_{i=1}^{n} N_i \tag{3}$$

Only *n*-1 of the fluxes J_i are independent because the diffusion fluxes sum to zero

$$\sum_{i=1}^{n} J_i = 0 \tag{4}$$

Also, only (*n*-1) of the chemical potential gradients $\frac{d\mu_i}{dz}$ are independent, because of the Gibbs-Duhem relationship

$$x_1 \frac{d\mu_1}{dz} + x_2 \frac{d\mu_2}{dz} + \cdots x_n \frac{d\mu_n}{dz} = 0 \tag{5}$$

It is convenient therefore to choose the (n-1) independent chemical potential gradients $\frac{d(\mu_i - \mu_n)}{dz}$ as driving forces for diffusion. In (n-1) dimensional matrix notation, the Onsager formulation is written as

$$(J) = -c_t [L] \frac{1}{RT} \frac{d(\mu - \mu_n)}{dz} \tag{6}$$

The units of the elements L_{ij} are the same as those for Fick diffusivities, i.e. $m^2\ s^{-1}$. The matrix of Onsager coefficients $[L]$ is symmetric because of the Onsager Reciprocal Relations (ORR)[2]

$$L_{ij} = L_{ji} \tag{7}$$

In proceeding further, we define a (n-1) dimensional matrix [H], that is the Hessian of the molar Gibbs free energy, G

$$H_{ij} = \frac{1}{RT} \frac{\partial^2 G}{\partial x_i \partial x_j} = \frac{1}{RT} \frac{\partial^2 G}{\partial x_i \partial x_i} = H_{ji}; \quad i, j = 1,2 \ldots n-1 \tag{8}$$

where G, the molar Gibbs free energy for the n-component mixture, is the sum of two contributions

$$G = G^{ex} + RT \sum_{i=1}^{n} x_i \ln(x_i); \quad G^{ex} = RT \sum_{i=1}^{n} x_i \ln(\gamma_i) \tag{9}$$

where γ_i is the activity coefficient of component i. Equation (9) can also be written in terms of the μ_i, that is the chemical potential or partial molar Gibbs free energy:

$$G = \sum_{i=1}^{n} x_i \mu_i = RT \sum_{i=1}^{n} x_i \ln(\gamma_i x_i) \tag{10}$$

When carrying out the partial differentiations of G, required in equation (8), it is important to note that all n of the mole fractions cannot be varied independently. So, we re-write equation (10), in terms of the n-1 independent mole fractions

$$G = \sum_{i=1}^{n} x_i \mu_i = \sum_{i=1}^{n-1} x_i (\mu_i - \mu_n) + \mu_n \tag{11}$$

In view of equations (8), and (11), we obtain

$$H_{ij} = \frac{1}{RT}\frac{\partial(\mu_i - \mu_n)}{\partial x_j} = \frac{1}{RT}\frac{\partial(\mu_j - \mu_n)}{\partial x_i} = H_{ji}; \quad i, j = 1,2\ldots n-1 \tag{12}$$

Combining equations (6), and (12) we get

$$(J) = -c_t[L][H]\frac{d(x)}{dz} \tag{13}$$

The second law of thermodynamics dictates that the rate of entropy production must be positive definite

$$\sigma = -\frac{1}{T}\sum_{i=1}^{n}\frac{d\mu_i}{dz}J_i = -\frac{1}{T}\sum_{i=1}^{n-1}\frac{d(\mu_i - \mu_n)}{dz}J_i \geq 0 \tag{14}$$

Substituting the Onsager equations (6) for the diffusion fluxes

$$\sigma = \sum_{i=1}^{n-1}\sum_{j=1}^{n-1}L_{ij}\frac{d(\mu_i - \mu_n)}{dz}\frac{d(\mu_j - \mu_n)}{dz} \geq 0 \tag{15}$$

Equation (15) implies that the Onsager matrix [L] be positive definite, i.e.

$$|L| \geq 0; \quad \text{second law of thermodynamics} \tag{16}$$

If we define a (n-1) × (n-1) dimensional Fick diffusivity matrix $[D]$

$$(J) = -c_t[D]\frac{d(x)}{dz} \tag{17}$$

we obtain the inter-relationship

$$[D] = [L][H] \tag{18}$$

Equation (18) underscores the direct influence of mixture thermodynamics on the Fick diffusivites D_{ij}. It is worthy of note that the Fick diffusivity matrix $[D]$, which is a product of two symmetric matrices, $[L]$ and $[H]$ is not symmetric.

For stable single phase fluid mixtures, we must have $|H| \geq 0$. Also, in view of the second law of thermodynamics we have $|L| \geq 0$. In view of equation (18), the condition of phase stability translates to

$$|D| \geq 0; \quad |L| \geq 0; \quad |H| \geq 0; \quad \text{phase stability} \tag{19}$$

Equation (19) implies that all the eigenvalues of the Fick matrix [D] are positive definite. It is interesting to note that thermodynamic stability considerations do not require the diagonal elements D_{ii} to be positive definite. If recourse is made to the kinetic theory of gases, it can be shown that the diagonal elements D_{ii} are individually positive definite for mixtures of ideal gases. The off-diagonal elements $D_{ij}(i \neq j)$ can be either positive or negative, even for ideal gas mixtures. Indeed, the sign of $D_{ij}(i \neq j)$ also depends on the component numbering.

The Onsager approach does not offer any clues about the estimation of the elements of $[L]$ using information on the diffusivities of the binary pairs in the *n*-component mixtures.

For *n*-component non-ideal fluid mixtures, the M-S equations represent a balance between the force exerted per mol of species *i* with the drag, or friction, experienced with each of the partner species in the mixture. For a ternary mixture we write

$$\begin{aligned}
-\frac{d\mu_1}{dz} &= \frac{RT}{Đ_{12}} x_2(u_1 - u_2) + \frac{RT}{Đ_{13}} x_3(u_1 - u_3) \\
-\frac{d\mu_2}{dz} &= \frac{RT}{Đ_{12}} x_1(u_2 - u_1) + \frac{RT}{Đ_{23}} x_3(u_2 - u_3) \\
-\frac{d\mu_3}{dz} &= \frac{RT}{Đ_{13}} x_1(u_3 - u_1) + \frac{RT}{Đ_{23}} x_3(u_3 - u_2)
\end{aligned} \tag{20}$$

The M-S pair diffusivities $Đ_{ij}$ can be interpreted as the *inverse drag coefficient* between species *i* and species *j*. Equation (20) can be generalized to *n*-component mixtures:

$$-\frac{1}{RT}\frac{d\mu_i}{dz} = \sum_{\substack{j=1 \\ j \neq i}}^{n} \frac{x_j(u_i - u_j)}{Đ_{ij}}; \quad i = 1,2,\ldots n \tag{21}$$

By multiplying both sides of equation (21) by x_i after introducing the expressions for fluxes $N_i \equiv c_i u_i = J_i + x_i N_t; \quad N_t = \sum_{i=1}^{n} N_i$ we obtain

$$-\frac{x_i}{RT}\frac{d\mu_i}{dz} = \sum_{\substack{j=1 \\ j\neq i}}^{n} \frac{x_j N_i - x_i N_j}{c_t Đ_{ij}} = \sum_{\substack{j=1 \\ j\neq i}}^{n} \frac{x_j J_i - x_i J_j}{c_t Đ_{ij}}; \quad i = 1,2,\ldots n \tag{22}$$

where the second equality arises from application of equations (3), and (4). The $\frac{x_i}{RT}\frac{d\mu_i}{dz}$ is the generalization of the mole fraction gradients, used as driving forces for ideal gas mixtures. Indeed, for ideal gas mixtures, equation (22) simplify to yield

$$\begin{aligned}
-\frac{dx_1}{dz} &= \frac{x_2 N_1 - x_1 N_2}{c_t Đ_{12}} + \frac{x_3 N_1 - x_1 N_3}{c_t Đ_{13}}; \\
-\frac{dx_2}{dz} &= \frac{x_1 N_2 - x_2 N_1}{c_t Đ_{12}} + \frac{x_3 N_2 - x_2 N_3}{c_t Đ_{23}} \\
-\frac{dx_3}{dz} &= \frac{x_1 N_3 - x_3 N_1}{c_t Đ_{13}} + \frac{x_2 N_3 - x_3 N_2}{c_t Đ_{23}}
\end{aligned} \tag{23}$$

The ORR imply that the M-S pair diffusivities are symmetric

$$Đ_{ij} = Đ_{ji}; \quad i, j = 1,2...n \tag{24}$$

Insertion of the Maxwell-Stefan diffusion eq. (21) into (14) we obtain on re-arrangement[3]

$$\sigma = \frac{1}{2} c_t R \sum_{i=1}^{n}\sum_{j=1}^{n} \frac{x_i x_j}{Đ_{ij}} \left| u_i - u_j \right|^2 \geq 0 \tag{25}$$

For mixtures of ideal gases for which the $Đ_{ij}$ are independent of composition the positive definite condition (25) can only be satisfied if

$$Đ_{ij} \geq 0; \quad \text{(ideal gas mixtures)} \tag{26}$$

Equation (26) was first derived by Hirschfelder, Curtiss and Bird.[4] For non-ideal liquid mixtures the $Đ_{ij}$ are composition dependent in general and a result analogous to eq. (26) cannot be derived.[3]

The M-S pair diffusivities $Đ_{ij}$ for gaseous mixtures at low pressures can be estimated to a good level of accuracy using the Fuller-Schettler-Giddings (FSG)[5] method.

$$Đ_{ij} = \frac{1.43\times10^{-7}T^{1.75}}{p\sqrt{M_{ij}}\left[\left(v_i^{1/3}\right)+\left(v_j^{1/3}\right)\right]^2} \quad \mathrm{m^2 s^{-1}} \tag{27}$$

where p is the pressure (expressed in atmospheres), $M_{ij} = \frac{2}{\frac{1}{M_i}+\frac{1}{M_j}}$ is the mean molecular weight of the mixture (expressed in g mol^{-1}), v_i, and v_j are the diffusion volumes (expressed in cm^3 mol^{-1}) whose values are obtained by summing the contributions of the volumes of the constituent atoms in the molecular species (the values are tabulated in Table 11.1 of Reid, Prausnitz, and Poling.[6]

According to the FSG estimation procedure, the product of $Đ_{ij}$ and the total pressure, p, is a function only of temperature and is also independent of composition. For gaseous mixtures at high pressures, the experimental data of Takahashi and Hongo[7] for M-S diffusivities of CO_2(trace amounts)/C_2H_4 mixtures, and CO_2/C_2H_4(trace amounts) mixtures at 298.2 K, 323.2 K, and 348.2 K demonstrate quite clearly, and dramatically, that the assumption $p\,Đ_{ij}$ = constant, implicit in the FSG estimation with Equation (27), becomes increasingly poor as p increases; see Figures 1a, 1b, and 1c. The departures from the FSG Equation (27), is primarily to be attributed to the departures of fluid densities from the ideal gas prescription. The experimental data of Takahashi and Hongo[7] conforms quite well with the modified prescription

$$Đ_{ij} = \frac{1.43\times10^{-7}T^{1.75}}{p\sqrt{M_{ij}}\left[\left(v_i^{1/3}\right)+\left(v_j^{1/3}\right)\right]^2} Z \tag{28}$$

The predictions of equation (28) are shown by the continuous solid lines in Figures 1a, 1b, and 1c. It is noteworthy that the experimental data for CO_2(trace amounts)/C_2H_4 mixtures, and CO_2/C_2H_4(trace amounts) mixtures are not coincidental. To understand the departures from the FSG prescription, Figures 1d, 1e, and 1f present calculations of the compressibility factor, Z, using the Peng-Robinson Equation of State (PR EOS) at the three different temperatures. The compressibility factors for

CO_2(trace amounts)/C_2H_4 mixtures, and CO_2/C_2H_4(trace amounts) mixtures are not the same, and this explains the differences in the corresponding diffusivity values.

For non-ideal liquid mixtures, the chemical potential of component *i*, μ_i are related to the gradients of the component activities, $a_i = \gamma_i x_i$:

$$\mu_i = \mu_i^0 + RT\ln(a_i) = \mu_i^0 + RT\ln(\gamma_i x_i) \tag{29}$$

where γ_i is the activity coefficient.

For gaseous mixtures at high pressure, the chemical potential of component *i*, μ_i are related to the gradients of the component fugacities, $f_i = \phi_i p_i = \phi_i x_i p$:

$$\mu_i = \mu_i^0 + RT\ln(f_i) = \mu_i^0 + RT\ln(\phi_i x_i p) \tag{30}$$

where ϕ_i is the activity coefficient and *p* is the total gas pressure.

It is helpful to express the left member of equation (22) in terms of the mole fraction gradients by introducing an (*n*-1) × (*n*-1) matrix of thermodynamic factors $[\Gamma]$:

$$\frac{x_i}{RT}\frac{d\mu_i}{dz} = x_i\frac{d\ln a_i}{dz} = \sum_{j=1}^{n-1}\Gamma_{ij}\frac{dx_j}{dz};\quad \Gamma_{ij} = \delta_{ij} + x_i\frac{\partial\ln\gamma_i}{\partial x_j};\quad i,j = 1,2\ldots n-1 \tag{31}$$

For non-ideal ternary liquid mixtures, the elements of $[\Gamma]$ can be calculated from Van Laar, Wilson, UNIQUAC or NRTL models describing phase equilibrium thermodynamics.[8, 9]

The analogous expression for high pressure gaseous mixtures is

$$\frac{x_i}{RT}\frac{d\mu_i}{dz} = x_i\frac{d\ln f_i}{dz} = \sum_{j=1}^{n-1}\Gamma_{ij}\frac{dx_j}{dz};\quad \Gamma_{ij} = \delta_{ij} + x_i\frac{\partial\ln\phi_i}{\partial x_j};\quad i,j = 1,2\ldots n-1 \tag{32}$$

The elements of $[\Gamma]$ can be calculated by analytic differentiation of an Equation of State (EOS) such as the Peng-Robinson (PR) EOS. For binary mixtures, explicit analytic expressions for $\Gamma = x_1\frac{\partial\ln f_1}{\partial x_1} = \delta_{ij} + x_1\frac{\partial\ln\phi_1}{\partial x_1}$ for PR EOS are provided in the paper by Tuan et al.[10]

We also define a (*n*-1) × (*n*-1) matrix of inverse diffusivities $[B]$ whose elements are given by

$$B_{ii} = \frac{x_i}{Đ_{in}} + \sum_{\substack{k=1 \\ k\neq i}}^{n} \frac{x_k}{Đ_{ik}}; \quad B_{ij(i\neq j)} = -x_i\left(\frac{1}{Đ_{ij}} - \frac{1}{Đ_{in}}\right); \quad i, j = 1,2...n-1 \tag{33}$$

Combining equations (22), (31), and (33), we can re-cast equation (22) into (n-1) dimensional matrix notation

$$(J) = -c_t[B]^{-1}[\Gamma]\frac{d(x)}{dz} = -c_t[\Lambda][\Gamma]\frac{d(x)}{dz} \tag{34}$$

where we have additionally defined

$$[\Lambda] = [B]^{-1} \tag{35}$$

For an ideal gas mixture, we have

$$[\Lambda] = [B]^{-1} = [D]; \quad \text{ideal gas mixture} \tag{36}$$

Comparing equations (13), (17), and (34), we get the inter-relationship between Fick, M-S and Onsager coefficients

$$[L][H] = [D] = [B]^{-1}[\Gamma] = [\Lambda][\Gamma] \tag{37}$$

For a binary mixture, n = 2, we get

$$D_{12} = Đ_{12}\Gamma \tag{38}$$

Specifically, for a ternary mixture, n = 3, we derive

$$\begin{bmatrix} D_{11} & D_{12} \\ D_{21} & D_{22} \end{bmatrix} = \frac{1}{B_{11}B_{22} - B_{12}B_{21}} \begin{bmatrix} \frac{x_2}{Đ_{23}} + \frac{x_1}{Đ_{12}} + \frac{x_3}{Đ_{23}} & x_1\left(\frac{1}{Đ_{12}} - \frac{1}{Đ_{13}}\right) \\ x_2\left(\frac{1}{Đ_{12}} - \frac{1}{Đ_{23}}\right) & \frac{x_1}{Đ_{13}} + \frac{x_2}{Đ_{12}} + \frac{x_3}{Đ_{13}} \end{bmatrix} \begin{bmatrix} \Gamma_{11} & \Gamma_{12} \\ \Gamma_{21} & \Gamma_{22} \end{bmatrix} \tag{39}$$

Equation (39) simplifies to yield

$$\begin{bmatrix} D_{11} & D_{12} \\ D_{21} & D_{22} \end{bmatrix} = \begin{bmatrix} \Lambda_{11} & \Lambda_{12} \\ \Lambda_{21} & \Lambda_{22} \end{bmatrix} \begin{bmatrix} \Gamma_{11} & \Gamma_{12} \\ \Gamma_{21} & \Gamma_{22} \end{bmatrix} = \frac{\begin{bmatrix} Đ_{13}\left(x_1Đ_{23} + (1-x_1)Đ_{12}\right) & x_1Đ_{23}\left(Đ_{13} - Đ_{12}\right) \\ x_2Đ_{13}\left(Đ_{23} - Đ_{12}\right) & Đ_{23}\left(x_2Đ_{13} + (1-x_2)Đ_{12}\right) \end{bmatrix}}{x_1Đ_{23} + x_2Đ_{13} + x_3Đ_{12}} \begin{bmatrix} \Gamma_{11} & \Gamma_{12} \\ \Gamma_{21} & \Gamma_{22} \end{bmatrix} \tag{40}$$

Equation (40) also shows that the component numbering alters the sign of the cross-coefficients; negative cross-coefficients are nothing to be alarmed about as they occur routinely *even for ideal gas mixtures*.

The determinant of $[B]$ for a ternary mixture is

$$|B| = \frac{x_1}{Đ_{12}Đ_{13}} + \frac{x_2}{Đ_{12}Đ_{23}} + \frac{x_3}{Đ_{13}Đ_{23}} = \frac{1}{|\Lambda|}; \quad |\Lambda| = \frac{Đ_{12}Đ_{13}Đ_{23}}{x_1Đ_{23}+x_2Đ_{13}+x_3Đ_{12}} \tag{41}$$

We also have

$$|\Lambda|^{1/2} = \sqrt{\frac{Đ_{12}Đ_{13}Đ_{23}}{x_1Đ_{23}+x_2Đ_{13}+x_3Đ_{12}}} \tag{42}$$

The quantity $|\Lambda|^{1/2}$ can be interpreted as an "average" magnitude of M-S diffusivity in the ternary mixture; we will return to this later. The values of the Fick and Onsager diffusivities are dependent on the choice of the reference velocity frame, that has been chosen in the foregoing set of expressions as the molar average mixture velocity. For converting the diffusivities from one reference velocity frame to another, explicit expressions are provided in Taylor and Krishna.[8] An important advantage of the M-S formulation, is that the pair diffusivities $Đ_{ij}$ are independent of the choice of the reference velocity frame. Further discussions of the characteristic differences between the Onsager, M-S and Fickian formulations are available in Taylor and Krishna.[8]

The thermodynamic factor $[\Gamma]$ is related to the Hessian matrix

$$\begin{bmatrix} H_{11} & H_{12} \\ H_{21} & H_{22} \end{bmatrix} = \frac{1}{x_3}\begin{bmatrix} \frac{(1-x_2)}{x_1} & 1 \\ 1 & \frac{(1-x_1)}{x_2} \end{bmatrix}\begin{bmatrix} \Gamma_{11} & \Gamma_{12} \\ \Gamma_{21} & \Gamma_{22} \end{bmatrix};$$
$$\begin{bmatrix} \Gamma_{11} & \Gamma_{12} \\ \Gamma_{21} & \Gamma_{22} \end{bmatrix} = \begin{bmatrix} (1-x_1)x_1 & -x_1x_2 \\ -x_1x_2 & (1-x_2)x_2 \end{bmatrix}\begin{bmatrix} H_{11} & H_{12} \\ H_{21} & H_{22} \end{bmatrix} \tag{43}$$

Combining equation (37), and (43), we obtain the following relation between $[L]$ and $[\Lambda]$ matrices

$$\begin{bmatrix} L_{11} & L_{12} \\ L_{21} & L_{22} \end{bmatrix}\begin{bmatrix} H_{11} & H_{12} \\ H_{21} & H_{22} \end{bmatrix} = \begin{bmatrix} \Lambda_{11} & \Lambda_{12} \\ \Lambda_{21} & \Lambda_{22} \end{bmatrix}\begin{bmatrix} \Gamma_{11} & \Gamma_{12} \\ \Gamma_{21} & \Gamma_{22} \end{bmatrix} = \begin{bmatrix} \Lambda_{11} & \Lambda_{12} \\ \Lambda_{21} & \Lambda_{22} \end{bmatrix}\begin{bmatrix} (1-x_1)x_1 & -x_1x_2 \\ -x_1x_2 & (1-x_2)x_2 \end{bmatrix}\begin{bmatrix} H_{11} & H_{12} \\ H_{21} & H_{22} \end{bmatrix} \tag{44}$$

Equation (44) in combination with equation (40) yields

$$\begin{bmatrix} L_{11} & L_{12} \\ L_{21} & L_{22} \end{bmatrix} = \begin{bmatrix} \Lambda_{11} & \Lambda_{12} \\ \Lambda_{21} & \Lambda_{22} \end{bmatrix} \begin{bmatrix} (1-x_1)x_1 & -x_1x_2 \\ -x_1x_2 & (1-x_2)x_2 \end{bmatrix}$$
$$= \frac{\begin{bmatrix} Đ_{13}\left(x_1Đ_{23}+(1-x_1)Đ_{12}\right) & x_1Đ_{23}\left(Đ_{13}-Đ_{12}\right) \\ x_2Đ_{13}\left(Đ_{23}-Đ_{12}\right) & Đ_{23}\left(x_2Đ_{13}+(1-x_2)Đ_{12}\right) \end{bmatrix}}{x_1Đ_{23}+x_2Đ_{13}+x_3Đ_{12}} \begin{bmatrix} (1-x_1)x_1 & -x_1x_2 \\ -x_1x_2 & (1-x_2)x_2 \end{bmatrix} \tag{45}$$

It is straightforward to verify that the Onsager relations (7) are satisified.

2. Darken and Vignes interpolation formulae for binary liquid mixtures

For binary liquid mixtures $n = 2$, the (n-1) dimensional matrix equations (31), and (37) simplify to yield

$$D_{12} = Đ_{12}\Gamma = L_{12}H = \frac{L_{12}}{x_1x_2}\Gamma; \quad \Gamma = \left(1+\frac{\partial \ln \gamma_1}{\partial \ln x_1}\right) \tag{46}$$

In the pioneering papers by Darken[11, 12] the following expression is postulated for the composition dependence of the Fick diffusivity D_{12}

$$D_{12} = \left(x_2D_{1,self} + x_1D_{2,self}\right)\left(1+\frac{\partial \ln \gamma_1}{\partial \ln x_1}\right) \tag{47}$$

where $D_{1,\text{self}}$ and $D_{2,\text{self}}$ are *tracer*, or *self*- diffusivities of components 1 and 2, respectively, in the binary mixture.

Darken[11, 12] was one of the first to recognize the need to use activity gradients as proper driving forces when setting up the phenomenological relations to describe diffusion. The thermodynamic factor Γ is also referred to as the "Darken correction factor". Combining equations (46) and (47) we obtain the following expression for the composition dependence of the M-S diffusivity $Đ_{12}$ for a binary mixture

$$Đ_{12} = x_2D_{1,self} + x_1D_{2,self} \tag{48}$$

The $D_{1,\text{self}}$ and $D_{2,\text{self}}$ are more easily accessible, both experimentally[13-15] and from Molecular Dynamics (MD) simulations,[16] than the $Đ_{12}$.

A somewhat more accurate interpolation formula is the empirical Vignes relation[16, 17]

$$Đ_{12} = \left(Đ_{12}^{x_1 \to 1}\right)^{x_1} \left(Đ_{12}^{x_2 \to 1}\right)^{x_2} \tag{49}$$

where the limiting values of the M-S diffusivities are

$$D_{2,self}^{x_1 \to 1} = Đ_{12}^{x_1 \to 1}; \quad D_{1,self}^{x_2 \to 1} = Đ_{12}^{x_2 \to 1} \tag{50}$$

Krishna and van Baten[16] have conducted a comprehensive set of MD simulations to determine $D_{i,self}$, $D_{j,self}$, and $Đ_{ij}$ for a variety of binary and ternary mixtures containing linear alkanes, with carbon numbers in the range of 1 – 16 at 333 K and 30 MPa. The computational details are provided in Krishna and van Baten;[16] some salient details are provided hereunder.

The MD simulations are based on the united atom model that considers the CH_x groups as single, chargeless interaction centers with their own effective potentials. The beads in the chain are connected by harmonic bonding potentials. A harmonic cosine bending potential models the bond bending between three neighboring beads, a Ryckaert-Bellemans potential controls the torsion angle. The beads in a chain separated by more than three bonds interact with each other through a Lennard-Jones potential. The Lennard-Jones potentials are shifted and cut at 12 Å. The force fields have been given in detail in other publications[36, 37]. The size of the simulation box was taken to be either 25 Å×25 Å×25 Å or 30 Å×30 Å×30 Å. Periodic boundary conditions were employed.

Diffusion in a system of N molecules is simulated using Newton's equations of motion until the system properties, on average, no longer change in time. The Verlet algorithm is used for time integration. The energy drift of the entire system is monitored to ensure that the time steps taken were not too large. A time step of 2 fs was used in all simulations. N molecules are inserted into the simulation box at random positions as long as no overlaps occur with other particles. During the initializing period we perform an NVT MC simulation to rapidly achieve an equilibrium molecular arrangement. After the initialization step, we assign velocities to the pseudo-atoms from the Maxwell-Boltzmann distribution at the desired average temperature. The total momentum of the system is set to zero. Next, we equilibrate the system further by performing a NVT MD simulation using the Nosé-Hoover thermostat. When the equilibration is completed, the production run starts. For every cycle, the

statistics for determining the mean square displacements (MSDs) in the NVT ensemble are updated. The MSDs are determined for time intervals ranging from 2 fs to 1 ns. In order to do this, an order-*N* algorithm, as detailed in Chapter 4 of Frenkel and Smit[23] is implemented.

The self-diffusivities were determined from the formula

$$D_{i,self} = \frac{1}{6N_i} \lim_{\Delta t \to \infty} \frac{1}{\Delta t} \left\langle \left(\sum_{l=1}^{N_i} \left(\mathbf{r}_{l,i}(t + \Delta t) - \mathbf{r}_{l,i}(t) \right)^2 \right) \right\rangle \tag{51}$$

where $\mathbf{r}_{l,i}(t)$ denotes the position vector of molecule l of species i , N_i is the number of molecules of species i, and the notation $\langle \cdots \rangle$ denotes ensemble averaging.

The values of the self-diffusivities at the limiting compositions, $D_{i,self}^{x_j \to 1}$, determined from MD simulations are provided in Table 1.

The elements of the n-dimensional matrix $[\Omega]$ defined by

$$x_i \mathbf{u}_i = -\frac{1}{RT} \sum_{j=1}^{n} \Omega_{ij} \nabla \mu_j; \quad i = 1,2,...n \tag{52}$$

are determined from

$$\Omega_{ij} = \frac{1}{6} \lim_{\Delta t \to \infty} \frac{1}{N} \frac{1}{\Delta t} \left\langle \left(\sum_{l=1}^{N_i} \left(\mathbf{r}_{l,i}(t + \Delta t) - \mathbf{r}_{l,i}(t) \right) \right) \bullet \left(\sum_{k=1}^{N_j} \left(\mathbf{r}_{k,j}(t + \Delta t) - \mathbf{r}_{k,j}(t) \right) \right) \right\rangle \tag{53}$$

where N_i and N_j are the number of molecules of species i and j, respectively, in the simulations box and N represents the total number of molecules. The $\Omega_{ij} = \Omega_{ji}$ coefficients defined by Eq. (52) correspond to a reference frame in which the mass average mixture velocity is zero, i.e. $\sum_{i=1}^{n} \omega_i \mathbf{u}_i = 0$. This implies that the $\Omega_{ij} = \Omega_{ji}$ coefficients are constrained by

$$\sum_i M_i \Omega_{ij} = 0 \tag{54}$$

where M_i represents the molar mass of species i. The elements Λ_{ij}, defined by equation (35), are related to the coefficients Ω_{ij} by

$$\Lambda_{ij} = (1-x_i)\left(\frac{\Omega_{ij}}{x_j} - \frac{\Omega_{in}}{x_n}\right) - x_i \sum_{k=1;k\neq i}^{k=n}\left(\frac{\Omega_{kj}}{x_j} - \frac{\Omega_{kn}}{x_n}\right); \quad i,j = 1,2,...n-1 \tag{55}$$

We discuss and analyze the MD simulation data below.

Figure 2 presents the MD simulation data of Krishna and van Baten[16] on $D_{i,self}$, $D_{j,self}$, and $Đ_{ij}$ for the methane(1)/ethane(2), methane(1)/n-hexane(3), and ethane(2)/n-hexane(3) binary mixtures. The continuous solid lines are the calculations of $Đ_{ij}$ using the Darken interpolation equation (48) using as input the MD simulated values of $D_{1,self}$, $D_{2,self}$, and $D_{3,self}$.

For the three binary mixtures methane(1)/ethane(2), methane(1)/n-hexane(3), and ethane(2)/n-hexane(3), we can determine the M-S diffusivities (units: 10^{-8} m^2 s^{-1}) at the limiting compositions as follows:

methane(1)/ethane(2): $Đ_{12}^{x_1\to 1} = \quad 5.3; \quad Đ_{12}^{x_2\to 1} = 2.58$

methane(1)/n-hexane(3): $Đ_{13}^{x_1\to 1} = \quad 3; \quad Đ_{13}^{x_3\to 1} = 1.05$

ethane(2)/n-hexane(3): $Đ_{23}^{x_2\to 1} = \quad 1.09; \quad Đ_{23}^{x_3\to 1} = 0.84$

Also shown in Figure 2 are the calculations using the Vignes interpolation formula (49) using the values at either ends of the composition range.

Figure 3 presents the MD simulation data of Krishna and van Baten[16] on $D_{i,self}$, $D_{j,self}$, and $Đ_{ij}$ for the binary methane(1)/ethane(2), methane(1)/propane(3), and ethane(2)/propane (3) mixtures. The continuous solid lines are the calculations of $Đ_{ij}$ using either the Darken interpolation equation (48), or the Vignes interpolation formula (49).

Figure 4 presents MD simulation data of Krishna and van Baten[16] on $D_{i,self}$, $D_{j,self}$, and $Đ_{ij}$ for the binary methane(1)/propane(2), methane(1)/n-hexane(3), and propane(2)/n-hexane (3) mixtures. The continuous solid lines are the calculations of $Đ_{ij}$ using either the Darken interpolation equation (48), or the Vignes interpolation formula (49).

Figure 5 presents MD simulation data of Krishna and van Baten[16] on $D_{i,self}$, $D_{j,self}$, and $Đ_{ij}$ for the binary ethane(1)/propane(2), ethane(1)/n-butane(3), and propane(2)/n-butane (3) mixtures. The continuous solid lines are the calculations of $Đ_{ij}$ using either the Darken interpolation equation (48), or the Vignes interpolation formula (49).

Figure 6 presents MD simulation data of Krishna and van Baten[16] on $D_{i,self}$, $D_{j,self}$, and $Đ_{ij}$ for the binary propane(1)/n-butane(2), propane(1)/n-pentane(3), and n-butane(2)/n-pentane (3) mixtures. The continuous solid lines are the calculations of $Đ_{ij}$ using either the Darken interpolation equation (48), or the Vignes interpolation formula (49).

The results presented in Figures 2,3, 4, 5, and 6 demonstrate the accuracy of both the Darken and Vignes interpolation formulae. A visual inspection shows that the Vignes interpolation formula (49) to be slightly superior for the investigated mixtures.

Generally speaking, the factoring out of the effects of non-ideal mixture thermodynamics (by use of $\frac{D_{12}}{\Gamma} = Đ_{12}$) results in a milder variation of the M-S diffusivity as compared to the Fick diffusivity.

The Vignes interpolation formula (49) offers the possibility of interpolation using data at either ends of the composition scale. To verify this, Figures 7a, 7b, and 7c present comparison of the Fick, and M-S, and Onsager diffusivities for (a) acetone (1) – water (2), (b) ethanol (1) – water (2) and (c) methanol(1)/n-hexane (2) mixtures along with the estimations using equation (49). We see that that the interpolation formula is of good accuracy. Further examination of the validity of the Vignes interpolation formula in available in published works.[8, 18-22]

The Onsager diffusivity is related to the M-S diffusivity by equation (37) which simplifies for binary mixtures to

$$L_{12} = x_1 x_2 Đ_{12} = \frac{D_{12}}{\Gamma} \tag{56}$$

The L_{12} vanishes at either ends of the composition scale (cf. Figure 7) and this characteristic makes it less desirable for use in practical applications.[3, 8, 23-25]

Figure 8 presents the comparison the Fick diffusivities, D_{12}, with the Maxwell-Stefan, $Đ_{12}$, diffusivities for (a) water (1) – methanol (2), (b) water (1) - ethanol(3), and (c) methanol (2) - ethanol (3) mixtures at 298 K. The M-S diffusivities are better behaved as regards their composition dependence in comparison with the Fick diffusivities.

For binary gaseous mixtures at high pressures, the influence of the compressibility factor needs to be additionally accounted for. The influence of influence of the total pressure, p, on the Fick diffusivity of binary gas mixtures can be estimated by combining the FSG equation (27) with the PR EOS for estimating Z, and Γ:

$$D_{ij} = \frac{1.43\times10^{-7}T^{1.75}}{p\sqrt{M_{ij}}\left[\left(v_i^{1/3}\right)+\left(v_j^{1/3}\right)\right]^2} Z\left(1+\frac{\partial \ln \phi_1}{\partial \ln x_1}\right) \tag{57}$$

The influence of increased pressures on the estimations of the Fick diffusivities are illustrated for $CH_4(1)/C_3H_8(2)$ mixtures at 298.15 K and x_1 = 0.7 in Figure 9. Influence of pressure on (a) compressibility factor, calculated using the Peng-Robinson Equation of State (PR EOS), (b) thermodynamic factor, Γ, calculated using PR EOS, and (c) Fick diffusivity of $CH_4(1)/C_3H_8(2)$ mixtures at T = 298.15 K and x_1= 0.7. Of particular interest is the variation of the Fick diffusivity with pressure. For the range 1 – 100 bar, the value of D_{12} decreases with increasing pressure. However, for p >100 bar, the diffusivity values are nearly independent of pressure.

The influence of fluid compositions on the diffusivities of $CH_4(1)/C_3H_8(2)$ mixtures at 298.15 K are shown in Figure 10. We note that the Fick diffusivities exhibit a pronounced increase in values for x_1 > 0.7. This increase in the diffusivity is confirmed by the experimental data of Sigmund, as reported in Figure 2a of Leahy-Dios and Firoozabadi, discussed below.[26]

Figure 11a presents the experimental data of Sigmund, as reported in Figure 2a of Leahy-Dios and Firoozabadi,[26] for Fick diffusivities of CH_4/C_3H_8 mixtures at T = 311 K and p = 137.8 bar. For an ideal gas mixture, the Fick diffusivities are expected to be independent of composition. The departures from this expectation is attributable to two separate factors: (a) the variation of the compressibility factor, Z, with composition (as shown in the PR EOS calculations in Figure 11b), and the thermodynamic

correction factor, $\Gamma = \left(1 + \frac{\partial \ln \phi_1}{\partial \ln x_1}\right)$ (as shown in the PR EOS calculations in Figure 11c); here ϕ_1 the fugacity coefficient. The continuous solid line in Figure 11a represents calculations using $D_{12} = \left(Đ_{12}^{x_1 \to 1}\right)^{x_1} \left(Đ_{12}^{x_2 \to 1}\right)^{x_2} \left(1 + \frac{\partial \ln \phi_1}{\partial \ln x_1}\right) Z$ with input of the empirical values $Đ_{12}^{x_1 \to 1} = 1.21 \times 10^{-7}$ m^{2}s^{-1}, and $Đ_{12}^{x_2 \to 1} = 0.38 \times 10^{-7}$ m^{2}s^{-1}; there is good agreement between the combined Vignes-PR EOS model and the experimental data. The dashed line in Figure 11a are calculations of the M-S diffusivity $Đ_{12} = \left(Đ_{12}^{x_1 \to 1}\right)^{x_1} \left(Đ_{12}^{x_2 \to 1}\right)^{x_2} Z$.

Figure 11d presents the experimental data of Sigmund, as reported in Figure 2c of Leahy-Dios and Firoozabadi,[26] for Fick diffusivities of CH_4/C_3H_8 mixtures at T = 311 K and p there is good agreement between this estimation and the experimental data.= 206.8 bar. The continuous solid line in Figure 11d represents calculations using $D_{12} = \left(Đ_{12}^{x_1 \to 1}\right)^{x_1} \left(Đ_{12}^{x_2 \to 1}\right)^{x_2} \left(1 + \frac{\partial \ln \phi_1}{\partial \ln x_1}\right) Z$ with input the empirical values $Đ_{12}^{x_1 \to 1} = 0.81 \times 10^{-7}$ m^{2}s^{-1}, and $Đ_{12}^{x_2 \to 1} = 0.26 \times 10^{-7}$ m^{2}s^{-1}; there is good agreement between the combined Vignes-PR EOS model and the experimental data. The dashed line in Figure 11d are calculations of the M-S diffusivity $Đ_{12} = \left(Đ_{12}^{x_1 \to 1}\right)^{x_1} \left(Đ_{12}^{x_2 \to 1}\right)^{x_2} Z$.

Figures 12a,b presents the experimental data of Tuan et al.[10] for the dependence of the Fick diffusivity of methyl oleate (MO) (component 2) in supercritical CO_2 (component 1), indicated by green squares, on the mole fraction of MO for T = 313.15 K, and (a) p = 10.6 MPa, and (b) p = 11.5 MPa. The strong decrease in the Fick diffusivity is primarily attributable to the influence of the thermodynamic correction factor, $\Gamma = \left(1 + \frac{\partial \ln \phi_1}{\partial \ln x_1}\right)$, values of which, calculated using the PR EOS, are also indicated in Figures 12a,b.

3. Darken and Vignes interpolation formulae for ternary liquid mixtures

For diffusion in *n*-component non-ideal liquid mixtures, the matrix of Fick diffusivities $[D]$ has significant non-diagonal contributions caused by (a) differences in the binary pair M-S diffusivities, $Đ_{ij}$, and (b) strong coupling introduced by the matrix of thermodynamic factors $[\Gamma]$.

The description of the composition dependence of the M-S diffusivities $Đ_{ij}$ in liquid mixtures containing three or more species is much less developed. Krishna and van Baten[16] postulate that the M-S diffusivity of the *i-j* pair in the ternary *i-j-k* mixture depends on $D_{i,self}$ and $D_{j,self}$ in this mixture, but weighted with mole fractions on a *k*-free basis, i.e.

$$Đ_{ij} = \frac{x_i}{x_i + x_j} D_{j,self} + \frac{x_j}{x_i + x_j} D_{i,self} \tag{58}$$

Each of the three M-S pair diffusivities $Đ_{ij}$ depends on six infinite dilution parameters

$$Đ_{12}^{x_1 \to 1}; \quad Đ_{12}^{x_2 \to 1}; \quad Đ_{13}^{x_1 \to 1}; \quad Đ_{13}^{x_3 \to 1}; \quad Đ_{23}^{x_2 \to 1}; \quad Đ_{23}^{x_3 \to 1} \tag{59}$$

These limiting values of $Đ_{ij}$ at the edges of the ternary composition space are

$$\begin{aligned}
&Đ_{12}^{x_1 \to 1} = D_{2,self}^{x_1 \to 1}; \quad Đ_{12}^{x_2 \to 1} = D_{1,self}^{x_2 \to 1}; \quad Đ_{12}^{x_3 \to 1} = \frac{x_1}{x_1 + x_2} D_{2,self}^{x_3 \to 1} + \frac{x_2}{x_1 + x_2} D_{1,self}^{x_3 \to 1}; \\
&Đ_{13}^{x_1 \to 1} = D_{3,self}^{x_1 \to 1}; \quad Đ_{13}^{x_3 \to 1} = D_{1,self}^{x_3 \to 1}; \quad Đ_{13}^{x_2 \to 1} = \frac{x_1}{x_1 + x_3} D_{3,self}^{x_2 \to 1} + \frac{x_3}{x_1 + x_3} D_{1,self}^{x_2 \to 1}; \\
&Đ_{23}^{x_2 \to 1} = D_{3,self}^{x_2 \to 1}; \quad Đ_{23}^{x_3 \to 1} = D_{2,self}^{x_3 \to 1}; \quad Đ_{23}^{x_3 \to 1} = \frac{x_2}{x_2 + x_3} D_{3,self}^{x_1 \to 1} + \frac{x_3}{x_2 + x_3} D_{2,self}^{x_1 \to 1};
\end{aligned} \tag{60}$$

Noting that the following limiting values hold

$$\begin{aligned}
&Đ_{12}^{x_1 \to 1} = D_{2,self}^{x_1 \to 1}; \quad Đ_{12}^{x_2 \to 1} = D_{1,self}^{x_2 \to 1}; \\
&Đ_{13}^{x_1 \to 1} = D_{3,self}^{x_1 \to 1}; \quad Đ_{13}^{x_3 \to 1} = D_{1,self}^{x_3 \to 1}; \\
&Đ_{23}^{x_2 \to 1} = D_{3,self}^{x_2 \to 1}; \quad Đ_{23}^{x_3 \to 1} = D_{2,self}^{x_3 \to 1};
\end{aligned} \tag{61}$$

we derive

$$
\begin{aligned}
&Đ_{12}^{x_1\to 1} = D_{2,self}^{x_1\to 1}; \quad Đ_{12}^{x_2\to 1} = D_{1,self}^{x_2\to 1}; \quad Đ_{12}^{x_3\to 1} = \frac{x_1}{x_1+x_2} Đ_{23}^{x_3\to 1} + \frac{x_2}{x_1+x_2} Đ_{13}^{x_3\to 1};\\
&Đ_{13}^{x_1\to 1} = D_{3,self}^{x_1\to 1}; \quad Đ_{13}^{x_3\to 1} = D_{1,self}^{x_3\to 1}; \quad Đ_{13}^{x_2\to 1} = \frac{x_1}{x_1+x_3} Đ_{23}^{x_2\to 1} + \frac{x_3}{x_1+x_3} Đ_{12}^{x_2\to 1};\\
&Đ_{23}^{x_2\to 1} = D_{3,self}^{x_2\to 1}; \quad Đ_{23}^{x_3\to 1} = D_{2,self}^{x_3\to 1}; \quad Đ_{23}^{x_3\to 1} = \frac{x_2}{x_2+x_3} Đ_{13}^{x_1\to 1} + \frac{x_3}{x_2+x_3} Đ_{12}^{x_1\to 1};
\end{aligned}
\tag{62}
$$

Eq. (62) is the proper estimation procedure for $Đ_{ij}^{x_j\to 1}$ that is consistent with the Darken relation.

For a ternary mixture, Wesselingh and Bollen[27] have suggested the following extension of the Vignes interpolation formula (49)

$$
Đ_{ij} = \left(Đ_{ij}^{x_i\to 1}\right)^{x_i} \left(Đ_{ij}^{x_j\to 1}\right)^{x_j} \left(Đ_{ij}^{x_k\to 1}\right)^{x_k} \tag{63}
$$

For the estimation of $Đ_{ij}^{x_k\to 1}$, the *i* - *j* pair diffusivity when both *i* and *j* are present in infinitely dilute concentrations. Krishna and van Baten[16] suggest the extension of the Darken relations (62) to obtain

$$
\begin{aligned}
Đ_{12}^{x_3\to 1} &= \left(Đ_{13}^{x_3\to 1}\right)^{x_1/(x_1+x_2)} \left(Đ_{23}^{x_3\to 1}\right)^{x_2/(x_1+x_2)}\\
Đ_{13}^{x_2\to 1} &= \left(Đ_{12}^{x_2\to 1}\right)^{x_1/(x_1+x_3)} \left(Đ_{23}^{x_2\to 1}\right)^{x_3/(x_1+x_3)}\\
Đ_{23}^{x_1\to 1} &= \left(Đ_{12}^{x_1\to 1}\right)^{x_2/(x_2+x_3)} \left(Đ_{13}^{x_1\to 1}\right)^{x_3/(x_2+x_3)}
\end{aligned}
\tag{64}
$$

For the special case of an equimolar mixture we obtain

$$
\begin{aligned}
Đ_{12}^{x_3\to 1} &= \sqrt{\left(Đ_{13}^{x_3\to 1} Đ_{23}^{x_3\to 1}\right)}\\
Đ_{13}^{x_2\to 1} &= \sqrt{\left(Đ_{12}^{x_2\to 1} Đ_{23}^{x_2\to 1}\right)}\\
Đ_{23}^{x_3\to 1} &= \sqrt{\left(Đ_{12}^{x_1\to 1} Đ_{13}^{x_1\to 1}\right)}
\end{aligned}
\tag{65}
$$

The simplified interpolation formula (65) was proposed by Wesselingh and Bollen.[27]

Liu, Bardow and Vlugt[18] have suggested the following procedure for estimation of $Đ_{ij}^{x_k\to 1}$

$$
Đ_{12}^{x_3\to 1} = \frac{D_{1,self}^{x_3\to 1} D_{2,self}^{x_3\to 1}}{D_{3,self}^{x_3\to 1}}; \quad Đ_{13}^{x_2\to 1} = \frac{D_{1,self}^{x_2\to 1} D_{3,self}^{x_2\to 1}}{D_{2,self}^{x_2\to 1}}; \quad Đ_{23}^{x_1\to 1} = \frac{D_{2,self}^{x_1\to 1} D_{3,self}^{x_1\to 1}}{D_{1,self}^{x_1\to 1}} \tag{66}
$$

While $D_{3,self}^{x_3\to 1}$, $D_{2,self}^{x_2\to 1}$, $D_{1,self}^{x_1\to 1}$ are accessible from MD simulations, these self-diffusivity values cannot be estimated on the basis of M-S diffusivities of the constituent binary pairs in ternary mixtures.

4. MD data for diffusivities in ternary mixtures on n-alkanes

Krishna and van Baten[16] have performed MD simulations to determine the diffusivities in a wide variety of ternary mixtures consisting of n-alkanes. We re-analyse their data on the following five systems.

methane(1)/ethane(2)/n-hexane(3)

methane(1)/ethane(2)/propane(3)

methane(1)/propane (2)/n-hexane(3)

ethane(1)/propane (2)/n-butane(3)

propane(1)/n-butane (2)/n-pentane(3)

MD simulations of diffusivities in ternary mixtures, such as those reported by Krishna and van Baten,[16] do not directly yield the values of the constituent pair diffusivities, $Đ_{ij}$. Rather, the MD simulations yield the four elements of the matrix [Λ], defined by equation (35). The inversion of [Λ] needs to be first performed in order to determine the elements of [B]. For a ternary mixture, the M-S $Đ_{ij}$ can be determined explicitly using the following relations that are derived by Krishna and van Baten,[16] :

$$Đ_{13} = \frac{1}{B_{11} + \dfrac{x_2 B_{12}}{x_1}} \tag{67}$$

$$Đ_{12} = \frac{1}{B_{11} - \dfrac{(x_1 + x_3)}{x_1} B_{12}} = \frac{1}{B_{22} - \dfrac{(x_2 + x_3)}{x_2} B_{21}} \tag{68}$$

$$Đ_{23} = \frac{1}{B_{22} + \dfrac{x_1 B_{21}}{x_2}} \tag{69}$$

The procedure of first inverting the MD simulated values of matrix [Λ], to obtain the $Đ_{ij}$ from equations (67), (68), and (69) is fraught with numerical inaccuracies. Therefore, let us first compare the MD simulated values of the four elements of the matrix [Λ] with estimations using the Vignes interpolation formula (63), combined with either equation (65) or equation (66). The parity plots for the

four elements Λ_{11}, Λ_{12}, Λ_{21}, and Λ_{22} are shown in Figures 13, 14, 15, 16, and 17 for the five different ternary mixtures investigated by Krishna and van Baten.[16] The upper left corner presents the parity plots using the Liu-Bardow-Vlugt[18] interpolation formula (66), while the bottom right corner presents the parity plots with the Wesselingh-Bollen interpolation formula (65). Generally speaking, the estimations of the diagonal elements Λ_{11}, and Λ_{22} should be expected to be more accurate than the estimations of the off-diagonal elements Λ_{12}, and Λ_{21}. This is indeed the case for all five ternary mixtures. The two estimation procedures of Wesselingh-Bollen and Liu-Bardow-Vlugt[18] yield predictions of four elements Λ_{11}, Λ_{12}, Λ_{21}, and Λ_{22} that are practically identical.

The square root of the determinant $|\Lambda|^{1/2}$ may be viewed as a measure of the "magnitude" of the M-S diffusivity that characterizes diffusion in a ternary mixture. Figure 18 presents comparisons of the values of MD simulated values of $|\Lambda|^{1/2}$ for the five different mixtures with calculations of $|\Lambda|^{1/2} = \sqrt{\frac{Đ_{12}Đ_{13}Đ_{23}}{x_1Đ_{23}+x_2Đ_{13}+x_3Đ_{12}}}$ with the $Đ_{ij}$ using Vignes interpolation formula (63), combined with (65). Such an estimate of the "magnitude" of the M-S diffusivity in ternary mixtures is useful for estimation of the elements of Fick matrix [D] for ternary mixtures, as we will discuss later.

A different procedure for estimation of $|\Lambda|^{1/2}$ is presented in Figure 19. Here we present comparisons of the values of MD simulated values of $|\Lambda|^{1/2}$ for the five different mixtures with calculations of $\left(D_{1,self}\right)^{x_1}\left(D_{2,self}\right)^{x_2}\left(D_{3,self}\right)^{x_3}$ where the component self-diffusivities are also values determined from MD simulations. The accuracy of this estimation is comparable to those based on Vignes interpolation, presented in Figure 18.

Let us now turn to the estimations of the M-S diffusivities $Đ_{12}$, $Đ_{13}$, and $Đ_{23}$ using Vignes interpolation formula (63), combined with equation (65) for the five different mixtures. Figure 20, Figure 21, Figure 22, Figure 23, Figure 24, and Figure 25 present comparisons of the estimations of the M-S diffusivities $Đ_{12}$, $Đ_{13}$, and $Đ_{23}$ using the Vignes interpolation formula (63), combined with equation

(65) along with the $Đ_{ij}$ values determined from equations (67), (68), and (69) for the five different ternary mixtures.

Figure 20 presents the MD simulation data of Krishna and van Baten[16] on $Đ_{12}$, $Đ_{13}$, and $Đ_{23}$ in the ternary methane(1)/ethane(2)/n-hexane(3) mixtures: $x_1 = 0.2$, varying x_2, x_3; $x_2 = 0.2$, varying x_1, x_3; $x_3 = 0.2$, varying x_1, x_2. The continuous solid lines are the calculations of $Đ_{ij}$ using Vignes interpolation formula (63), combined with equation (65). The estimations of $Đ_{12}$, and $Đ_{13}$ are of good accuracy but the estimates of $Đ_{23}$ are not of the same accuracy.

Figure 21 presents the MD simulation data of Krishna and van Baten[16] on $Đ_{12}$, $Đ_{13}$, and $Đ_{23}$ in the ternary methane(1)/ethane(2)/n-hexane(3) mixtures: vary x_1, with $x_2/x_3 = 1$; vary x_2, with $x_1/x_3 = 1$; vary x_3, with $x_1/x_2 = 1$. The continuous solid lines are the calculations of $Đ_{ij}$ using Vignes interpolation formula (63), combined with equation (65). As in the previous case, we note that the estimations of $Đ_{12}$, and $Đ_{13}$ are of good accuracy but the estimates of $Đ_{23}$ are not of the same accuracy.

Similar conclusions about the accuracy of the Vignes interpolation formula (63) are reached for the other four mixtures; see Figure 22, Figure 23, Figure 24, and Figure 25.

5. MD simulations of diffusivities in water/methanol/ethanol mixtures

Parez et al.[28] have published MD simulated values $|\Lambda|^{1/2}$ for water(1)/methanol(2)/ethanol(3) mixtures. Figure 26 presents a plot of the $|\Lambda|^{1/2}$ data as a function of the mole fraction of methanol (component 2). We see that the data shows a very simple correlation with the methanol compositon. This MD simulated values are in reasonably good agreement with calculations using $|\Lambda|^{1/2} = \left(D_{1,self}\right)^{x_1}\left(D_{2,self}\right)^{x_2}\left(D_{3,self}\right)^{x_3}$, taking $D_{1,\text{self}} = 10.3$, $D_{2,\text{self}} = 18$, $D_{3,\text{self}} = 9.1$ with units 10^{-10} m^2 s^{-1}.

6. Fick diffusivity matrix [*D*] for acetone/benzene/CCl_4 mixtures

Cullinan and Toor,[29] have presented experimental data for the elements of the Fick diffusivity matrix [*D*] for acetone(1)/benzene(2)/CCl_4(3) mixtures. Let us now examine whether we can estimate the elements of the Fick diffusivity matrix [*D*] for acetone(1)/benzene(2)/CCl_4(3) mixtures using data on the

infinite dilution M-S diffusivity values. For this purpose, we need to examine diffusivities in each of the binary pairs. Figure 27 presents the experimental data on the Fick diffusivities for (a) acetone(1)/benzene(2), (b) acetone(1)/CCl_4(3), and (c) benzene (2)/ CCl_4(3) mixtures as a function of composition. Also shown in Figure 27 are the M-S diffusivities, calculated from $Đ_{12} = \frac{D_{12}}{\Gamma}$. The required NRTL parameters for calculation of thermodynamic factors are provided in Table 2. The benzene/CCl_4 mixtures are ideal, and consequently $\Gamma \approx 1; \quad Đ_{12} \approx D_{12}$. For acetone/benzene mixtures, the Vignes interpolation formula (49) is of reasonable accuracy, whereas for acetone/CCl_4, the M-S diffusivity does not accurately follow the composition dependence prescribed by equation (49). On the basis of the diffusivity data of the three binary pairs, we determine the following six M-S diffusivity values at either ends of the composition ranges (units: 10^{-9} m^2 s^{-1})

$$\begin{aligned}
&Đ_{12}^{x_1\to 1} = 4.15; \quad Đ_{12}^{x_2\to 1} = 2.75; \quad \text{for acetone(1)/benzene(2) binary mixture} \\
&Đ_{13}^{x_1\to 1} = 3.57; \quad Đ_{13}^{x_3\to 1} = 1.7; \quad \text{for acetone(1)/CCl}_4\text{(3) binary mixture} \\
&Đ_{23}^{x_2\to 1} = 1.91; \quad Đ_{23}^{x_3\to 1} = 1.42 \quad \text{for benzene(2)/CCl}_4\text{(3) binary mixture}
\end{aligned} \tag{70}$$

Equation (70) in combination with the Vignes interpolation formula (63), with equation (65) allows the estimation of $[\Lambda]=[B]^{-1}$. We are unable to use the Liu-Bardow-Vlugt[18] interpolation formula (66) because the data on $D_{3,self}^{x_3\to 1}$, $D_{2,self}^{x_2\to 1}$, $D_{1,self}^{x_1\to 1}$ cannot be determined from the experimental M-S diffusivity data on binary pairs. Post-multiplication of $[\Lambda]$ with the matrix of thermodynamic factors $[\Gamma]$ allows estimation of the Fick diffusivity matrix [*D*]

$$[D]=[B]^{-1}[\Gamma]=[\Lambda][\Gamma] \tag{71}$$

Figure 28 presents a comparison of the experimental data on Fick diffusivity matrix [*D*] with the estimations. The required NRTL parameters for calculation of thermodynamic factors $[\Gamma]$ are provided in Table 2. We observe that the diagonal elements D_{11} and D_{22} are predicted fairly well, as is to be expected. However, the estimations of the off-diagonal elements D_{12} and D_{21} are somewhat poorer. Nevertheless, the estimations of the cross-coefficients are of the right order of magnitude and sign.

Figure 29 presents a plot of $|\Lambda|^{1/2} = \frac{|D|^{1/2}}{|\Gamma|^{1/2}}$ as a function of the mole fraction of acetone in acetone(1)/benzene(2)/carbon-tetrachloride(3) mixtures at 298 K. The square root of determinants $|D|$, and $|\Gamma|$ are representative of the "magnitudes" of [D], and $[\Gamma]$ respectively. The ratio $\frac{|D|^{1/2}}{|\Gamma|^{1/2}}$ can be viewed as the "magnitude" of the Maxwell-Stefan diffusivity in the *ternary* mixture. The ratio $|\Lambda|^{1/2} = \frac{|D|^{1/2}}{|\Gamma|^{1/2}}$ appears to show a simple dependence on the mole fraction of acetone, quite similar to that observed for the variation of the M-S diffusivity in acetone/benzene, and acetone/CCl_4 mixtures; see Figure 27. The crosses in Figure 29 represent calculations using the formula $|\Lambda|^{1/2} = \sqrt{\frac{Đ_{12}Đ_{13}Đ_{23}}{x_1Đ_{23}+x_2Đ_{13}+x_3Đ_{12}}}$ where the $Đ_{12}$, $Đ_{13}$, and $Đ_{23}$ are calculated using Vignes interpolation formula (63), combined with Wesselingh-Bollen interpolation (65).

We shall now estimate the Fick diffusivity matrix [D] from $[D]=|\Lambda|^{1/2}[\Gamma]$ with $|\Lambda|^{1/2} = \sqrt{\frac{Đ_{12}Đ_{13}Đ_{23}}{x_1Đ_{23}+x_2Đ_{13}+x_3Đ_{12}}}$, where the $Đ_{12}$, $Đ_{13}$, and $Đ_{23}$ are calculated using Vignes interpolation formula (63), combined with Wesselingh-Bollen interpolation (65).

The parity plots are presented in Figure 30. The estimations of the Fick diffusivity matrix [D] using this simplified procedure is about the same level of accuracy as the more rigorous Vignes interpolation formula (63). We observe that the diagonal elements D_{11} and D_{22} are predicted fairly well, as is to be expected. However, the estimations of the off-diagonal elements D_{12} and D_{21} are somewhat poorer. Nevertheless, the estimations of the cross-coefficients are of the right order of magnitude and sign. We conclude therefore that a good estimate of the Fick diffusivity matrix is $[D]=|\Lambda|^{1/2}[\Gamma]$ where the "average" M-S diffusivity can be estimated using the Vignes interpolation formula.

7. Fick diffusivity matrix [*D*] for acetone/benzene/methanol mixtures

We now analyze the experimental data of Alimadadian and Colver;[30] for acetone(1)/benzene(2)/methanol(3) mixtures. Figure 31 presents a comparison of the Fick and Maxwell-Stefan diffusivities for (a) acetone(1)/benzene(2), (b) acetone(1)/methanol (3), and (c) benzene (2)/methanol (3) mixtures. The thermodynamic factors are calculated using NRTL parameters reported by Kooijman and Taylor[31] and reproduced in Table 3. Please note that the acetone-benzene parameters are not the same as those reported above in Table 2. This explains that the M-S diffusivities for acetone-benzene mixtures shown in Figure 31a are significantly higher than the corresponding values in Figure 27a.

On the basis of the diffusivity data of the three binary pairs, we determine the following six M-S diffusivity values at either ends of the composition ranges

$$\begin{aligned}
&Đ_{12}^{x_1\to 1} = 4.15; \quad Đ_{12}^{x_2\to 1} = 2.75; \quad \text{for acetone(1)/benzene(2) binary mixture}\\
&Đ_{13}^{x_1\to 1} = 5.3; \quad Đ_{13}^{x_3\to 1} = 2.7; \quad \text{for acetone(1)/methanol(3) binary mixture}\\
&Đ_{23}^{x_2\to 1} = 4.3; \quad Đ_{23}^{x_3\to 1} = 3 \quad \text{for benzene(2)/methanol(3) binary mixture}
\end{aligned} \tag{72}$$

Alimadadian and Colver;[30] report the elements of the Fick matrix [*D*] for acetone(1)/benzene(2)/methanol(3) mixtures at 9 different compositions. Figure 32 presents data on $\frac{|D|^{1/2}}{|\Gamma|^{1/2}}$ as a function of the mole fraction of acetone for acetone(1)/benzene(2)/methanol(3) mixtures, where the matrix of thermodynamic factors is determined from the NRTL parameters in Table 3. We again note that factoring out the thermodynamic influences yields much milder, well-behaved, composition dependences. The crosses in Figure 32 represent calculations using the formula $|\Lambda|^{1/2} = \sqrt{\frac{Đ_{12}Đ_{13}Đ_{23}}{x_1Đ_{23}+x_2Đ_{13}+x_3Đ_{12}}}$ where the $Đ_{12}$, $Đ_{13}$, and $Đ_{23}$ are calculated using Vignes interpolation formula (63), combined with Wesselingh-Bollen interpolation (65).

Figure 33 presents a comparison of the experimental data of Alimadadian and Colver;[30] for the elements of the estimate the Fick diffusivity matrix with estimates using $[D]=|\Lambda|^{1/2}[\Gamma]$ with

$|\Lambda|^{1/2} = \sqrt{\frac{Đ_{12}Đ_{13}Đ_{23}}{x_1Đ_{23}+x_2Đ_{13}+x_3Đ_{12}}}$. The M-S binary pair diffusivities $Đ_{12}$, $Đ_{13}$, and $Đ_{23}$ are calculated using Vignes interpolation formula (63), combined with Wesselingh-Bollen interpolation (65) and equation (72). We observe that the diagonal elements D_{11} and D_{22} are predicted fairly well, as is to be expected. However, the estimations of the off-diagonal elements D_{12} and D_{21} are somewhat poorer. Nevertheless, the estimations of the cross-coefficients are of the right order of magnitude and sign.

The reasonably good estimates provided by $[D]=|\Lambda|^{1/2}[\Gamma]$ implies that the coupling effects of the Fick diffusivity matrix have their origins in the coupling of the matrix of thermodynamic factors. In order to verify this conclusion, Figure 34 plots the ratio $\frac{D_{12}D_{21}}{D_{11}D_{22}}$ against the corresponding value of the ratio $\frac{\Gamma_{12}\Gamma_{21}}{\Gamma_{11}\Gamma_{22}}$. We note a near-linear dependence, confirming that diffusional coupling largely originate from thermodynamic coupling.

8. Fick diffusivity matrix [*D*] for methanol/1-propanol/iso-butanol mixtures

We now analyse the experimental data of Shuck and Toor[32] for methanol(1)/1-propanol(2)/iso-butanol(3) mixtures.. Figure 35 presents data on $\frac{|D|^{1/2}}{|\Gamma|^{1/2}}$ as a function of the mole fraction of methanol for methanol(1)/1-propanol(2)/iso-butanol(3) mixtures, where the matrix of thermodynamic factors is determined from the NRTL parameters in Table 4. We note that factoring out the thermodynamic influences yields much milder, well-behaved, composition dependences. The crosses in Figure 32 represent calculations using the formula $|\Lambda|^{1/2} = \sqrt{\frac{Đ_{12}Đ_{13}Đ_{23}}{x_1Đ_{23}+x_2Đ_{13}+x_3Đ_{12}}}$ where the $Đ_{12}$, $Đ_{13}$, and $Đ_{23}$ are calculated using Vignes interpolation formula (63), combined with Wesselingh-Bollen interpolation (65).

Figure 36 presents a comparison of the experimental data of Shuck and Toor[32] for the elements of the estimate the Fick diffusivity matrix with estimates using $[D]=|\Lambda|^{1/2}[\Gamma]$ with

$|\Lambda|^{1/2} = \sqrt{\frac{Đ_{12}Đ_{13}Đ_{23}}{x_1Đ_{23}+x_2Đ_{13}+x_3Đ_{12}}}$. The M-S binary pair diffusivities $Đ_{12}$, $Đ_{13}$, and $Đ_{23}$ are calculated using Vignes interpolation formula (63), combined with combined with Wesselingh-Bollen interpolation (65). We observe that the diagonal elements D_{11} and D_{22} are predicted fairly well, as is to be expected. However, the estimations of the off-diagonal elements D_{12} and D_{21} are somewhat poorer. Nevertheless, the estimations of the cross-coefficients are of the right order of magnitude and sign.

The reasonably good estimates provided by $[D]=|\Lambda|^{1/2}[\Gamma]$ implies that the coupling effects of the Fick diffusivity matrix have their origins in the coupling of the matrix of thermodynamic factors. In order to verify this conclusion, Figure 37 plots the ratio $\frac{D_{12}D_{21}}{D_{11}D_{22}}$ against the corresponding value of the ratio $\frac{\Gamma_{12}\Gamma_{21}}{\Gamma_{11}\Gamma_{22}}$. We note a near-linear dependence, confirming that diffusional coupling largely originate from thermodynamic coupling.

9. Fick diffusivity matrix [*D*] for 2-propanol/glycerol/water mixtures

The elements of the Fick diffusivity matrix [*D*] for ternary mixtures of 2-propanol/glycerol/water mixtures, measured in a diaphragm cell at 323 K, have been reported by Riede and Schlünder.[33] Their data, presented in the original paper in graphical form has also been conveniently tabulated by Mutoru and Firoozabadi;[34] see Table 3 of the Supplementary Material accompanying their publication. The NRTL parameters for the binary pairs of 2-propanol/glycerol/water mixtures are provided in Table 2 of Zhang et al.[35]

In Figure 38, the ratio $\frac{|D|^{1/2}}{|\Gamma|^{1/2}}$ is plotted as a function of the mole fraction of glycerol. We see that the ratio $\frac{|D|^{1/2}}{|\Gamma|^{1/2}}$ shows a mild dependence on the composition, emphasizing that the "factoring out" of thermodynamic influences simplifies the description of ternary diffusion.

10. Rehfeldt data on Fick diffusivity matrix [*D*] for four different ternary mixtures

A fairly comprehensive evaluation and discussion of the procedures for estimation of [*D*] is contained in the paper by Rehfeldt and Stichlmair,[36] and in the dissertation of Rehfeldt.[37] They report experimental data on the Fick diffusivity matrix [*D*] for (a) methanol(1)/1-butanol(2)/1-propanol, (b) acetone(1)/water(2)/1-propanol(3), (c) acetone(1)/1-butanol(2)/1-propanol(3), and (d) 1-propanol(1)/1-chlorobutane(2)/n-heptane(3) mixtures at 298 K.

Before proceeding with the comparing the experimental data on [*D*] with estimations, we shall first present experimental data on the constituent binary pairs for the four ternary mixtures in order to extract the infinite dilution M-S diffusivity values.

Figures 39, 40, 41, and 42 present data on Fick diffusivities of the constituent binary pairs for the four respective mixtures. Also shown are the M-S diffusivities, along with the estimations using the Vignes interpolation formula (49). The calculation of thermodynamic factors are based on the Wilson parameters reported in Table 9.2 of the dissertation of Rehfeldt.[37] The values of the infinite dilution M-S diffusivities are also indicated in Figures 39, 40, 41, and 42. Figures 43, 44, 45, and 46 present parity plots for the four elements of [*D*] comparing experimental data with the estimations using $[D]=[B]^{-1}[\Gamma]=[\Lambda][\Gamma]$ along with the Vignes interpolation formula (63), combined with Wesselingh-Bollen interpolation (65). For all four mixtures, the Vignes interpolation provides a reasonable prediction of the elements of the Fick diffusivity matrix.

Figure 47 presents a plot of the ratio $\frac{D_{12}D_{21}}{D_{11}D_{22}}$ of the elements of the Fick diffusivity matrix [*D*] in 1-propanol(1)/1-chlorobutane(2)/n-heptane(3) mixtures plotted against the corresponding value of the ratio $\frac{\Gamma_{12}\Gamma_{21}}{\Gamma_{11}\Gamma_{22}}$. We see that the diffusional coupling effects are linked to thermodynamic coupling.

In Figure 48, the ratio $\frac{|D|^{1/2}}{|\Gamma|^{1/2}}$ is plotted as a function of the mole fraction of component 1 in four different mixtures. We see that the ratio $\frac{|D|^{1/2}}{|\Gamma|^{1/2}}$ shows a mild dependence on the composition, emphasizing that the "factoring out" of thermodynamic influences simplifies the description of ternary diffusion. The crosses in Figure 48 represent calculations using the formula $|\Lambda|^{1/2} = \sqrt{\frac{Đ_{12}Đ_{13}Đ_{23}}{x_1Đ_{23}+x_2Đ_{13}+x_3Đ_{12}}}$ where the $Đ_{12}$, $Đ_{13}$, and $Đ_{23}$ are calculated using Vignes interpolation formula (63), combined with Wesselingh-Bollen interpolation (65).

A simple procedure for estimation of the Fick matrix [D] is $[D]=|\Lambda|^{1/2}[\Gamma]$ with $|\Lambda|^{1/2} = \sqrt{\frac{Đ_{12}Đ_{13}Đ_{23}}{x_1Đ_{23}+x_2Đ_{13}+x_3Đ_{12}}}$. Figures 49, 50, 51, and 52 present parity plots for the four elements of [D] comparing experimental data with the estimations using $[D]=|\Lambda|^{1/2}[\Gamma]$. The M-S binary pair diffusivities $Đ_{12}$, $Đ_{13}$, and $Đ_{23}$ are calculated using Vignes interpolation formula (63), combined with Wesselingh-Bollen interpolation (65). We observe that the diagonal elements D_{11} and D_{22} are predicted fairly well, as is to be expected. However, the estimations of the off-diagonal elements D_{12} and D_{21} are somewhat poorer. Nevertheless, the estimations of the cross-coefficients are of the right order of magnitude and sign.

Comparing the estimations in Figures 43, 44, 45, and 46 with the corresponding ones in Figures 49, 50, 51, and 52 leads us to conclude that the estimations using the simple formula $[D]=|\Lambda|^{1/2}[\Gamma]$ are no less accurate than using $[D]=[B]^{-1}[\Gamma]=[\Lambda][\Gamma]$.

11. Phase stability in binary mixtures of liquids and alloys: influence on diffusion

Non-ideal mixture thermodynamics has a strong influence on diffusion of binary mixtures of liquids and alloyws in the vicinity of phase transition regions. To understand the diffusion characteristics of

binary mixtures near phase transition point, we need to examine the mixture thermodynamics in more detail, starting with the calculations of the Gibbs free energy

$$\frac{G}{RT} = \frac{G^{ex}}{RT} + \left(x_1 \ln x_1 + x_2 \ln x_2\right); \quad \frac{G^{ex}}{RT} = \left(x_1 \ln \gamma_1 + x_2 \ln \gamma_2\right) \tag{73}$$

As illustration, let us consider a binary alloy of Fe(1)/Cr(2). The phase equilibrium thermodynamic data are provided by Soriano-Vargas et al.[38] The regular solution model is used to described the Gibbs excess free energy

$$\frac{G^{ex}}{RT} = \left(x_1 \ln \gamma_1 + x_2 \ln \gamma_2\right) = A x_1 x_2 = \frac{18600.0 + 0.1T}{RT} x_1 x_2 \tag{74}$$

Figures 53a, and 53b present calculations of the Gibbs free energy for binary mixtures at (a) T = 1200 K, and (b) T = 800 K. At T = 1200 K, the free energy curve is "bow shaped", indicating that the mixtures are miscible in all proportions. However, we note that the free energy at 800 K, exhibits two minima, and one maximum; see Figure 53b. For temperatures lower than 1125 K, we note two minima, corresponding to

$$\frac{\partial G}{\partial x_1} = 0 \tag{75}$$

From the data on the vanishing of the first derivative $\frac{\partial G}{\partial x_1}$, we can determine the compositions of the two liquid phases that are in equilibrium with each other. The two points thus obtained at various values of T, yields the binodal curve (indicated in green) in Figure 53c.

The vanishing of the second derivative of the Gibbs free energy

$$\frac{\partial^2 G}{\partial x_1^2} = 0 \tag{76}$$

delineates the limits of phase instability; this defines the spinodal curve. The second derivative of the Gibbs free energy is simply related to the thermodynamic factor,

$$\frac{1}{RT}\frac{\partial^2 G}{\partial x_1^2} = H = \frac{\Gamma}{x_1 x_2} \tag{77}$$

where Γ, defined by (31), reduces for $n = 2$ to

$$\Gamma = \left(1 + \frac{\partial \ln \gamma_1}{\partial \ln x_1}\right) \tag{78}$$

The calculations of $\frac{\partial^2 G}{\partial x_1^2} = 0$ yields the points that lie on the spinodal curve (indicated in red) in Figure 53c. The Upper Critical Solution Temperature (UCST) represents the confluence of the binodal and spinodal curves; the UCST for this system is determined to be 1125 K. For any (x_1, T) conditions outside the region delineated by the binodal curve, diffusion acts in a manner to smear out concentration gradients and fluctuations. For any (x_1, T) conditions within the spinodal region, we have phase separation, i.e. de-mixing. The region between the binodal and spinodal envelopes is meta-stable.

At the spinodal composition, the Fick diffusivity must vanish

$$\frac{1}{RT}\frac{\partial^2 G}{\partial x_1^2} = H = \frac{\Gamma}{x_1 x_2} = 0; \quad D_{12} = 0 \tag{79}$$

The activity coefficients, γ_i, of Fe(1) and Cr(2) in solution, as a function of the atom fraction of Fe(1), can be calculated from

$$\ln \gamma_1 = A x_2^2; \quad \ln \gamma_2 = A x_1^2; \quad A = \frac{18600.0 + 0.1T}{RT} \tag{80}$$

For the derivation of equation (80), see Appendix D of Taylor and Krishna.[8] The calculations of the activity coefficients at 800 K are presented in Figure 53d.

Figure 53e presents calculations of the thermodynamic activity $a_i = \gamma_i x_i$ as a function of the atom fraction of Fe(1) for a chosen temperature of 800 K. In the unstable region, we note that the activity of either component decreases while the corresponding atom fraction of that component increases. This underscores the phenomenon of spinodal decomposition within the unstable region.

For visualization of the spinodal decomposition in the Fe(1)/Cr(2) system, obtained by solution of the Cahn-Hilliard[39, 40] equation, see the following videos on YouTube

https://www.youtube.com/watch?v=wHYfOAOt3vE

For verification of the fact that the Fick diffusivities tends to vanish at the spinodal composition, we consider seven sets of experiments for partially miscible binary fluid mixtures.

Consider first the experiments reported by Vitagliano et al.[41], the Fick diffusivities, D_{12}, for triethylamine (1)/water (2) mixtures, measured at two different temperatures 292.15 K, and 293.15 K, both slightly above the value of UCST = 291.5 K; see Figure 54a. The diffusivities were measured at varying compositions approaching the spinodal curve from either side of the spinodal curves; see Figure 54b. Their data clearly demonstrate that the diffusivities vanish at spinodal composition, in agreement with the expectations of Equation (79).

Consider the experimental data for 1-butanol (1)/water (2) mixtures measured at 298.15 K and presented in Table 2 of Pertler et al.[42]; see Figure 55. The diffusivities were measured at varying compositions on either side of the spinodal compositions. Their data clearly demonstrate that the diffusivities tend to vanish as the spinodal compositions are approached from either end of the spinodal curve, in agreement with the expectations of Equation (79).

Figure 56 presents the experimental data of Thiel et al.[43] for Fick diffusivities, D_{12}, for methyl isopropyl ketone(1)/water(2) mixtures, measured at 293.15 K (water rich region) and 298.15 (MIPK rich region) for various compositions on either side of the spinodal compositions. Their data clearly demonstrate that the diffusivities tend to vanish as the spinodal compositions are approached from either end of the spinodal curve, in agreement with the expectations of Equation (79).

Figure 57 presents the experimental data of Grossmann and Winkelmann,[44] and Pertler et al.[42] for Fick diffusivities, D_{12}, for glycerol(1)/acetone(2) mixtures, measured at 298.15 K for various compositions in the acetone-rich region to the left of the spinodal composition. The data show that the Fick diffusivities reduce in magnitude as the spinodal composition is approached.

Figure 58 shows the experimental data of McKeigue and Gulari[45] for Fick diffusivities, D_{12}, for methanol(1)/CS_2(2) mixtures, measured at 293.15 K for various compositions in the CS_2-rich region to the left of the spinodal composition. The data show that the Fick diffusivities tend to vanish as the spinodal composition is approached.

Consider diffusivities in regions close to vapor/liquid phase transitions. Figures 59a, and 59b present experimental data of Dysthe and Hafskjold[46] for Fick diffusivities of CH_4(1)/n-$C_{10}H_{22}$(2) mixtures at T = 303.5 K and p = 40, 50 and 60 MPa. The sharp well in the Fick diffusivity data at x_1 = 0.903 is caused by the proximity to the spinodal compositions, plotted in Figure 59c.

Experimental data of Dysthe and Hafskjold[46] for Fick diffusivities of CH_4(1)/n-$C_{10}H_{22}$(2) mixtures at T = 303.5 K with varying total pressures at the critical composition x_1= 0.903 are shown in Figure 59d. The Fick diffusivity progressively decreases in magnitude as the pressure is reduced, and D_{12} = 0 at p = 31.5 MPa; this pressure dependence of the Fick diffusivity is opposite to the expectations for ideal gas mixtures.

The composition dependence of the Fick diffusivities is dictated by a combination of the composition dependence of the compressibility factor, Z (PR EOS calculations shown in Figure 59e) and the thermodynamic factor, $\Gamma = \left(1 + \frac{\partial \ln \phi_1}{\partial \ln x_1}\right)$ (PR EOS calculations shown in Figure 59f). The continuous solid lines in Figures 59a, 59b and 59d represent calculations using $D_{12} = \left(Đ_{12}^{x_1 \to 1}\right)^{x_1} \left(Đ_{12}^{x_2 \to 1}\right)^{x_2} \left(1 + \frac{\partial \ln \phi_1}{\partial \ln x_1}\right) Z$. The values $Đ_{12}^{x_1 \to 1} = 12 \times 10^{-9}\ \mathrm{m^2 s^{-1}} \left[\frac{40}{p}\right]$, and $Đ_{12}^{x_2 \to 1} = 0.7 \times 10^{-9}\ \mathrm{m^2 s^{-1}} \left[\frac{40}{p}\right]$ were chosen to match the diffusivities at either ends of the composition range at the specified pressure p (expressed in MPa). Our combined Vignes - PR EOS model captures the essential characteristics of the composition dependence of the experimental Fick diffusivities over the entire range of compositions and pressures.

Figure 60a presents experimental data of Ago and Nishiumi[47] for diffusivity of benzene in supercritical CO_2 as a function of the total pressure. The measurements were made in a Taylor dispersion tube with varying amounts of benzene injection into the tube. We note that with increased

injection of benzene, the variation of the diffusivity with the total system pressure p is significantly affected. For injection of 5.7 mL and 13.1 mL of benzene, we note a sharp increase in the diffusivity at $p \approx 8$ MPa. In order to rationalize the experimental results, we use a similar approach as adopted in the foregoing example for $CH_4(1)$/n-$C_{10}H_{22}(2)$ mixtures. Figures 60b, and 60c present calculations of the compressibility factor, and the thermodynamic factor, Γ, using the Peng-Robinson Equation of State (PR EOS). These calculations have been performed at four different benzene compositions, x_1 = 0.005, 0.007, 0.01, and 0.013. The deep well in Γ the at $p \approx 8$ MPa for x_1 = 0.01, and 0.013. The calculations of the Fick diffusivity using $D_{12} = Đ_0\left(1+\frac{\partial \ln \phi_1}{\partial \ln x_1}\right)Z; \quad Đ_0 = 7.5\times10^{-7}\,\mathrm{m^2 s^{-1}}$ are shown in Figure 60d for x_1 = 0.005, 0.007, 0.01, and 0.013. These model calculations are able to rationalize the characteristics of the experimental diffusivities in Figure 60a; the key factor appears to be deep well in the thermodynamic factor, Γ.

12. Phase stability in ternary mixtures: influence on diffusion

Let us first consider phase stability in ternary liquid mixtures that can undergo phase separation yielding two liquid phase phases that are in equilibrium with each other. Figure 61 is a schematic showing liquid/liquid phase equilibrium for a hypothetical ternary liquid mixture. The binodal and spinodal curves converge at the plait point. The region between the spinodal and binodal envelopes is meta-stable (indicated in yellow). Let us consider ternary liquid mixtures of two different compositions A and B that are brought into contact (cf. Figure 61). The average mixture composition (M) falls within in the two-phase region. Each of the mixtures A and B will equilibrate to the compositions at the two ends of the tie-line corresponding to the mixture composition M; these compositions are different from those of A and B. The technology of liquid-liquid extraction is essentially based on the separation that is effected as a consequence of the fact that phase equilibration yields compositions that are distinctly different from the starting ones A and B. The design and development of liquid-liquid extraction processes is crucially dependent on our ability to describe (a) liquid-liquid phase equilibrium

thermodynamics, and (b) composition trajectories and fluxes in both the adjoining phases as these approach equilibrium or stationary states.

The phase stability is dictated by the determinant of the Hessian matrix of the Gibbs free energy, $|H|$.

At the plait point, the binodal and spinodal curves converge. Outside the region delineated by the spinodal curve, we have

$$|H| > 0; \quad |\Gamma| > 0; \quad \text{phase stability} \tag{81}$$

Also, in view of the second law of thermodynamics (cf. equation (16)), we have $|L| > 0$. In view of equation (37), the condition of phase stability translates to Equation (19) which implies that both the eigenvalues of the Fick matrix [*D*] are positive definite.

Within the region delineated by the spinodal curve, we require

$$|H| < 0; \quad |\Gamma| < 0; \quad |D| < 0; \quad \text{phase instability} \tag{82}$$

Equation (82) implies that one of eigenvalues of the Fick diffusivity matrix [*D*] must be negative.

The region between the binodal and spinodal curves is meta-stable. At the plait point, and along the spinodal curve we must have

$$|H| = 0; \quad |\Gamma| = 0; \quad |D| = 0; \quad \text{spinodal curve} \tag{83}$$

So, the determinant $|\Gamma|$ also vanishes along the spinodal curve, and at the plait point, i.e. $|\Gamma| = 0$.

13. Diffusivities in glycerol/acetone/water mixtures

We now examine the influence of phase stability on diffusion in glycerol(1)/acetone(2)/water(3) mixtures for which the liquid-liquid phase equilibrium data has been provided by Krishna et al.[9] The experimental data on the binodal curve, and the tie lines are shown in Figure 62. The composition of the plait point is x_{glycerol}= 0.1477, x_{acetone}= 0.4163 and x_{water}= 0.4360. Krishna et al[9] also provide the NRTL parameters describing phase equilibrium.

Grossmann and Winkelmann[44, 48, 49] have reported data on the Fick diffusivity matrix [D] for glycerol(1)/acetone(2)/water(3) mixtures at 75 different compositions, in the acetone-rich and water-rich regions as indicated in Figure 62. As illustration, at x_1= 0.18, x_2 = 0.22, x_3 = 0.6, $[D]=\begin{bmatrix}0.294 & 0.127\\ 0.148 & 0.213\end{bmatrix}\times 10^{-9}$ m^2 s^{-1}, signaling strong diffusional coupling. We may consider $|D|^{1/2}$ to be representative of the magnitude of the matrix of Fick diffusivities. Figure 63 presents a plot of $|D|^{1/2}$ as a function of the mole fraction of glycerol, x_1. We note that $|D|^{1/2}$ tends to vanish as the plait point composition is approached, in conformity with the restraint imposed by equation (83).

The matrix of thermodynamic factors at the composition x_1= 0.18, x_2 = 0.22, x_3 = 0.6 is calculated to be $[\Gamma]=\begin{bmatrix}1.83 & 0.73\\ 0.478 & 0.444\end{bmatrix}$. Thermodynamic coupling effects contribute to large off-diagonal elements of the matrix of Fick diffusivities $[D]$. In order to demonstrate that the coupling effects in the Fick diffusivity matrix have their origins in the coupling effects of the matrix of thermodynamic factors, Figure 64 presents a plot of the ratio $\frac{D_{12}D_{21}}{D_{11}D_{22}}$ of the elements of the Fick diffusivity matrix [D] for glycerol(1)/acetone(2)/water(3) mixtures as a function of the ratio $\frac{\Gamma_{12}\Gamma_{21}}{\Gamma_{11}\Gamma_{22}}$. We see a unique dependence between the two sets of data. Along the spinodal curve, both of these ratios tend to unity values, in view of equation (83). The important message emerging from Figure 64 is that diffusional coupling effects become of increasing importance as the compositions approach values corresponding to the spinodal curve.

In order to demonstrate the well-behavedness of the M-S diffusivities, Figure 65a presents a plot of the ratio $\frac{|D|^{1/2}}{|\Gamma|^{1/2}}$ for glycerol(1)/acetone(2)/water(3) mixtures, plotted as a function of the mole fractions of acetone, x_2, and water x_3. The square root of determinants $|D|$, and $|\Gamma|$ are representative of the

"magnitudes" of [D], and $[\Gamma]$ respectively. The ratio $\frac{|D|^{1/2}}{|\Gamma|^{1/2}}$ can be viewed as the "magnitude" of the Maxwell-Stefan diffusivity in the *ternary* mixture. The variation of $\frac{|D|^{1/2}}{|\Gamma|^{1/2}}$ appears to be strongly dependent on the composition of acetone in the mixture. To confirm this, Figure 65b plots $\frac{|D|^{1/2}}{|\Gamma|^{1/2}}$ as a function of the mole fraction of acetone, x_2. We note that the entire data set appears to fall within a narrow band; these results are analogous to those presented earlier for acetone(1)/benzene(2)/CCl_4(3), acetone(1)/benzene(2)/methanol(3), methanol(1)/1-butanol(2)/1-propanol, acetone(1)/water(2)/1-propanol(3), acetone(1)/1-butanol(2)/1-propanol(3), and 1-propanol(1)/1-chlorobutane(2)/n-heptane(3) mixtures.

In Figure 65b, the crosses represent a model fit of the data using $|\Lambda|^{1/2} = (D_{1,self})^{x_1} (D_{2,self})^{x_2} (D_{3,self})^{x_3}$, taking $D_{1,\text{self}}$= 0.01, $D_{2,\text{self}}$= 3.2, $D_{3,\text{self}}$= 0.5 with units 10^{-9} m^2 s^{-1}.

Figure 66 presents a comparison of experimental data for the Fick diffusivity matrix [D] for glycerol(1)/acetone(2)/water(3) mixtures with the estimations using $[D]=|\Lambda|^{1/2}[\Gamma]$ based on $|\Lambda|^{1/2} = (D_{1,self})^{x_1} (D_{2,self})^{x_2} (D_{3,self})^{x_3}$. The estimations of the cross-coefficients are of the right order of magnitude and sign.

14. Diffusivities in water/chloroform/acetic acid mixtures

Figure 67 shows the experimental data for liquid/liquid equilibrium in water(1)/chloroform(2)/acetic-acid(3) mixtures. The binodal curve is indicated in green. The spinodal curve is indicated by the red line. The experimental data of Vitagliano et al.[50] for Fick diffusivity matrix [D] of water(1)/chloroform(2)/acetic-acid(3) mixtures at six different compositions (cf. Figure 67) also confirm the expectations of Equations (19), and (83). We note that values of the determinant $|D|$ progressively decreases in magnitude as the compositions become increasingly poorer in acetic acid. At

the plait point (composition: $x_1 = 0.375$, $x_2 = 0.261$ and $x_3 = 0.364$) the matrix of Fick diffusivities determined by Vitagliano et al.[50] by extrapolation of their data is $[D] = \begin{bmatrix} 0.92 & 0.40 \\ 0.37 & 0.161 \end{bmatrix} \times 10^{-9}$ $m^2\ s^{-1}$. It can be confirmed that the determinant vanishes, i.e. $|D| = 0$.

More recent measurements reported by Buzatu et al.[51] for Fick diffusivity matrix [D] of water(1)/chloroform(2)/acetic-acid(3) mixtures at five different compositions are shown in Figure 68.

Figure 69 presents a plot of $|D|^{1/2}$ as a function of (1- x_3) for water(1)/chloroform(2)/acetic-acid(3) mixtures for the two data sets. The magnitude of $|D|^{1/2}$ reduces progressively as the plait point composition is approached; this is in conformity with the restraint imposed by equation (83).

In order to demonstrate that the coupling effects in the Fick diffusivity matrix have their origins in the coupling effects of the matrix of thermodynamic factors, Figure 70 presents a plot of the ratio $\frac{D_{12}D_{21}}{D_{11}D_{22}}$ of the elements of the Fick diffusivity matrix [D] for water(1)/chloroform(2)/acetic-acid(3) mixtures as a function of the ratio $\frac{\Gamma_{12}\Gamma_{21}}{\Gamma_{11}\Gamma_{22}}$. We see a unique dependence between the two sets of data. Along the spinodal curve, both of these ratios tend to unity values, in view of equation (83). The important message emerging from Figure 64 is that diffusional coupling effects become of increasing importance as the compositions approach values corresponding to the spinodal curve.

In order to demonstrate the well-behavedness of the M-S diffusivities, Figure 71 presents a plot of ratio $\frac{|D|^{1/2}}{|\Gamma|^{1/2}}$ for water(1)/chloroform(2)/acetic-acid(3) mixtures as a function of (1- x_3). The square root of determinants $|D|$, and $|\Gamma|$ are representative of the "magnitudes" of [D], and $[\Gamma]$ respectively. The ratio $\frac{|D|^{1/2}}{|\Gamma|^{1/2}}$ can be viewed as the "magnitude" of the Maxwell-Stefan diffusivity in the *ternary* mixture. The variation of $\frac{|D|^{1/2}}{|\Gamma|^{1/2}}$ appears to be strongly dependent on (1- x_3) in the mixture. The crosses represent

a model fit of the data using $|\Lambda|^{1/2} = (D_{1,self})^{x_1} (D_{2,self})^{x_2} (D_{3,self})^{x_3}$, taking $D_{1,\text{self}}$= 0.4, $D_{2,\text{self}}$= 0.8, $D_{3,\text{self}}$= 1.1 with units 10^{-9} m^2 s^{-1}.

Figure 72 presents comparisons of experimental data for the Fick diffusivity matrix [D] for water(1)/chloroform(2)/acetic-acid(3) mixtures with the estimations using $[D] = |\Lambda|^{1/2} [\Gamma]$ based on $|\Lambda|^{1/2} = (D_{1,self})^{x_1} (D_{2,self})^{x_2} (D_{3,self})^{x_3}$, taking $D_{1,\text{self}}$= 0.4, $D_{2,\text{self}}$= 0.8, $D_{3,\text{self}}$= 1.1 with units 10^{-9} m^2 s^{-1}. The estimations of the cross-coefficients are of the right order of magnitude and sign.

15. Diffusivities in water/2-propanol/cyclohexane mixtures

Clark and Rowley[52] report experimental data for the determinant of the Fick diffusivity matrix [D] for water(1)/2-propanol(2)/cyclohexane(3) mixtures as ($T - T_c$) where T is the temperature at which the diffusivities are measured, and critical temperature T_c = 303.67 K; see Figure 73. The elements of the Fick matrix of diffusivities were measured at a constant composition corresponding to that at the plait point at 303.67 K: x_1 = 0.367, x_2= 0.389, x_3= 0.244. Examination of the values of the Fick diffusivity matrix (also indicated in Figure 73), we see that the coupling effects get increasingly stronger as T_c is approached; concomitantly the magnitude of $|D|^{1/2}$ gets progressively smaller in magnitude.

16. Equilibration trajectories in ternary liquid mixtures

In homogeneous single-phase regions, sizable magnitudes of cross-coefficients of the Fick diffusivity matrix often lead to serpentine equilibration trajectories and uphill diffusion.[53] To demonstrate this let us consider inter-diffusion of glycerol(1)/acetone(2)/water(3) mixtures that ensues when two different compositions (in the left and right compartments in Figure 74 are brought in contact. The initial composition of the left compartment is: $x_{1,\text{L}}$ = 0.08, $x_{2,\text{L}}$= 0.55 and $x_{3,\text{L}}$ = 0.37. The initial composition of the right compartment is: $x_{1,\text{R}}$ = 0.12, $x_{2,\text{R}}$ = 0.314, and $x_{3,\text{R}}$ = 0.566. The composition at equilibrium is $x_{1,\text{eq}}$ = 0.1, $x_{2,\text{eq}}$ = 0.432 and $x_{3,\text{eq}}$ = 0.468. We note that there is no driving force for the transfer of glycerol, component 1. The transient equilibration process is described by the coupled two-dimensional matrix equation

$$\begin{pmatrix} x_1 \\ x_2 \end{pmatrix} = \frac{1}{2}\begin{pmatrix} x_{1L} + x_{1,R} \\ x_{2L} + x_{2,R} \end{pmatrix} + \frac{1}{2} erf\left[-\frac{z}{\sqrt{4t}} \begin{bmatrix} D_{11} & D_{12} \\ D_{21} & D_{22} \end{bmatrix}^{-1/2} \right] \begin{pmatrix} x_{1R} - x_{1L} \\ x_{2R} - x_{2L} \end{pmatrix} \tag{84}$$

At the equilibrated composition, $x_{1,eq}$ = 0.1, $x_{2,eq}$ = 0.432 and $x_{3,eq}$ = 0.468, Grossmann and Winkelmann[44, 48, 49] report the Fick diffusivity matrix as $[D] = \begin{bmatrix} 0.4901 & 0.2267 \\ 0.4585 & 0.3991 \end{bmatrix} \times 10^{-9}$ $m^2\ s^{-1}$. The equilibration trajectory, calculated using equation (84) and shown by the dashed line, follows a serpentine path, as depicted in Figure 74. The continuous solid line in Figure 74 show the equilibration trajectories calculated using the simple estimation procedure $[D] = |\Lambda|^{1/2}[\Gamma]$ where the "magnitude" of the M-S diffusivity is estimated from $|\Lambda|^{1/2} = (D_{1,self})^{x_1} (D_{2,self})^{x_2} (D_{3,self})^{x_3}$, taking $D_{1,self}$= 0.01, $D_{2,self}$= 3.2, $D_{3,self}$= 0.5 with units 10^{-9} $m^2\ s^{-1}$. The matrix of thermodynamic factors at the composition $x_{1,eq}$ = 0.1, $x_{2,eq}$ = 0.432 and $x_{3,eq}$ = 0.468 is calculated to be $[\Gamma] = \begin{bmatrix} 1.44 & 0.533 \\ 0.958 & 0.41 \end{bmatrix}$. The simplified procedure essentially captures the serpentine nature of the equilibration path.

Figure 75 presents the calculations of the equilibration trajectories obtained for a different set of intial compositions in the left and right compartments. The initial composition of the left compartment is: $x_{1,L}$ = 0.05, $x_{2,L}$= 0.28 and $x_{3,L}$ = 0.67. The initial composition of the right compartment is: $x_{1,R}$ = 0.31, $x_{2,R}$ = 0.16 and $x_{3,R}$ = 0.53. The composition at equilibrium is $x_{1,eq}$ = 0.18, $x_{2,eq}$ = 0.22 and $x_{3,eq}$ = 0.6. At the equilibrated composition, Grossmann and Winkelmann:[44, 48, 49]. report the Fick diffusivity matrix as $[D] = \begin{bmatrix} 0.2938 & 0.1271 \\ 0.1483 & 0.2127 \end{bmatrix} \times 10^{-9}$ $m^2\ s^{-1}$. The equilibration trajectory follows a serpentine path, shown by the dashed line, as depicted in Figure 75. The continuous solid line in Figure 75 show the equilibration trajectories calculated using the simple estimation procedure $[D] = |\Lambda|^{1/2}[\Gamma]$ where the "magnitude" of the M-S diffusivity is estimated from $|\Lambda|^{1/2} = (D_{1,self})^{x_1} (D_{2,self})^{x_2} (D_{3,self})^{x_3}$, taking $D_{1,self}$= 0.01, $D_{2,self}$= 3.2, $D_{3,self}$= 0.5 with units 10^{-9} $m^2\ s^{-1}$. The simplified procedure essentially captures the serpentine nature of the equilibration path.

17. Foray of equilibration trajectory into meta-stable regions

Curvilinear equilibration trajectories may foray into meta-stable regions of the phase diagram. The foray into meta-stable regions is demonstrated by the equilibration trajectories in 34 different ternary liquid mixtures, that are partially miscible:

water(1)/chloroform(2)/acetic-acid(3)

glycerol(1)/acetone(2)/water(3)

water(1)/DMSO(2)/THF(3)

water(1)/acetone(2)/phenol(3)

water(1)/acetone(2)/TCE(3)

water(1)/2-propanol(2)/phenol(3)

water(1)/trichloroacetic acid (2)/antipyrine(3)

acetone(1)/ethyl-acetate(2)/water(3)

propyl acetate (1)/formic acid(2)/water(3)

furfural(1)/formic acid(2)/water (3)

1-butanol (1)/methanol(2)/water(3)

water(1)/acetic acid(2)/dichloromethane(3)

water(1)/acetic acid(2)/1-hexanol(3)

toluene(1)/acetaldehyde(2)/water(3)

1-hexanol(1)/nitromethane(2)/water(3)

4-methyl-2-pentanone(1)/acetonitrile(2)/water(3)

acetonitrile(1)/1-propanol(2)/hexane(3)

water(1)/caprolactam(2)/toluene(3)

water(1)/caprolactam(2)/benzene (3)

toluene(1)/propionic-acid (2)/water(3)

ethylacetate(1)/propionic-acid (2)/water(3)

water(1)/acetic acid(2)/isophorone(3)

water(1)/acetic acid(2)/ethylacetate(3)

water(1)/acetic acid(2)/MTBE (3)

ethanol (1)/toluene(2)/n-decane(3)

water(1)/ethanol(2)/benzene(3)

NMP(1)/propylbenzene(2)/dodecane(3)

NMP(1)/propylbenzene(2)/tetradecane(3)

heptane(1)/toluene(2)/sulpholane(3)

[omim][Cl](1)/ethanol(2)/TAEE(3)

[bmim][TfO](1)/ethanol(2)/TAEE(3)

water(1)/acetone(2)/toluene(3)

water(1)/ethanol(2)/cyclohexane(3)

toluene(1)/ethanol(2)/water(3)

In each of the mixtures investigated, we determine the composition trajectories followed when homogeneous mixtures of two different compositions (in the left and right compartments) are brought into contact. We choose the equilibrated composition to lie on the bimodal curve, or on a tangent to the bimodal curve. In every case, except one, the straight-line equilibration trajectory (indicated by dotted lines in the Figures to be discussed below) lies entirely in the homogeneous, single-phase region; i.e. no emulsification is possible. By contrast, the equilibration trajectory calculated using equation (84) follows a serpentine path that exhibits a foray into the meta-stable region. This suggests the possibility of spontaneous emulsification for each mixture.

water(1)/chloroform(2)/acetic-acid(3)

The first system we consider is water(1)/chloroform(2)/acetic-acid(3) mixtures. We performed simulations in which the initial composition of the left compartment is: $x_{1,L} = 0.55$, $x_{2,L} = 0.1$ and $x_{3,L} = 0.35$; the initial composition of the right compartment is: $x_{1,R} = 0.13$, $x_{2,R} = 0.38$ and $x_{3,R} = 0.49$. The composition at equilibrium is $x_{1,eq} = 0.34$, $x_{2,eq} = 0.24$ and $x_{3,eq} = 0.42$. The average composition corresponds to the fifth data set of Vitagliano et al;[50] for that reason we take the values of the Fick

diffusivity matrix as $[D]=\begin{bmatrix}0.309 & 0.368\\ 0.344 & 0.939\end{bmatrix}\times 10^{-9}$ $m^2\ s^{-1}$; $|D|=0.164\times 10^{-18}$ $m^4\ s^{-2}$. We note that composition trajectory in the left chamber has forayed into the meta-stable region; see Figure 76. A linear equilibration trajectory, shown by the dotted line in Figure 76, remains in the homogeneous single-phase region.

glycerol(1)/acetone(2)/water(3)

Let us examine the trajectory followed during equilibration of homogenous mixtures of two different compositions for the system glycerol(1)/acetone(2)/water(3). The composition of the equilibrated mixture is $x_{1,eq}$ = 0.5, $x_{2,eq}$ = 0.17 and $x_{3,eq}$ = 0.33, which point lies on a tangent to the binodal curve. At the average composition, the matrix of thermodynamic factors is calculated from phase equilibrium thermodynamics: $[\Gamma]=\begin{bmatrix}2.3 & 1.37\\ 0.149 & 0.464\end{bmatrix}$. The "magnitude" of the M-S diffusivity is estimated from $|\Lambda|^{1/2}=(D_{1,self})^{x_1}(D_{2,self})^{x_2}(D_{3,self})^{x_3}$ taking $D_{1,self}$= 0.01, $D_{2,self}$= 3.2, $D_{3,self}$= 0.5 with units 10^{-9} $m^2\ s^{-1}$; the value $|\Lambda|^{1/2}=0.095\times 10^{-9}$ $m^2\ s^{-1}$. We assume that the matrix of Fick diffusivities is $[D]=|\Lambda|^{1/2}[\Gamma]$; the calculated value is i.e. $[D]=\begin{bmatrix}0.223 & 0.133\\ 0.0144 & 0.045\end{bmatrix}\times 10^{-9}$ $m^2\ s^{-1}$. Using this diffusivity estimate, we calculated the equilibration trajectory. We note that the serpentine trajectory has penetrated the binodal envelope; see Figure 77. This indicates the spontaneous emulsification is feasible. A linear equilibration trajectory (shown by dotted line) does not foray into the meta-stable zone.

water(1)/DMSO(2)/THF(3)

Let us examine the trajectory followed during equilibration of homogenous mixtures of two different compositions for the system water(1)/DMSO(2)/THF(3). We have carried out two sets of simulations for equilibration of homogeneous mixtures at 293.15 K, using the NRTL parameters from two different sources: Olaya et al.[54] and Zuber et al.[55]

For the first set of simulations using the NRTL parameters of Olaya et al.,[54] the composition of the equilibrated mixture is $x_{1,eq}$ = 0.625, $x_{2,eq}$ = 0.21 and $x_{3,eq}$ = 0.165, which point lies in the homogeneous

region above the binodal curve. At the average composition, the matrix of thermodynamic factors is calculated from phase equilibrium thermodynamics: $[\Gamma]=\begin{bmatrix} 1.614 & -3.535 \\ -1.2974 & 3.766 \end{bmatrix}$. We assume that the matrix of Fick diffusivities is the product of a scalar diffusivity $|\Lambda|^{1/2}=1\times10^{-9}$ $\mathrm{m^2\ s^{-1}}$ multiplied by $[\Gamma]$; i.e. $[D]=\begin{bmatrix} 1.614 & -3.535 \\ -1.2974 & 3.766 \end{bmatrix}\times10^{-9}$ $\mathrm{m^2\ s^{-1}}$. Using this diffusivity estimate, we calculated the equilibration trajectory. We note that the serpentine trajectory has penetrated the binodal envelope; see Figure 78. This indicates the spontaneous emulsification is feasible. A linear equilibration trajectory (shown by dotted line) does not foray into the meta-stable zone.

For the second set of simulations using the NRTL parameters of Zuber et al.,[55] the composition of the equilibrated water(1)/DMSO(2)/THF(3). mixture is $x_{1,\mathrm{eq}}$ = 0.7, $x_{2,\mathrm{eq}}$ = 0.16 and $x_{3,\mathrm{eq}}$ = 0.14, which point lies on a tangent to the binodal curve. At the average composition, the matrix of thermodynamic factors is calculated from phase equilibrium thermodynamics: $[\Gamma]=\begin{bmatrix} 0.948 & -2.458 \\ -0.6091 & 2.756 \end{bmatrix}$. We assume that the matrix of Fick diffusivities is the product of a scalar diffusivity $|\Lambda|^{1/2}=1\times10^{-9}$ $\mathrm{m^2\ s^{-1}}$ multiplied by $[\Gamma]$; i.e. $[D]=\begin{bmatrix} 0.948 & -2.458 \\ -0.6091 & 2.756 \end{bmatrix}\times10^{-9}$ $\mathrm{m^2\ s^{-1}}$. Using this diffusivity estimate, we calculated the equilibration trajectory. We note that the serpentine trajectory has penetrated the binodal envelope; see Figure 79. This indicates the spontaneous emulsification is feasible. A linear equilibration trajectory (shown by dotted line) does not foray into the meta-stable zone.

water(1)/acetone(2)/phenol(3), and water(1)/acetone(2)/TCE(3)

Let us examine the trajectory followed during equilibration of homogenous mixtures of two different compositions for the system water(1)/acetone(2)/phenol(3). The composition of the equilibrated mixture is $x_{1,\mathrm{eq}}$ = 0.42, $x_{2,\mathrm{eq}}$ = 0.42 and $x_{3,\mathrm{eq}}$ = 0.15, which point lies in the single-phase region on a tangent to the binodal curve. At the average composition, the matrix of thermodynamic factors is calculated from phase equilibrium thermodynamics: $[\Gamma]=\begin{bmatrix} 1.648\times10^{-3} & -0.3437 \\ 2.013 & 3.1942 \end{bmatrix}$. We assume that the matrix of Fick

diffusivities is the product of a scalar diffusivity $|\Lambda|^{1/2} = 1\times10^{-9}$ $m^2\ s^{-1}$ multiplied by $[\Gamma]$; i.e. $[D] = \begin{bmatrix} 1.648\times10^{-3} & -0.3437 \\ 2.013 & 3.1942 \end{bmatrix}\times10^{-9}$ $m^2\ s^{-1}$. Using this diffusivity estimate, we calculated the equilibration trajectory. We note that the serpentine trajectory has penetrated the binodal envelope; see Figure 80. This indicates the spontaneous emulsification is feasible. A linear equilibration trajectory (shown by dotted line) does not foray into the meta-stable zone.

Let us examine the trajectory followed during equilibration of homogenous mixtures of two different compositions for the system water(1)/acetone(2)/TCE(3) where TCE = 1,1,2-trichlorethane. The composition of the equilibrated mixture is $x_{1,eq}$ = 0.05, $x_{2,eq}$ = 0.08 and $x_{3,eq}$ = 0.87., which point lies in the single-phase region on a tangent to the binodal curve. At the average composition, the matrix of thermodynamic factors is calculated from phase equilibrium thermodynamics: $[\Gamma] = \begin{bmatrix} 0.3792 & -0.1983 \\ -0.246 & 1.106 \end{bmatrix}$. We assume that the matrix of Fick diffusivities is the product of a scalar diffusivity $|\Lambda|^{1/2} = 1\times10^{-9}$ $m^2\ s^{-1}$ multiplied by $[\Gamma]$; i.e. $[D] = \begin{bmatrix} 0.3792 & -0.1983 \\ -0.246 & 1.106 \end{bmatrix}\times10^{-9}$ $m^2\ s^{-1}$. Using this diffusivity estimate, we calculated the equilibration trajectory. We note that the serpentine trajectory has penetrated the binodal envelope; see Figure 81. This indicates the spontaneous emulsification is feasible. A linear equilibration trajectory (shown by dotted line) does not foray into the meta-stable zone.

water(1)/2-propanol(2)/phenol(3)

Let us examine the trajectory followed during equilibration of homogenous mixtures of two different compositions for the system water(1)/2-propanol(2)/phenol(3). The composition of the equilibrated mixture is $x_{1,eq}$ = 0.61, $x_{2,eq}$ = 0.22 and $x_{3,eq}$ = 0.17, which point lies in the single-phase region on a tangent to the binodal curve. At the average composition, the matrix of thermodynamic factors is calculated from phase equilibrium thermodynamics: $[\Gamma] = \begin{bmatrix} 0.049 & -0.4195 \\ 1.342 & 2.964 \end{bmatrix}$. We assume that the matrix of Fick diffusivities is the product of a scalar diffusivity $|\Lambda|^{1/2} = 1\times10^{-9}$ $m^2\ s^{-1}$ multiplied by $[\Gamma]$; i.e.

$[D]=\begin{bmatrix}0.049 & -0.4195\\ 1.342 & 2.964\end{bmatrix}\times 10^{-9}$ $\mathrm{m^2\ s^{-1}}$. Using this diffusivity estimate, we calculated the equilibration trajectory. We note that the serpentine trajectory has penetrated the binodal envelope; see Figure 82. This indicates the spontaneous emulsification is feasible. A linear equilibration trajectory (shown by dotted line) does not foray into the meta-stable zone.

water(1)/trichloroacetic acid (2)/antipyrine(3)

Let us examine the trajectory followed during equilibration of homogenous mixtures of two different compositions for the system water(1)/trichloroacetic acid (2)/antipyrine(3). The composition of the equilibrated mixture is $x_{1,\mathrm{eq}} = 0.35$, $x_{2,\mathrm{eq}} = 0.32$ and $x_{3,\mathrm{eq}} = 0.33$, which point lies above the binodal curve in the single-phase region on a tangent to the binodal curve. At the average composition, the matrix of thermodynamic factors is calculated from phase equilibrium thermodynamics: $[\Gamma]=\begin{bmatrix}0.7169 & -0.1595\\ 3.094 & 7.312\end{bmatrix}$. We assume that the matrix of Fick diffusivities is the product of a scalar diffusivity $|\Lambda|^{1/2}=1\times 10^{-9}$ $\mathrm{m^2\ s^{-1}}$ multiplied by $[\Gamma]$; i.e. $[D]=\begin{bmatrix}0.7169 & -0.1595\\ 3.094 & 7.312\end{bmatrix}\times 10^{-9}$ $\mathrm{m^2\ s^{-1}}$. Using this diffusivity estimate, we calculated the equilibration trajectory. We note that the serpentine trajectory has penetrated the binodal envelope; see Figure 83. This indicates the spontaneous emulsification is feasible. A linear equilibration trajectory (shown by dotted line) does not foray into the meta-stable zone.

acetone(1)/ethyl-acetate(2)/water(3)

Let us examine the trajectory followed during equilibration of homogenous mixtures of two different compositions for the system acetone(1)/ethyl-acetate(2)/water(3). The composition of the equilibrated mixture is $x_{1,\mathrm{eq}} = 0.28$, $x_{2,\mathrm{eq}} = 0.415$ and $x_{3,\mathrm{eq}} = 0.305$, which point lies on the binodal curve. At the average composition, the matrix of thermodynamic factors is calculated from phase equilibrium thermodynamics: $[\Gamma]=\begin{bmatrix}1.18 & -0.097\\ -0.649 & 0.2257\end{bmatrix}$. We assume that the matrix of Fick diffusivities is the product of a scalar diffusivity $|\Lambda|^{1/2}=1\times 10^{-9}$ $\mathrm{m^2\ s^{-1}}$ multiplied by $[\Gamma]$; i.e.

$[D]=\begin{bmatrix} 1.18 & -0.097 \\ -0.649 & 0.2257 \end{bmatrix}\times 10^{-9}$ $\mathrm{m^2\ s^{-1}}$. Using this diffusivity estimate, we calculated the equilibration trajectory. We note that the serpentine trajectory has penetrated the binodal envelope; see Figure 84. This indicates the spontaneous emulsification is feasible. A linear equilibration trajectory (shown by dotted line) does not foray into the meta-stable zone.

propyl acetate (1)/formic acid(2)/water(3)

Let us examine the trajectory followed during equilibration of homogenous mixtures of two different compositions for the system n-propyl acetate (1)/formic acid(2)/water(3). The composition of the equilibrated mixture is $x_{1,eq}$ = 0.5, $x_{2,eq}$ = 0.17 and $x_{3,eq}$ = 0.33, which point lies on the binodal curve. At the average composition, the matrix of thermodynamic factors is calculated from phase equilibrium thermodynamics: $[\Gamma]=\begin{bmatrix} 0.1786 & -1.561 \\ 0.243 & 3.485 \end{bmatrix}$. We assume that the matrix of Fick diffusivities is the product of a scalar diffusivity $|\Lambda|^{1/2}=1\times 10^{-9}$ $\mathrm{m^2\ s^{-1}}$ multiplied by $[\Gamma]$; i.e. $[D]=\begin{bmatrix} 0.1786 & -1.561 \\ 0.243 & 3.485 \end{bmatrix}\times 10^{-9}$ $\mathrm{m^2\ s^{-1}}$. Using this diffusivity estimate, we calculated the equilibration trajectory. We note that the serpentine trajectory has penetrated the binodal envelope; see Figure 85. This indicates the spontaneous emulsification is feasible. A linear equilibration trajectory (shown by dotted line) does not foray into the meta-stable zone.

furfural(1)/formic acid(2)/water (3)

Let us examine the trajectory followed during equilibration of homogenous mixtures of two different compositions for the system furfural(1)/formic acid(2)/water (3). The composition of the equilibrated mixture is $x_{1,eq}$ = 0.58, $x_{2,eq}$ = 0.054 and $x_{3,eq}$ = 0.366, which point lies on the binodal curve. At the average composition, the matrix of thermodynamic factors is calculated from phase equilibrium thermodynamics: $[\Gamma]=\begin{bmatrix} 0.2602 & 0.392 \\ 0.271 & 1.72 \end{bmatrix}$. We assume that the matrix of Fick diffusivities is the product of a scalar diffusivity $|\Lambda|^{1/2}=1\times 10^{-9}$ $\mathrm{m^2\ s^{-1}}$ multiplied by $[\Gamma]$; i.e. $[D]=\begin{bmatrix} 0.2602 & 0.392 \\ 0.271 & 1.72 \end{bmatrix}\times 10^{-9}$ $\mathrm{m^2\ s^{-1}}$.

Using this diffusivity estimate, we calculated the equilibration trajectory. We note that the serpentine trajectory has penetrated the binodal envelope; see Figure 86. This indicates the spontaneous emulsification is feasible. A linear equilibration trajectory (shown by dotted line) does not foray into the meta-stable zone.

1-butanol (1)/methanol(2)/water(3)

Let us examine the trajectory followed during equilibration of homogenous mixtures of two different compositions for the system 1-butanol (1)/methanol(2)/water(3). The composition of the equilibrated mixture is $x_{1,eq}$ = 0.3, $x_{2,eq}$ = 0.046 and $x_{3,eq}$ = 0.654, which point lies on the binodal curve. At the average composition, the matrix of thermodynamic factors is calculated from phase equilibrium thermodynamics: $[\Gamma]=\begin{bmatrix} 0.273 & 0.484 \\ 0.198 & 1.74 \end{bmatrix}$. We assume that the matrix of Fick diffusivities is the product of a scalar diffusivity $|\Lambda|^{1/2} = 1\times10^{-9}$ $\mathrm{m^2\,s^{-1}}$ multiplied by $[\Gamma]$; i.e. $[D]=\begin{bmatrix} 0.273 & 0.484 \\ 0.198 & 1.74 \end{bmatrix}\times10^{-9}$ $\mathrm{m^2\,s^{-1}}$. Using this diffusivity estimate, we calculated the equilibration trajectory. We note that the serpentine trajectory has penetrated the binodal envelope; see Figure 87. This indicates the spontaneous emulsification is feasible. A linear equilibration trajectory (shown by dotted line) does not foray into the meta-stable zone.

water(1)/acetic acid(2)/dichloromethane(3)

Let us examine the trajectory followed during equilibration of homogenous mixtures of two different compositions for the system water(1)/acetic acid(2)/dichloromethane(3). The composition of the equilibrated mixture is $x_{1,eq}$ = 0.13, $x_{2,eq}$ = 0.25 and $x_{3,eq}$ = 0.62, which point lies on the binodal curve. At the average composition, the matrix of thermodynamic factors is calculated from phase equilibrium thermodynamics: $[\Gamma]=\begin{bmatrix} 0.536 & -0.895 \\ -0.904 & 2.56 \end{bmatrix}$. We assume that the matrix of Fick diffusivities is the product of a scalar diffusivity $|\Lambda|^{1/2} = 1\times10^{-9}$ $\mathrm{m^2\,s^{-1}}$ multiplied by $[\Gamma]$; i.e. $[D]=\begin{bmatrix} 0.536 & -0.895 \\ -0.904 & 2.56 \end{bmatrix}\times10^{-9}$ $\mathrm{m^2\,s^{-1}}$. Using this diffusivity estimate, we calculated the equilibration

trajectory. We note that the serpentine trajectory has penetrated the binodal envelope; see Figure 88. This indicates the spontaneous emulsification is feasible. A linear equilibration trajectory (shown by dotted line) does not foray into the meta-stable zone.

water(1)/acetic acid(2)/1-hexanol(3)

Let us examine the trajectory followed during equilibration of homogenous mixtures of two different compositions for the system water(1)/acetic acid(2)/1-hexanol(3). The composition of the equilibrated mixture is $x_{1,eq}$ = 0.425, $x_{2,eq}$ = 0.19 and $x_{3,eq}$ = 0.385, which point lies on the binodal curve. At the average composition, the matrix of thermodynamic factors is calculated from phase equilibrium thermodynamics: $[\Gamma]=\begin{bmatrix} 0.4158 & -0.6816 \\ -0.1967 & 1.1194 \end{bmatrix}$. We assume that the matrix of Fick diffusivities is the product of a scalar diffusivity $|\Lambda|^{1/2} = 1\times10^{-9}$ m^2 s^{-1} multiplied by $[\Gamma]$; i.e. $[D]=\begin{bmatrix} 0.4158 & -0.6816 \\ -0.1967 & 1.1194 \end{bmatrix}\times10^{-9}$ m^2 s^{-1}. Using this diffusivity estimate, we calculated the equilibration trajectory. We note that the serpentine trajectory has penetrated the binodal envelope; see Figure 89. This indicates the spontaneous emulsification is feasible. A linear equilibration trajectory (shown by dotted line) does not foray into the meta-stable zone.

toluene(1)/acetaldehyde(2)/water(3)

Let us examine the trajectory followed during equilibration of homogenous mixtures of two different compositions for the system toluene(1)/acetaldehyde(2)/water(3). The composition of the equilibrated mixture is $x_{1,eq}$ = 0.4075, $x_{2,eq}$ = 0.545 and $x_{3,eq}$ = 0.0475, which point lies on the binodal curve. At the average composition, the matrix of thermodynamic factors is calculated from phase equilibrium thermodynamics: $[\Gamma]=\begin{bmatrix} -0.236 & -1.095 \\ 0.674 & 1.72 \end{bmatrix}$. We assume that the matrix of Fick diffusivities is the product of a scalar diffusivity $|\Lambda|^{1/2} = 1\times10^{-9}$ m^2 s^{-1} multiplied by $[\Gamma]$; i.e.

$[D]=\begin{bmatrix} -0.236 & -1.095 \\ 0.674 & 1.72 \end{bmatrix}\times 10^{-9}$ $\mathrm{m^2\ s^{-1}}$. Using this diffusivity estimate, we calculated the equilibration trajectory. We note that the serpentine trajectory has penetrated the binodal envelope; see Figure 90. This indicates the spontaneous emulsification is feasible. A linear equilibration trajectory (shown by dotted line) does not foray into the meta-stable zone.

1-hexanol(1)/nitromethane(2)/water(3)

Let us examine the trajectory followed during equilibration of homogenous mixtures of two different compositions for the system 1-hexanol(1)/nitromethane(2)/water(3). The composition of the equilibrated mixture is $x_{1,eq} = 0.22$, $x_{2,eq} = 0.56$ and $x_{3,eq} = 0.22$, which point lies on the binodal curve. At the average composition, the matrix of thermodynamic factors is calculated from phase equilibrium thermodynamics: $[\Gamma]=\begin{bmatrix} 0.854 & 0.1733 \\ -0.2546 & 0.1526 \end{bmatrix}$. We assume that the matrix of Fick diffusivities is the product of a scalar diffusivity $|\Lambda|^{1/2} = 1\times 10^{-9}$ $\mathrm{m^2\ s^{-1}}$ multiplied by $[\Gamma]$; i.e. $[D]=\begin{bmatrix} 0.854 & 0.1733 \\ -0.2546 & 0.1526 \end{bmatrix}\times 10^{-9}$ $\mathrm{m^2\ s^{-1}}$. Using this diffusivity estimate, we calculated the equilibration trajectory. We note that the serpentine trajectory has penetrated the binodal envelope; see Table 91. This indicates the spontaneous emulsification is feasible. A linear equilibration trajectory (shown by dotted line) does not foray into the meta-stable zone.

4-methyl-2-pentanone(1)/acetonitrile(2)/water(3)

Let us examine the trajectory followed during equilibration of homogenous mixtures of two different compositions for the system 4-methyl-2-pentanone(1)/acetonitrile(2)/water(3). The composition of the equilibrated mixture is $x_{1,eq} = 0.09$, $x_{2,eq} = 0.54$, and $x_{3,eq} = 0.37$, which point lies on the binodal curve.

At the average composition, the matrix of thermodynamic factors is calculated from phase equilibrium thermodynamics: $[\Gamma]=\begin{bmatrix} 0.5 & -0.229 \\ -0.647 & 0.5817 \end{bmatrix}$. We assume that the matrix of Fick diffusivities is the product of a scalar diffusivity $|\Lambda|^{1/2} = 1\times 10^{-9}$ $\mathrm{m^2\ s^{-1}}$ multiplied by $[\Gamma]$; i.e.

$[D]=\begin{bmatrix} 0.5 & -0.229 \\ -0.647 & 0.5817 \end{bmatrix}\times 10^{-9}$ $\mathrm{m^2\ s^{-1}}$. Using this diffusivity estimate, we calculated the equilibration trajectory. We note that the serpentine trajectory has penetrated the binodal envelope; see Figure 92. This indicates the spontaneous emulsification is feasible. A linear equilibration trajectory (shown by dotted line) does not foray into the meta-stable zone.

acetonitrile(1)/1-propanol(2)/hexane(3)

Let us examine the trajectory followed during equilibration of homogenous mixtures of two different compositions for the system acetonitrile(1)/1-propanol(2)/hexane(3). Two different composition trajectories have been determined that correspond to left hand side of diagram: $x_{1,eq} = 0.575$, $x_{2,eq} = 0.24$ and $x_{3,eq} = 0.185$, and the right hand side of diagram: $x_{1,eq} = 0.175$, $x_{2,eq} = 0.17$ and $x_{3,eq} = 0.655$. In both cases the equilibrated compositions lie on the binodal curve, one either side of the plait point.

Consider first the trajectory at the left hand side of the phase diagram. At the average composition, the matrix of thermodynamic factors is calculated from phase equilibrium thermodynamics: $[\Gamma]=\begin{bmatrix} 0.133 & -1.79 \\ 0.017 & 2.53 \end{bmatrix}$. We assume that the matrix of Fick diffusivities is the product of a scalar diffusivity $|\Lambda|^{1/2} = 1\times 10^{-9}$ $\mathrm{m^2\ s^{-1}}$ multiplied by $[\Gamma]$; i.e. $[D]=\begin{bmatrix} 0.133 & -1.79 \\ 0.017 & 2.53 \end{bmatrix}\times 10^{-9}$ $\mathrm{m^2\ s^{-1}}$. Using this diffusivity estimate, we calculated the equilibration trajectory. We note that the serpentine trajectory has penetrated the binodal envelope; see Figure 93. This indicates the spontaneous emulsification is feasible. A linear equilibration trajectory (shown by dotted line) does not foray into the meta-stable zone.

Consider next the trajectory at the right hand side of the phase diagram. At the average composition, the matrix of thermodynamic factors is calculated from phase equilibrium thermodynamics: $[\Gamma]=\begin{bmatrix} 0.452 & -0.819 \\ -0.565 & 1.6 \end{bmatrix}$. We assume that the matrix of Fick diffusivities is the product of a scalar diffusivity $|\Lambda|^{1/2} = 1\times 10^{-9}$ $\mathrm{m^2\ s^{-1}}$ multiplied by $[\Gamma]$; i.e. $[D]=\begin{bmatrix} 0.452 & -0.819 \\ -0.565 & 1.6 \end{bmatrix}\times 10^{-9}$ $\mathrm{m^2\ s^{-1}}$. Using

this diffusivity estimate, we calculated the equilibration trajectory. We note that the serpentine trajectory has penetrated the binodal envelope; see Figure 93. This indicates the spontaneous emulsification is feasible. A linear equilibration trajectory (shown by dotted line) does not foray into the meta-stable zone.

water(1)/caprolactam(2)/toluene(3)

Let us examine the trajectory followed during equilibration of homogenous mixtures of two different compositions for the system water(1)/caprolactam(2)/toluene(3). The composition of the equilibrated mixture is chosen to be $x_{1,eq}$ = 0.645, $x_{2,eq}$ = 0.27 and $x_{3,eq}$ = 0.085, which point lies on the binodal curve. At the average composition, the matrix of thermodynamic factors is calculated from phase equilibrium thermodynamics: $[\Gamma]=\begin{bmatrix} -0.187 & -1.524 \\ 0.44 & 2.12 \end{bmatrix}$. We assume that the matrix of Fick diffusivities is the product of a scalar diffusivity $|\Lambda|^{1/2} = 1\times10^{-9}$ m^2 s^{-1} multiplied by $[\Gamma]$; i.e. $[D]=\begin{bmatrix} -0.187 & -1.524 \\ 0.44 & 2.12 \end{bmatrix}\times10^{-9}$ m^2 s^{-1}. Using this estimate, we calculated the equilibration trajectory. We note that the serpentine trajectory has penetrated the binodal envelope; see Figure 94. This indicates the spontaneous emulsification is feasible. A linear equilibration trajectory (shown by dotted line) does not foray into the meta-stable zone.

water(1)/caprolactam(2)/benzene (3)

Let us examine the trajectory followed during equilibration of homogenous mixtures of two different compositions for the system water(1)/caprolactam(2)/benzene (3) for the equilibrium composition. The composition of the equilibrated mixture is chosen to be x_1= 0.125, x_2 = 0.17, x_3 = 0.705 which point lies on the binodal curve. At the average composition, the matrix of thermodynamic factors is calculated from phase equilibrium thermodynamics: $[\Gamma]=\begin{bmatrix} 0.598 & -0.911 \\ -0.882 & 2.11 \end{bmatrix}$. We assume that the matix of Fick diffusivities is the product of scalar diffusivity $|\Lambda|^{1/2} = 1\times10^{-9}$ m^2 s^{-1} multiplied by $[\Gamma]$; i.e. $[D]=\begin{bmatrix} 0.598 & -0.911 \\ -0.882 & 2.11 \end{bmatrix}\times10^{-9}$ m^2 s^{-1}. Using this estimate, we calculated the equilibration trajectory. We

note that the serpentine trajectory has penetrated the binodal envelope; see Figure 95. This indicates the spontaneous emulsification is feasible. A linear equilibration trajectory (shown by dotted line) does not foray into the meta-stable zone.

toluene(1)/propionic-acid (2)/water(3)

Let us examine the trajectory followed during equilibration of homogenous mixtures of two different compositions for the system toluene(1)/propionic-acid (2)/water(3). The composition of the equilibrated mixture is chosen to be $x_{1,eq} = 0.47$, $x_{2,eq} = 0.24$ and $x_{3,eq} = 0.29$, which point lies on the binodal curve. At the average composition, the matrix of thermodynamic factors is calculated from phase equilibrium thermodynamics: $[\Gamma]=\begin{bmatrix} 0.318 & -0.3 \\ 0.178 & 1.196 \end{bmatrix}$. We assume that the matrix of Fick diffusivities is the product of scalar diffusivity $|\Lambda|^{1/2} = 1\times10^{-9}$ $m^2\ s^{-1}$ multiplied by $[\Gamma]$; i.e. $[D]=\begin{bmatrix} 0.318 & -0.3 \\ 0.178 & 1.196 \end{bmatrix}\times10^{-9}$ $m^2\ s^{-1}$. Using this estimate, we calculated the equilibration trajectory. We note that the serpentine trajectory has penetrated the binodal envelope; see Figure 96. This indicates the spontaneous emulsification is feasible. A linear equilibration trajectory (shown by dotted line) does not foray into the meta-stable zone.

ethylacetate(1)/propionic-acid (2)/water(3)

Let us examine the trajectory followed during equilibration of homogenous mixtures of two different compositions for the system ethylacetate(1)/propionic-acid(2)/water(3). The composition of the equilibrated mixture is chosen to be $x_{1,eq} = 0.675$, $x_{2,eq} = 0.13$ and $x_{3,eq} = 0.195$, which point lies on the binodal curve. At the average composition, the matrix of thermodynamic factors is calculated from phase equilibrium thermodynamics: $[\Gamma]=\begin{bmatrix} -0.0358 & -1.7447 \\ 0.5700 & 3.6379 \end{bmatrix}$. We assume that the matrix of Fick diffusivities is the product of scalar diffusivity $|\Lambda|^{1/2} = 1\times10^{-9}$ $m^2\ s^{-1}$ multiplied by $[\Gamma]$; i.e. $[D]=\begin{bmatrix} -0.0358 & -1.7447 \\ 0.5700 & 3.6379 \end{bmatrix}\times10^{-9}$ $m^2\ s^{-1}$. Using this estimate, we calculated the equilibration trajectory. We note that the serpentine trajectory has penetrated the binodal envelope; see Figure 97.

This indicates the spontaneous emulsification is feasible. A linear equilibration trajectory (shown by dotted line) does not foray into the meta-stable zone.

water(1)/acetic acid(2)/isophorone(3)

Let us examine the trajectory followed during equilibration of homogenous mixtures of two different compositions for the system water(1)/acetic acid(2)/isophorone(3). Isophorone is an β-unsaturated cyclic ketone. The composition of the equilibrated mixture is chosen to be $x_{1,eq}$ = 0.365, $x_{2,eq}$ = 0.155 and $x_{3,eq}$ = 0.48, which point lies on a tangent to the binodal curve. At the average composition, the matrix of thermodynamic factors is calculated from phase equilibrium thermodynamics: $[\Gamma]=\begin{bmatrix} 0.5558 & -0.6106 \\ -0.0923 & 1.591 \end{bmatrix}$. We assume that the matrix of Fick diffusivities is the product of scalar diffusivity $|\Lambda|^{1/2} = 1\times10^{-9}$ $m^2\ s^{-1}$ multiplied by $[\Gamma]$; i.e. $[D]=\begin{bmatrix} 0.5558 & -0.6106 \\ -0.0923 & 1.591 \end{bmatrix}\times10^{-9}$ $m^2\ s^{-1}$. Using this estimate, we calculated the equilibration trajectory. We note that the serpentine trajectory has penetrated the binodal envelope; see Figure 98. This indicates the spontaneous emulsification is feasible. A linear equilibration trajectory (shown by dotted line) does not foray into the meta-stable zone.

water(1)/acetic acid(2)/ethylacetate(3)

Let us examine the trajectory followed during equilibration of homogenous mixtures of two different compositions for the system water(1)/acetic acid(2)/ethylacetate(3). The composition of the equilibrated mixture is chosen to be $x_{1,eq}$ = 0.36, $x_{2,eq}$ = 0.11 and $x_{3,eq}$ = 0.53, which point lies on the binodal curve. At the average composition, the matrix of thermodynamic factors is calculated from phase equilibrium thermodynamics: $[\Gamma]=\begin{bmatrix} 0.3748 & -1.23 \\ -0.2363 & 2.041 \end{bmatrix}$. We assume that the matrix of Fick diffusivities is the product of scalar diffusivity $|\Lambda|^{1/2} = 1\times10^{-9}$ $m^2\ s^{-1}$ multiplied by $[\Gamma]$; i.e. $[D]=\begin{bmatrix} 0.3748 & -1.23 \\ -0.2363 & 2.041 \end{bmatrix}\times10^{-9}$ $m^2\ s^{-1}$. Using this estimate, we calculated the equilibration trajectory. We note that the serpentine trajectory has penetrated the binodal envelope; see Figure 99. This indicates the spontaneous emulsification is

feasible. A linear equilibration trajectory (shown by dotted line) does not foray into the meta-stable zone.

water(1)/acetic acid(2)/MTBE (3)

Let us examine the trajectory followed during equilibration of homogenous mixtures of two different compositions for the system water(1)/acetic acid(2)/MTBE (3). The composition of the equilibrated mixture is chosen to be $x_{1,eq} = 0.32$, $x_{2,eq} = 0.22$ and $x_{3,eq} = 0.46$, which point lies on the binodal curve. At the average composition, the matrix of thermodynamic factors is calculated from phase equilibrium thermodynamics: $[\Gamma]=\begin{bmatrix} 0.1986 & -0.8834 \\ 0.0689 & 2.565 \end{bmatrix}$. We assume that the matrix of Fick diffusivities is the product of scalar diffusivity $|\Lambda|^{1/2} = 1\times10^{-9}$ $m^2\ s^{-1}$ multiplied by $[\Gamma]$; i.e. $[D]=\begin{bmatrix} 0.1986 & -0.8834 \\ 0.0689 & 2.565 \end{bmatrix}\times10^{-9}$ $m^2\ s^{-1}$. Using this estimate, we calculated the equilibration trajectory. We note that the serpentine trajectory has penetrated the binodal envelope; see Figure 100. This indicates the spontaneous emulsification is feasible. A linear equilibration trajectory (shown by dotted line) does not foray into the meta-stable zone.

ethanol (1)/toluene(2)/n-decane(3)

Let us examine the trajectory followed during equilibration of homogenous mixtures of two different compositions for the system ethanol (1)/toluene(2)/n-decane(3). The composition of the equilibrated mixture is chosen to be $x_{1,eq} = 0.31$, $x_{2,eq} = 0.375$ and $x_{3,eq} = 0.315$, which point lies on the binodal curve. At the average composition, the matrix of thermodynamic factors is calculated from phase equilibrium thermodynamics: $[\Gamma]=\begin{bmatrix} 0.083 & -0.0209 \\ 0.5102 & 1.065 \end{bmatrix}$. We assume that the matrix of Fick diffusivities is the product of scalar diffusivity $|\Lambda|^{1/2} = 1\times10^{-9}$ $m^2\ s^{-1}$ multiplied by $[\Gamma]$; i.e. $[D]=\begin{bmatrix} 0.083 & -0.0209 \\ 0.5102 & 1.065 \end{bmatrix}\times10^{-9}$ $m^2\ s^{-1}$. Using this estimate, we calculated the equilibration trajectory. We note that the serpentine trajectory has penetrated the binodal envelope; see Figure 101. This indicates the spontaneous emulsification is

feasible. A linear equilibration trajectory (shown by dotted line) does not foray into the meta-stable zone.

water(1)/ethanol(2)/benzene(3)

Let us examine the trajectory followed during equilibration of homogenous mixtures of two different compositions for the system water(1)/ethanol(2)/benzene(3). The composition of the equilibrated mixture is chosen to be $x_{1,eq}$ = 0.085, $x_{2,eq}$ = 0.225 and $x_{3,eq}$ = 0.69, which point lies on a tangent to the binodal curve. At the average composition, the matrix of thermodynamic factors is calculated from phase equilibrium thermodynamics: $[\Gamma]=\begin{bmatrix} 0.6809 & -0.4738 \\ -1.01 & 0.8943 \end{bmatrix}$. We assume that the matrix of Fick diffusivities is the product of scalar diffusivity $|\Lambda|^{1/2}=1\times10^{-9}$ $m^2\ s^{-1}$ multiplied by $[\Gamma]$; i.e. $[D]=\begin{bmatrix} 0.6809 & -0.4738 \\ -1.01 & 0.8943 \end{bmatrix}\times10^{-9}$ $m^2\ s^{-1}$. Using this estimate, we calculated the equilibration trajectory. We note that the serpentine trajectory has penetrated the binodal envelope; see Figure 102. This indicates the spontaneous emulsification is feasible. A linear equilibration trajectory (shown by dotted line) does not foray into the meta-stable zone.

NMP(1)/propylbenzene(2)/dodecane(3), and NMP(1)/propylbenzene(2)/tetradecane(3)

Solvents such as NMP (=N-methyl-2-pyrrolidone), and sulpholane are used in the petroleum industry for aromatics from non-aromatic hydrocarbons.

Let us examine the trajectory followed during equilibration of homogenous mixtures of two different compositions for the system NMP(1)/propylbenzene(2)/dodecane(3). The composition of the equilibrated mixture is chosen to be $x_{1,eq}$ = 0.25, $x_{2,eq}$ = 0.155 and $x_{3,eq}$ = 0.6, which point lies on a tangent to the binodal curve. At the average composition, the matrix of thermodynamic factors is calculated from phase equilibrium thermodynamics: $[\Gamma]=\begin{bmatrix} 0.3081 & -0.3568 \\ -0.0821 & 1.1072 \end{bmatrix}$. We assume that the matrix of Fick diffusivities is the product of scalar diffusivity $|\Lambda|^{1/2}=1\times10^{-9}$ $m^2\ s^{-1}$ multiplied by $[\Gamma]$; i.e. $[D]=\begin{bmatrix} 0.3081 & -0.3568 \\ -0.0821 & 1.1072 \end{bmatrix}\times10^{-9}$ $m^2\ s^{-1}$. Using this estimate, we calculated the equilibration

trajectory. We note that the serpentine trajectory has penetrated the binodal envelope; see Figure 103. This indicates the spontaneous emulsification is feasible. A linear equilibration trajectory (shown by dotted line) does not foray into the meta-stable zone.

Let us examine the trajectory followed during equilibration of homogenous mixtures for the system NMP(1)/propylbenzene(2)/tetradecane(3). Consider first the equilibration of a mixture that lies on the left of the diagram with the average composition: $x_{1,eq} = 0.81$, $x_{2,eq} = 0.13$ and $x_{3,eq} = 0.06$, which point lies on a tangent to the binodal curve. At the average composition, the matrix of thermodynamic factors is calculated from phase equilibrium thermodynamics: $[\Gamma] = \begin{bmatrix} -0.0524 & -1.038 \\ 0.5064 & 1.803 \end{bmatrix}$. We assume that the matrix of Fick diffusivities is the product of scalar diffusivity $|\Lambda|^{1/2} = 1 \times 10^{-9}$ $m^2\ s^{-1}$ multiplied by $[\Gamma]$; i.e. $[D] = \begin{bmatrix} -0.0524 & -1.038 \\ 0.5064 & 1.803 \end{bmatrix} \times 10^{-9}$ $m^2\ s^{-1}$. Using this estimate, we calculated the equilibration trajectory. We note that the serpentine trajectory has penetrated the binodal envelope; see Figure 104. This indicates the spontaneous emulsification is feasible. A linear equilibration trajectory (shown by dotted line) does not foray into the meta-stable zone.

Consider next the equilibration of the ternary NMP(1)/propylbenzene(2)/tetradecane(3) mixture that lies on the right of the diagram with the average composition: $x_{1,eq} = 0.23$, $x_{2,eq} = 0.15$ and $x_{3,eq} = 0.62$, which point lies on a tangent to the binodal curve. At the average composition, the matrix of thermodynamic factors is calculated from phase equilibrium thermodynamics: $[\Gamma] = \begin{bmatrix} 0.3773 & -0.3802 \\ -0.0713 & 1.416 \end{bmatrix}$. We assume that the matrix of Fick diffusivities is the product of scalar diffusivity $|\Lambda|^{1/2} = 1 \times 10^{-9}$ $m^2\ s^{-1}$ multiplied by $[\Gamma]$; i.e. $[D] = \begin{bmatrix} 0.3773 & -0.3802 \\ -0.0713 & 1.416 \end{bmatrix} \times 10^{-9}$ $m^2\ s^{-1}$. Using this estimate, we calculated the equilibration trajectory. We note that the serpentine trajectory has penetrated the binodal envelope; see Figure 104. This indicates the spontaneous emulsification is feasible. A linear equilibration trajectory (shown by dotted line) does not foray into the meta-stable zone.

Heptane(1)/toluene(2)/sulpholane(3)

Let us examine the trajectory followed during equilibration of homogenous mixtures of two different compositions for the system heptane(1)/toluene(2)/sulpholane(3). The composition of the equilibrated mixture is chosen to be $x_{1,eq} = 0.33$, $x_{2,eq} = 0.595$, and $x_{3,eq} = 0.075$, which point lies on a tangent to the binodal curve. At the average composition, the matrix of thermodynamic factors is calculated from phase equilibrium thermodynamics: $[\Gamma] = \begin{bmatrix} 0.0689 & -0.6949 \\ 0.2493 & 1.2025 \end{bmatrix}$. We assume that the matrix of Fick diffusivities is the product of scalar diffusivity $|\Lambda|^{1/2} = 1 \times 10^{-9}$ m^2 s^{-1} multiplied by $[\Gamma]$; i.e. $[D] = \begin{bmatrix} 0.0689 & -0.6949 \\ 0.2493 & 1.2025 \end{bmatrix} \times 10^{-9}$ m^2 s^{-1}. Using this estimate, we calculated the equilibration trajectory. We note that the serpentine trajectory has penetrated the binodal envelope; see Figure 105. This indicates the spontaneous emulsification is feasible. A linear equilibration trajectory (shown by dotted line) does not foray into the meta-stable zone.

[omim][Cl](1)/ethanol(2)/TAEE(3), and [bmim][TfO](1)/ethanol(2)/TAEE(3)

There is increasing amount of fundamental and technological interest in the use of ionic liquids in separations in liquid-liquid extraction. We shall examine the diffusion trajectories in ternary mixtures of [omim][Cl](1)/ethanol(2)/TAEE(3). Here we denote the ionic liquid 1-octyl-3-methylimidazolium chloride in the abbreviated form [omim][Cl]. TAEE is the abbreviated name for tert-amyl ethyl ether. Two different phase equilibrium models are used for this purpose: UNIQUAC and NRTL, with two different parameter sources.

Let us first examine the trajectory followed during equilibration of homogenous mixtures of two different compositions for the system [omim][Cl](1)/ethanol(2)/TAEE(3) using the UNIQUAC parameters of Santiago et al.[56]

The composition of the equilibrated mixture is chosen to be $x_{1,eq} = 0.3$, $x_{2,eq} = 0.33$ and $x_{3,eq} = 0.37$, which point lies on a tangent to the binodal curve. At the average composition, the matrix of thermodynamic factors is calculated from phase equilibrium thermodynamics: $[\Gamma] = \begin{bmatrix} 2.498 & -3.1605 \\ -2.3352 & 4.603 \end{bmatrix}$.

We assume that the matrix of Fick diffusivities is the product of scalar diffusivity $|\Lambda|^{1/2} = 1\times10^{-9}$ $m^2\ s^{-1}$ multiplied by $[\Gamma]$; i.e. $[D]=\begin{bmatrix} 2.498 & -3.1605 \\ -2.3352 & 4.603 \end{bmatrix}\times10^{-9}$ $m^2\ s^{-1}$. Using this estimate, we calculated the equilibration trajectory. We note that the serpentine trajectory has penetrated the binodal envelope; see Figure 106. This indicates the spontaneous emulsification is feasible. A linear equilibration trajectory (shown by dotted line) does not foray into the meta-stable zone.

Next we examine the trajectory followed during equilibration of homogenous mixtures of two different compositions for the system [omim][Cl](1)/ethanol(2)/TAEE(3) using the NRTL parameters of Aznar.[57] The composition of the equilibrated mixture is chosen to be $x_{1,eq} = 0.4$, $x_{2,eq} = 0.375$ and $x_{3,eq} = 0.225$, which point lies on a tangent to the binodal curve. At the average composition, the matrix of thermodynamic factors is calculated from phase equilibrium thermodynamics: $[\Gamma]=\begin{bmatrix} 1.652 & -1.949 \\ -1.306 & 2.607 \end{bmatrix}$.

We assume that the matrix of Fick diffusivities is the product of scalar diffusivity $|\Lambda|^{1/2} = 1\times10^{-9}$ $m^2\ s^{-1}$ multiplied by $[\Gamma]$; i.e. $[D]=\begin{bmatrix} 1.652 & -1.949 \\ -1.306 & 2.607 \end{bmatrix}\times10^{-9}$ $m^2\ s^{-1}$. Using this estimate, we calculated the equilibration trajectory. We note that the serpentine trajectory has penetrated the binodal envelope; see Figure 107. This indicates the spontaneous emulsification is feasible. A linear equilibration trajectory (shown by dotted line) does not foray into the meta-stable zone.

We also investigation the diffusion trajectories using a different ionic liquid [bmim][TfO] = 1-butyl-3-methylimidazolium trifluoromethanesulfonate. The phase equilibrium data for [bmim][TfO](1)/ethanol(2)/TAEE(3) mixtures utilizes the UNIQUAC parameters of Santiago et al.[56]

The composition of the equilibrated mixture is chosen to be $x_{1,eq} = 0.24$, $x_{2,eq} = 0.37$ and $x_{3,eq} = 0.39$, that lies on a tangent to the binodal curve. At the average composition, the matrix of thermodynamic factors is calculated from phase equilibrium thermodynamics: $[\Gamma]=\begin{bmatrix} 0.7471 & -1.729 \\ -0.89037 & 3.457 \end{bmatrix}$. We assume that the matrix of Fick diffusivities is the product of scalar diffusivity $|\Lambda|^{1/2} = 1\times10^{-9}$ $m^2\ s^{-1}$ multiplied by

$[\Gamma]$; i.e. $[D]=\begin{bmatrix} 0.7471 & -1.729 \\ -0.89037 & 3.457 \end{bmatrix}\times 10^{-9}$ $m^2\ s^{-1}$. Using this estimate, we calculated the equilibration trajectory. We note that the serpentine trajectory has penetrated the binodal envelope; see Figure 108. This indicates the spontaneous emulsification is feasible. A linear equilibration trajectory (shown by dotted line) does not foray into the meta-stable zone.

water(1)/acetone(2)/toluene(3)

Let us examine the trajectory followed during equilibration of homogenous mixtures of two different compositions for the system water(1)/acetone(2)/toluene(3). The composition of the equilibrated mixture is chosen to be $x_{1,eq}$= 0.425, $x_{2,eq}$ = 0.487, $x_{3,eq}$ = 0.088, which point lies on a tangent to the binodal curve. At the average composition, the matrix of thermodynamic factors is calculated from phase equilibrium thermodynamics: $[\Gamma]=\begin{bmatrix} -0.3805 & -0.6848 \\ 0.9492 & 1.567 \end{bmatrix}$. We assume that the matrix of Fick diffusivities is the product of scalar diffusivity $|\Lambda|^{1/2}=1\times 10^{-9}$ $m^2\ s^{-1}$ multiplied by $[\Gamma]$; i.e. $[D]=\begin{bmatrix} -0.3805 & -0.6848 \\ 0.9492 & 1.567 \end{bmatrix}\times 10^{-9}$ $m^2\ s^{-1}$. It is particularly noteworthy that the Γ_{11}, and D_{11} are both negative; thermodynamic stability only requires that the determinants of $[\Gamma]$ and $[D]$ be positive definite. Using this diffusivity estimate, we calculated the diffusion trajectory. We note that the serpentine trajectory has penetrated the binodal envelope and entered the metable region; see Figure 109. This indicates the spontaneous emulsification is feasible. A linear equilibration trajectory (shown by dotted line) does not foray into the meta-stable zone.

water(1)/ethanol(2)/cyclohexane(3)

Let us examine the trajectory followed during equilibration of homogenous mixtures of two different compositions for the system water(1)/ethanol(2)/cyclohexane(3). The composition of the equilibrated mixture is chosen to be $x_{1,eq}$= 0.2, $x_{2,eq}$ = 0.59, $x_{3,eq}$ = 0.21, which point lies on a tangent to the binodal curve. At the average composition, the matrix of thermodynamic factors is calculated from phase equilibrium thermodynamics: $[\Gamma]=\begin{bmatrix} 0.335 & -0.3193 \\ -0.3493 & 0.5158 \end{bmatrix}$. We assume that the matrix of Fick diffusivities

is the product of scalar diffusivity $|\Lambda|^{1/2} = 1\times10^{-9}$ $m^2\ s^{-1}$ multiplied by $[\Gamma]$; i.e. $[D]=\begin{bmatrix} 0.335 & -0.3193 \\ -0.3493 & 0.5158 \end{bmatrix}\times10^{-9}$ $m^2\ s^{-1}$. It is particularly noteworthy that the Γ_{11}, and D_{11} are both negative; thermodynamic stability only requires that the determinants of $[\Gamma]$ and $[D]$ be positive definite. Using this diffusivity estimate, we calculated the diffusion trajectory. We note that the serpentine trajectory has penetrated the binodal envelope and entered the metable region; see Figure 110. This indicates the spontaneous emulsification is feasible. A linear equilibration trajectory (shown by dotted line) does not foray into the meta-stable zone.

toluene(1)/ethanol(2)/water(3)

Consider inter-diffusion of toluene(1)/ethanol(2)/water(3) mixtures; the composition (in mole tractions) of the mixture at equilibrium $x_{1,eq}$ = 0.01, $x_{2,eq}$ = 0.188 and $x_{3,eq}$ = 0.802, which point already lies in the meta-stable zone between the binodal and spinodal envelopes. At the average composition, the matrix of thermodynamic factors is calculated from phase equilibrium thermodynamics: $[\Gamma]=\begin{bmatrix} 0.715 & -0.1028 \\ -1.656 & 0.343 \end{bmatrix}$. We assume that the matrix of Fick diffusivities is the product of scalar diffusivity $|\Lambda|^{1/2} = 1\times10^{-9}$ $m^2\ s^{-1}$ multiplied by $[\Gamma]$; i.e. $[D]=\begin{bmatrix} 0.715 & -0.1028 \\ -1.656 & 0.343 \end{bmatrix}\times10^{-9}$ $m^2\ s^{-1}$. Using this diffusivity estimate, we calculated the diffusion trajectory. We note that the serpentine trajectory has penetrated the spinodal envelope and entered unstable region; see Figure 111; this implies phase splitting. A linear equilibration trajectory (dotted line) remains within the meta-stable zone and does not anticipate spinodal decomposition.

18. Notation

a_i	component activity, dimensionless
$[B]$	matrix defined by Equations (33), m^{-2} s
c_i	molar concentration of species *i*, mol m^{-3}
c_t	total molar concentration of mixture, mol m^{-3}
$Đ_{ij}$	M-S exchange coefficient, m^2 s^{-1}
$Đ_{12}$	M-S diffusivity for binary pair 1-2, m^2 s^{-1}
D_{12}	Fick diffusivity for binary mixture, m^2 s^{-1}
$\left[D\right]$	Fick diffusivity matrix, m^2 s^{-1}
$\left\|D\right\|$	Determinant of the Fick diffusivity matrix, m^4 s^{-2}
$\left\|D\right\|^{1/2}$	Square-root of determinant of $\left[D\right]$, m^2 s^{-1}
D_i	Fick diffusivity of species *i* in porous material, m^2 s^{-1}
$D_{i,self}$	self-diffusivity of species *i*, m^2 s^{-1}
G	Gibbs free energy, J mol^{-1}
G^{ex}	Excess Gibbs free energy, J mol^{-1}
$[H]$	Hessian of the Gibbs free energy defined by equation (8), dimensionless
J_i	molar diffusion flux of species *i* with respect to u, mol m^{-2} s^{-1}
$\left[L\right]$	Onsager diffusivity matrix in fluid phases, m^2 s^{-1}
M_i	molar mass of species *i*, kg mol^{-1}
n	number of species in the mixture, dimensionless
N_i	molar flux of species *i* in laboratory fixed reference frame, mol m^{-2} s^{-1}
N_t	molar flux of total mixture in laboratory fixed reference frame, mol m^{-2} s^{-1}
p_i	partial pressure of species *i* in mixture, Pa
p_t	total system pressure, Pa
R	gas constant, 8.314 J mol^{-1} K^{-1}
t	time, s
T	absolute temperature, K

x_i	mole fraction of component *i* in bulk fluid phase, dimensionless
u	molar average mixture velocity, m s^{-1}
$\overline{V}_i$	partial molar volume of species *i,* m^3 mol^{-1}
z	direction coordinate, m
Z	compressibility factor, calculated in this article using the PR ESO, dimensionless

Greek letters

δ_{ij}	Kronecker delta, dimensionless
γ_i	activity coefficient of component *i*, dimensionless
ϕ_i	fugacity coefficient of component *i*, dimensionless
Γ_{ij}	thermodynamic factors, dimensionless
$[\Gamma]$	matrix of thermodynamic factors, dimensionless
$\lvert\Gamma\rvert^{1/2}$	Square-root of determinant of $[\Gamma]$, dimensionless
$[\Lambda]$	matrix defined by Equations (33), (35), m^2 s^{-1}
$\lvert\Lambda\rvert^{1/2}$	Square-root of determinant of $[\Lambda]$, m^2 s^{-1}
μ_i^0	molar chemical potential at standard state, J mol^{-1}
μ_i	molar chemical potential, J mol^{-1}
σ	rate of entropy production, J m^{-3} s^{-1} K^{-1}

Subscripts

A	referring to site A
B	referring to site B
i	referring to component *i*
n	referring to component *n*
t	referring to total mixture
T	thermal diffusion

Table 1. Self-diffusivities $D_{i,self}^{x_j \to 1}$ in units of 10^{-8} m^2 s^{-1} for linear alkanes at 333 K and 30 MPa. The rows indicate species *i* and the columns, species *j*. The tabulated data is from Krishna and van Baten.[16]

	C1	C2	C3	nC4	nC5	nC6	nC7	nC8	nC9	nC10
C1	7.00	2.58	1.50	1.05		1.05		1.05		1.05
C2	5.30	1.95	1.23	0.92		0.84		0.83		0.83
C3	4.52	1.63	1.03	0.79	0.72	0.75				
nC4	3.83	1.44	0.92	0.69	0.65					
nC5			0.83	0.62	0.59					
nC6	3.00	1.09	0.77			0.56				
nC7							0.44			
nC8	2.36	0.97						0.40		
nC9									0.34	
nC10	1.86	0.82								0.34

As illustration, for the system, C1/C2/nC6, we have

$$D_{1,self}^{x_2 \to 1} = 7; \quad D_{1,self}^{x_2 \to 1} = 2.58; \quad D_{1,self}^{x_3 \to 1} = 1.50$$
$$D_{2,self}^{x_2 \to 1} = 5.3; \quad D_{2,self}^{x_2 \to 1} = 1.95; \quad D_{2,self}^{x_3 \to 1} = 0.84$$
$$D_{3,self}^{x_2 \to 1} = 3; \quad D_{3,self}^{x_2 \to 1} = 1.09; \quad D_{3,self}^{x_3 \to 1} = 0.56$$

Table 2. NRTL parameters for acetone(1)/benzene(2)/carbon-tetrachloride(3) at 298 K. These parameters are from Example 3.3.1 of Taylor and Krishna.[8] See also Kooijman and Taylor.[31]

	$\tau_{ij} = A_{ij}/T$	$\tau_{ji} = A_{ji}/T$	$\alpha_{ij} = \alpha_{ji}$
	dimensionless	dimensionless	dimensionless
acetone(1)/benzene(2)	-0.46504	0.76432	0.2
acetone(1)/carbon-tetrachloride(3)	-0.4279	1.5931	0.2
benzene(2)/carbon-tetrachloride(3)	-0.51821	0.7338	0.2

Table 3. NRTL parameters for acetone(1)/benzene(2)/methanol(3) mixtures at 298 K. The parameters are as reported by Kooijman and Taylor.[31] Please note that the acetone-benzene parameters are not the same as those reported above in Table 2.

	$\tau_{ij} = A_{ij}/T$	$\tau_{ji} = A_{ji}/T$	$\alpha_{ij} = \alpha_{ji}$
	dimensionless	dimensionless	dimensionless
acetone(1)/benzene(2)	-0.40727	1.378	0.29998
acetone(1)/methanol(3)	1.371	-0.528	0.2942
benzene(2)/methanol(3)	2.3	1.316	0.5023

Table 4. NRTL parameters for methanol(1)/1-propanol(2)/iso-butanol (3) mixtures at 298 K. The parameters are as reported by Kooijman and Taylor.[31]

	$\tau_{ij} = A_{ij}/T$	$\tau_{ji} = A_{ji}/T$	$\alpha_{ij} = \alpha_{ji}$
	dimensionless	dimensionless	dimensionless
methanol(1)/ 1-propanol(2)	1.295	-0.75	0.3086
methanol(1)/ iso-butanol (3)	1.41	-0.926	0.3018
1-propanol(2)/ iso-butanol (3)	0.859	-0.654	0.2791

Table 5. NRTL parameters for glyercol(1)/acetone(2)/water(3) at 298 K. These parameters are from Krishna et al.[9]

	$\tau_{ij} = A_{ij}/T$	$\tau_{ji} = A_{ji}/T$	$\alpha_{ij} = \alpha_{ji}$
	dimensionless	dimensionless	dimensionless
glycerol(1)/acetone(2)	0.868	2.467	0.2
glycerol(1)/water(3)	-1.29	-1.52	0.2
acetone(2)/water(3)	-0.665	2.095	0.2

Table 6. UNIQUAC parameters for water(1)/chloroform(2)/acetic-acid(3) at 298 K. These parameters are from Pertler.[58] These parameters needed re-adjustment in order to match the experimental solubility data of Othmer and Ku.[59] The following are the adjusted values used in the calculations.

	r_i	q_i
	dimensionless	dimensionless
water(1)	0.92	1.4
chloroform(2)	2.87	2.41
acetic-acid(3)	2.2024	2.072

	$\tau_{ij} = \exp(-A_{ij}/T)$	$\tau_{ji} = \exp(-A_{ji}/T)$
	dimensionless	dimensionless
water(1)/chloroform(2)	0.4285	0.229
water(1)/acetic-acid(3)	1.274	1.312
chloroform(2)/acetic-acid(3)	1.388	0.885

Table 7. NRTL parameters for water(1)/DMSO(2)/THF(3) at 293.15 K. These parameters are taken from Table 1 of Olaya et al.[54]

	$\tau_{ij} = A_{ij}/T$	$\tau_{ji} = A_{ji}/T$	$\alpha_{ij} = \alpha_{ji}$
	dimensionless	dimensionless	dimensionless
water(1)/DMSO(2)	1.1545	-5.296	0.2
water(1)/THF(3)	1.7842	-0.787	0.2
DMSO(2)/THF(3)	4.3595	-1.4228	0.2

Table 8. NRTL parameters for water(1)/DMSO(2)/THF(3) at 293.15 K. These parameters are taken from Table 1 of Zuber et al.[55]

	$\tau_{ij} = A_{ij}/T$	$\tau_{ji} = A_{ji}/T$	$\alpha_{ij} = \alpha_{ji}$
	dimensionless	dimensionless	dimensionless
water(1)/DMSO(2)	-0.5902	-3.5184	0.2
water(1)/THF(3)	1.8997	0.2437	0.2
DMSO(2)/THF(3)	1.615	-1.373	0.2

Table 9. NRTL parameters for water(1)/acetone(2)/phenol(3) at 323.15 K. These parameters are taken from Table 2 of Zuber et al.[55]

	$\tau_{ij} = A_{ij}/T$	$\tau_{ji} = A_{ji}/T$	$\alpha_{ij} = \alpha_{ji}$
	dimensionless	dimensionless	dimensionless
water(1)/acetone(2)	0.1024	1.826	0.2
water(1)/phenol(3)	5.332	-1.585	0.2
acetone(2)/phenol(3)	-1.504	-2.78	0.2

Table 10. NRTL parameters for water(1)/acetone(2)/TCE(3) at 298.15 K. These parameters are taken from Table 8-31 of Reid, Prausnitz and Poling.[6]

	$\tau_{ij} = A_{ij}/T$	$\tau_{ji} = A_{ji}/T$	$\alpha_{ij} = \alpha_{ji}$
	dimensionless	dimensionless	dimensionless
water(1)/acetone(2)	1.388	0.75701	0.3
water(1)/TCE(3)	5.98775	3.60977	0.2485
acetone(2)/TCE(3)	-0.20102	-0.19920	0.3

Table 11. NRTL parameters for water(1)/2-propanol(2)/phenol(3) at 298.15 K. These parameters are taken from Table 3 of Rogošic et al.[60] Please note that the Table 3 of this paper has reversed the subscripts 2, and 3. This error has been corrected in the values reported in the Table below.

	$\tau_{ij} = A_{ij}/T$	$\tau_{ji} = A_{ji}/T$	$\alpha_{ij} = \alpha_{ji}$
	dimensionless	dimensionless	dimensionless
water(1)/2-propanol(2)	0.6362	0.9474	0.3
water(1)/phenol(3)	4.8511	–0.9032	0.3
2-propanol(2)/phenol(3)	–1.8055	–2.1517	0.2

Table 12. NRTL parameters for water(1)/trichloroacetic acid (2)/antipyrine(3) at 303.15 K. These parameters are taken from Table 2 of Olaya et al.[54]

	$\tau_{ij} = A_{ij}/T$	$\tau_{ji} = A_{ji}/T$	$\alpha_{ij} = \alpha_{ji}$
	dimensionless	dimensionless	dimensionless
water(1)/trichloro-acetic acid(2)	3.022	-2.2055	0.2
water(1)/antipyrine(3)	-1.809	2.4313	0.2
trichloro-acetic acid (2)/ antipyrine (3)	-5.233	-6.583	0.2

Table 13. UNIQUAC parameters for acetone(1)/ethyl-acetate(2)/water(3) at 293 K. These parameters are from Pertler.[58]

	r_i	q_i
	dimensionless	dimensionless
acetone(1)	2.5735	2.336
ethyl-acetate(2)	3.4786	3.116
water(3)	0.92	1.4

	$\tau_{ij} = \exp(-A_{ij}/T)$	$\tau_{ji} = \exp(-A_{ji}/T)$
	dimensionless	dimensionless
acetone(1)/ethyl-acetate(2)	1.3068	0.827
acetone(1)/water(3)	0.488	1.328
ethyl-acetate(2)/water(3)	0.2538	0.7705

Table 14. NRTL parameters for propyl acetate(1)/formic acid(2)/water (3) at 298 K. These parameters are taken from Table 2 of Reyes-Labarta et al.[61]

	$\tau_{ij} = A_{ij}/T$	$\tau_{ji} = A_{ji}/T$	$\alpha_{ij} = \alpha_{ji}$
	dimensionless	dimensionless	dimensionless
Propyl acetate(1)/ formic acid(2)	-5.098	-1.567	0.2
Propyl acetate(1)/ water(3)	0.793	7.87	0.2
Formic acid (2)/ water(3)	-2.03	-3.97	0.2

Table 15. NRTL parameters for furfural(1)/formic acid(2)/water (3) at 298 K. These parameters are taken from Table 2 of Reyes-Labarta et al.[61]

	$\tau_{ij} = A_{ij}/T$	$\tau_{ji} = A_{ji}/T$	$\alpha_{ij} = \alpha_{ji}$
	dimensionless	dimensionless	dimensionless
Furfural(1)/ formic acid(2)	3.0975	-1.662	0.2
Furfural(1)/ water(3)	0.1044	4.126	0.2
Formic acid (2)/ water(3)	1.387	-3.525	0.2

Table 16. NRTL parameters for 1-butanol (1)/methanol(2)/water(3) at 298 K. These parameters are taken from Table 2 of Reyes-Labarta et al.[61]

	$\tau_{ij} = A_{ij}/T$	$\tau_{ji} = A_{ji}/T$	$\alpha_{ij} = \alpha_{ji}$
	dimensionless	dimensionless	dimensionless
1-butanol(1)/ methanol(2)	-6.296	-1.004	0.3
1-butanol(1)/ water(3)	-0.4596	5.638	0.3
methanol (2)/ water(3)	-0.628	-9.11	0.2

Table 17. NRTL parameters for water(1)/acetic acid(2)/dichloromethane (3) at 298 K. These parameters are taken from Table 2 of Reyes-Labarta et al.[61]

	$\tau_{ij} = A_{ij}/T$	$\tau_{ji} = A_{ji}/T$	$\alpha_{ij} = \alpha_{ji}$
	dimensionless	dimensionless	dimensionless
water(1)/acetic acid(2)	-5.95	-1.49	0.2
water(1)/ dichloromethane(3)	3.98	2.08	0.2
Acetic acid (2)/ dichloromethane(3)	-0.73	-5.2	0.3

Table 18. NRTL parameters for water(1)/acetic acid(2)/1-hexanol(3) at 298 K. These parameters are taken from Table 3 of Fahim et al.[62]

	$\tau_{ij} = \left(a_{ij}^0 + b_{ij}\left(T - 273.15\right)\right)/T$	$\tau_{ji} = \left(a_{ji}^0 + b_{ji}\left(T - 273.15\right)\right)/T$	$\alpha_{ij} = \alpha_{ji}$
	dimensionless	dimensionless	dimensionless
water(1)/acetic acid(2)	1.2199	-0.3239	0.2
water(1)/ 1-hexanol(3)	6.9513	-0.3454	0.2
Acetic acid (2)/ 1-hexanol(3)	-0.3616	0.9906	0.2

Table 19. NRTL parameters for toluene(1)/acetaldehyde(2)/water(3) at 298 K. These parameters are taken from Table 2 of Reyes-Labarta et al.[61]

	$\tau_{ij} = A_{ij}/T$	$\tau_{ji} = A_{ji}/T$	$\alpha_{ij} = \alpha_{ji}$
	dimensionless	dimensionless	dimensionless
toluene(1)/ acetaldehyde(2)	0.155	0.085	0.2
toluene(1)/ water(3)	6.5	11.22	0.2
acetaldehyde (2)/ water(3)	1.93	-0.21	0.2

Table 20. NRTL parameters for 1-hexanol(1)/nitromethane(2)/water(3) at 298 K. These parameters are taken from Table 2 of Reyes-Labarta et al.[61]

	$\tau_{ij} = A_{ij}/T$	$\tau_{ji} = A_{ji}/T$	$\alpha_{ij} = \alpha_{ji}$
	dimensionless	dimensionless	dimensionless
1-hexanol (1)/ nitromethane (2)	2.165	-0.1017	0.2
1-hexanol (1)/ water(3)	-0.299	9.026	0.2
nitromethane (2)/ water(3)	1.3524	2.319	0.2

Table 21. NRTL parameters for 4-methyl-2-pentanone(1)/acetonitrile(2)/water(3) at 298 K. These parameters are taken from Table 2 of Reyes-Labarta et al.[61]

	$\tau_{ij} = A_{ij}/T$	$\tau_{ji} = A_{ji}/T$	$\alpha_{ij} = \alpha_{ji}$
	dimensionless	dimensionless	dimensionless
toluene(1)/ acetaldehyde(2)	-0.0665	0.9023	0.2
toluene(1)/ water(3)	1.357	5.391	0.2
acetaldehyde (2)/ water(3)	-0.133	2.62	0.2

Table 22. NRTL parameters for acetonitrile(1)/1-propanol(2)/hexane(3) at 298 K. These parameters are taken from Table 2 of Reyes-Labarta et al.[61]

	$\tau_{ij} = A_{ij}/T$	$\tau_{ji} = A_{ji}/T$	$\alpha_{ij} = \alpha_{ji}$
	dimensionless	dimensionless	dimensionless
acetonitrile(1)/ 1-propanol(2)	-0.857	-2.01	0.2
acetonitrile(1)/ hexane(3)	2.25	1.43	0.2
1-propanol(2)/ hexane (3)	1.44	-2.41	0.2

Table 23. UNIQUAC parameters for water(1)/caprolactam(2)/toluene(3) at 298.15 K. These parameters are from Table 1, Chapter 7 of the PhD dissertation of Bollen.[63]

	r_i	q_i
	dimensionless	dimensionless
water(1)	0.92	1.4
caprolactam(2)	4.6106	3.724
toluene(3)	3.9928	2.968

	$\tau_{ij} = A_{ij}/T$	$\tau_{ji} = A_{ji}/T$
	dimensionless	dimensionless
water(1)/caprolactam(2)	0.1027043	3.647516849
water(1)/ toluene(3)	0.2563201	0.0964476
caprolactam(2)/toluene(3)	0.3324973	1.4351863

Table 24. UNIQUAC parameters for water(1)/caprolactam(2)/benzene(3) at 298.15 K. These parameters are from Table 1, Chapter 7 of the PhD dissertation of Bollen.[63]

	r_i	q_i
	dimensionless	dimensionless
water(1)	0.92	1.4
caprolactam(2)	4.6106	3.724
benzene(3)	3.1878	2.4

	$\tau_{ij} = A_{ij}/T$	$\tau_{ji} = A_{ji}/T$
	dimensionless	dimensionless
water(1)/caprolactam(2)	1.5339381	1.7321924
water(1)/ benzene(3)	0.3259823	0.1101953
caprolactam(2)/benzene(3)	1.4594085	0.8758174

Table 25. UNIQUAC parameters for toluene(1)/water(2)/propionic-acid(2)/water(3) at 298.15 K. These parameters are from Table 6 of Kim and Park.[64] However, there is some uncertainty about the units of the energy parameters listed in Table 6 because the units are not specified. Furthermore, equation (16) of Kim and Park[64] appears to contain a typo. Due to the combination of the uncertainties, our binodal curve do not correspond with the experimental data. Therefore, the calculations presented here must be viewed as being consistent for a partially miscible (hypothetical) mixture for which the following set of UNIQUAC parameters are valid.

	r_i	q_i
	dimensionless	dimensionless
toluene(1)	3.9928	2.968
Propionic-acid(2)	2.9	2.58
water(3)	0.92	1.4

	$\tau_{ij} = \exp(-A_{ij}/T)$	$\tau_{ji} = \exp(-A_{ji}/T)$
	dimensionless	dimensionless
toluene(1) / propionic-acid (2)	1.08985977	0.86688385
toluene(1)/ water(3)	0.81980947	0.3296506
Propionic-acid (2)/ water(3)	1.21111669	0.61226107

Table 26. UNIQUAC parameters for ethylacetate(1)/propionic-acid(2)/water(3) at 298.15 K. These parameters are from Table 6 of Kim and Park.[64] However, there is some uncertainty about the units of the energy parameters listed in Table 6 because the units are not specified. Furthermore, equation (16) of Kim and Park[64] appears to contain a typo. Due to the combination of the uncertainties, our binodal curve do not correspond with the experimental data. Therefore, the calculations presented here must be viewed as being consistent for a partially miscible (hypothetical) mixture for which the following set of UNIQUAC parameters are valid.

	r_i	q_i
	dimensionless	dimensionless
ethylacetate(1)	3.4786	3.116
Propionic-acid(2)	2.9	2.58
water(3)	0.92	1.4

	$\tau_{ij} = \exp(-A_{ij}/T)$	$\tau_{ji} = \exp(-A_{ji}/T)$
	dimensionless	dimensionless
ethylacetate (1)/ propionic-acid (2)	0.94875404	2.69011546
ethylacetate (1)/ water(3)	0.19953302	0.33562196
Propionic-acid (2)/ water(3)	3.28217216	1.9470615

Table 27. NRTL parameters for water(1)/acetic acid(2)/isophorone(3) at 298.15 K. The parameters are from Colombo et al.[65]

	$\tau_{ij} = A_{ij}/T$	$\tau_{ji} = A_{ji}/T$	$\alpha_{ij} = \alpha_{ji}$
	dimensionless	dimensionless	dimensionless
water(1)/acetic acid (2)	0.7074	0.2455	0.2
water(1)/isophorone(3)	6.466	-0.2852	0.2
Acetic acid(2)/ Isophorone(3)	-1.489	1.381	0.2

Table 28. NRTL parameters for water(1)/acetic acid(2)/ethylacetate(3) at 298.15 K. The parameters are from Colombo et al.[65]

	$\tau_{ij} = A_{ij}/T$	$\tau_{ji} = A_{ji}/T$	$\alpha_{ij} = \alpha_{ji}$
	dimensionless	dimensionless	dimensionless
water(1)/acetic acid (2)	-0.2651	-0.5147	0.2
water(1)/ethyl acetate(3)	4.3205	0.5055	0.2
Acetic acid(2)/ Ethyl acetate(3)	-2.545	3.224	0.2

Table 29. NRTL parameters for water(1)/acetic acid(2)/MTBE (3) at 298.15 K. The parameters are from Zhang and Wang.[66]

	$\tau_{ij} = A_{ij}/T$	$\tau_{ji} = A_{ji}/T$	$\alpha_{ij} = \alpha_{ji}$
	dimensionless	dimensionless	dimensionless
water(1)/acetic acid (2)	0.354	-1.2151	0.47
water(1)/MTBE(3)	3.9737	1.2998	0.2
Acetic acid(2)/ MTBE(3)	-0.2774	-2.8068	0.37

Table 30. NRTL parameters for ethanol (1)/toluene(2)/n-decane(3) at 298.15 K. The parameters are from Mohsen-Nia.[67]

	$\tau_{ij} = A_{ij}/T$	$\tau_{ji} = A_{ji}/T$	$\alpha_{ij} = \alpha_{ji}$
	dimensionless	dimensionless	dimensionless
ethanol(1)/toluene(2)	1.9193	0.6687	0.293
ethanol(1)/n-decane(3)	0.465	2.3092	0.2
toluene(2)/n-decane(3)	-0.7673	0.7246	0.2

Table 31. UNIQUAC parameters for water (1)/ethanol(2)/benzene(3) at 298.15 K. These parameters are taken from Example 05.20 of Gmehling et al.[68]

	r_i	q_i
	dimensionless	dimensionless
water(1)	0.92	1.4
ethanol(2)	2.1055	1.972
benzene(3)	3.1878	2.4

	$\tau_{ij} = A_{ij}/T$	$\tau_{ji} = A_{ji}/T$
	dimensionless	dimensionless
water(1)/ethanol(2)	0.1713	2.9060
Water(1)/benzene(3)	0.354	0.0117
ethanol(2)/benzene(3)	1.359	0.3625

Table 32. NRTL parameters for NMP(1)/propylbenzene(2)/dodecane(3) at 298 K. The parameters are from Al-Jimaz et al.[69]

	τ_{ij}	τ_{ji}	$\alpha_{ij} = \alpha_{ji}$
	dimensionless	dimensionless	dimensionless
NMP(1)/ propylbenzene(2)	0.0539	0.1769	0.2
NMP(1)/dodecane(3)	2.938	0.5403	0.2
propylbenzene(2)/ dodecane(3)	0.9102	-1.004	0.2

Table 33. NRTL parameters for NMP(1)/propylbenzene(2)/tetradecane(3) at 298 K. The parameters are from Al-Jimaz et al.[69]

	$\tau_{ij} = A_{ij}/T$	$\tau_{ji} = A_{ji}/T$	$\alpha_{ij} = \alpha_{ji}$
	dimensionless	dimensionless	dimensionless
NMP(1)/ propylbenzene(2)	-2.8661	1.5931	0.2
NMP(1)/tetradecane(3)	3.4745	0.4103	0.2
propylbenzene(2)/ tetradecane(3)	0.2851	-2.678	0.2

Table 34. NRTL parameters for heptane(1)/toluene(2)/sulpholane(3) at 373.15 K. The parameters are from Steltenpohl and Graczová.[70]

	$\tau_{ij} = A_{ij}/T$	$\tau_{ji} = A_{ji}/T$	$\alpha_{ij} = \alpha_{ji}$
	dimensionless	dimensionless	dimensionless
heptane(1)/ toluene(2)	-0.33049669	0.73432311	0.3
heptane(1)/ sulpholane(3)	3.15538119	2.13985359	0.1866
toluene(2)/ sulpholane(3)	1.4355933	0.57965228	0.5288

Table 35. UNIQUAC parameters for [omim][Cl](1)/ethanol(2)/TAEE(3) at 298 K. The parameters are from Tables 2, 3, and 4 of Santiago et al.[56]

	r_i	q_i
	dimensionless	dimensionless
[omim][Cl]	9.6165	7.698
ethanol(2)	2.5755	2.588
TAEE(3)	5.417	4.712

	$\tau_{ij} = \exp(-A_{ij}/T)$	$\tau_{ji} = \exp(-A_{ji}/T)$
	dimensionless	dimensionless
[omim][Cl](1)/ethanol(2)	1.874373291	4.720604883
[omim][Cl](1)/TAEE(3)	1.410892816	0.169936683
ethanol(2)/TAEE(3)	3.744325482	0.048064224

Table 36. NRTL parameters for [omim][Cl](1)/ethanol(2)/TAEE(3) at 298 K. The parameters are from Aznar.[57]

	$\tau_{ij} = A_{ij}/T$	$\tau_{ji} = A_{ji}/T$	$\alpha_{ij} = \alpha_{ji}$
	dimensionless	dimensionless	dimensionless
[omim][Cl](1)/ethanol(2)	-1.674	-3.035	0.2
[omim][Cl](1)/TAEE(3)	1.365	9.3245	0.204
ethanol(2)/TAEE(3)	0.3034	1.399	0.307

Table 37. UNIQUAC parameters for [bmim][TfO](1)/ethanol(2)/TAEE(3) at 298 K. The parameters are from Tables 2, 3, and 4 of Santiago et al.[56]

	r_i	q_i
	dimensionless	dimensionless
[bmim][TfO]	8.9463	7.135
ethanol(2)	2.5755	2.588
TAEE(3)	5.417	4.712

	$\tau_{ij} = \exp(-A_{ij}/T)$	$\tau_{ji} = \exp(-A_{ji}/T)$
	dimensionless	dimensionless
[bmim][TfO](1)/ethanol(2)	0.8331298	2.91830955
[bmim][TfO](1)/TAEE(3)	1.4677043	0.004246414
ethanol(2)/TAEE(3)	3.74432548	0.048064224

Table 38. NRTL parameters for water(1)/acetone(2)/toluene(3) at 298 K. These parameters are from the DECHEMA Dortmund data bank, as reported in Table 1 of Springer et al.[71]

	$\tau_{ij} = A_{ij}/T$	$\tau_{ji} = A_{ji}/T$	$\alpha_{ij} = \alpha_{ji}$
	dimensionless	dimensionless	dimensionless
Water(1)/acetone(2)	2.1942	1.267	0.5859
water(1)/toluene(3)	7.2509	9.5281	0.2
acetone(2)/toluene(3)	-0.4187	1.2285	0.295

Table 39. NRTL parameters for water(1)/ethanol(2)/cyclohexane (3) at 298 K. These parameters are from the DECHEMA Dortmund data bank, as reported in Table 1 of Springer et al.[71]

	τ_{ij}	τ_{ji}	$\alpha_{ij} = \alpha_{ji}$
	dimensionless	dimensionless	dimensionless
Water(1)/ethanol(2)	1.8707	0.0976	0.3475
water(1)/cyclohexane(3)	14.84	5.6653	0.21159
ethanol(2)/cyclohexane(3)	1.4786	2.408	0.46261

Table 40. NRTL parameters for toluene(1)/ethanol(2)/water(3) at 298 K. The toluene/water parameters are from Wang et al.[72] The remaining parameters are from the DECHEMA Dortmund data bank; the ethanol/toluene τ_{ji} has been modified to match experimental binodal data.[73, 74]

	τ_{ij}	τ_{ji}	$\alpha_{ij} = \alpha_{ji}$
	dimensionless	dimensionless	dimensionless
toluene(1)/ethanol(2)	1.938	0.6	0.529
toluene(1)/water(3)	15.219	7.529	0.2
ethanol(2)/water(3)	-0.0978	2.096	0.293

19. References

(1) Onsager, L. Theories and Problems of Liquid Diffusion, *Annals N.Y. Acad. Sci.* **1945**, *46*, 241-265.

(2) de Groot, S. R.; Mazur, P. Non-Equilibrium Thermodynamics; North-Holland Publishing Co.: Amsterdam, 1962.

(3) Standart, G. L.; Taylor, R.; Krishna, R. The Maxwell-Stefan formulation of irreversible thermodynamics for simultaneous heat and mass transfer, *Chem. Eng. Commun.* **1979**, *3*, 277-289.

(4) Hirschfelder, J. O.; Curtiss, C. F.; Bird, R. B. Molecular theory of gases and liquids; Second Corrected Printing, John Wiley: New York, USA, 1964.

(5) Fuller, E. N.; Schettler, P. D.; Giddings, J. C. A new method for prediction of binary gas-phase diffusion coefficients, *Ind. Eng. Chem.* **1966**, *58*, 19-27.

(6) Reid, R.C.; Prausnitz, J. M.; Poling, B. E. The Properties of Gases and Liquids; 4th Edition, McGraw-Hill: New York, 1986.

(7) Takahashi, S.; Hongo, M. Diffusion Coefficients of Gases at High Pressures in the CO_2 - C_2H_4 System, *J. Chem. Eng. Japan.* **1982**, *15*, 57-59.

(8) Taylor, R.; Krishna, R. Multicomponent mass transfer; John Wiley: New York, 1993.

(9) Krishna, R.; Low, C. Y.; Newsham, D. M. T.; Olivera Fuentes, C. G.; Paybarah, A. Liquid Liquid Equilibrium in the System Glycerol Water Acetone at 25 ^{o}C, *Fluid Phase Equilib.* **1989**, *45*, 115-120.

(10) Tuan, D. Q.; Zollweg, J. A.; Rizvi, S. S. H. Concentration Dependence of the Diffusion Coefficient of Lipid in Supercritical Carbon Dioxide, *Ind. Eng. Chem. Res.* **1999**, *38*, 2787-2793.

(11) Darken, L. S. Diffusion, Mobility and Their Interrelation through Free Energy in Binary Metallic Systems, *Trans. AIME* **1948**, *175*, 184-201.

(12) Darken, L. S. Diffusion of Carbon in Austenite with a Discontinuity in Composition, *Trans. AIME* **1949**, *180*, 430-438.

(13) Shieh, J. C.; Lyons, P. A. Transport Properties of Liquid n-Alkanes, *J. Phys. Chem.* **1969**, *73*, 3258-3264.

(14) Bidlack, D. L.; Anderson, D. K. Mutual diffusion in the system hexane-hexadecane, *J. Phys. Chem.* **1964**, *68*, 206-208.

(15) Helbaek, M.; Hafskjold, B.; Dysthe, D. K.; Sorland, G. H. Self-diffusion coefficients of methane or ethane mixtures with hydrocarbons at high pressure by NMR, *J. Chem. Eng. Data* **1996**, *41*, 598-603.

(16) Krishna, R.; van Baten, J. M. The Darken relation for multicomponent diffusion in liquid mixtures of linear alkanes. An investigation using Molecular Dynamics (MD) simulations, *Ind. Eng. Chem. Res.* **2005**, *44*, 6939-6947.

(17) Krishna, R.; van Baten, J. M. Unified Maxwell-Stefan description of binary mixture diffusion in micro- and meso- porous materials, *Chem. Eng. Sci.* **2009**, *64*, 3159-3178.

(18) Liu, X.; Bardow, A.; Vlugt, T. J. H. Multicomponent Maxwell-Stefan Diffusivities at Infinite Dilution, *Ind. Eng. Chem. Res.* **2011**, *50*, 4776-4782.

(19) Krishna, R.; van Baten, J. M. MD simulations of diffusivities in methanol – n-hexane mixtures near the liquid-liquid phase splitting region, *Chem Eng Technol* **2006**, *29*, 516-519.

(20) Krishna, R.; van Baten, J. M. Validating the Darken relation for diffusivities in fluid mixtures of varying densities by use of MD simulations, *Chem Eng Technol* **2006**, *29*, 761-765.

(21) Wesselingh, J. A.; Krishna, R. Mass transfer in multicomponent mixtures; VSSD: Delft, 2000.

(22) Hsu, Y.-D.; Chen, Y.-P. Correlation of the mutual diffusion coefficients of binary liquid mixtures, *Fluid Phase Equilibr.* **1998**, *152*, 149-168.

(23) Krishna, R.; Standart, G. L. Mass and energy transfer in multicomponent systems, *Chem. Eng. Commun.* **1979**, *3*, 201-275.

(24) Krishna, R. A Unified Theory of Separation Processes Based on Irreversible Thermodynamics, *Chem. Eng. Commun.* **1987**, *59*, 33-64.

(25) Krishna, R.; van Baten, J. M. Onsager coefficients for binary mixture diffusion in nanopores, *Chem. Eng. Sci.* **2008**, *63*, 3120-3140.

(26) Leahy-Dios, A.; Firoozabadi, A. Unified Model for Nonideal Multicomponent Molecular Diffusion Coefficients, *A.I.Ch.E.J.* **2007**, *53*, 2932-2939.

(27) Wesselingh, J. A.; Bollen, A. M. Multicomponent diffusivities from the free volume theory, *Chem. Eng. Res. Des.* **1997**, *75*, 590-602.

(28) Parez, S.; Guevara-Carrion, G.; Hasse, H.; Vrabec, J. Mutual diffusion in the ternary mixture of water + methanol + ethanol and its binary subsystems, *Phys. Chem. Chem. Phys.* **2013**, *15*, 3985-4001.

(29) Cullinan, H. T.; Toor, H. L. Diffusion in the Three-Component Liquid System: Acetone-Benzene Carbon Tetrachloride, *J. Phys. Chem.* **1965**, *69*, 3941-3949.

(30) Alimadadian, A.; Colver, C. P. A New Technique for the Measurement of Ternary Diffusion Coefficients in Liquid Systems, *Can. J. Chem. Eng.* **1976**, *54*, 208-213.

(31) Kooijman, H. A.; Taylor, R. Estimation of Diffusion-Coefficients in Multicomponent Liquid- Systems, *Ind. Eng. Chem. Res.* **1991**, *30*, 1217-1222.

(32) Shuck, F. O.; Toor, H. L. Diffusion in the Three Component Liquid System Methyl Alcohol - n-Propyl Alchohol - Isobutyl alcohol, *J. Phys. Chem.* **1963**, *67*, 540-545.

(33) Riede, T.; Schlünder, E. U. Diffusivities of the Ternary Liquid Mixture 2-Propanol-Water-Glycerol and Three-Component Mass Transfer in Liquids, *Chem. Eng. Sci.* **1991**, *46*, 609-617.

(34) Mutoru, J. W.; Firoozabadi, A. Form of multicomponent Fickian diffusion coefficients matrix, *J. Chem. Thermodynamics* **2011**, *43*, 1192-1203.

(35) Zhang, L.; Zhang, W.; Yang, B. Experimental Measurement and Modeling of Ternary Vapor−Liquid Equilibrium for Water + 2-Propanol + Glycerol, *J. Chem. Eng. Data* **2014**, *59*, 3825-3830.

(36) Rehfeldt, S.; Stichlmair, J. Measurement and prediction of multicomponent diffusion coefficients in four ternary liquid systems, *Fluid Phase Equilib.* **2010**, *290*, 1-14.

(37) Rehfeldt, S. Mehrkomponentendiffusion in Flüssigkeiten, Technische Universität München, München, 2009.

(38) Soriano-Vargas, O.; Avila-Davila, E. O.; Lopez-Hirata, V. M.; Dorantes-Rosales, H. J.; Gonzalez-Velazquez, J. L. Spinodal Decomposition in an Fe-32 at %Cr Alloy during Isothermal Aging, *Mater. Trans., J.I.M.,* **2009**, *50*, 1753-1757.

(39) Cahn, J. W.; Hilliard, J. E. Free Energy of a Nonuniform System. II. Nucleation in a Two-Component Incompressible Fluid, *J. Chem. Phys.* **1959**, *31*, 688-699.

(40) Cahn, J. W. On Spinodal Decomposition, *J. Chem. Phys.* **1961**, *9*, 795-801.

(41) Vitagliano, V.; Sartorio, R.; Chiaravalle, E.; Ortona, O. Diffusion and Viscosity in Water-Triethylamine Mixtures at 19 and 20 “C, *J. Chem. Eng. Data* **1980**, *25*, 121-124.

(42) Pertler, M.; Blass, E.; Stevens, G. W. Fickian diffusion in binary mixtures that form two liquid phases, *A.I.Ch.E.J.* **1986**, *42*, 910-920.

(43) Thiel, P.; Paschke, A.; Winkelmann, J. Diffusion Coefficients, Viscosities and Densities in the Binary Subsystems of Methyl Isopropyl Ketone - n-Butyl acetate - Water, *Ber. Bunsen Phys. Chem.* **1993**, *97*, 1119-1124.

(44) Grossmann, T.; Winkelmann, J. Ternary Diffusion Coefficients of Glycerol + Acetone + Water by Taylor Dispersion Measurements at 298.15 K, *J. Chem. Eng. Data* **2005**, *50*, 1396-1403.

(45) McKeigue, K.; Gulari, E. Light Scattering Measurements of Diffusion in Binary Solutions Containing an Associating Component, *J. Phys. Chem.* **1984**, *88*, 3472-3479.

(46) Dysthe, D. K.; Hafskjold, B. Inter- and Intradiffusion in Liquid Mixtures of Methane and n-Decane, *Int. J. Thermophys.* **1995**, *16*, 1213-1224.

(47) Ago, K.; Nishiumi, H. Calculation of Mutual Diffusion Coefficients near the Critical Region from the Peng-Robinson Equation of State, *Ind. Eng. Chem. Res.* **1998**, *37*, 1692-1695.

(48) Grossmann, T.; Winkelmann, J. Ternary Diffusion Coefficients of Glycerol + Acetone + Water by Taylor Dispersion Measurements at 298.15 K. 2. Acetone-Rich Region, *J. Chem. Eng. Data* **2007**, *52*, 336-340.

(49) Grossmann, T.; Winkelmann, J. Ternary Diffusion Coefficients of Glycerol + Acetone + Water by Taylor Dispersion Measurements at 298.15 K. 3. Water-Rich Region, *J. Chem. Eng. Data* **2007**, *52*, 341-344.

(50) Vitagliano, V.; Sartorio, R.; Scala, S.; Spaduzzi, D. Diffusion in a Ternary System and the Critical Mixing Point, *J. Solution Chem.* **1978**, *7*, 605-621.

(51) Buzatu, D.; Buzatu, F. D.; Paduano, L.; Sartorio, R. Diffusion Coefficients for the Ternary System Water + Chloroform + Acetic Acid at 25 °C, *J. Solution Chem.* **2007**, *36*, 1373-1384.

(52) Clark, W. M.; Rowley, R. L. Ternary Liquid Diffusion Coefficients Near Plait Points, *Int. J. Thermophys.* **1986**, *6*, 631-642.

(53) Krishna, R. Uphill Diffusion in Multicomponent Mixtures, *Chem. Soc. Rev.* **2015**, *44*, 2812-2836.

(54) Olaya, M. M.; Reyes-Labarta, J. A.; Velasco, R.; Ibarra, I.; Marcilla, A. Modelling liquid–liquid equilibria for island type ternary systems, *Fluid Phase Equilib.* **2008**, *265*, 184-191.

(55) Zuber, A.; Raimundo, R.; Mafra, M. R.; Filho, L. C.; Oliveira, J. V.; Corazza, M. L. Thermodynamic Modeling of Ternary Liquid-Liquid Systems with Forming Immiscibility Islands, *Braz. Arch. Biol. Technol.* **2013**, *56*, 1034-1042.

(56) Santiago, R. S.; Santos, G. R.; Aznar, M. UNIQUAC correlation of liquid–liquid equilibrium in systems involving ionic liquids: The DFT–PCM approach, *Fluid Phase Equilib.* **2009**, *278*, 54-61.

(57) Aznar, M. Correlation of (Liquid + Liquid) Equilibrium of Systems Including Ionic Liquids, *Braz. J. Chem. Eng.* **2007**, *24*, 143-149.

(58) Pertler, M. Die Mehrkomponenten-Diffuson in nicht vollständig mischbaren Flüssigkeiten, Technische Universität München, München, 1996.

(59) Othmer, D. F.; Ku, P. L. Solubility Data for Ternary Liquid Systems. Acetic Acid and Formic Acid Distributed between Chloroform and Water, *J. Chem. Eng. Data* **1960**, *5*, 42-44.

(60) Rogošic, M.; Bakula, M.; Župan, M. Liquid-liquid Equilibria in the Ternary Systems H_2O– Phenol – 2-Butanone and H_2O– Phenol – 2-Propanol, *Chem. Biochem. Eng. Quaterly* **2012**, *26*, 155-162.

(61) Reyes-Labarta, J. A.; Olaya, M. M.; Velasco, R.; Serrano, M. D.; Marcilla, A. Correlation of the liquid–liquid equilibrium data for specific ternary systems with one or two partially miscible binary subsystems, *Fluid Phase Equilib.* **2009**, *278*, 9-14.

(62) Fahim, M. A.; Al-Muhtaseb, S. A.; Al-Nashef, I. M. Liquid-Liquid Equilibria of the Ternary System Water + Acetic Acid + 1-Hexanol, *J. Chem. Eng. Data* **1997**, *42*, 183-186.

(63) Bollen, A. M. Collected tales on mass transfer in liquids, Ph.D. Dissertation, Rijksuniversiteit Groningen, Groningen, 1999. http://dissertations.ub.rug.nl/faculties/science/1999/a.m.bollen/

(64) Kim, J.-K.; Park, D.-W. Liquid-Liquid Equilibrium for the Ternary Systems of Solvents+Water+Propionic Acid at 25 ^{o}C and Atmospheric Pressure, *Korean J. Chem. Eng.* **2005**, *22*, 256-263.

(65) Colombo, A.; Battilana, P.; Ragaini, V.; Bianchi, C. L. Liquid-Liquid Equilibria of the Ternary Systems Water + Acetic Acid + Ethyl Acetate and Water + Acetic Acid + Isophorone (3,5,5-Trimethyl-2-cyclohexen-1-one), *J. Chem. Eng. Data* **1999**, *44*, 35-39.

(66) Zhang, H.; Wang, T. Measurement and Correlation of Liquid-Liquid Equilibrium Data for Water + Acetic Acid + Methyl tert-Butyl Ether + NaCl, *J. Chem. Eng. Data* **2009**, *54*, 945-949.

(67) Mohsen-Nia, M. Ternary liquid–liquid equilibria for mixtures of (ethanol1toluene1n-decane), *Phys. Chem. Liq.* **2007**, *45*, 541-548.

(68) Kärger, J.; Ruthven, D. M.; Theodorou, D. N. Diffusion in Nanoporous Materials; Wiley - VCH: Weinheim, 2012.

(69) Al-Jimaz, A. S.; Fandary, M. S.; Al-Kandary, J. A.; Fahim, M. A. Liquid–liquid equilibria for n-alkanes (C12, C14,C17) + propylbenzene +NMP mixtures at temperatures between 298 and 328K, *Fluid Phase Equilib.* **2005**, *231*, 163-170.

(70) Steltenpohl, P.; Graczová, E. Application of extended NRTL equation for ternary liquid–liquid and vapor–liquid–liquid equilibria description, *Chemical Papers* **2010**, *64*, 310-317. http://dx.doi.org/doi:10.2478/s11696-010-0006-x.

(71) Springer, P. A. M.; Baur, R.; Krishna, R. Composition trajectories for heterogeneous azeotropic distillation in a bubble-cap tray column: Influence of mass transfer, *Chem. Eng. Res. Des.* **2003**, *81*, 413-426.

(72) Wang, H.; Wang, Q.; Xiong, Z.; Chen, C. Liquid–liquid equilibria for ternary system water + toluene + benzaldehyde at (303.2–343.2) K, *Fluid Phase Equilib.* **2014**, *383*, 43-48.

(73) Ruiz, F.; Prats, D.; Gomis, V. Quaternary Liquid-Liquid Equilibrium: Water-Ethanol-ChtoroformToluene at 25 °C. Experimental Determination and Graphical and Analytical Correlation of Equillbrium Data, *J. Chem. Eng. Data* **1985**, *30*, 412-416.

(74) Washburn, E. R.; Beguin, A. E.; Beckford, O. C. The Ternary System: Ethyl Alcohol, Toluene and Water at 25°, *J. Am. Chem. Soc.* **1939**, *61*, 1694-1695.

(75) Tyn, M. T.; Calus, W. F. Temperature and Concentration Dependence of Mutual Diffusion Coefficients of Some Binary Liquid Systems, *J. Chem. Eng. Data* **1975**, *20*, 310-316.

(76) Königer, A.; Meier, B.; Köhler, W. Measurement of the Soret, diffusion, and thermal diffusion coefficients of three binary organic benchmark mixtures and of ethanol–water mixtures using a beam deflection technique, *Philos. Mag.* **2009**, *89*, 907-923.

(77) Clark, W. M.; Rowley, R. L. The mutual diffusion coefficient of methanol - n-hexane near the consolute point, *A.I.Ch.E.J.* **1986**, *32*, 1125-1131.

(78) Derlacki, Z. J.; Easteal, A. J.; Edge, A. V. J.; Woolf, L. A.; Roksandic, Z. DiffusIon Coefficients of Methanol and Water and the Mutual Dlffusion Coefficient in Methanol-Water Solutions at 278 and 298 K, *J. Phys. Chem.* **1995**, *89*, 5318-5322.

(79) Anderson, D. K.; Hall, J. R.; Babb, A. L. Mutual diffusion in non-ideal binary liquid mixtures, *J. Phys. Chem.* **1958**, *62*, 404-408.

(80) Caldwell, C. S.; Babb, A. L. Diffusion in Ideal Binary Liquid Mixtures, *J. Phys. Chem.* **1956**, *60*, 51-56.

(81) Ren, Z.; Fei, W.; Bart, H.-J. Ternary Diffusion Coefficients of 1-Hexanol-Hexane-Toluene and 1-Propanol-Water-Ethylene Glycol by Taylor Dispersion Method, *Tsinghua Science and Technology* **2005**, *10*, 523-528.

(82) Zhu, Q.; Moggridge, G. D.; D'Agostino, C. A local composition model for the prediction of mutual diffusion coefficients in binary liquid mixtures from tracer diffusion coefficients, *Chem. Eng. Sci.* **2015**, *132*, 250-258.

(83) Counsell, J. F.; Everett, D. H.; Munn, R. J. Recent redeterminations of the phase diagram of the system: triethylamine + water, *Pure. Appl. Chem.* **1961**, *2*, 335-338.

(84) Kohler, F.; Rice, O. K. Coexistence Curve of the Triethylamine-Water System, *J. Chem. Phys.* **1957**, *26*, 1614-1618.

20. Caption for Figures

Figure 1. (a, b, c) Experimental data of Takahashi and Hongo[7] for M-S diffusivities of CO_2(trace amounts)/C_2H_4 mixtures, and CO_2/C_2H_4(trace amounts) mixtures at (a) 298.2 K, (b) 323.2 K, and (c) 348.2 K for a range of pressures. (d, e, f) Calculations of the compressibility factor using the Peng-Robinson Equation of State (PR EOS) of CO_2(trace amounts)/C_2H_4 mixtures, and CO_2/C_2H_4(trace amounts) mixtures at (d) 298.2 K, (e) 323.2 K, and (f) 348.2 K for a range of pressures.

Figure 2. MD simulation data of Krishna and van Baten[16] on $D_{i,self}$, $D_{j,self}$, and $Đ_{ij}$ for the binary methane(1)/ethane(2), methane(1)/n-hexane(3), and ethane(2)/n-hexane(3) mixtures. The continuous solid lines are the calculations of $Đ_{ij}$ using either the Darken interpolation equation (48), or the Vignes interpolation formula (49). The values of the self-diffusivities at the limiting compositions, $D_{i,self}^{x_j \to 1}$, are provided in Table 1.

$$Đ_{12}^{x_1 \to 1} = 5.3; \quad Đ_{12}^{x_2 \to 1} = 2.5; \quad Đ_{13}^{x_1 \to 1} = 3; \quad Đ_{13}^{x_3 \to 1} = 1.05; \quad Đ_{23}^{x_2 \to 1} = 1.09; \quad Đ_{23}^{x_3 \to 1} = 0.84.$$

Figure 3. MD simulation data of Krishna and van Baten[16] on $D_{i,self}$, $D_{j,self}$, and $Đ_{ij}$ for the binary methane(1)/ethane(2), methane(1)/propane(3), and ethane(2)/propane (3) mixtures. The continuous solid lines are the calculations of $Đ_{ij}$ using either the Darken interpolation equation (48), or the Vignes interpolation formula (49). The values of the self-diffusivities at the limiting compositions, $D_{i,self}^{x_j \to 1}$, are provided in Table 1.

$$Đ_{12}^{x_1 \to 1} = 5.3; \quad Đ_{12}^{x_2 \to 1} = 2.5; \quad Đ_{13}^{x_1 \to 1} = 4.52; \quad Đ_{13}^{x_3 \to 1} = 1.5; \quad Đ_{23}^{x_2 \to 1} = 1.63; \quad Đ_{23}^{x_3 \to 1} = 1.23.$$

Figure 4. MD simulation data of Krishna and van Baten[16] on $D_{\mathrm{i,self}}$, $D_{\mathrm{j,self}}$, and $Đ_{\mathrm{ij}}$ for the binary methane(1)/propane(2), methane(1)/n-hexane(3), and propane(2)/n-hexane (3) mixtures. The continuous solid lines are the calculations of $Đ_{\mathrm{ij}}$ using either the Darken interpolation equation (48), or the Vignes interpolation formula (49). The values of the self-diffusivities at the limiting compositions, $D_{i,self}^{x_j \to 1}$, are provided in Table 1.

$$Đ_{12}^{x_1 \to 1} = 4.52; \quad Đ_{12}^{x_2 \to 1} = 1.5; \quad Đ_{13}^{x_1 \to 1} = 3; \quad Đ_{13}^{x_3 \to 1} = 1.05; \quad Đ_{23}^{x_2 \to 1} = 0.77; \quad Đ_{23}^{x_3 \to 1} = 0.75.$$

Figure 5. MD simulation data of Krishna and van Baten[16] on $D_{\mathrm{i,self}}$, $D_{\mathrm{j,self}}$, and $Đ_{\mathrm{ij}}$ for the binary ethane(1)/propane(2), ethane(1)/n-butane(3), and propane(2)/n-butane (3) mixtures. The continuous solid lines are the calculations of $Đ_{\mathrm{ij}}$ using either the Darken interpolation equation (48), or the Vignes interpolation formula (49). The values of the self-diffusivities at the limiting compositions, $D_{i,self}^{x_j \to 1}$, are provided in Table 1.

$$Đ_{12}^{x_1 \to 1} = 1.63; \quad Đ_{12}^{x_2 \to 1} = 1.23; \quad Đ_{13}^{x_1 \to 1} = 1.44; \quad Đ_{13}^{x_3 \to 1} = 0.92; \quad Đ_{23}^{x_2 \to 1} = 0.92; \quad Đ_{23}^{x_3 \to 1} = 0.79.$$

Figure 6. MD simulation data of Krishna and van Baten[16] on $D_{\mathrm{i,self}}$, $D_{\mathrm{j,self}}$, and $Đ_{\mathrm{ij}}$ for the binary propane(1)/n-butane(2), propane(1)/n-pentane(3), and n-butane(2)/n-pentane (3) mixtures. The continuous solid lines are the calculations of $Đ_{\mathrm{ij}}$ using either the Darken interpolation equation (48), or the Vignes interpolation formula (49). The values of the self-diffusivities at the limiting compositions, $D_{i,self}^{x_j \to 1}$, are provided in Table 1.

$$Đ_{12}^{x_1 \to 1} = 0.92; \quad Đ_{12}^{x_2 \to 1} = 0.79; \quad Đ_{13}^{x_1 \to 1} = 0.83; \quad Đ_{13}^{x_3 \to 1} = 0.72; \quad Đ_{23}^{x_2 \to 1} = 0.62; \quad Đ_{23}^{x_3 \to 1} = 0.65.$$

Figure 7. Comparison of the Fick diffusivities, D_{12}, with the Maxwell-Stefan, $Đ_{12}$, and Onsager, L_{12}, diffusivities for (a) acetone (1) – water (2), (b) ethanol(1)-water(2), and (c) methanol(1)-n-hexane (2) mixtures. The experimental data on D_{12} are from Tyn and Calus,[75] Grossmann and Winkelmann,[44] Königer et al,[76] and Clark and Rowley[77] The $Đ_{12}$ are obtained by correcting for the thermodynamic factor $Đ_{12} = \frac{D_{12}}{\Gamma}$. Also shown are the calculations using the Vignes interpolation formula (49). The Onsager coefficients L_{12} are calculated using equation (46).

Figure 8. Comparison of the Fick diffusivities, D_{12}, with the Maxwell-Stefan, $Đ_{12}$, diffusivities for (a) water (1) – methanol (2), (b) water (1) - ethanol(3), and (c) methanol (2) - ethanol (3) mixtures at 298 K. The experimental data for the binaries are from Parez et al.[28] with addition of the water/methanol data of Derlacki et al.[78] The thermodynamic factors are calculated using the Wilson parameters reported in Table 4 of Parez et al.[28] Also shown are the calculations using the Vignes interpolation formula (49) with the values of the infinite dilution M-S diffusivities:

$$Đ_{12}^{x_1\to 1} = 1.5; \quad Đ_{12}^{x_2\to 1} = 2.2; \quad Đ_{13}^{x_1\to 1} = 1.3; \quad Đ_{13}^{x_3\to 1} = 1.2; \quad Đ_{23}^{x_2\to 1} = 1.23; \quad Đ_{23}^{x_3\to 1} = 2.03.$$

Figure 9. Influence of pressure on (a) compressibility factor, calculated using the Peng-Robinson Equation of State (PR EOS), (b) thermodynamic factor, Γ, calculated using PR EOS, and (c) Fick diffusivity of $CH_4(1)/C_3H_8(2)$ mixtures at $T = 298.15$ K and $x_1 = 0.7$.

Figure 10. Influence of composition on (a) compressibility factor, calculated using the Peng-Robinson Equation of State (PR EOS), (b) thermodynamic factor, Γ, calculated using PR EOS, and (c) Fick diffusivity of $CH_4(1)/C_3H_8(2)$ mixtures at $T = 298.15$ K.

Figure 11. (a) Experimental data of Sigmund, as reported in Figure 2a of Leahy-Dios and Firoozabadi,[26] for Fick diffusivities of $CH_4(1)/C_3H_8(2)$ mixtures at T = 311 K and p = 137.8 bar. (b) Calculations of the compressibility factor using the Peng-Robinson Equation of State (PR EOS). (c) Calculations of the thermodynamic factor, Γ, using PR EOS. (d) Experimental data of Sigmund, as reported in Figure 2c of Leahy-Dios and Firoozabadi,[26] for Fick diffusivities of $CH_4(1)/C_3H_8(2)$ mixtures at T = 311 K and p = 206.8 bar.

Figure 12. Experimental data of Tuan et al.[10] for the dependence of the Fick diffusivity of methyl oleate (MO) (component 2) in supercritical CO_2 (component 1), indicated by green squares, on the mole fraction of MO for T = 313.15 K, and (a) p = 10.6 MPa, and (b) p = 11.5 MPa. Also shown by the continuous solid lines are the calculations of the thermodynamic factor using the PR EOS.

Figure 13. MD simulation data of Krishna and van Baten[16] on the elements of [Λ] for ternary methane(1)/ethane(2)/n-hexane(3) mixtures compared with the estimations using Vignes interpolation formula (63), combined with either equation (65) or equation (66).

Figure 14. MD simulation data of Krishna and van Baten[16] on the elements [Λ] for ternary methane(1)/ethane(2)/propane (3) mixtures compared with the estimations using Vignes interpolation formula (63), combined with either equation (65) or equation (66).

Figure 15. MD simulation data of Krishna and van Baten[16] on the elements of [Λ] for ternary methane(1)/propane(2)/n-hexane (3) mixtures compared with the estimations using Vignes interpolation formula (63), combined with either equation (65) or equation (66).

Figure 16. MD simulation data of Krishna and van Baten[16] on the elements of [Λ] for ternary ethane(1)/propane(2)/n-butane(3) mixtures compared with the estimations using Vignes interpolation formula (63), combined with either equation equation (65) or equation (66).

Figure 17. MD simulation data of Krishna and van Baten[16] on the elements of [Λ] for ternary propane(1)/n-butane(2)/n-pentane (3) mixtures compared with the estimations using Vignes interpolation formula (63), combined either equation (65) or equation (66).

Figure 18. Comparison of the values of MD simulated values (red circles) of $|\Lambda|^{1/2}$ with calculations (crosses) using the formula $|\Lambda|^{1/2} = \sqrt{\frac{Đ_{12}Đ_{13}Đ_{23}}{x_1Đ_{23}+x_2Đ_{13}+x_3Đ_{12}}}$ where the $Đ_{12}$, $Đ_{13}$, and $Đ_{23}$ are calculated using Vignes interpolation formula (63), combined with Wesselingh-Bollen interpolation (65).

Figure 19. Comparison of the values of MD simulated values of $|\Lambda|^{1/2}$ with calculations of $\left(D_{1,self}\right)^{x_1}\left(D_{2,self}\right)^{x_2}\left(D_{3,self}\right)^{x_3}$ where the component self-diffusivities are also values determined from MD simulations.

Figure 20. MD simulation data of Krishna and van Baten[16] on $Đ_{12}$, $Đ_{13}$, and $Đ_{23}$ in the ternary methane(1)/ethane(2)/n-hexane(3) mixtures: $x_1 = 0.2$, varying x_2, x_3; $x_2 = 0.2$, varying x_1, x_3; $x_3 = 0.2$,

varying x_1, x_2. The continuous solid lines are the calculations of $Đ_{ij}$ using Vignes interpolation formula (63), combined with Wesselingh-Bollen interpolation (65).

Figure 21. MD simulation data of Krishna and van Baten[16] on $Đ_{12}$, $Đ_{13}$, and $Đ_{23}$ in the ternary methane(1)/ethane(2)/n-hexane(3) mixtures: vary x_1, with x_2/x_3= 1; vary x_2, with x_1/x_3= 1; vary x_3, with x_1/x_2= 1. The continuous solid lines are the calculations of $Đ_{ij}$ using Vignes interpolation formula (63), combined with Wesselingh-Bollen interpolation (65).

Figure 22. MD simulation data of Krishna and van Baten[16] on $Đ_{12}$, $Đ_{13}$, and $Đ_{23}$ in the ternary methane(1)/ethane(2)/propane(3) mixtures: vary x_1, with x_2/x_3= 1; vary x_2, with x_1/x_3= 1; vary x_3, with x_1/x_2= 1. The continuous solid lines are the calculations of $Đ_{ij}$ using Vignes interpolation formula (63), combined with Wesselingh-Bollen interpolation (65).

Figure 23. MD simulation data of Krishna and van Baten[16] on $Đ_{12}$, $Đ_{13}$, and $Đ_{23}$ in the ternary methane(1)/propane(2)/n-hexane(3) mixtures: vary x_1, with x_2/x_3= 1; vary x_2, with x_1/x_3= 1; vary x_3, with x_1/x_2= 1. The continuous solid lines are the calculations of $Đ_{ij}$ using Vignes interpolation formula (63), combined with Wesselingh-Bollen interpolation (65).

Figure 24. MD simulation data of Krishna and van Baten[16] on $Đ_{12}$, $Đ_{13}$, and $Đ_{23}$ in the ternary ethane(1)/propane(2)/n-butane(3) mixtures: vary x_1, with x_2/x_3= 1; vary x_2, with x_1/x_3= 1; vary x_3, with x_1/x_2= 1. The continuous solid lines are the calculations of $Đ_{ij}$ using Vignes interpolation formula (63), combined with Wesselingh-Bollen interpolation (65).

Figure 25. MD simulation data of Krishna and van Baten[16] on $Đ_{12}$, $Đ_{13}$, and $Đ_{23}$ in the ternary propane(1)/n-butane(2)/n-pentane(3) mixtures: vary x_1, with x_2/x_3= 1; vary x_2, with x_1/x_3= 1; vary x_3, with x_1/x_2= 1. The continuous solid lines are the calculations of $Đ_{ij}$ using Vignes interpolation formula (63), combined with Wesselingh-Bollen interpolation (65).

Figure 26. Comparison of the values of MD simulated values (from Parez et al.[28], denoted as red circles) of $|\Lambda|^{1/2}$ for water(1)/methanol(2)/ethanol(3) mixtures, as a function of the mole fraction of methanol (component 2), with calculations (crosses) data using $|\Lambda|^{1/2} = \left(D_{1,self}\right)^{x_1}\left(D_{2,self}\right)^{x_2}\left(D_{3,self}\right)^{x_3}$, taking $D_{1,\text{self}}$= 10.3, $D_{2,\text{self}}$= 18, $D_{3,\text{self}}$= 9.1 with units 10^{-10} m^2 s^{-1}.

Figure 27. Comparison of the Fick and Maxwell-Stefan diffusivities for (a) acetone(1)/benzene(2), (b) acetone(1)/carbon tetrachloride (3), and (c) benzene (2)/carbon tetrachloride (3) mixtures. The Fick diffusivity data are culled from Cullinan and Toor[29], Anderson et al.[79], and Caldwell and Babb.[80] Also shown are the calculations using the Vignes interpolation formula (49). The required NRTL parameters for calculation of thermodynamic factors are provided in Table 2.

Figure 28. Comparison of the experimental data of Cullinan and Toor[29] for the elements of the Fick diffusivity matrix [D] for acetone(1)/benzene(2)/carbon-tetrachloride(3) mixtures with the estimations using Vignes interpolation formula (63), combined with Wesselingh-Bollen interpolation (65). The required NRTL parameters for calculation of thermodynamic factors are provided in Table 2. Also plotted are two additional data points for [D] that are reported in Table 2 of Ren et al.[81]

Figure 29. The ratio $|\Lambda|^{1/2} = \frac{|D|^{1/2}}{|\Gamma|^{1/2}}$ plotted as a function of the mole fraction of acetone in acetone(1)/benzene(2)/carbon-tetrachloride(3) mixtures at 298 K. The crosses represent calculations using the formula $|\Lambda|^{1/2} = \sqrt{\frac{Đ_{12}Đ_{13}Đ_{23}}{x_1Đ_{23}+x_2Đ_{13}+x_3Đ_{12}}}$ where the $Đ_{12}$, $Đ_{13}$, and $Đ_{23}$ are calculated using Vignes interpolation formula (63), combined with Wesselingh-Bollen interpolation (65). Also plotted are two additional data points for [D] that are reported in Table 2 of Ren et al.[81]

Figure 30. Comparison of the experimental data of Cullinan and Toor[29] for the elements of the Fick diffusivity matrix [D] for acetone(1)/benzene(2)/carbon-tetrachloride(3) mixtures with the estimations using $[D] = |\Lambda|^{1/2}[\Gamma]$, where $|\Lambda|^{1/2} = \sqrt{\frac{Đ_{12}Đ_{13}Đ_{23}}{x_1Đ_{23}+x_2Đ_{13}+x_3Đ_{12}}}$ and the $Đ_{12}$, $Đ_{13}$, and $Đ_{23}$ are calculated using Vignes interpolation formula (63), combined with Wesselingh-Bollen interpolation (65). The required NRTL parameters for calculation of thermodynamic factors are provided in Table 2. Also plotted are two additional data points for [D] that are reported in Table 2 of Ren et al.[81]

Figure 31. Comparison of the Fick and Maxwell-Stefan diffusivities for (a) acetone(1)/benzene(2), (b) acetone(1)/methanol (3), and (c) benzene (2)/methanol (3) mixtures. The Fick diffusivity data are culled from Cullinan and Toor[29], Anderson et al.[79], Zhu et al.[82], and Alimadadian and Colver.[30] Also shown are the calculations using the Vignes interpolation formula (49). The required NRTL parameters for calculation of thermodynamic factors are provided in Table 3.

Figure 32. The ratio $\frac{|D|^{1/2}}{|\Gamma|^{1/2}}$ plotted as a function of the mole fraction of acetone in acetone(1)/benzene(2)/methanol(3) mixtures. The Fick diffusivity data are from Alimadadian and Colver;[30] the NRTL parameters are provided in Table 3. The crosses represent calculations using the formula $|\Lambda|^{1/2} = \sqrt{\frac{Đ_{12}Đ_{13}Đ_{23}}{x_1Đ_{23}+x_2Đ_{13}+x_3Đ_{12}}}$ where the $Đ_{12}$, $Đ_{13}$, and $Đ_{23}$ are calculated using Vignes interpolation formula (63), combined with Wesselingh-Bollen interpolation (65).

Figure 33. Comparison of the experimental data of Alimadadian and Colver;[30] for the elements of the Fick diffusivity matrix [D] for acetone(1)/benzene(2)/methanol(3) mixtures with the estimations using $[D]=|\Lambda|^{1/2}[\Gamma]$, where $|\Lambda|^{1/2} = \sqrt{\frac{Đ_{12}Đ_{13}Đ_{23}}{x_1Đ_{23}+x_2Đ_{13}+x_3Đ_{12}}}$ and the $Đ_{12}$, $Đ_{13}$, and $Đ_{23}$ are calculated using Vignes interpolation formula (63), combined with Wesselingh-Bollen interpolation (65). The NRTL parameters are provided in Table 3.

Figure 34. The ratio $\frac{D_{12}D_{21}}{D_{11}D_{22}}$ of the elements of the Fick diffusivity matrix [D] for acetone(1)/benzene(2)/methanol (3) mixtures (experimental data of Alimadadian and Colver[30]) plotted against the corresponding value of the ratio $\frac{\Gamma_{12}\Gamma_{21}}{\Gamma_{11}\Gamma_{22}}$.

Figure 35. The ratio $\frac{|D|^{1/2}}{|\Gamma|^{1/2}}$ plotted as a function of the mole fraction of methanol in methanol(1)/1-propanol(2)/iso-butanol(3) mixtures. The Fick diffusivity data are from Shuck and Toor[32]; the NRTL parameters are provided in Table 4. The crosses represent calculations using the formula $|\Lambda|^{1/2} = \sqrt{\frac{Đ_{12}Đ_{13}Đ_{23}}{x_1Đ_{23}+x_2Đ_{13}+x_3Đ_{12}}}$ where the $Đ_{12}$, $Đ_{13}$, and $Đ_{23}$ are calculated using Vignes interpolation formula (63), combined with Wesselingh-Bollen interpolation (65), along with the M-S diffusivities as provided by Kooijman and Taylor.[31]

$$Đ_{12}^{x_1\to 1}=1.966;\quad Đ_{12}^{x_2\to 1}=0.804;\quad Đ_{13}^{x_1\to 1}=1.83;\quad Đ_{13}^{x_3\to 1}=0.587;\quad Đ_{23}^{x_2\to 1}=0.584;\quad Đ_{23}^{x_3\to 1}=0.398.$$

Figure 36. Comparison of the experimental data of Shuck and Toor[32] for the elements of the Fick diffusivity matrix [D] for methanol(1)/1-propanol(2)/iso-butanol(3) mixtures with the estimations using $[D]=|\Lambda|^{1/2}[\Gamma]$, where $|\Lambda|^{1/2} = \sqrt{\frac{Đ_{12}Đ_{13}Đ_{23}}{x_1Đ_{23}+x_2Đ_{13}+x_3Đ_{12}}}$ and the $Đ_{12}$, $Đ_{13}$, and $Đ_{23}$ are calculated using Vignes interpolation formula (63), combined with Wesselingh-Bollen interpolation (65). The NRTL parameters are provided in Table 4.

Figure 37. The ratio $\frac{D_{12}D_{21}}{D_{11}D_{22}}$ of the elements of the Fick diffusivity matrix [D] for in methanol(1)/1-propanol(2)/iso-butanol(3) mixtures (experimental data of Shuck and Toor[32]) plotted against the corresponding value of the ratio $\frac{\Gamma_{12}\Gamma_{21}}{\Gamma_{11}\Gamma_{22}}$.

Figure 38. The ratio $\frac{|D|^{1/2}}{|\Gamma|^{1/2}}$ plotted as a function of the mole fraction of glycerol in 2-propanol(1)/glycerol(2)/iso-water(3) mixtures. The experimental data are from Riede and Schlünder.[33]

Figure 39. Experimental data of Rehfeldt[36, 37] for the Fick diffusivities of the constituent binary pairs of methanol(1)/1-butanol(2)/1-propanol(3) mixtures at 298 K. Also shown are the M-S diffusivities, along with the estimations using the Vignes interpolation formula (49). The calculation of thermodynamic factors are based on the Wilson parameters reported in Table 9.2 of the dissertation of Rehfeldt.[37]

Figure 40. Experimental data of Rehfeldt[36, 37] for the Fick diffusivities of the constituent binary pairs of acetone(1)/water(2)/1-propanol(3) mixtures at 298 K. Also shown are the M-S diffusivities, along with the estimations using the Vignes interpolation formula (49). The calculation of thermodynamic factors are based on the Wilson parameters reported in Table 9.2 of the dissertation of Rehfeldt.[37]

Figure 41. Experimental data of Rehfeldt[36, 37] for the Fick diffusivities of the constituent binary pairs of acetone(1)/1-butanol(2)/1-propanol(3) mixtures at 298 K. Also shown are the M-S diffusivities, along with the estimations using the Vignes interpolation formula (49). The calculation of thermodynamic factors are based on the Wilson parameters reported in Table 9.2 of the dissertation of Rehfeldt.[37]

Figure 42. Experimental data of Rehfeldt[36, 37] for the Fick diffusivities of the constituent binary pairs of 1-propanol(1)/1-chlorobutane(2)/n-heptane(3) mixtures at 298 K. Also shown are the M-S diffusivities, along with the estimations using the Vignes interpolation formula (49). The calculation of thermodynamic factors are based on the Wilson parameters reported in Table 9.2 of the dissertation of Rehfeldt.[37]

Figure 43. Comparison of experimental data of Rehfeldt[36, 37] for the Fick diffusivity matrix [*D*] for methanol(1)/1-butanol(2)/1-propanol mixtures at 298 K with the estimations using Vignes interpolation formula (63), combined with Wesselingh-Bollen interpolation (65), along with along with the M-S diffusivities that are determined from data on the constituent binary pairs

$$Đ_{12}^{x_1\to 1}=1.3;\quad Đ_{12}^{x_2\to 1}=0.48;\quad Đ_{13}^{x_1\to 1}=1.37;\quad Đ_{13}^{x_3\to 1}=0.68;\quad Đ_{23}^{x_2\to 1}=0.4;\quad Đ_{23}^{x_3\to 1}=0.51$$

The calculations of the the thermodynamic factor matrix $[\Gamma]$ are based on the Wilson parameters reported in Table 9.2 of the dissertation of Rehfeldt.[37]

Figure 44. Comparison of experimental data of Rehfeldt[36, 37] for the Fick diffusivity matrix [*D*] for acetone(1)/water(2)/1-propanol(3) mixtures at 298 K with the estimations using Vignes interpolation formula (63), combined with Wesselingh-Bollen interpolation (65), along with along with the M-S diffusivities that are determined from data on the constituent binary pairs

$$Đ_{12}^{x_1\to 1}=5.08;\quad Đ_{12}^{x_2\to 1}=1.28;\quad Đ_{13}^{x_1\to 1}=3.17;\quad Đ_{13}^{x_3\to 1}=1.13;\quad Đ_{23}^{x_2\to 1}=1.1;\quad Đ_{23}^{x_3\to 1}=0.68$$

The calculations of the the thermodynamic factor matrix $[\Gamma]$ are based on the Wilson parameters reported in Table 9.2 of the dissertation of Rehfeldt.[37]

Figure 45. Comparison of experimental data of Rehfeldt[36, 37] for the Fick diffusivity matrix [*D*] for acetone(1)/1-butanol(2)/1-propanol(3) mixtures at 298 K with the estimations using Vignes interpolation formula (63), combined with Wesselingh-Bollen interpolation (65), along with along with the M-S diffusivities that are determined from data on the constituent binary pairs

$Đ_{12}^{x_1\to 1}=2.79;\quad Đ_{12}^{x_2\to 1}=0.94;\quad Đ_{13}^{x_1\to 1}=3.17;\quad Đ_{13}^{x_3\to 1}=1.13;\quad Đ_{23}^{x_2\to 1}=0.4;\quad Đ_{23}^{x_3\to 1}=0.51$

The calculations of the the thermodynamic factor matrix $[\Gamma]$ are based on the Wilson parameters reported in Table 9.2 of the dissertation of Rehfeldt.[37]

Figure 46. Comparison of experimental data of Rehfeldt[36, 37] for the Fick diffusivity matrix [*D*] for 1-propanol(1)/1-chlorobutane(2)/n-heptane(3) mixtures at 298 K with the estimations using Vignes interpolation formula (63), combined with Wesselingh-Bollen interpolation (65), along with along with the M-S diffusivities that are determined from data on the constituent binary pairs

$Đ_{12}^{x_1\to 1}=1.2;\quad Đ_{12}^{x_2\to 1}=3.4;\quad Đ_{13}^{x_1\to 1}=1.5;\quad Đ_{13}^{x_3\to 1}=6;\quad Đ_{23}^{x_2\to 1}=2.8;\quad Đ_{23}^{x_3\to 1}=3.5$

The calculations of the the thermodynamic factor matrix $[\Gamma]$ are based on the Wilson parameters reported in Table 9.2 of the dissertation of Rehfeldt.[37]

Figure 47. The ratio $\frac{D_{12}D_{21}}{D_{11}D_{22}}$ of the elements of the Fick diffusivity matrix [*D*] in 1-propanol(1)/1-chlorobutane(2)/n-heptane(3) mixtures (experimental data of Rehfeldt[36, 37]) plotted against the corresponding value of the ratio $\frac{\Gamma_{12}\Gamma_{21}}{\Gamma_{11}\Gamma_{22}}$.

Figure 48. The ratio $|R|^{1/2} = \frac{|D|^{1/2}}{|\Gamma|^{1/2}}$ plotted as a function of the mole fraction of component 1 in four different mixtures: (a) methanol(1)/1-butanol(2)/1-propanol, (b) acetone(1)/water(2)/1-propanol(3), (c) acetone(1)/1-butanol(2)/1-propanol(3), and (d) 1-propanol(1)/1-chlorobutane(2)/n-heptane(3) mixtures at 298 K. The crosses represent calculations using the formula $|\Lambda|^{1/2} = \sqrt{\frac{Đ_{12}Đ_{13}Đ_{23}}{x_1Đ_{23}+x_2Đ_{13}+x_3Đ_{12}}}$ where the $Đ_{12}$, $Đ_{13}$, and $Đ_{23}$ are calculated using Vignes interpolation formula (63), combined with Wesselingh-Bollen interpolation (65).

Figure 49. Comparison of experimental data of Rehfeldt[36, 37] for the Fick diffusivity matrix [D] for methanol(1)/1-butanol(2)/1-propanol mixtures at 298 K with the estimations using $[D] = |\Lambda|^{1/2}[\Gamma]$, where $|\Lambda|^{1/2} = \sqrt{\frac{Đ_{12}Đ_{13}Đ_{23}}{x_1Đ_{23}+x_2Đ_{13}+x_3Đ_{12}}}$ and the $Đ_{12}$, $Đ_{13}$, and $Đ_{23}$ are calculated using Vignes interpolation formula (63), combined with Wesselingh-Bollen interpolation (65).

Figure 50. Comparison of experimental data of Rehfeldt[36, 37] for the Fick diffusivity matrix [D] for acetone(1)/water(2)/1-propanol(3) mixtures at 298 K with the estimations using $[D] = |\Lambda|^{1/2}[\Gamma]$, where $|\Lambda|^{1/2} = \sqrt{\frac{Đ_{12}Đ_{13}Đ_{23}}{x_1Đ_{23}+x_2Đ_{13}+x_3Đ_{12}}}$ and the $Đ_{12}$, $Đ_{13}$, and $Đ_{23}$ are calculated using Vignes interpolation formula (63), combined with Wesselingh-Bollen interpolation (65).

Figure 51. Comparison of experimental data of Rehfeldt[36, 37] for the Fick diffusivity matrix [D] for acetone(1)/1-butanol(2)/1-propanol(3) mixtures at 298 K with the estimations using $[D]=|\Lambda|^{1/2}[\Gamma]$, where $|\Lambda|^{1/2}=\sqrt{\frac{Đ_{12}Đ_{13}Đ_{23}}{x_1Đ_{23}+x_2Đ_{13}+x_3Đ_{12}}}$ and the $Đ_{12}$, $Đ_{13}$, and $Đ_{23}$ are calculated using Vignes interpolation formula (63), combined with Wesselingh-Bollen interpolation (65).

Figure 52. Comparison of experimental data of Rehfeldt[36, 37] for the Fick diffusivity matrix [D] for 1-propanol(1)/1-chlorobutane(2)/n-heptane(3) mixtures at 298 K with the estimations using $[D]=|\Lambda|^{1/2}[\Gamma]$, where $|\Lambda|^{1/2}=\sqrt{\frac{Đ_{12}Đ_{13}Đ_{23}}{x_1Đ_{23}+x_2Đ_{13}+x_3Đ_{12}}}$ and the $Đ_{12}$, $Đ_{13}$, and $Đ_{23}$ are calculated using Vignes interpolation formula (63), combined with Wesselingh-Bollen interpolation (65).

Figure 53. Phase equilibrium thermodynamics for Fe(1)/Cr(2) alloy mixtures. (a, b) Gibbs free energy at temperatures of (a) 1200 K, and (b) 800 K, as a function of the atom fraction of Fe(1). (c) Binodal and spinodal curves, as a function of the atom fraction of Fe(1). (d) Activity coefficients, γ_i, of Fe(1) and Cr(2) in solution, as a function of the atom fraction of Fe(1). (e) Activities, a_i, of Fe(1) and Cr(2) , as a function of the atom fraction of Fe(1).

Figure 54. (a) Liquid/liquid phase equilibrium for triethylamine (1) – water (2) mixture exhibiting LCST at 291.5 K. The experimental data for the binodal and spinodal curves are taken from Counsell et al.,[83] Kohler and Rice,[84] and Vitagliano et al.[41] (b) Experimental data of Vitagliano et al.[41] for Fick

diffusivities, D_{12}, for triethyamine(1)/water(2) mixtures, measured at two different temperatures 292.15 K, and 293.15 K, for various compositions on either side of the spinodal curves in (a).

Figure 55. Experimental data of Pertler et al.[42] for Fick diffusivities, D_{12}, for 1-butanol(1)/water(2) mixtures, measured at 298.15 K for various compositions on either side of the spinodal compositions. The UNIQUAC parameters are provided Table 3 of Pertler et al.[42]

Figure 56. Experimental data of Thiel et al.[43] for Fick diffusivities, D_{12}, for methyl isopropyl ketone(1)/water(2) mixtures, measured at 293.15 K (water rich region) and 298.15 (MIPK rich region) for various compositions on either side of the spinodal compositions. The UNIQUAC parameters are provided Table 3 of Pertler et al.[42]

Figure 57. Experimental data of Grossmann and Winkelmann,[44] and Pertler et al.[42] for Fick diffusivities, D_{12}, for glycerol(1)/acetone(2) mixtures, measured at 298.15 K for various compositions in the acetone-rich region to the left of the spinodal composition. The NRTL parameters are provided in Table 5.

Figure 58. Experimental data of McKeigue and Gulari[45] for Fick diffusivities, D_{12}, for methanol(1)/CS_2(2) mixtures, measured at 293.15 K for various compositions in the CS_2-rich region to the left of the spinodal composition. The UNIQUAC parameters are provided Table 3 of Pertler et al.[42]

Figure 59. (a) Experimental data of Dysthe and Hafskjold[46] for Fick diffusivities of $CH_4(1)$/n-$C_{10}H_{22}(2)$ mixtures at T = 303.5 K and p = 40 MPa. (b) Experimental data of Dysthe and Hafskjold[46] for Fick diffusivities of $CH_4(1)$/n-$C_{10}H_{22}(2)$ mixtures at T = 303.5 K and p = 40, 50 and 60 MPa. (c) Spinodal compostions for $CH_4(1)$/n-$C_{10}H_{22}(2)$ mixtures at T = 303.5 K. (d) Experimental data of Dysthe and Hafskjold[46] for Fick diffusivities of $CH_4(1)$/n-$C_{10}H_{22}(2)$ mixtures at T = 303.5 K and x_1= 0.903, with varying total pressures. (e) Calculations of the compressibility factor using the Peng-Robinson Equation of State (PR EOS) at five different pressures. (f) Calculations of the thermodynamic factor, Γ, using PR EOS at five different pressures.

Figure 60. (a) Experimental data of Ago and Nishiumi[47] for diffusivity of benzene in supercritical CO_2 as a function of the total pressure. The measurements are made in a Taylor dispersion tube with varying amounts of benzene injection into the tube. (c) Calculations of the compressibility factor using the Peng-Robinson Equation of State (PR EOS). (f) Calculations of the thermodynamic factor, Γ, using PR EOS. Calculations of the Fick diffusivities as a function of pressure and composition of benzene in the mixture using the PR EOS.

Figure 61. Schematic showing liquid/liquid phase equilibrium for a hypothetical ternary liquid mixture. The binodal and spinodal curves converge at the plait point. Consider two mixtures of compositions A and B are brought into contact. The average mixture composition (M) falls within in the two-phase region. Each of the mixtures A and B will equilibrate to the compositions at the two ends of the tie-line corresponding to the mixture composition M. The mixture with a composition M will split into two phases at either end of the tie-line.

Figure 62. The phase equilibrium diagram for glycerol(1)/acetone(2)/water(3) mixtures at 298 K.[9] The composition of the plait point is: x_{glycerol}= 0.1477, x_{acetone}= 0.4163 and x_{water}= 0.4360. Also indicated are the 75 compositions for which Grossmann and Winkelmann[44, 48, 49] have measured the Fick diffusivity matrix [D] for glycerol(1)/acetone(2)/water(3) mixtures. As indicated, at x_1= 0.18, x_2 = 0.22, x_3 = 0.6, $[D] = \begin{bmatrix} 0.294 & 0.127 \\ 0.148 & 0.213 \end{bmatrix} \times 10^{-9}$ m^2 s^{-1}, and $|D| = 0.044 \times 10^{-18}$ m^4 s^{-2}. The spinodal curve is calculated using the constraint $|H| = 0; \quad |\Gamma| = 0; \quad$ spinodal curve ; for this purpose the phase equilibrium is determined from the NRTL parameters in Table 5.

Figure 63. Plot of $|D|^{1/2}$ for glycerol(1)/acetone(2)/water(3) mixtures as a function of the mole fraction of glycerol, x_1.

Figure 64. The ratio $\frac{D_{12}D_{21}}{D_{11}D_{22}}$ of the elements of the Fick diffusivity matrix [D] for glycerol(1)/acetone(2)/water(3) mixtures plotted against the corresponding value of the ratio $\frac{\Gamma_{12}\Gamma_{21}}{\Gamma_{11}\Gamma_{22}}$.

Figure 65. The ratio $\frac{|D|^{1/2}}{|\Gamma|^{1/2}}$ for glycerol(1)/acetone(2)/water(3) mixtures plotted (a) as a function of the the mole fractions of acetone, x_2, and water x_3 and (b) only as a function of the mole fraction of acetone, x_2. In (b), the crosses represent a model fit of the data using $|\Lambda|^{1/2} = \left(D_{1,self}\right)^{x_1}\left(D_{2,self}\right)^{x_2}\left(D_{3,self}\right)^{x_3}$, taking $D_{1,\text{self}}$= 0.01, $D_{2,\text{self}}$= 3.2, $D_{3,\text{self}}$= 0.5 with units 10^{-9} m^2 s^{-1}.

Figure 66. Comparison of experimental data for the Fick diffusivity matrix [D] for glycerol(1)/acetone(2)/water(3) mixtures with the estimations using $[D]=|\Lambda|^{1/2}[\Gamma]$ with $|\Lambda|^{1/2}=(D_{1,self})^{x_1}(D_{2,self})^{x_2}(D_{3,self})^{x_3}$, taking $D_{1,\mathrm{self}}$= 0.01, $D_{2,\mathrm{self}}$= 3.2, $D_{3,\mathrm{self}}$= 0.5 with units 10^{-9} m^2 s^{-1}.

Figure 67. Experimental data of Vitagliano et al.[50] for Fick diffusivity matrix [D] of water(1)/chloroform(2)/acetic-acid(3) mixtures at six different compositions. The measured values of the Fick matrix [D], in units of 10^{-9} m^2 s^{-1}, are indicated. The composition of the plait point is x_1 = 0.375, x_2= 0.262, x_3= 0.363. The binodal curve is from the experimental data of Othmer and Ku.[59] The spinodal curve is obtained from the criterion of phase stability; the UNIQUAC parameters are provided in Table 6.

Figure 68. Experimental data of Buzatu et al.[51] for Fick diffusivity matrix [D] of water(1)/chloroform(2)/acetic-acid(3) mixtures at six different compositions. The measured values of the Fick matrix [D], in units of 10^{-9} m^2 s^{-1}, are indicated. The composition of the plait point is x_1 = 0.375, x_2= 0.262, x_3= 0.363. The binodal curve is from the experimental data of Othmer and Ku.[59] The spinodal curve is obtained from the criterion of phase stability; the UNIQUAC parameters are provided in Table 6.

Figure 69. Plot of $|D|^{1/2}$ as a function of (1- x_3) for water(1)/chloroform(2)/acetic-acid(3) mixtures.

Figure 70. The ratio $\frac{D_{12}D_{21}}{D_{11}D_{22}}$ of the elements of the Fick diffusivity matrix [D] for water(1)/chloroform(2)/acetic-acid(3) mixtures plotted against the corresponding value of the ratio $\frac{\Gamma_{12}\Gamma_{21}}{\Gamma_{11}\Gamma_{22}}$.

Figure 71. The ratio $\frac{|D|^{1/2}}{|\Gamma|^{1/2}}$ for water(1)/chloroform(2)/acetic-acid(3) mixtures plotted as a function of (1- x_3). The crosses represent a model fit of the data using $|\Lambda|^{1/2} = (D_{1,self})^{x_1}(D_{2,self})^{x_2}(D_{3,self})^{x_3}$, taking $D_{1,\text{self}}$= 0.4, $D_{2,\text{self}}$= 0.8, $D_{3,\text{self}}$= 1.1 with units 10^{-9} m^2 s^{-1}.

Figure 72. Comparison of experimental data for the Fick diffusivity matrix [D] for water(1)/chloroform(2)/acetic-acid(3) mixtures with the estimations using $[D]=|\Lambda|^{1/2}[\Gamma]$ with estimates based on $|\Lambda|^{1/2} = (D_{1,self})^{x_1}(D_{2,self})^{x_2}(D_{3,self})^{x_3}$, taking $D_{1,\text{self}}$= 0.4, $D_{2,\text{self}}$= 0.8, $D_{3,\text{self}}$= 1.1 with units 10^{-9} m^2 s^{-1}.

Figure 73. Experimental data of Clark and Rowley[52] for $|D|^{1/2}$ for water(1)/2-propanol(2)/cyclohexane(3) mixtures as function of ($T - T_c$) where T is the temperature at which the diffusivities are measured, with T_c = 303.67 K. The elements of the Fick matrix of diffusivities were measured at a constant composition of the plait point at 303.67 K: x_1 = 0.367, x_2= 0.389, x_3= 0.244. The measured values of the Fick matrix [D], in units of 10^{-10} m^2 s^{-1}, are also indicated.

Figure 74. Equilibration trajectories in glycerol(1)/acetone(2)/water(3) mixtures at 298 K for the equilibrium composition x_1= 0.1, x_2 = 0.432, x_3 = 0.468. The plot is in 2D composition space. The

dashed line represents simulations of transient trajectories using the Fick diffusivity matrix following the experimental data of Grossmann and Winkelmann:[44, 48, 49] $[D]=\begin{bmatrix}0.4901 & 0.2267\\ 0.4585 & 0.3991\end{bmatrix}\times 10^{-9}$ $m^2\ s^{-1}$. The continuous solid line is the trajectories calculated using $[D]=|\Lambda|^{1/2}[\Gamma]$ with $|\Lambda|^{1/2}=\left(D_{1,self}\right)^{x_1}\left(D_{2,self}\right)^{x_2}\left(D_{3,self}\right)^{x_3}$, taking $D_{1,\mathrm{self}}$= 0.01, $D_{2,\mathrm{self}}$= 3.2, $D_{3,\mathrm{self}}$= 0.5 with units 10^{-9} $m^2\ s^{-1}$: $|\Lambda|^{1/2}=0.754\times 10^{-9}$ $m^2\ s^{-1}$. The phase equilibrium is determined from the NRTL parameters in Table 5.

Figure 75. Equilibration trajectories in glycerol(1)/acetone(2)/water(3) mixtures at 298 K for the equilibrium composition x_1= 0.18, x_2 = 0.22, x_3 = 0.6. The plot is in 2D composition space. The dashed line represent simulations of transient trajectories using the Fick diffusivity matrix following the experimental data of Grossmann and Winkelmann:[44, 48, 49] $[D]=\begin{bmatrix}0.2938 & 0.1271\\ 0.1483 & 0.2127\end{bmatrix}\times 10^{-9}$ $m^2\ s^{-1}$. The continuous solid line represents the trajectory calculated using $[D]=|\Lambda|^{1/2}[\Gamma]$ with $|\Lambda|^{1/2}=\left(D_{1,self}\right)^{x_1}\left(D_{2,self}\right)^{x_2}\left(D_{3,self}\right)^{x_3}$, taking $D_{1,\mathrm{self}}$= 0.01, $D_{2,\mathrm{self}}$= 3.2, $D_{3,\mathrm{self}}$= 0.5 with units 10^{-9} $m^2\ s^{-1}$, yielding $|\Lambda|^{1/2}=0.372\times 10^{-9}$ $m^2\ s^{-1}$. The phase equilibrium is determined from the NRTL parameters in Table 5.

Figure 76. Transient inter-diffusion in a diffusion couple consisting of water(1)/chloroform(2)/acetic-acid(3) mixtures. The values of the Fick diffusivity matrix is $[D]=\begin{bmatrix}0.309 & 0.368\\ 0.344 & 0.939\end{bmatrix}\times 10^{-9}$ $m^2\ s^{-1}$; $|D|=0.164\times 10^{-18}$ $m^4\ s^{-2}$, corresponding to the fifth data set of Vitagliano et al.[50] The binodal curve is from the experimental data of Othmer and Ku.[59]

Figure 77. Trajectory followed during equilibration of homogenous mixtures of two different compositions for the system glycerol(1)/acetone(2)/water(3); the equilibrium composition $x_{1,eq}$ = 0.5, $x_{2,eq}$ = 0.17 and $x_{3,eq}$ = 0.33. The NRTL parameters for calculation of the phase equilibrium thermodynamics are provided in Table 5.

Figure 78. Trajectory followed during equilibration of homogenous mixtures of two different compositions for the system water(1)/DMSO(2)/THF(3); the equilibrium composition $x_{1,eq}$ = 0.625, $x_{2,eq}$ = 0.21 and $x_{3,eq}$ = 0.165. The NRTL parameters for calculation of the phase equilibrium thermodynamics are provided in Table 7.

Figure 79. Trajectory followed during equilibration of homogenous mixtures of two different compositions for the system water(1)/DMSO(2)/THF(3); the equilibrium composition $x_{1,eq}$ = 0.7, $x_{2,eq}$ = 0.16 and $x_{3,eq}$ = 0.14. The NRTL parameters for calculation of the phase equilibrium thermodynamics are provided in Table 8.

Figure 80. Trajectory followed during equilibration of homogenous mixtures of two different compositions for the system water(1)/acetone(2)/phenol(3); the equilibrium composition $x_{1,eq}$ = 0.42, $x_{2,eq}$ = 0.42 and $x_{3,eq}$ = 0.15. The NRTL parameters for calculation of the phase equilibrium thermodynamics are provided in Table 9.

Figure 81. Trajectory followed during equilibration of homogenous mixtures of two different compositions for the system water(1)/acetone(2)/TCE(3); the equilibrium composition $x_{1,eq}$ = 0.05, $x_{2,eq}$

= 0.08 and $x_{3,eq}$ = 0.87. The NRTL parameters for calculation of the phase equilibrium thermodynamics are provided in Table 10.

Figure 82. Trajectory followed during equilibration of homogenous mixtures of two different compositions for the system water(1)/2-propanol(2)/phenol(3); the equilibrium composition $x_{1,eq}$ = 0.61, $x_{2,eq}$ = 0.22 and $x_{3,eq}$ = 0.17. The NRTL parameters for calculation of the phase equilibrium thermodynamics are provided in Table 11.

Figure 83. Trajectory followed during equilibration of homogenous mixtures of two different compositions for the system water(1)/trichloroacetic acid (2)/antipyrine(3); the equilibrium composition $x_{1,eq}$ = 0.35, $x_{2,eq}$ = 0.32 and $x_{3,eq}$ = 0.33. The NRTL parameters for calculation of the phase equilibrium thermodynamics are provided in Table 12.

Figure 84. Trajectory followed during equilibration of homogenous mixtures of two different compositions for the system acetone(1)/ethyl-acetate(2)/water(3); the equilibrium composition $x_{1,eq}$ = 0.28, $x_{2,eq}$ = 0.415 and $x_{3,eq}$ = 0.305. The UNIQUAC parameters for calculation of the phase equilibrium thermodynamics are provided in Table 13.

Figure 85. Trajectory followed during equilibration of homogenous mixtures of two different compositions for the system propyl acetate (1)/formic acid(2)/water(3); the equilibrium composition

$x_{1,eq}$ = 0.5, $x_{2,eq}$ = 0.17 and $x_{3,eq}$ = 0.33. The NRTL parameters for calculation of the phase equilibrium thermodynamics are provided in Table 14.

Figure 86. Trajectory followed during equilibration of homogenous mixtures of two different compositions for the system furfural(1)/formic acid(2)/water (3); the equilibrium composition $x_{1,eq}$ = 0.58, $x_{2,eq}$ = 0.054 and $x_{3,eq}$ = 0.366. The NRTL parameters for calculation of the phase equilibrium thermodynamics are provided in Table 15.

Figure 87. Trajectory followed during equilibration of homogenous mixtures of two different compositions for the system 1-butanol (1)/methanol(2)/water(3); the equilibrium composition $x_{1,eq}$ = 0.3, $x_{2,eq}$ = 0.046 and $x_{3,eq}$ = 0.654. The NRTL parameters for calculation of the phase equilibrium thermodynamics are provided in Table 16.

Figure 88. Trajectory followed during equilibration of homogenous mixtures of two different compositions for the system water(1)/acetic acid(2)/dichloromethane(3); the equilibrium composition $x_{1,eq}$ = 0.13, $x_{2,eq}$ = 0.25 and $x_{3,eq}$ = 0.62. The NRTL parameters for calculation of the phase equilibrium thermodynamics are provided in Table 17.

Figure 89. Trajectory followed during equilibration of homogenous mixtures of two different compositions for the system water(1)/acetic acid(2)/1-hexanol(3); the equilibrium composition $x_{1,eq}$ = 0.425, $x_{2,eq}$ = 0.19 and $x_{3,eq}$ = 0.385. The NRTL parameters for calculation of the phase equilibrium thermodynamics are provided in Table 18.

Figure 90. Trajectory followed during equilibration of homogenous mixtures of two different compositions for the system toluene(1)/acetaldehyde(2)/water(3); the equilibrium composition is $x_{1,eq}$ = 0.4075, $x_{2,eq}$ = 0.545 and $x_{3,eq}$ = 0.0475. The NRTL parameters for calculation of the phase equilibrium thermodynamics are provided in Table 19.

Figure 91. Trajectory followed during equilibration of homogenous mixtures of two different compositions for the system 1-hexanol(1)/nitromethane(2)/water(3); the equilibrium composition is $x_{1,eq}$ = 0.22, $x_{2,eq}$ = 0.56 and $x_{3,eq}$ = 0.22. The NRTL parameters for calculation of the phase equilibrium thermodynamics are provided in Table 20.

Figure 92. Trajectory followed during equilibration of homogenous mixtures of two different compositions for the system 4-methyl-2-pentanone(1)/acetonitrile(2)/water(3); the equilibrium composition is $x_{1,eq}$ = 0.09, $x_{2,eq}$ = 0.54, and $x_{3,eq}$ = 0.37. The NRTL parameters for calculation of the phase equilibrium thermodynamics are provided in Table 21.

Figure 93. Trajectory followed during equilibration of homogenous mixtures of two different compositions for the system acetonitrile(1)/1-propanol(2)/hexane(3); the equilibrium compositions (left hand side of diagram) $x_{1,eq}$ = 0.575, $x_{2,eq}$ = 0.24 and $x_{3,eq}$ = 0.185, and (right hand side of diagram) $x_{1,eq}$ = 0.175, $x_{2,eq}$ = 0.17 and $x_{3,eq}$ = 0.655. The NRTL parameters for calculation of the phase equilibrium thermodynamics are provided in Table 22.

Figure 94. Trajectory followed during equilibration of homogenous mixtures of two different compositions for the system water(1)/caprolactam(2)/toluene(3); the equilibrium composition $x_{1,eq}$ = 0.645, $x_{2,eq}$ = 0.27 and $x_{3,eq}$ = 0.085. The UNIQUAC parameters for calculation of the phase equilibrium thermodynamics are provided in Table 23.

Figure 95. Trajectory followed during equilibration of homogenous mixtures of two different compositions for the system water(1)/caprolactam(2)/benzene (3); the equilibrium composition x_1= 0.125, x_2 = 0.17, x_3 = 0.705. The UNIQUAC parameters for calculation of the phase equilibrium thermodynamics are provided in Table 24.

Figure 96. Trajectory followed during equilibration of homogenous mixtures of two different compositions for the system for toluene(1)/propionic-acid (2)/water(3); the equilibrium composition $x_{1,eq}$ = 0.47, $x_{2,eq}$ = 0.24 and $x_{3,eq}$ = 0.29. The UNIQUAC parameters for calculation of the phase equilibrium thermodynamics are provided in Table 25.

Figure 97. Trajectory followed during equilibration of homogenous mixtures of two different compositions for the system for ethylacetate(1)/propionic-acid(2)/water(3); the equilibrium composition $x_{1,eq}$ = 0.675, $x_{2,eq}$ = 0.13 and $x_{3,eq}$ = 0.195. The UNIQUAC parameters for calculation of the phase equilibrium thermodynamics are provided in Table 26.

Figure 98. Trajectory followed during equilibration of homogenous mixtures of two different compositions for the system for water(1)/acetic acid(2)/isophorone(3); the equilibrium composition $x_{1,eq}$

= 0.365, $x_{2,eq}$ = 0.155 and $x_{3,eq}$ = 0.48. The NRTL parameters for calculation of the phase equilibrium thermodynamics are provided in Table 27.

Figure 99. Trajectory followed during equilibration of homogenous mixtures of two different compositions for the system for water(1)/acetic acid(2)/ethylacetate(3); the equilibrium composition $x_{1,eq}$ = 0.36, $x_{2,eq}$ = 0.11 and $x_{3,eq}$ = 0.53. The NRTL parameters for calculation of the phase equilibrium thermodynamics are provided in Table 28.

Figure 100. Trajectory followed during equilibration of homogenous mixtures of two different compositions for the system for water(1)/acetic acid(2)/MTBE (3); the equilibrium composition $x_{1,eq}$ = 0.32, $x_{2,eq}$ = 0.22 and $x_{3,eq}$ = 0.46. The NRTL parameters for calculation of the phase equilibrium thermodynamics are provided in Table 29.

Figure 101. Trajectory followed during equilibration of homogenous mixtures of two different compositions for the system for ethanol (1)/toluene(2)/n-decane(3); the equilibrium composition $x_{1,eq}$ = 0.31, $x_{2,eq}$ = 0.375 and $x_{3,eq}$ = 0.315. The NRTL parameters for calculation of the phase equilibrium thermodynamics are provided in Table 30.

Figure 102. Trajectories followed during equilibration of mixtures of two different compositions for the system water(1)/ethanol(2)/benzene(3) with the equilibrium composition $x_{1,eq}$ = 0.085, $x_{2,eq}$ = 0.225 and $x_{3,eq}$ = 0.69 that lies on a tangent to the binodal curve. The UNIQUAC parameters are provided in Table 31.

Figure 103. Trajectories followed during equilibration of mixtures of two different compositions for the system NMP(1)/propylbenzene(2)/dodecane(3) with the equilibrium composition $x_{1,eq}$ = 0.25, $x_{2,eq}$ = 0.155 and $x_{3,eq}$ = 0.6 that lies on a tangent to the binodal curve. The NRTL parameters are provided in Table 32.

Figure 104. Trajectories followed during equilibration of mixtures of two different compositions for the system NMP(1)/propylbenzene(2)/tetradecane(3) with the equilibrium compositions: (a, left of diagram) $x_{1,eq}$ = 0.81, $x_{2,eq}$ = 0.13 and $x_{3,eq}$ = 0.06, and (b, right of diagram) $x_{1,eq}$ = 0.23, $x_{2,eq}$ = 0.15 and $x_{3,eq}$ = 0.62 that both lie on tangents to the binodal curve. The NRTL parameters are provided in Table 33.

Figure 105. Trajectories followed during equilibration of mixtures of two different compositions for the system heptane(1)/toluene(2)/sulpholane(3) with the equilibrium compositions: $x_{1,eq}$ = 0.33, $x_{2,eq}$ = 0.595, and $x_{3,eq}$ = 0.075 that lies on a tangent to the binodal curve. The NRTL parameters are provided in Table 34.

Figure 106. Trajectories followed during equilibration of mixtures of two different compositions for the system [omim][Cl](1)/ethanol(2)/TAEE(3) with the equilibrium composition $x_{1,eq}$ = 0.3, $x_{2,eq}$ = 0.33 and $x_{3,eq}$ = 0.37 that lies on a tangent to the binodal curve. The UNIQUAC parameters are provided in Table 35.

Figure 107. Trajectories followed during equilibration of mixtures of two different compositions for the system [omim][Cl](1)/ethanol(2)/TAEE(3) with the equilibrium composition $x_{1,eq}$ = 0.4, $x_{2,eq}$ = 0.375 and $x_{3,eq}$ = 0.225 that lies on a tangent to the binodal curve. The NRTL parameters are provided in Table 36.

Figure 108. Trajectories followed during equilibration of mixtures of two different compositions for the system [bmim][TfO](1)/ethanol(2)/TAEE(3) with the equilibrium composition $x_{1,eq}$ = 0.24, $x_{2,eq}$ = 0.37 and $x_{3,eq}$ = 0.39 that lies on a tangent to the binodal curve. The UNIQUAC parameters are provided in Table 37.

Figure 109. Trajectory followed during equilibration of homogenous mixtures of two different compositions for the system water(1)/acetone(2)/toluene(3) with the equilibrium composition $x_{1,eq}$= 0.425, $x_{2,eq}$ = 0.487, $x_{3,eq}$ = 0.088. The NRTL parameters for calculation of the phase equilibrium thermodynamics are provided in Table 38.

Figure 110. Trajectory followed during equilibration of homogenous mixtures of two different compositions for the system water(1)/ethanol(2)/cyclohexane(3) with the equilibrium composition $x_{1,eq}$= 0.2, $x_{2,eq}$ = 0.59, $x_{3,eq}$ = 0.21. The NRTL parameters for calculation of the phase equilibrium thermodynamics are provided in Table 39.

Figure 111. Trajectories followed during equilibration of mixtures of two different compositions for the system toluene(1)/ethanol(2)/water(3) with the equilibrium composition $x_{1,eq}$ = 0.01, $x_{2,eq}$ = 0.188 and

$x_{3,eq}$ = 0.802 that lies within the meta-stable region. The NRTL parameters for toluene(1)/ethanol(2)/water(3) are provided in Table 40.

Gaseous Mixtures at High Pressures

Fig. S1

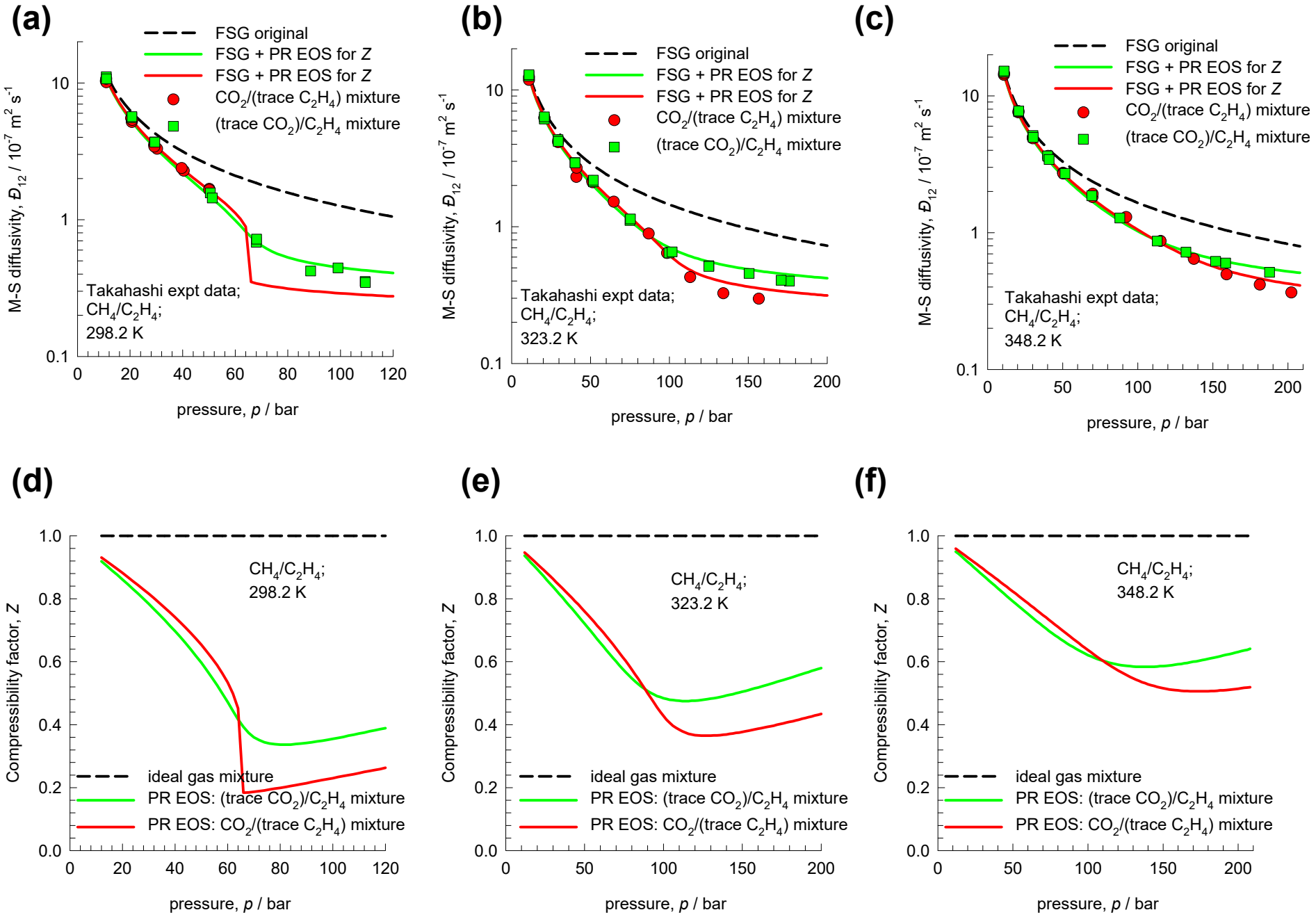

Fig. S2

C1/C2/nC6 system: interpolation binaries

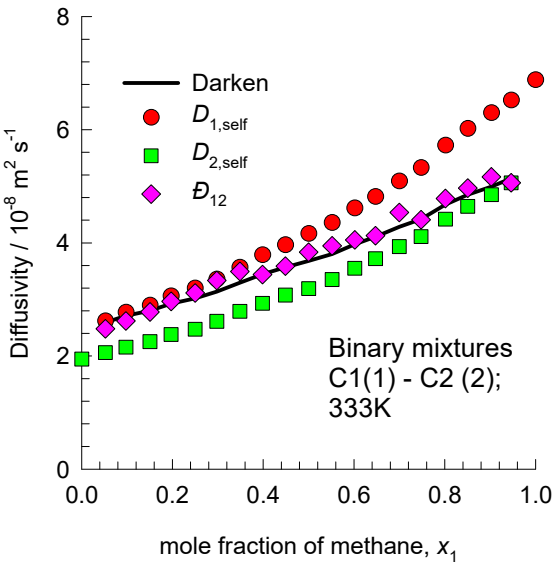

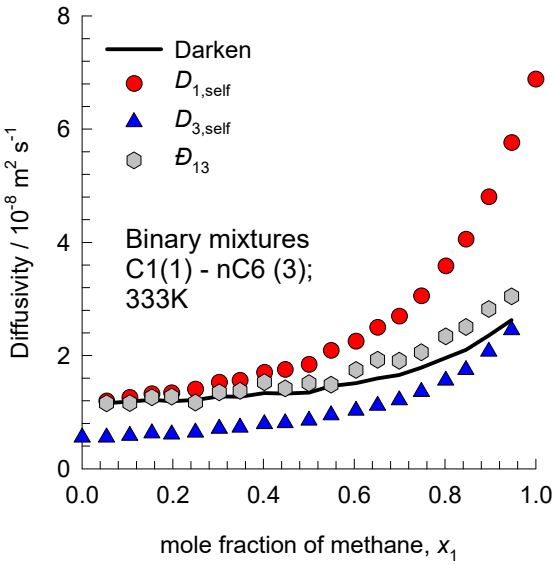

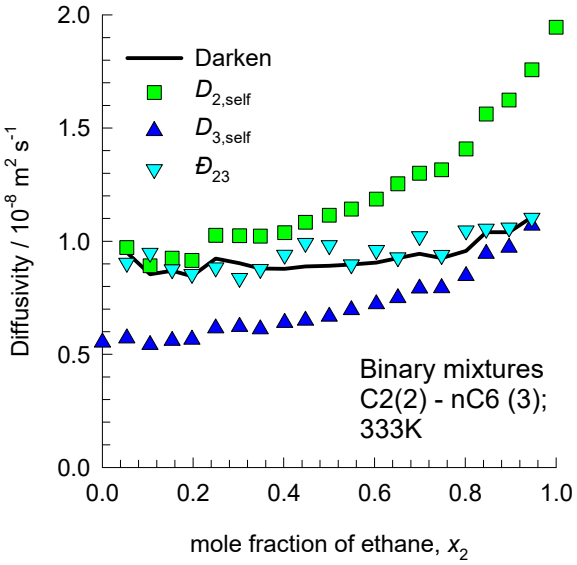

$$Đ_{12}^{x_1\to 1}=5.3;\quad Đ_{12}^{x_2\to 1}=2.5;\quad Đ_{13}^{x_1\to 1}=3;\quad Đ_{13}^{x_3\to 1}=1.05;\quad Đ_{23}^{x_2\to 1}=1.09;\quad Đ_{23}^{x_3\to 1}=0.84.$$

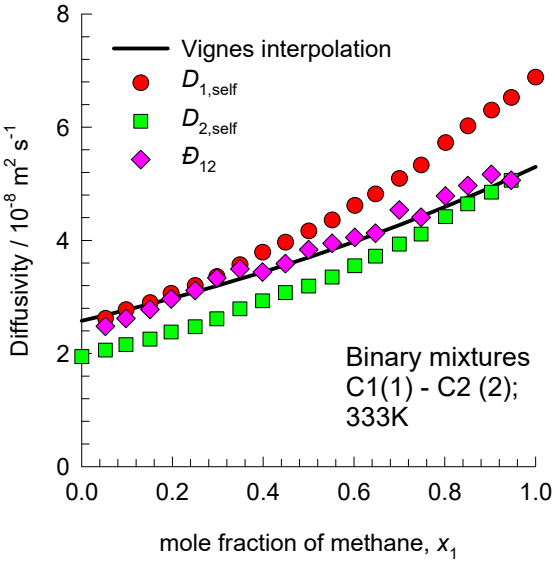

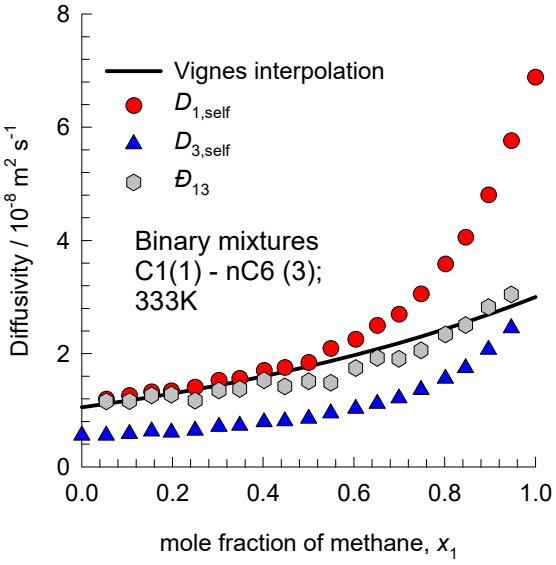

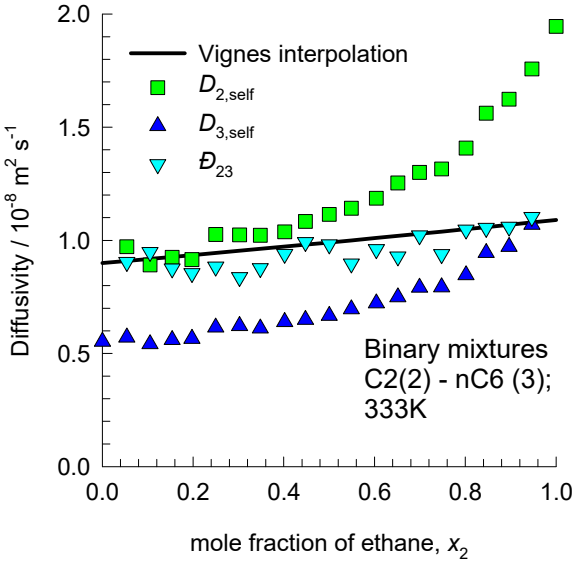

Fig. S3

C1/C2/C3 system: interpolation binaries

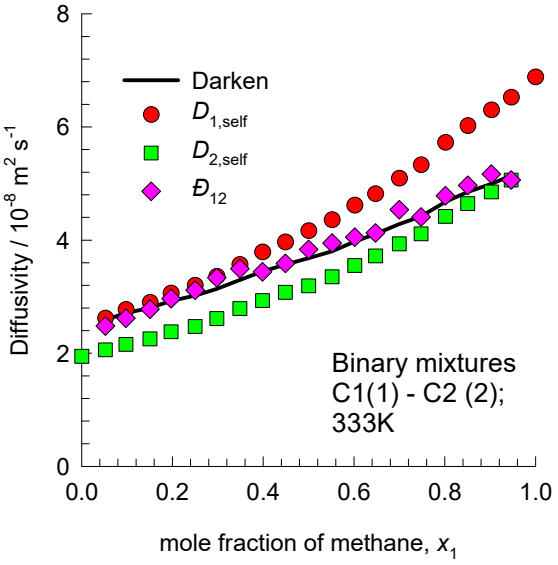

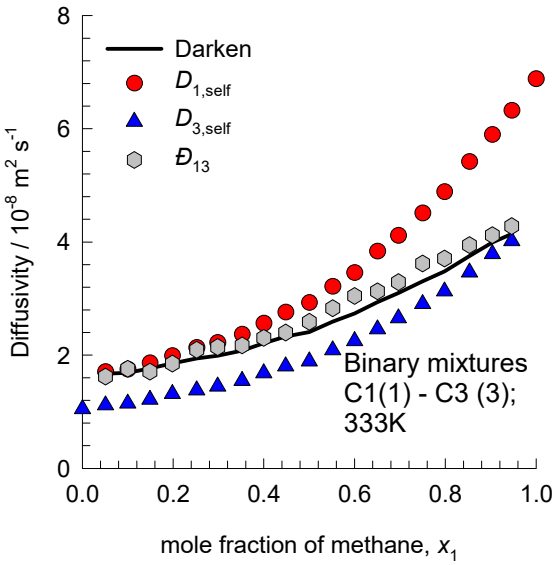

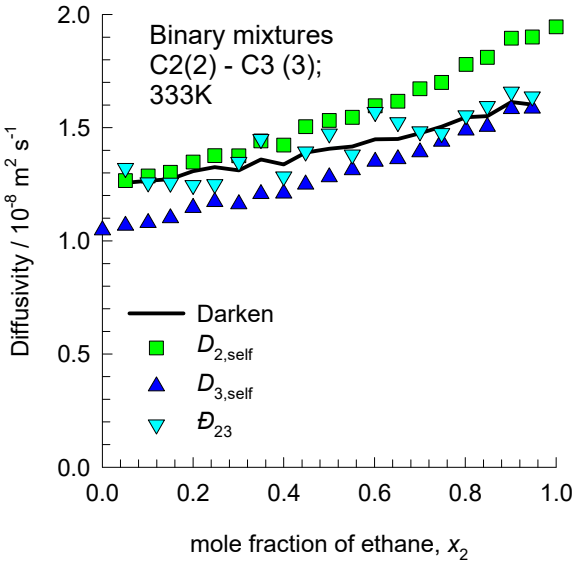

$$Đ_{12}^{x_1\to 1}=5.3;\quad Đ_{12}^{x_2\to 1}=2.5;\quad Đ_{13}^{x_1\to 1}=4.52;\quad Đ_{13}^{x_3\to 1}=1.5;\quad Đ_{23}^{x_2\to 1}=1.63;\quad Đ_{23}^{x_3\to 1}=1.23.$$

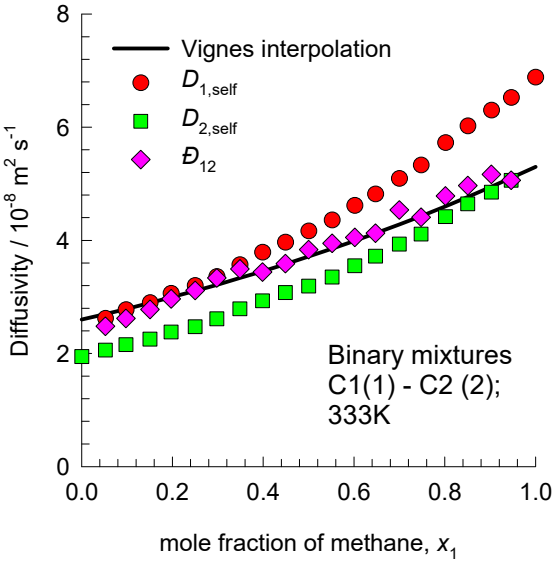

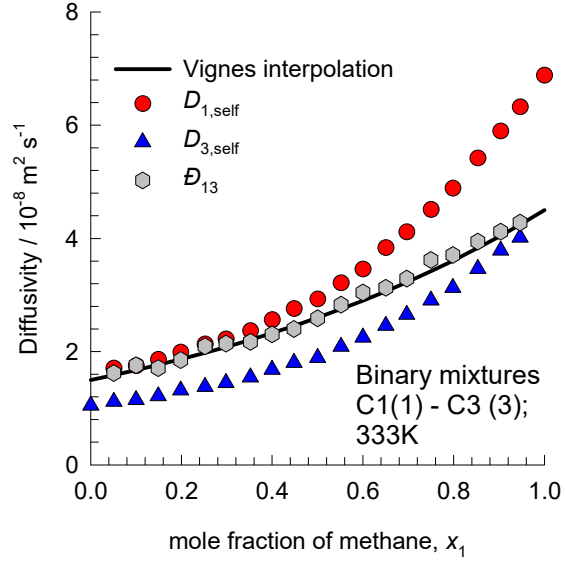

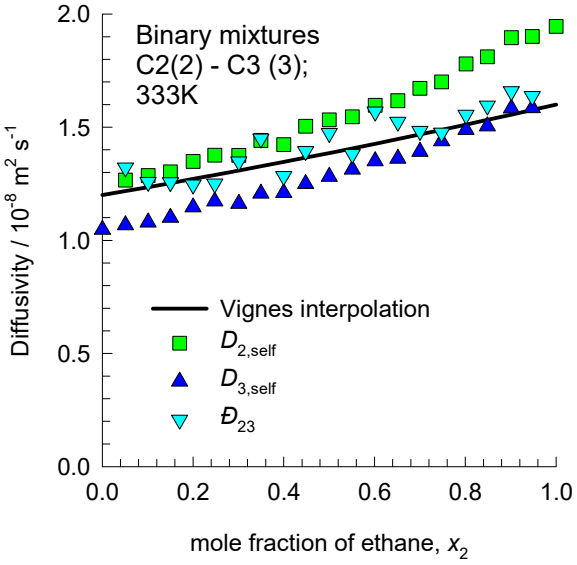

Fig. S4

C1/C3/nC6 system: interpolation binaries

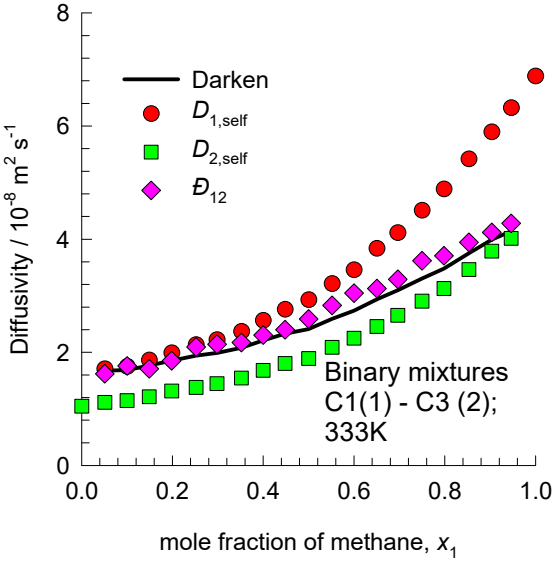

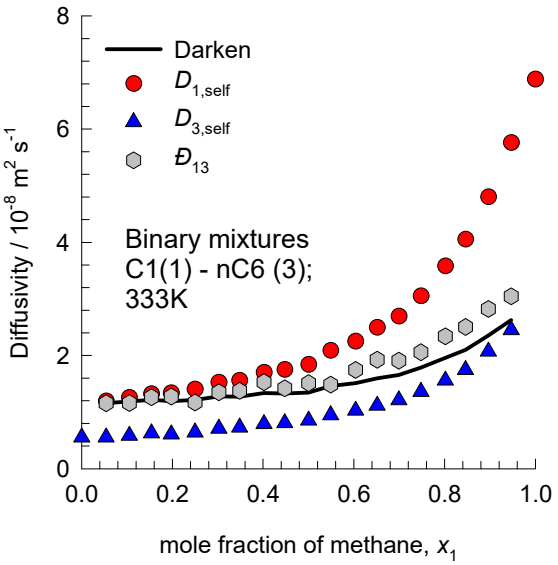

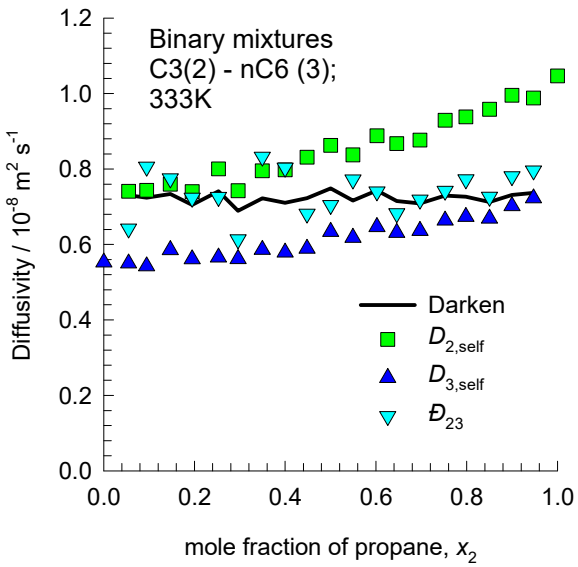

$$Đ_{12}^{x_1\to 1} = 4.52; \quad Đ_{12}^{x_2\to 1} = 1.5; \quad Đ_{13}^{x_1\to 1} = 3; \quad Đ_{13}^{x_3\to 1} = 1.05; \quad Đ_{23}^{x_2\to 1} = 0.77; \quad Đ_{23}^{x_3\to 1} = 0.75.$$

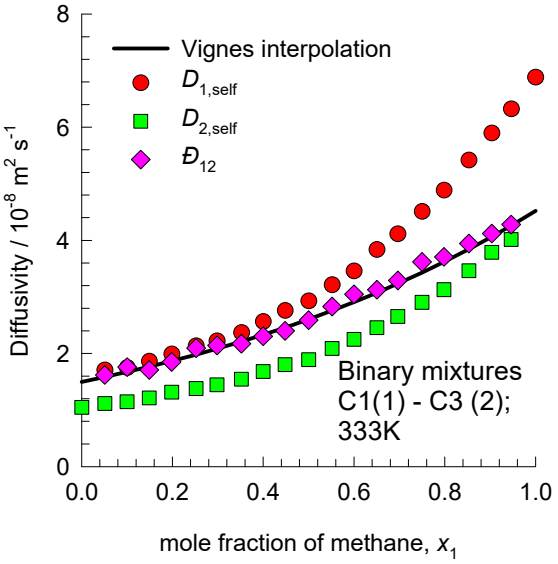

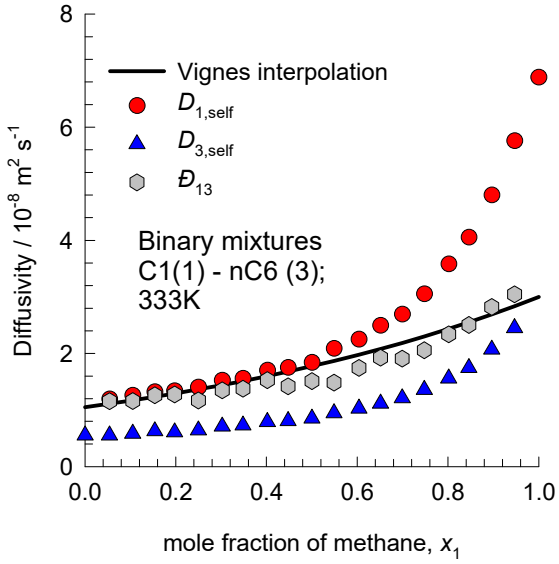

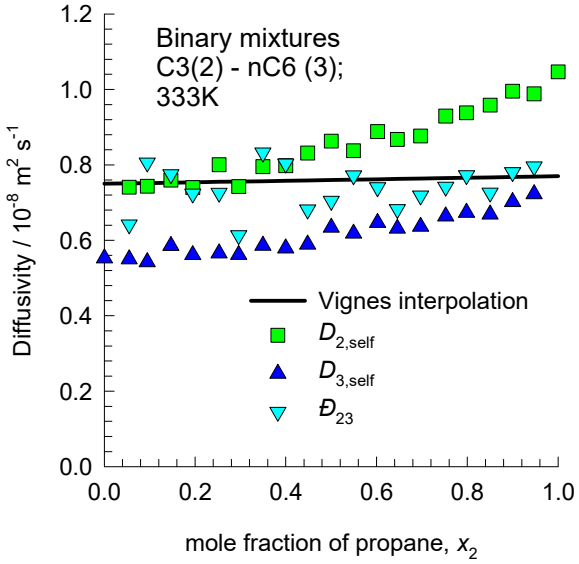

Fig. S5

C2/C3/nC4 system: interpolation binaries

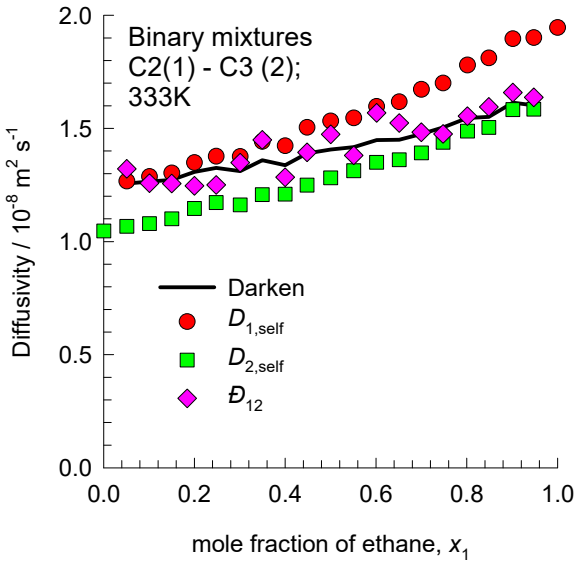

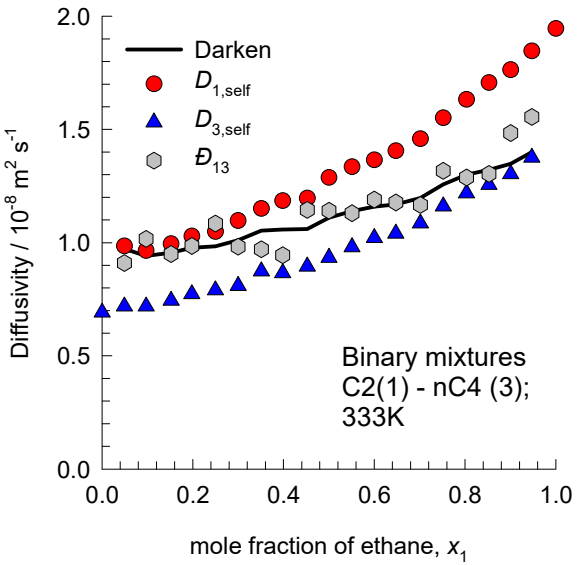

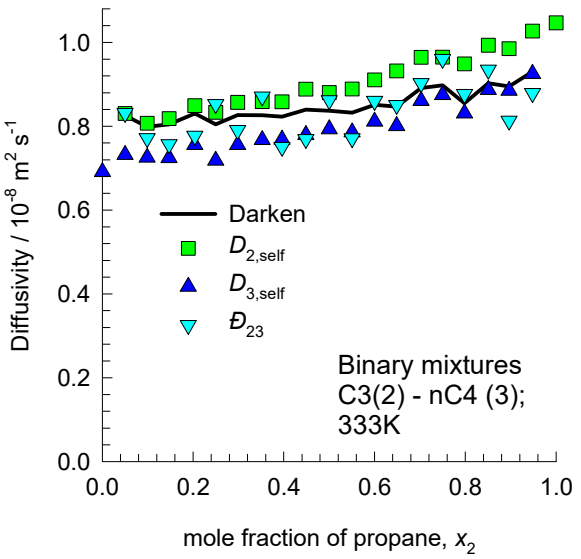

$$Đ_{12}^{x_1\to 1}=1.63;\quad Đ_{12}^{x_2\to 1}=1.23;\quad Đ_{13}^{x_1\to 1}=1.44;\quad Đ_{13}^{x_3\to 1}=0.92;\quad Đ_{23}^{x_2\to 1}=0.92;\quad Đ_{23}^{x_3\to 1}=0.79.$$

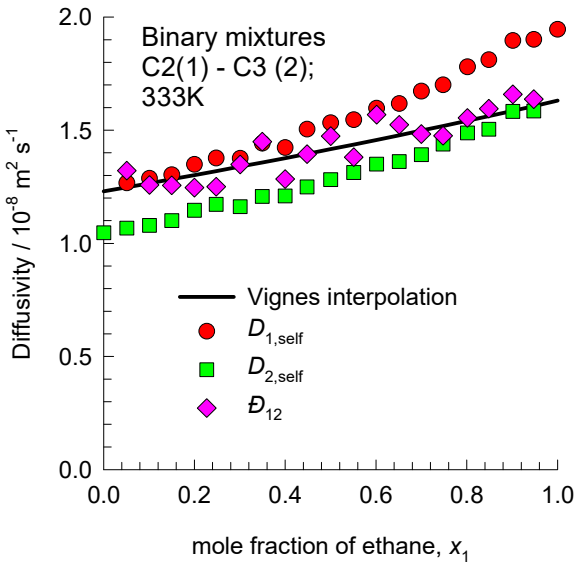

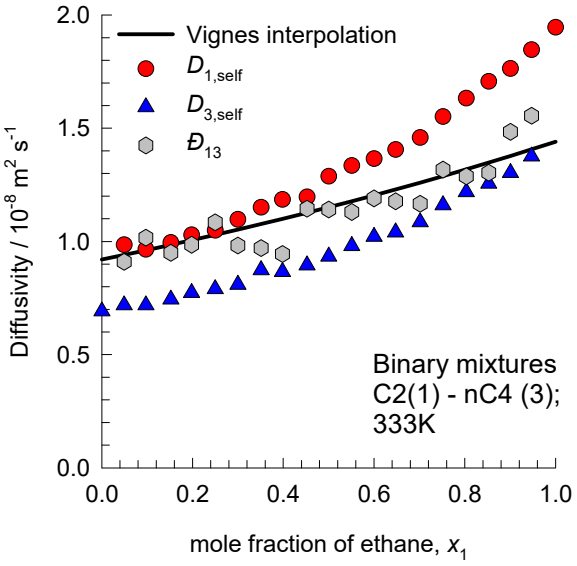

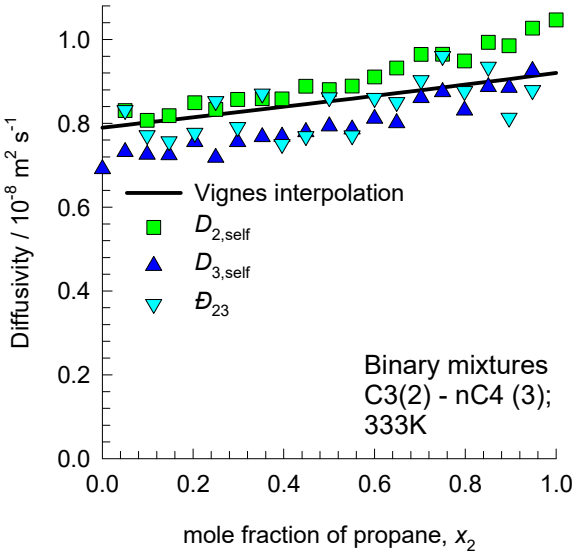

Fig. S6

C3/nC4/nC5 system: interpolation binaries

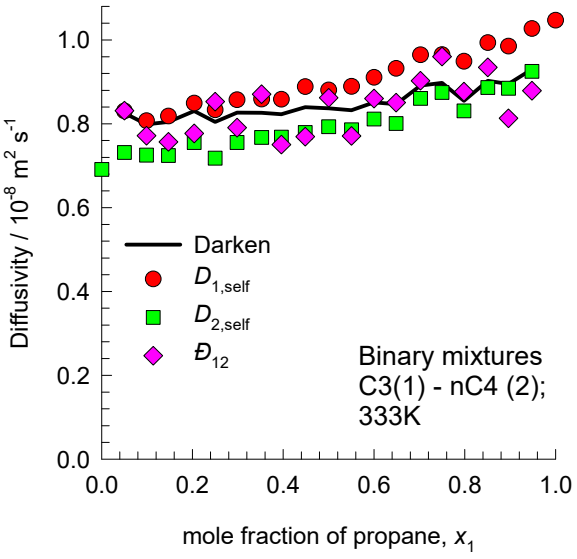

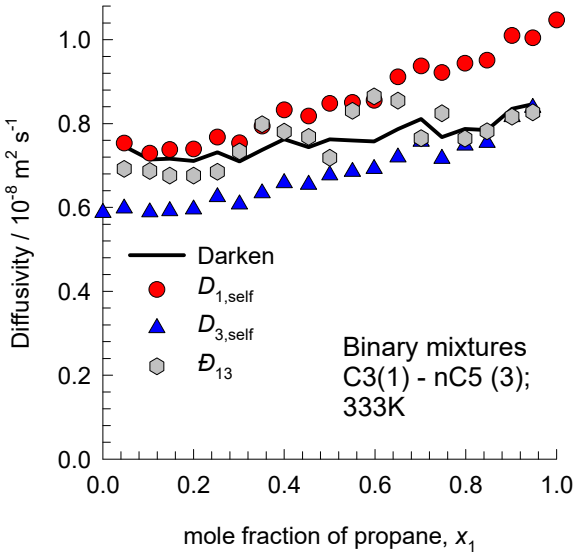

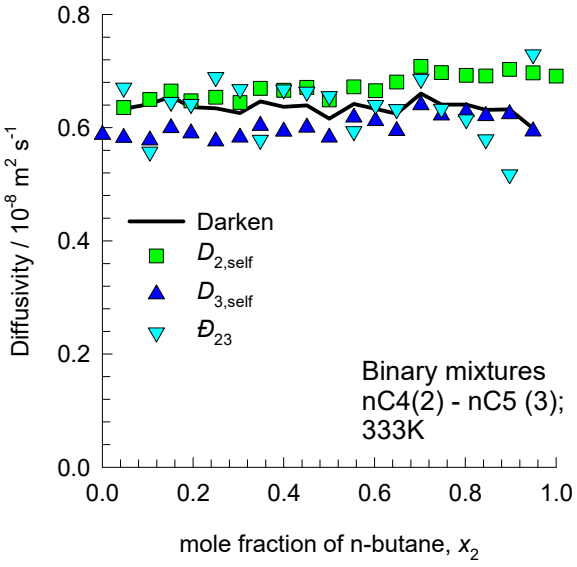

$$Đ_{12}^{x_1\to 1} = 0.92; \quad Đ_{12}^{x_2\to 1} = 0.79; \quad Đ_{13}^{x_1\to 1} = 0.83; \quad Đ_{13}^{x_3\to 1} = 0.72; \quad Đ_{23}^{x_2\to 1} = 0.62; \quad Đ_{23}^{x_3\to 1} = 0.65.$$

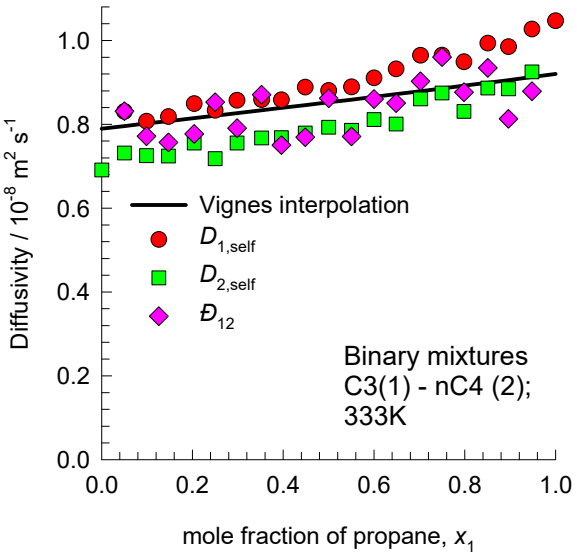

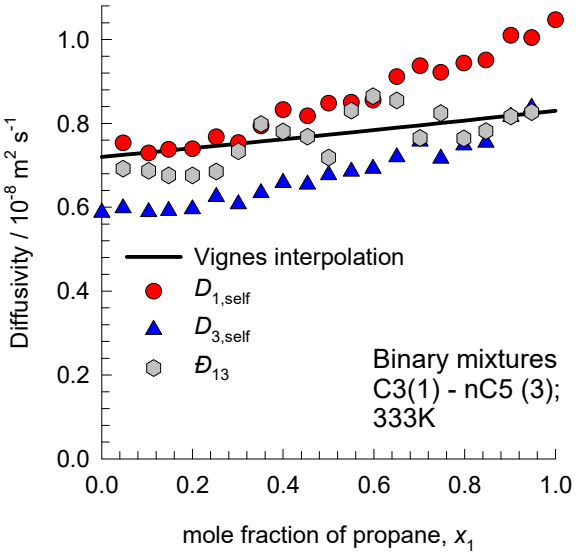

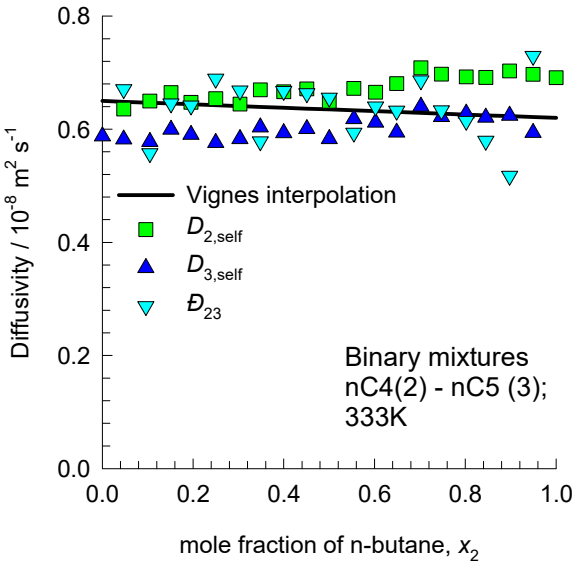

Fig. S7

Binaries: Fick, Onsager, M-S diffusivities

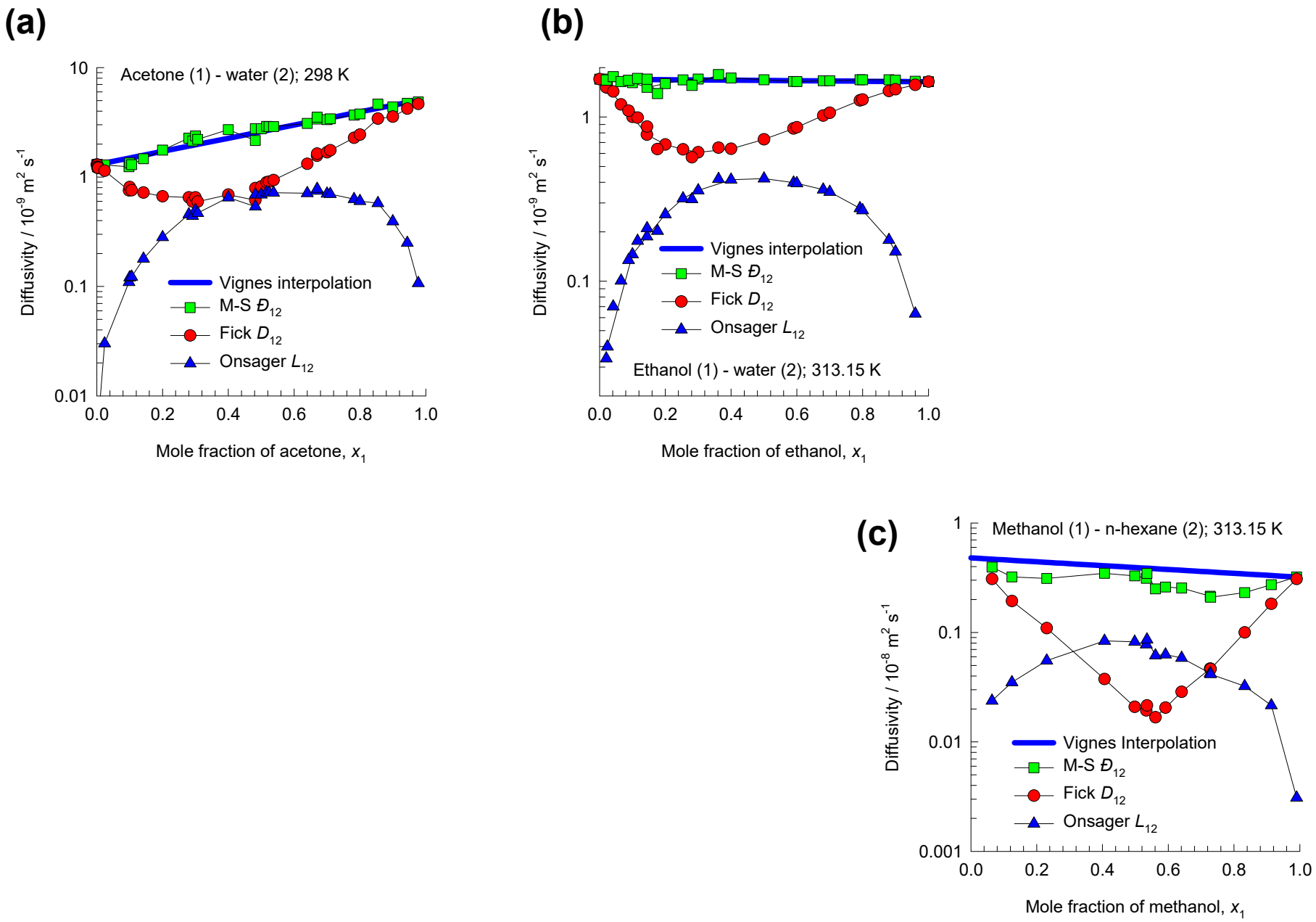

Fig. S8

Binaries: Fick, M-S diffusivities

(a)

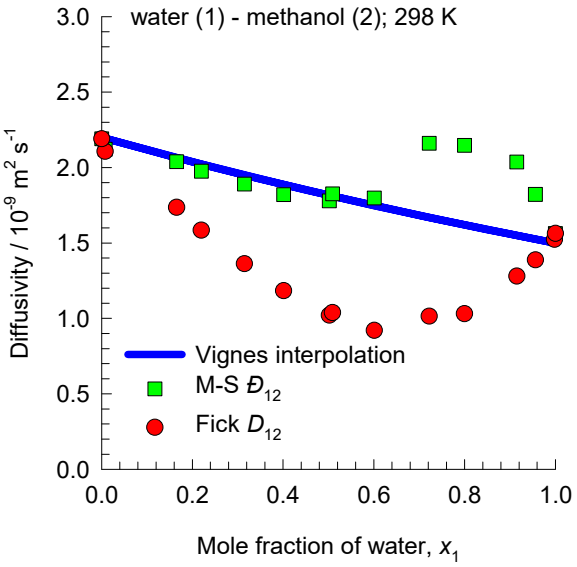

(b)

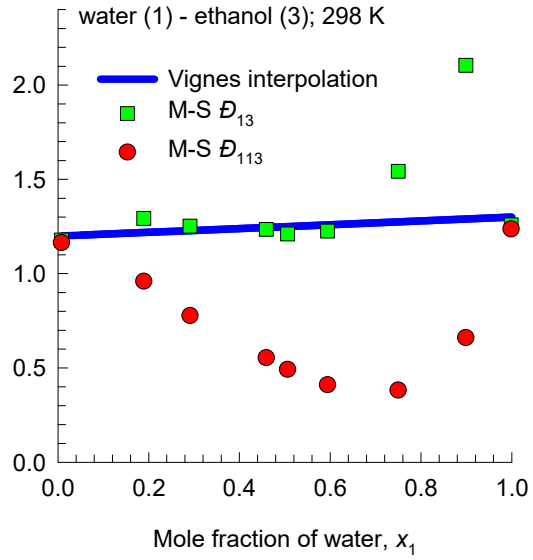

(c)

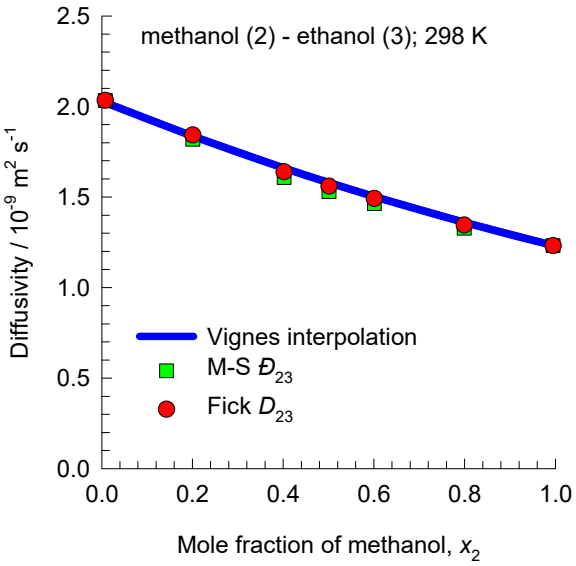

Methane/Propane mixtures: Influence of Pressure

Fig. S9

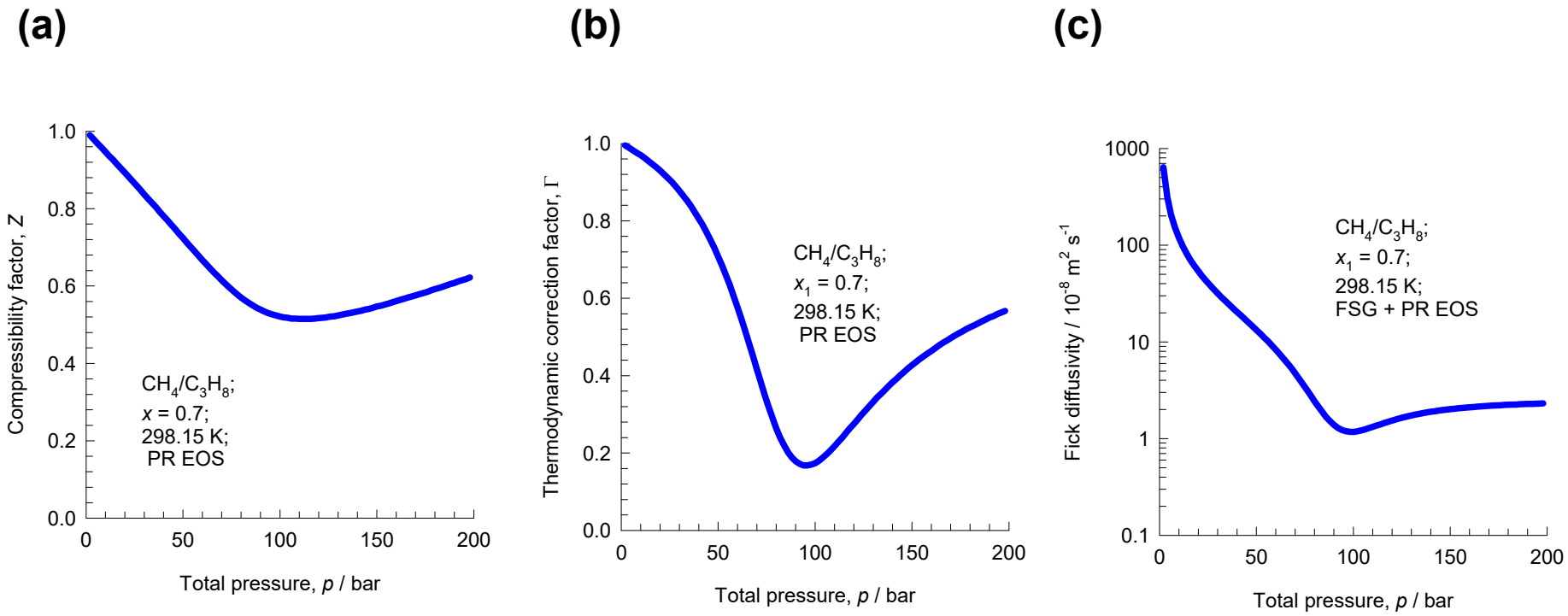

Fig. S10

Methane/Propane mixtures: Influence of composition and pressure

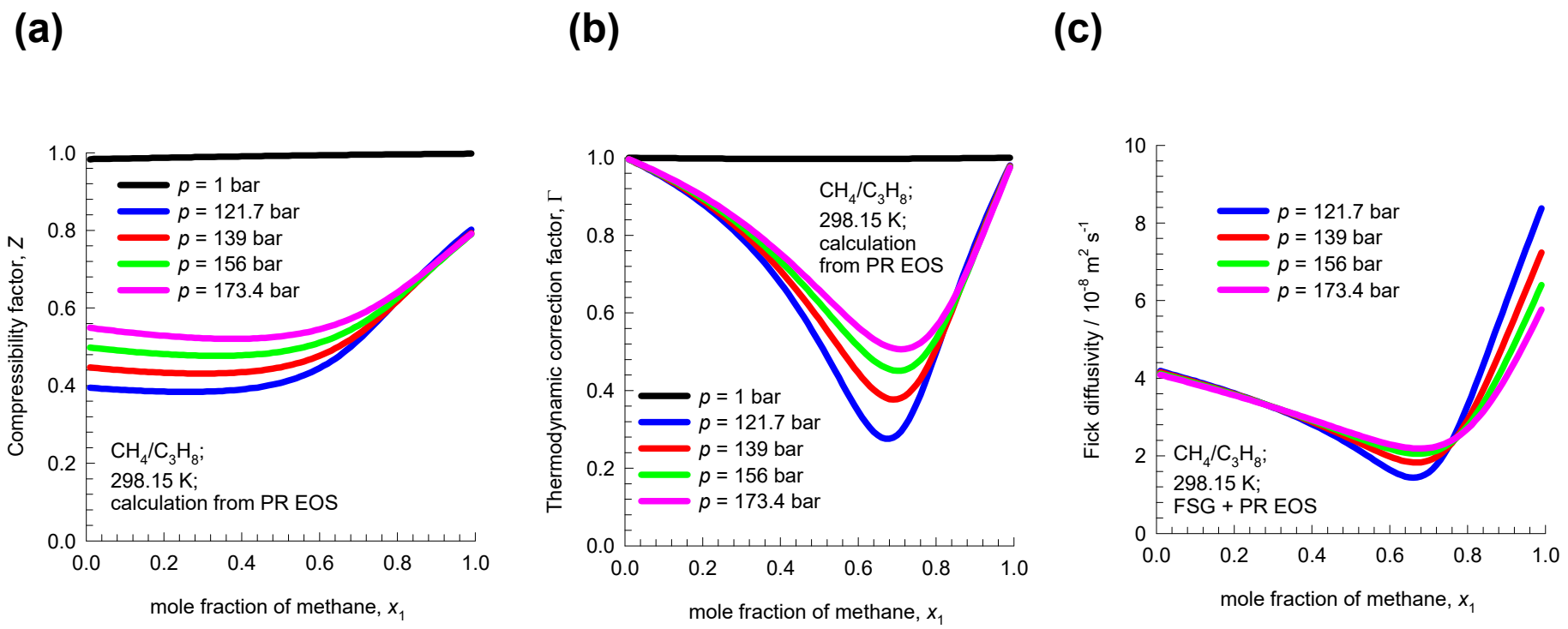

Diffusivities in Gaseous Mixtures at High Pressures

Fig. S11

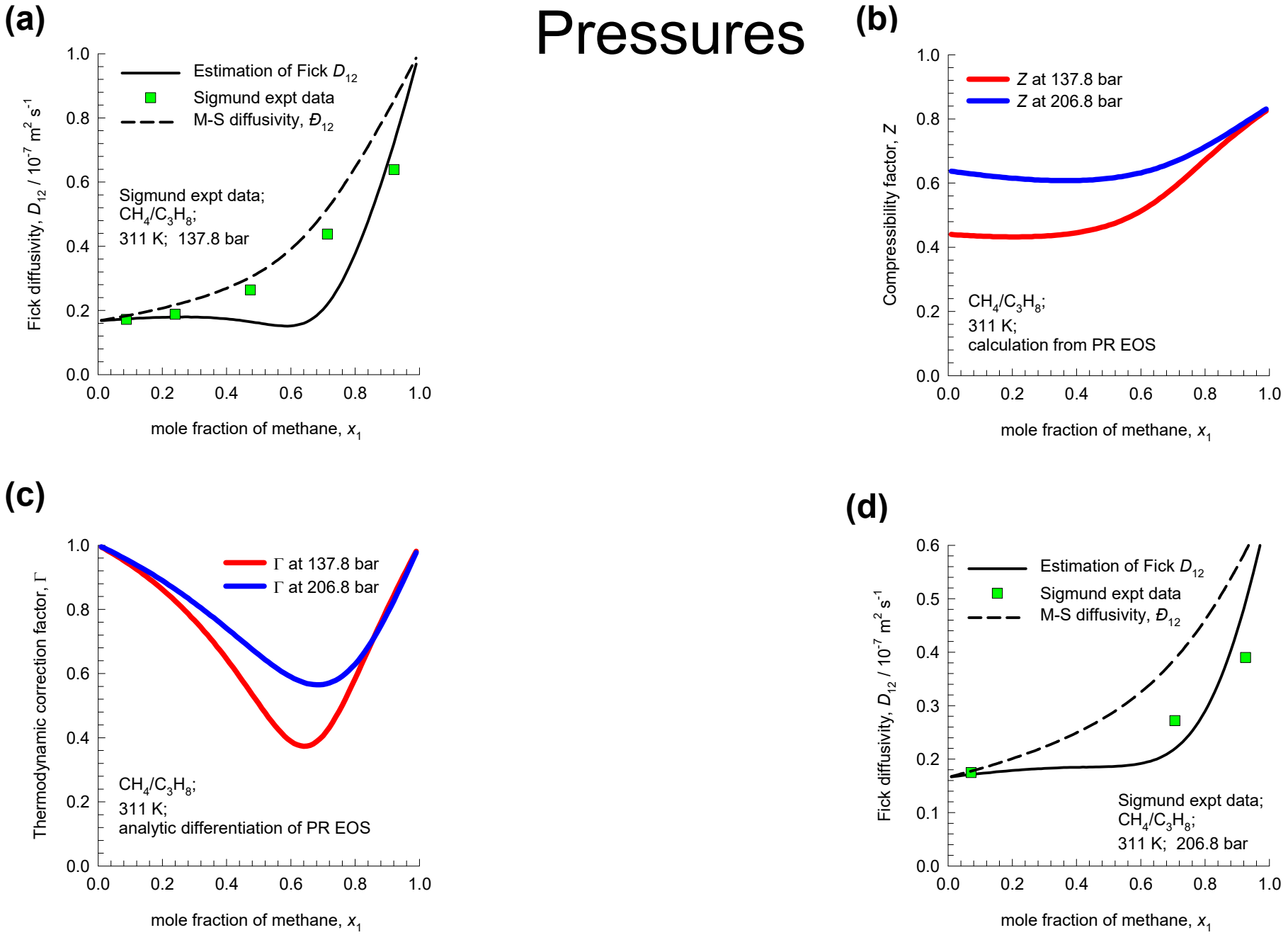

Diffusion in methyl oleate in supercritical CO_2

Fig. S12

(a)

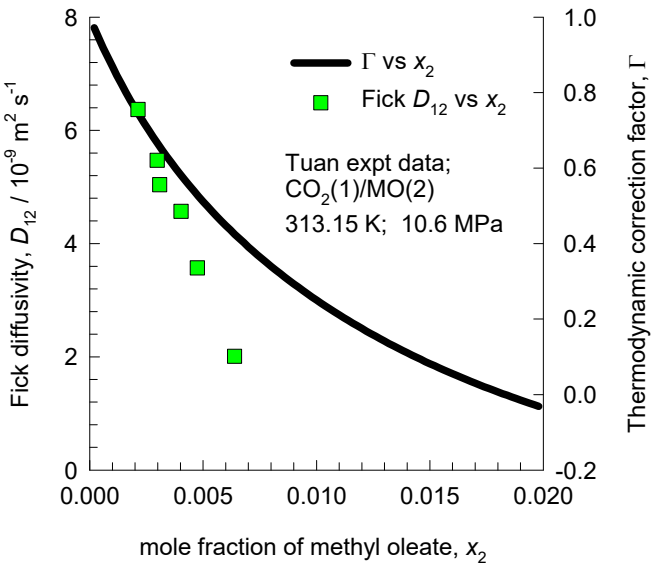

(b)

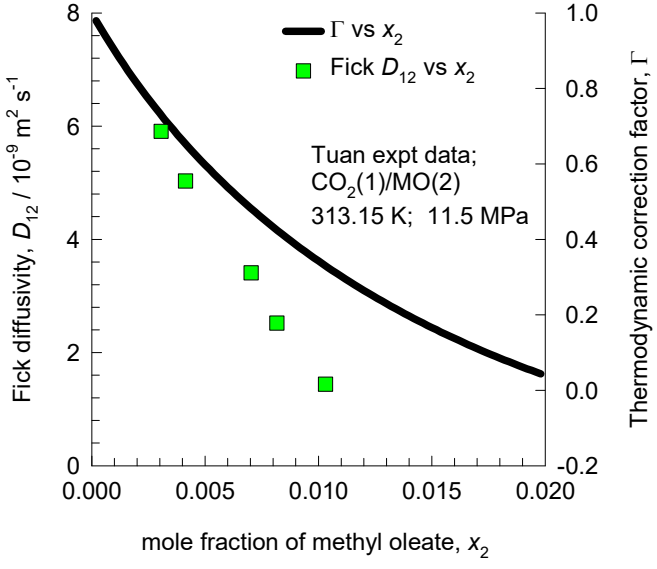

C1/C2/nC6 system: estimation of [Λ]

Fig. S13

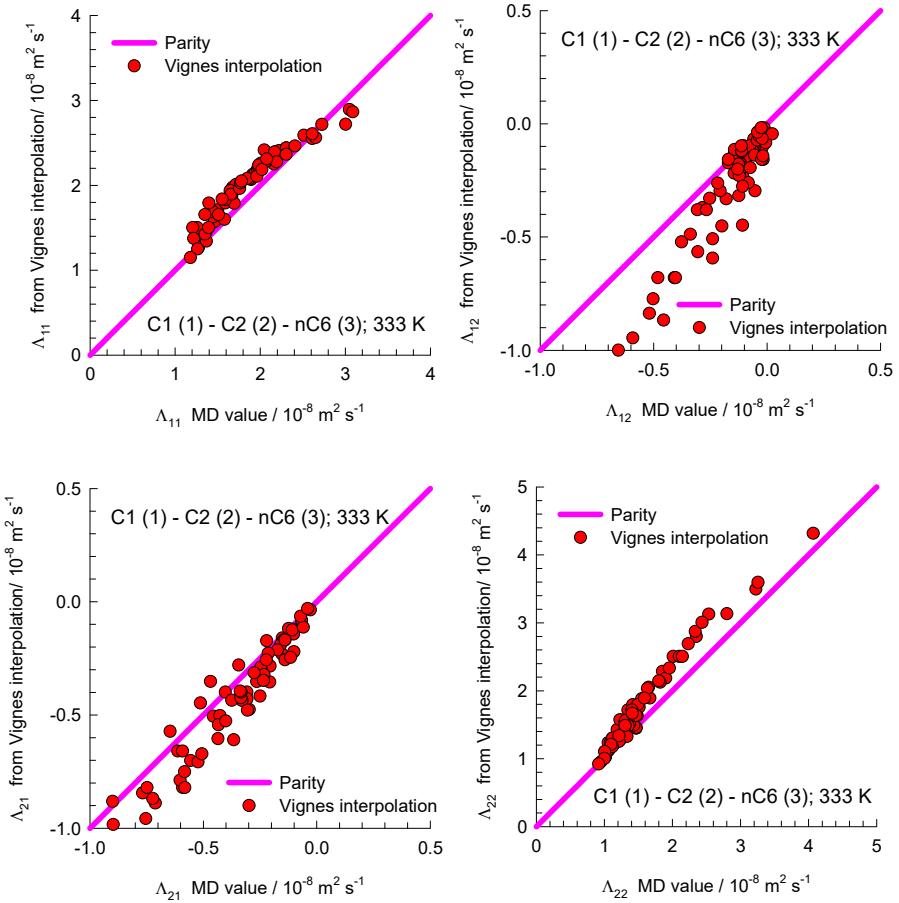

The parity plots shown above are obtained using the Vignes interpolation formula

$$Đ_{ij} = \left(Đ_{ij}^{x_i \to 1}\right)^{x_i} \left(Đ_{ij}^{x_j \to 1}\right)^{x_j} \left(Đ_{ij}^{x_k \to 1}\right)^{x_k}$$

combined with the Liu-Bardow-Vlugt interpolation

$$Đ_{12}^{x_3 \to 1} = \frac{D_{1,self}^{x_3 \to 1} D_{2,self}^{x_3 \to 1}}{D_{3,self}^{x_3 \to 1}}; \quad Đ_{13}^{x_2 \to 1} = \frac{D_{1,self}^{x_2 \to 1} D_{3,self}^{x_2 \to 1}}{D_{2,self}^{x_2 \to 1}}; \quad Đ_{23}^{x_1 \to 1} = \frac{D_{2,self}^{x_1 \to 1} D_{3,self}^{x_1 \to 1}}{D_{1,self}^{x_1 \to 1}}$$

The parity plots shown below are obtained using the Vignes interpolation formula

$$Đ_{ij} = \left(Đ_{ij}^{x_i \to 1}\right)^{x_i} \left(Đ_{ij}^{x_j \to 1}\right)^{x_j} \left(Đ_{ij}^{x_k \to 1}\right)^{x_k}$$

combined with the Wesselingh Bollen interpolation

$$Đ_{12}^{x_3 \to 1} = \sqrt{\left(Đ_{13}^{x_3 \to 1} Đ_{23}^{x_3 \to 1}\right)}$$

$$Đ_{13}^{x_2 \to 1} = \sqrt{\left(Đ_{12}^{x_2 \to 1} Đ_{23}^{x_2 \to 1}\right)}$$

$$Đ_{23}^{x_3 \to 1} = \sqrt{\left(Đ_{12}^{x_1 \to 1} Đ_{13}^{x_1 \to 1}\right)}$$

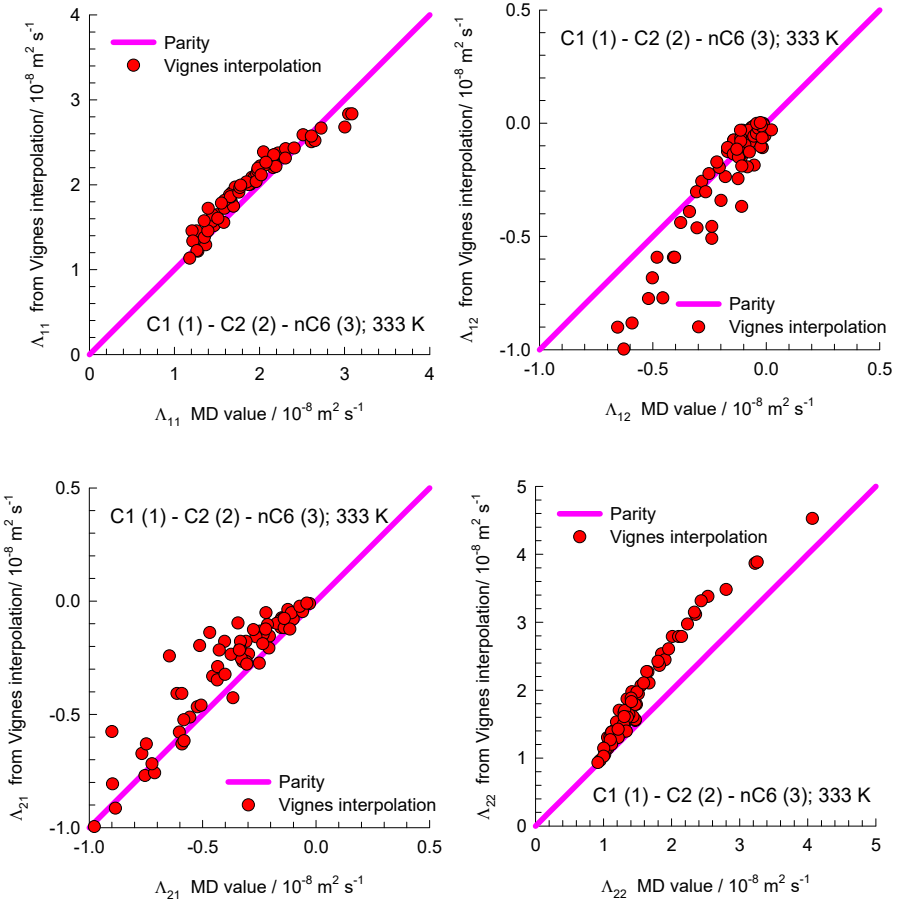

Fig. S14

C1/C2/C3 system: estimation of [Λ]

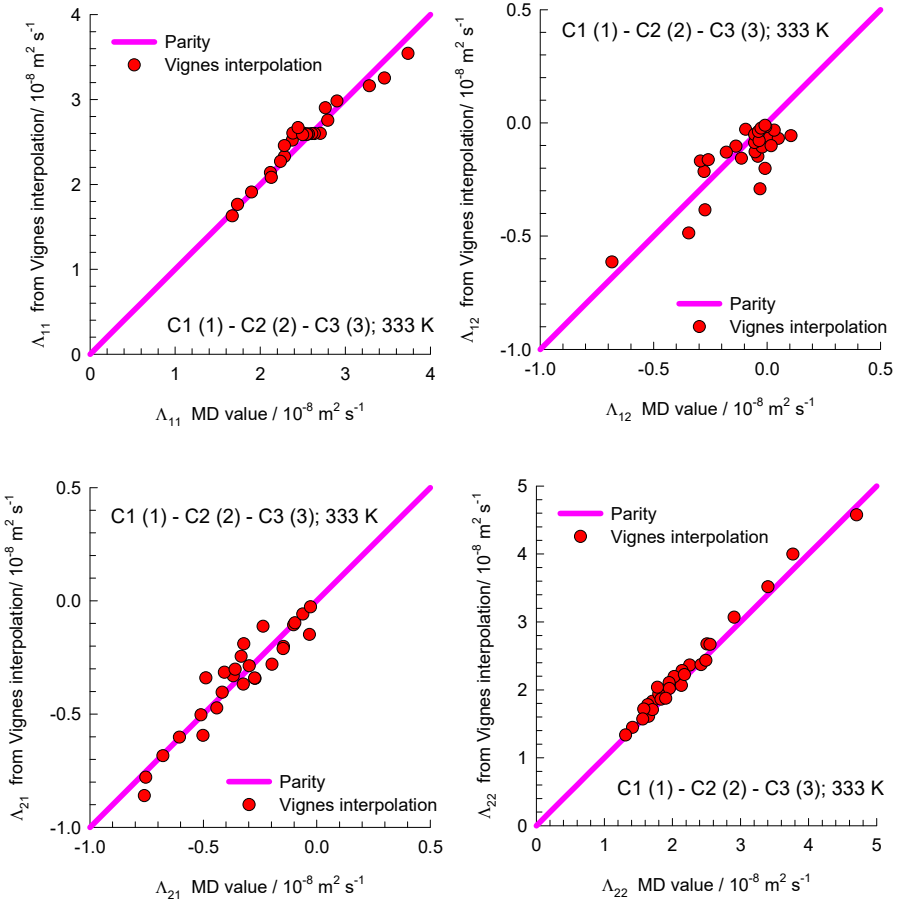

The parity plots shown above are obtained using the Vignes interpolation formula

$$Đ_{ij} = \left(Đ_{ij}^{x_i \to 1}\right)^{x_i} \left(Đ_{ij}^{x_j \to 1}\right)^{x_j} \left(Đ_{ij}^{x_k \to 1}\right)^{x_k}$$

combined with the Liu-Bardow-Vlugt interpolation

$$Đ_{12}^{x_3 \to 1} = \frac{D_{1,self}^{x_3 \to 1} D_{2,self}^{x_3 \to 1}}{D_{3,self}^{x_3 \to 1}}; \quad Đ_{13}^{x_2 \to 1} = \frac{D_{1,self}^{x_2 \to 1} D_{3,self}^{x_2 \to 1}}{D_{2,self}^{x_2 \to 1}}; \quad Đ_{23}^{x_1 \to 1} = \frac{D_{2,self}^{x_1 \to 1} D_{3,self}^{x_1 \to 1}}{D_{1,self}^{x_1 \to 1}}$$

The parity plots shown below are obtained using the Vignes interpolation formula

$$Đ_{ij} = \left(Đ_{ij}^{x_i \to 1}\right)^{x_i} \left(Đ_{ij}^{x_j \to 1}\right)^{x_j} \left(Đ_{ij}^{x_k \to 1}\right)^{x_k}$$

combined with the Wesselingh Bollen interpolation

$$Đ_{12}^{x_3 \to 1} = \sqrt{\left(Đ_{13}^{x_3 \to 1} Đ_{23}^{x_3 \to 1}\right)}$$

$$Đ_{13}^{x_2 \to 1} = \sqrt{\left(Đ_{12}^{x_2 \to 1} Đ_{23}^{x_2 \to 1}\right)}$$

$$Đ_{23}^{x_3 \to 1} = \sqrt{\left(Đ_{12}^{x_1 \to 1} Đ_{13}^{x_1 \to 1}\right)}$$

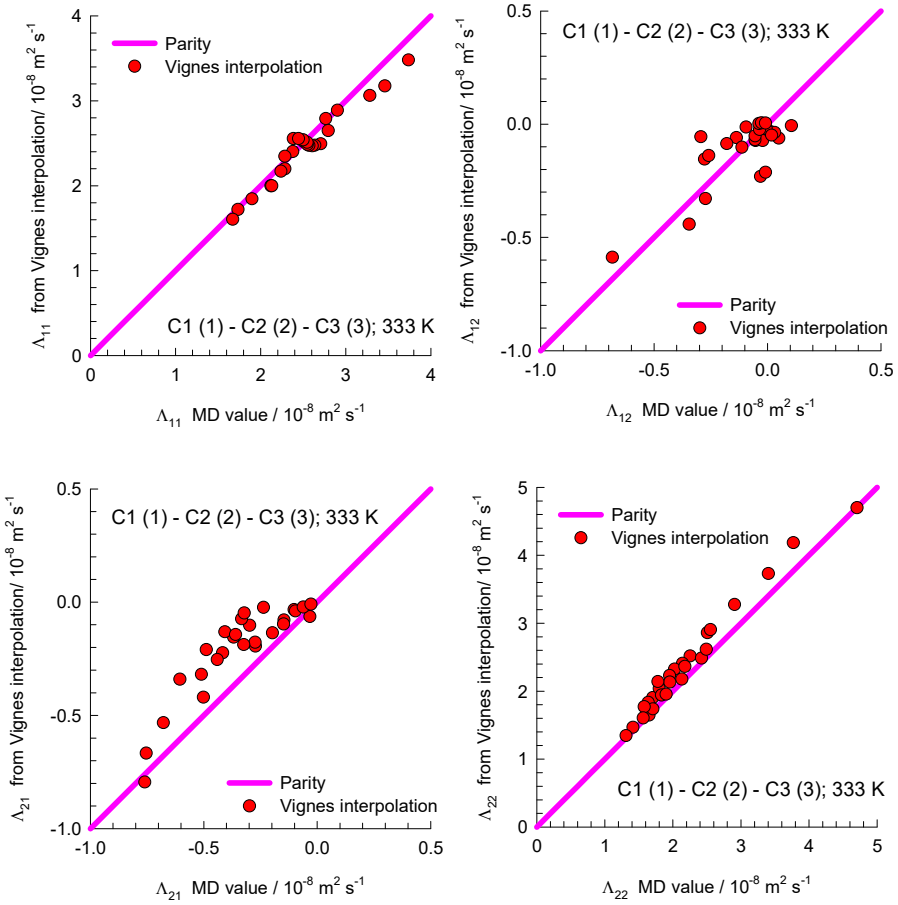

Fig. S15

C1/C3/nC6 system: estimation of [Λ]

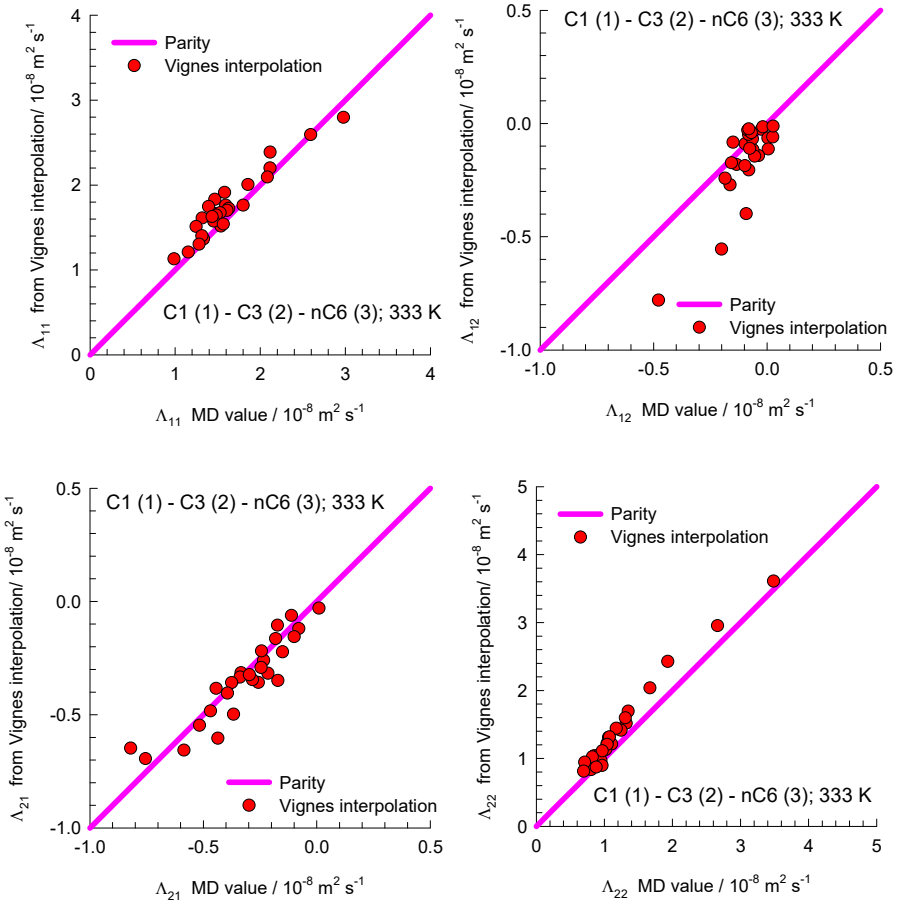

The parity plots shown above are obtained using the Vignes interpolation formula

$$Đ_{ij} = \left(Đ_{ij}^{x_i \to 1}\right)^{x_i} \left(Đ_{ij}^{x_j \to 1}\right)^{x_j} \left(Đ_{ij}^{x_k \to 1}\right)^{x_k}$$

combined with the Liu-Bardow-Vlugt interpolation

$$Đ_{12}^{x_3 \to 1} = \frac{D_{1,self}^{x_3 \to 1} D_{2,self}^{x_3 \to 1}}{D_{3,self}^{x_3 \to 1}}; \quad Đ_{13}^{x_2 \to 1} = \frac{D_{1,self}^{x_2 \to 1} D_{3,self}^{x_2 \to 1}}{D_{2,self}^{x_2 \to 1}}; \quad Đ_{23}^{x_1 \to 1} = \frac{D_{2,self}^{x_1 \to 1} D_{3,self}^{x_1 \to 1}}{D_{1,self}^{x_1 \to 1}}$$

The parity plots shown below are obtained using the Vignes interpolation formula

$$Đ_{ij} = \left(Đ_{ij}^{x_i \to 1}\right)^{x_i} \left(Đ_{ij}^{x_j \to 1}\right)^{x_j} \left(Đ_{ij}^{x_k \to 1}\right)^{x_k}$$

combined with the Wesselingh Bollen interpolation

$$Đ_{12}^{x_3 \to 1} = \sqrt{\left(Đ_{13}^{x_3 \to 1} Đ_{23}^{x_3 \to 1}\right)}$$

$$Đ_{13}^{x_2 \to 1} = \sqrt{\left(Đ_{12}^{x_2 \to 1} Đ_{23}^{x_2 \to 1}\right)}$$

$$Đ_{23}^{x_3 \to 1} = \sqrt{\left(Đ_{12}^{x_1 \to 1} Đ_{13}^{x_1 \to 1}\right)}$$

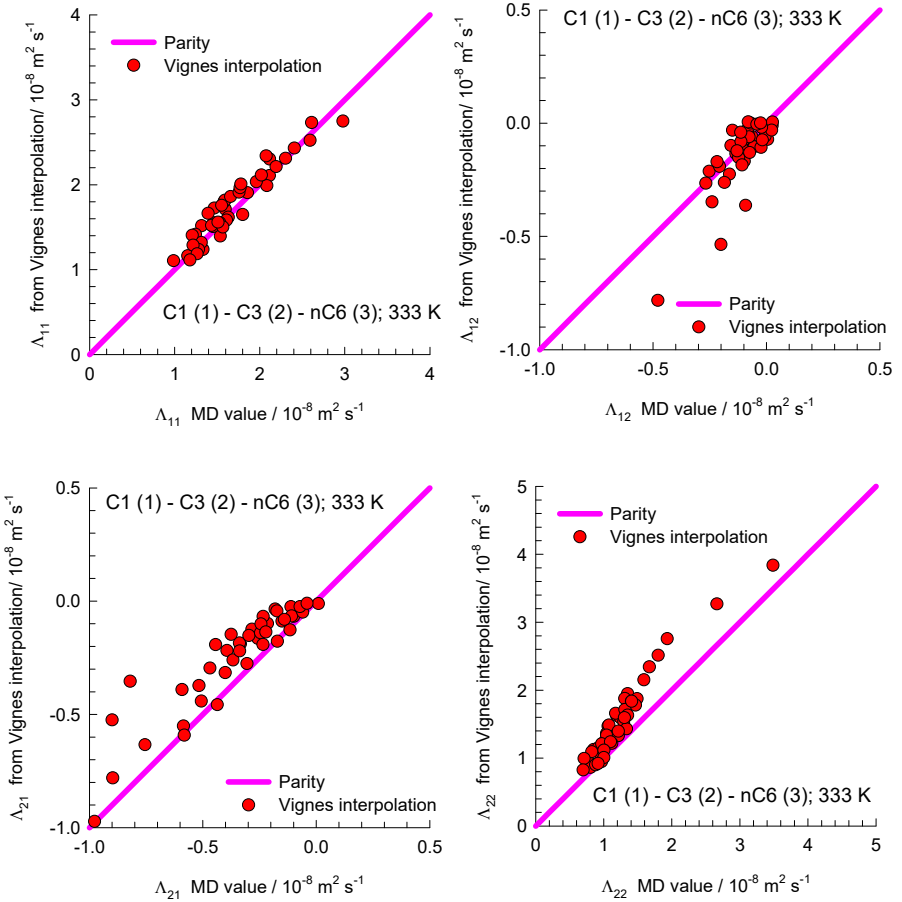

Fig. S16

C2/C3/nC4 system: estimation of [Λ]

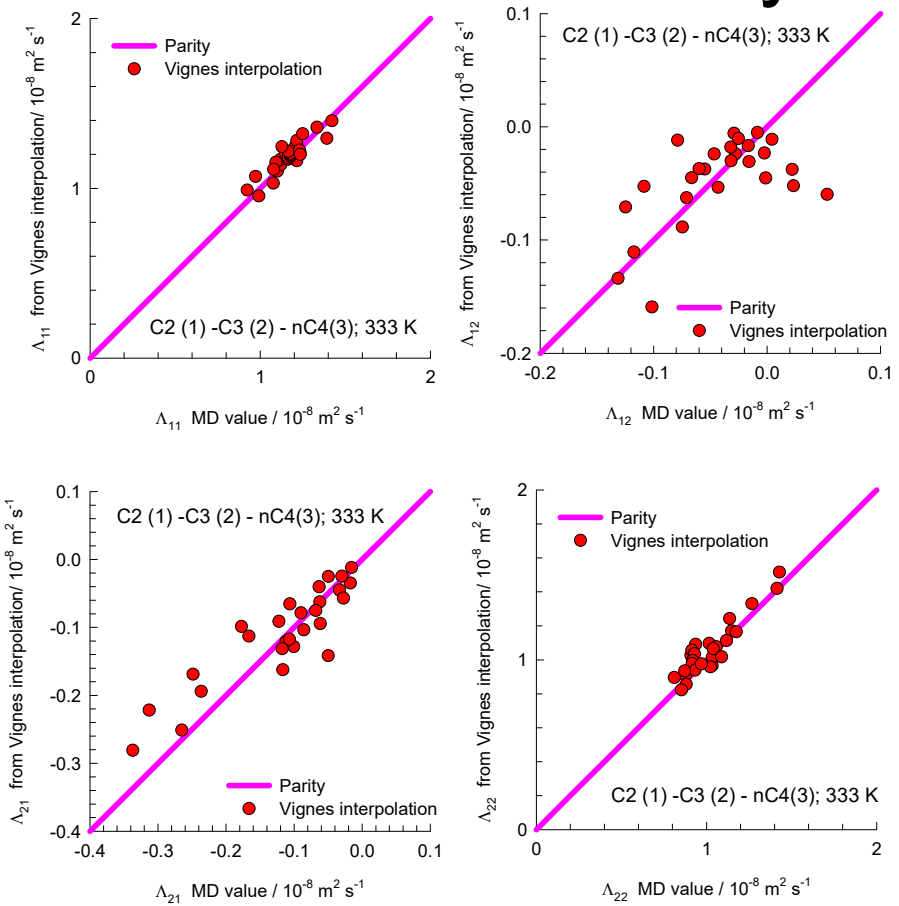

The parity plots shown above are obtained using the Vignes interpolation formula

$$Đ_{ij} = \left(Đ_{ij}^{x_i \to 1}\right)^{x_i} \left(Đ_{ij}^{x_j \to 1}\right)^{x_j} \left(Đ_{ij}^{x_k \to 1}\right)^{x_k}$$

combined with the Liu-Bardow-Vlugt interpolation

$$Đ_{12}^{x_3 \to 1} = \frac{D_{1,self}^{x_3 \to 1} D_{2,self}^{x_3 \to 1}}{D_{3,self}^{x_3 \to 1}}; \quad Đ_{13}^{x_2 \to 1} = \frac{D_{1,self}^{x_2 \to 1} D_{3,self}^{x_2 \to 1}}{D_{2,self}^{x_2 \to 1}}; \quad Đ_{23}^{x_1 \to 1} = \frac{D_{2,self}^{x_1 \to 1} D_{3,self}^{x_1 \to 1}}{D_{1,self}^{x_1 \to 1}}$$

The parity plots shown below are obtained using the Vignes interpolation formula

$$Đ_{ij} = \left(Đ_{ij}^{x_i \to 1}\right)^{x_i} \left(Đ_{ij}^{x_j \to 1}\right)^{x_j} \left(Đ_{ij}^{x_k \to 1}\right)^{x_k}$$

combined with the Wesselingh Bollen interpolation

$$Đ_{12}^{x_3 \to 1} = \sqrt{\left(Đ_{13}^{x_3 \to 1} Đ_{23}^{x_3 \to 1}\right)}$$

$$Đ_{13}^{x_2 \to 1} = \sqrt{\left(Đ_{12}^{x_2 \to 1} Đ_{23}^{x_2 \to 1}\right)}$$

$$Đ_{23}^{x_3 \to 1} = \sqrt{\left(Đ_{12}^{x_1 \to 1} Đ_{13}^{x_1 \to 1}\right)}$$

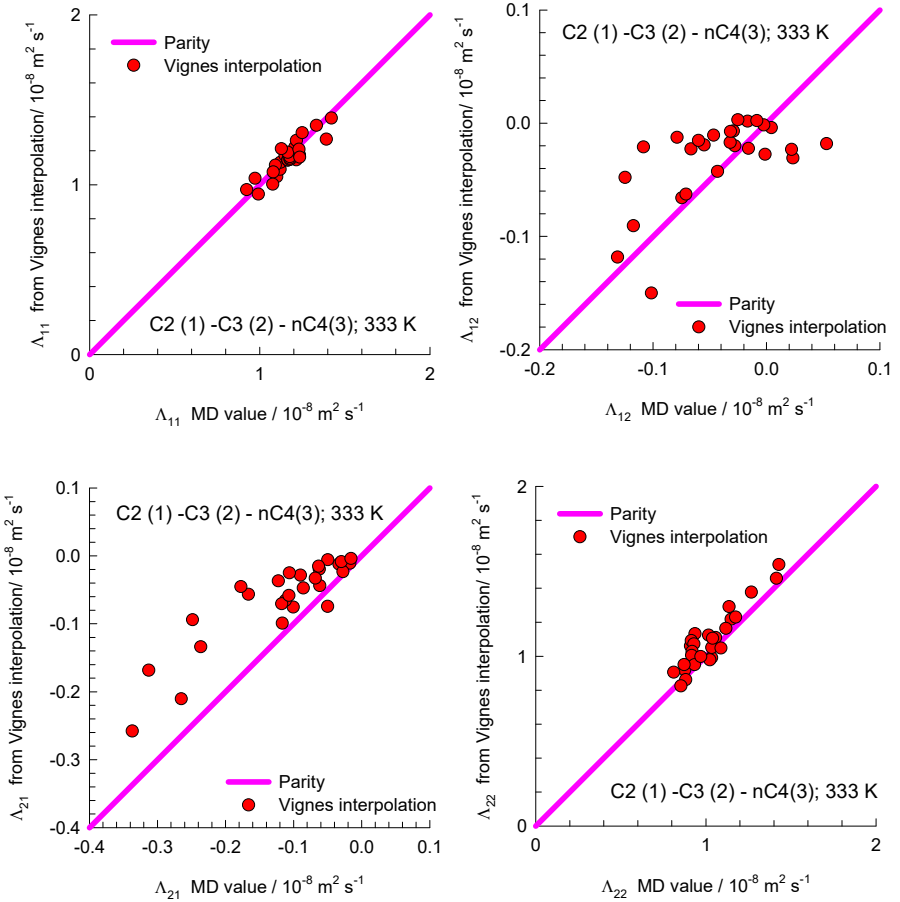

Fig. S17

C3/nC4/nC5 system: estimation of [Λ]

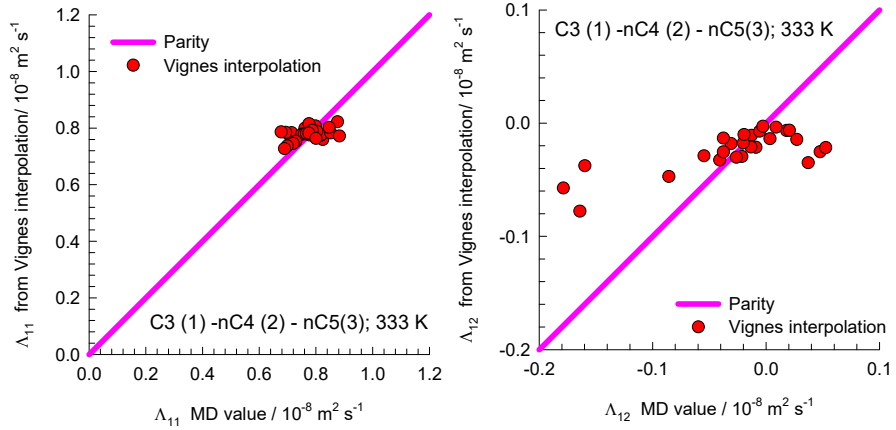

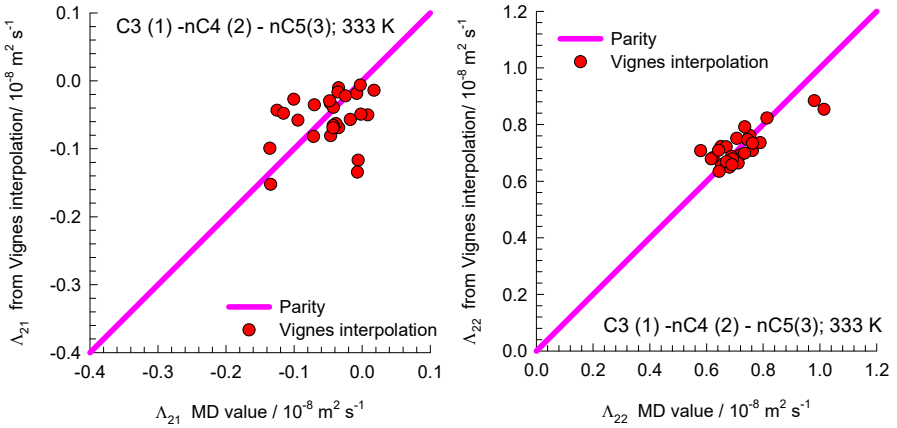

The parity plots shown above are obtained using the Vignes interpolation formula

$$Đ_{ij} = \left(Đ_{ij}^{x_i \to 1}\right)^{x_i} \left(Đ_{ij}^{x_j \to 1}\right)^{x_j} \left(Đ_{ij}^{x_k \to 1}\right)^{x_k}$$

combined with the Liu-Bardow-Vlugt interpolation

$$Đ_{12}^{x_3 \to 1} = \frac{D_{1,self}^{x_3 \to 1} D_{2,self}^{x_3 \to 1}}{D_{3,self}^{x_3 \to 1}}; \quad Đ_{13}^{x_2 \to 1} = \frac{D_{1,self}^{x_2 \to 1} D_{3,self}^{x_2 \to 1}}{D_{2,self}^{x_2 \to 1}}; \quad Đ_{23}^{x_1 \to 1} = \frac{D_{2,self}^{x_1 \to 1} D_{3,self}^{x_1 \to 1}}{D_{1,self}^{x_1 \to 1}}$$

The parity plots shown below are obtained using the Vignes interpolation formula

$$Đ_{ij} = \left(Đ_{ij}^{x_i \to 1}\right)^{x_i} \left(Đ_{ij}^{x_j \to 1}\right)^{x_j} \left(Đ_{ij}^{x_k \to 1}\right)^{x_k}$$

combined with the Wesselingh Bollen interpolation

$$Đ_{12}^{x_3 \to 1} = \sqrt{\left(Đ_{13}^{x_3 \to 1} Đ_{23}^{x_3 \to 1}\right)}$$

$$Đ_{13}^{x_2 \to 1} = \sqrt{\left(Đ_{12}^{x_2 \to 1} Đ_{23}^{x_2 \to 1}\right)}$$

$$Đ_{23}^{x_3 \to 1} = \sqrt{\left(Đ_{12}^{x_1 \to 1} Đ_{13}^{x_1 \to 1}\right)}$$

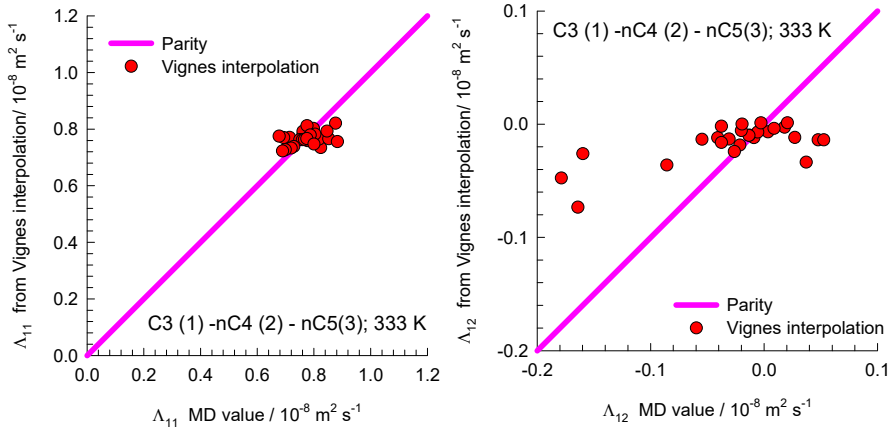

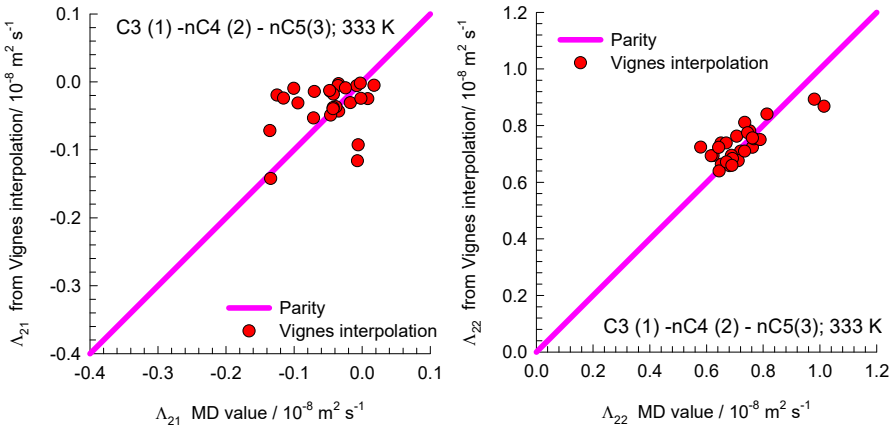

$|\Lambda|^{1/2}$: MD vs interpolation

Fig. S18

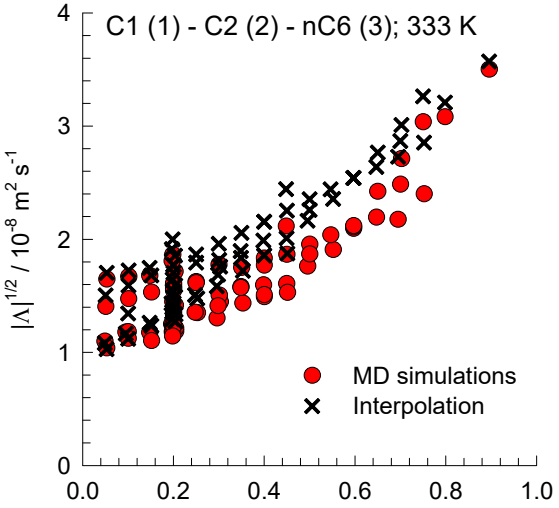

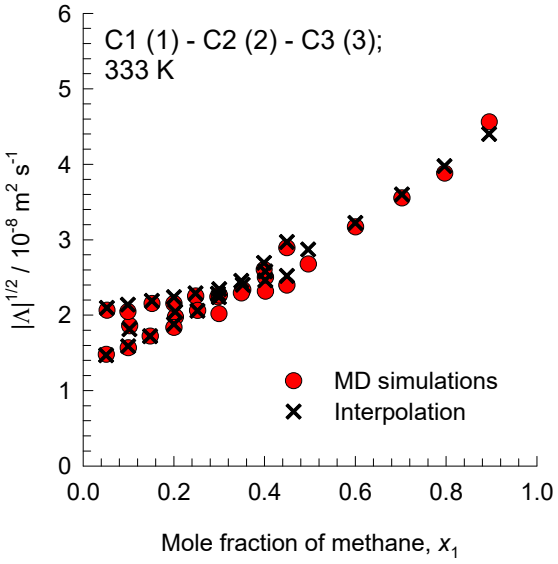

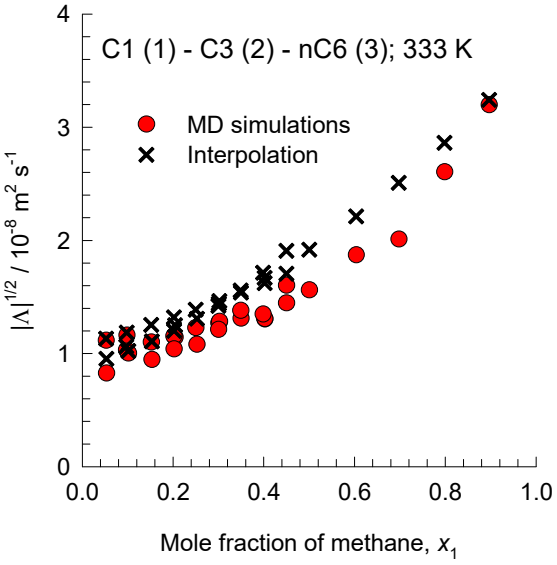

The values of $|\Lambda|^{1/2}$ obtained from MD simulations are compared with calculations using

$$|\Lambda|^{1/2} = \sqrt{\frac{Đ_{12}Đ_{13}Đ_{23}}{x_1Đ_{23}+x_2Đ_{13}+x_3Đ_{12}}}$$

combined with the Vignes interpolation formula

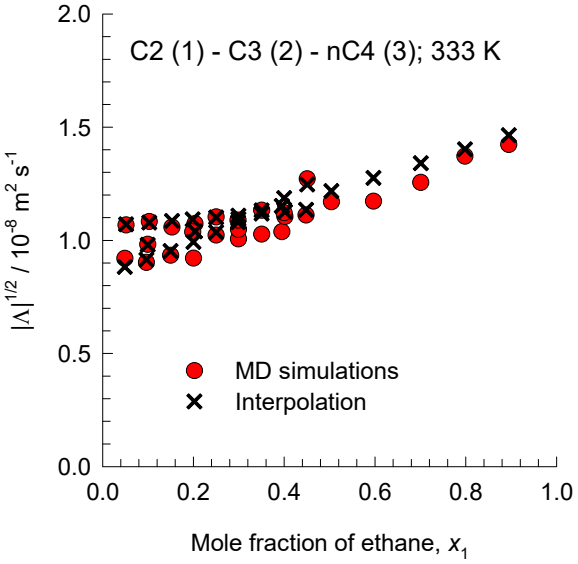

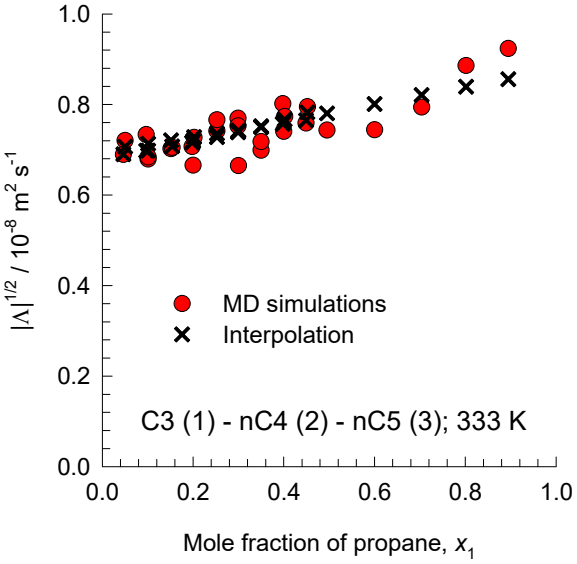

$|\Lambda|^{1/2}$: MD vs interpolation

Fig. S19

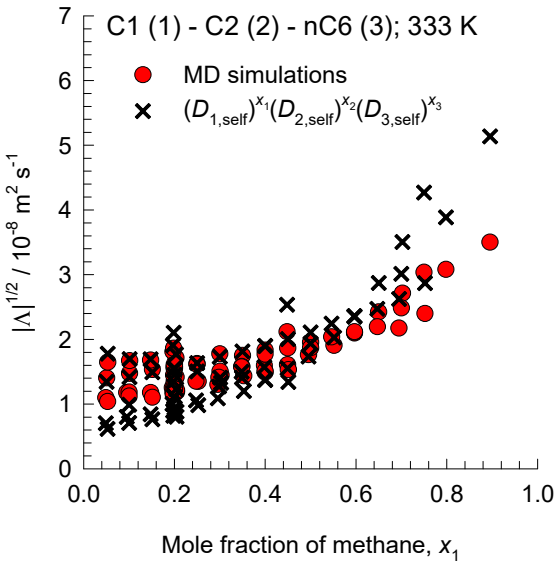

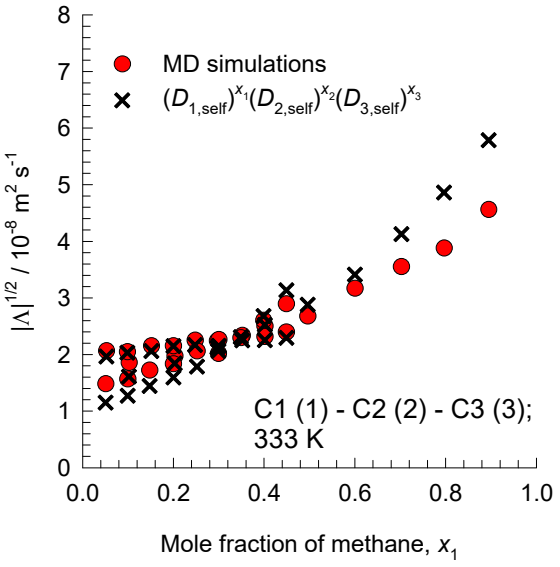

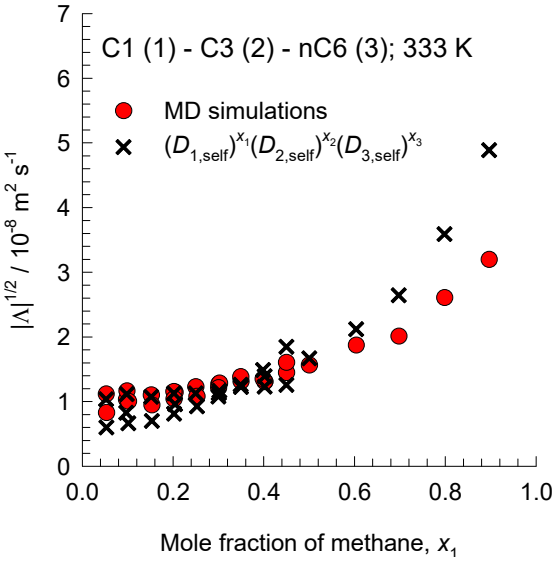

The self diffusivity values are from MD simulations.

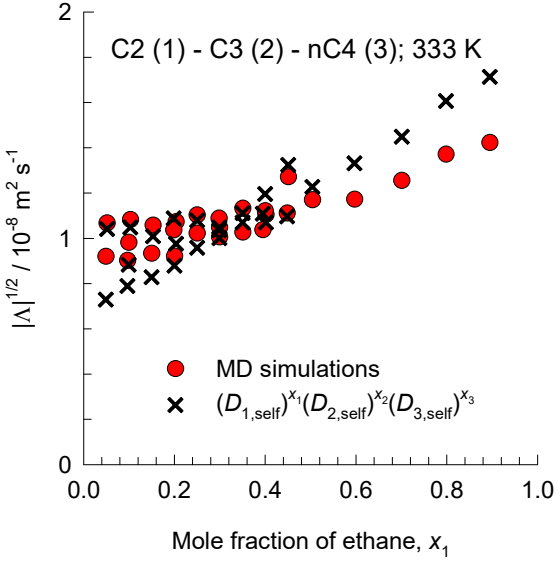

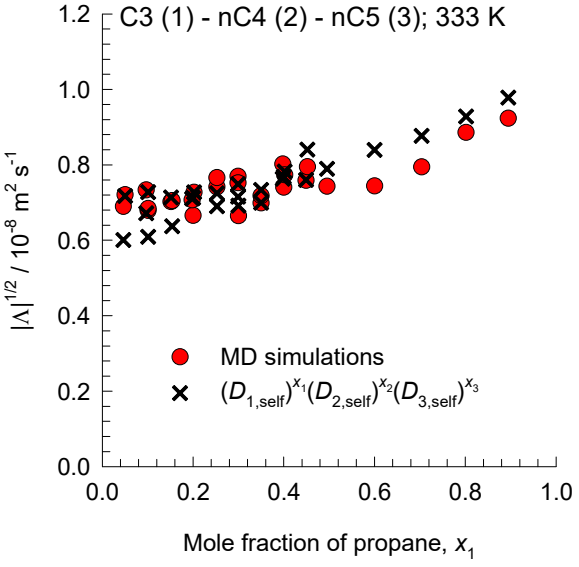

Fig. S20

C1/C2/nC6 system: interpolation ternaries

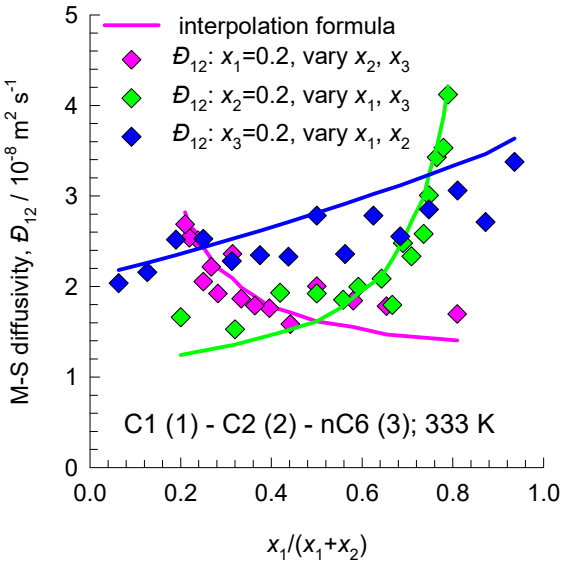

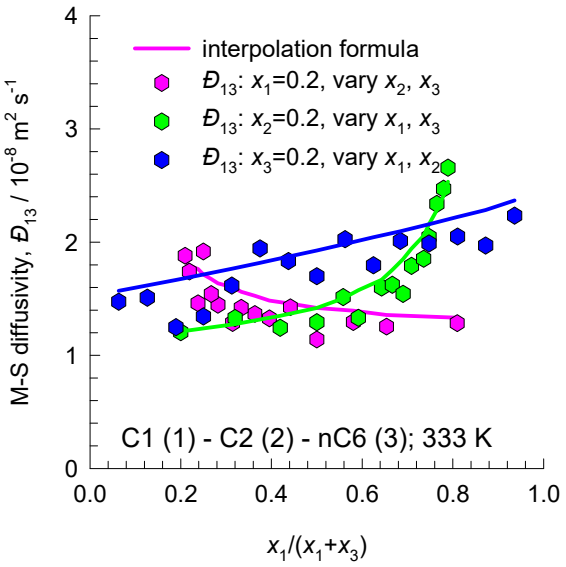

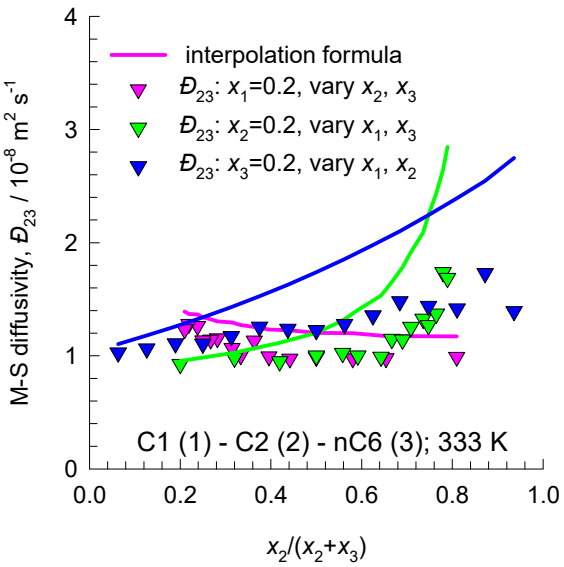

These parity plots are obtained using the Vignes interpolation formula

$$Đ_{ij} = \left(Đ_{ij}^{x_i \to 1}\right)^{x_i} \left(Đ_{ij}^{x_j \to 1}\right)^{x_j} \left(Đ_{ij}^{x_k \to 1}\right)^{x_k}$$

combined with the Wesselingh Bollen interpolation

$$Đ_{12}^{x_3 \to 1} = \sqrt{\left(Đ_{13}^{x_3 \to 1} Đ_{23}^{x_3 \to 1}\right)}$$

$$Đ_{13}^{x_2 \to 1} = \sqrt{\left(Đ_{12}^{x_2 \to 1} Đ_{23}^{x_2 \to 1}\right)}$$

$$Đ_{23}^{x_3 \to 1} = \sqrt{\left(Đ_{12}^{x_1 \to 1} Đ_{13}^{x_1 \to 1}\right)}$$

$$Đ_{12}^{x_1 \to 1} = 5.3; \quad Đ_{12}^{x_2 \to 1} = 2.5; \quad Đ_{13}^{x_1 \to 1} = 3; \quad Đ_{13}^{x_3 \to 1} = 1.05; \quad Đ_{23}^{x_2 \to 1} = 1.09; \quad Đ_{23}^{x_3 \to 1} = 0.84.$$

Fig. S21

C1/C2/nC6 system: interpolation ternaries

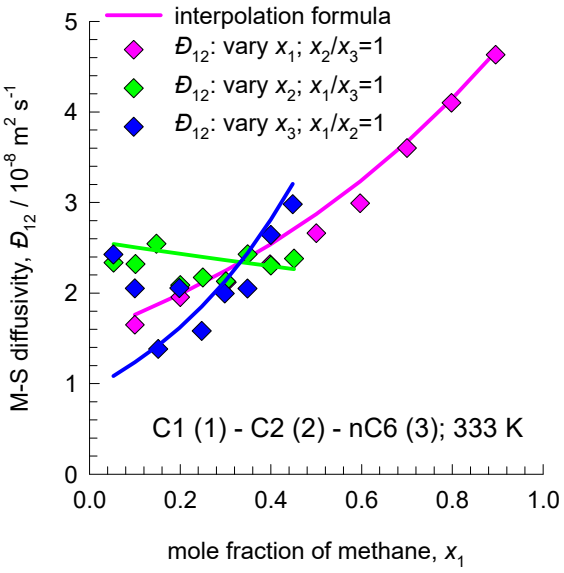

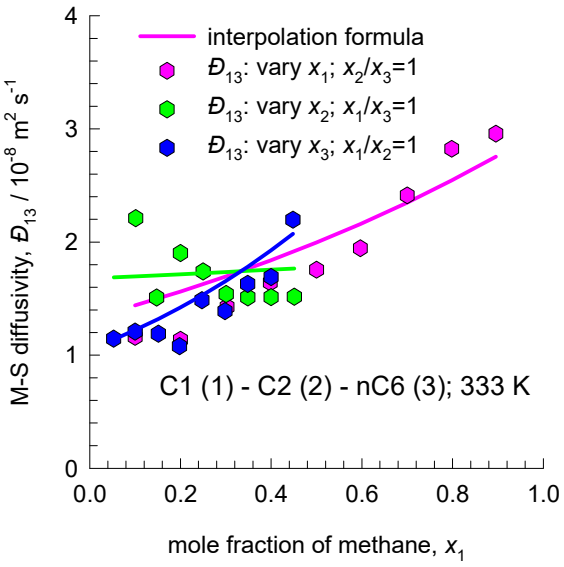

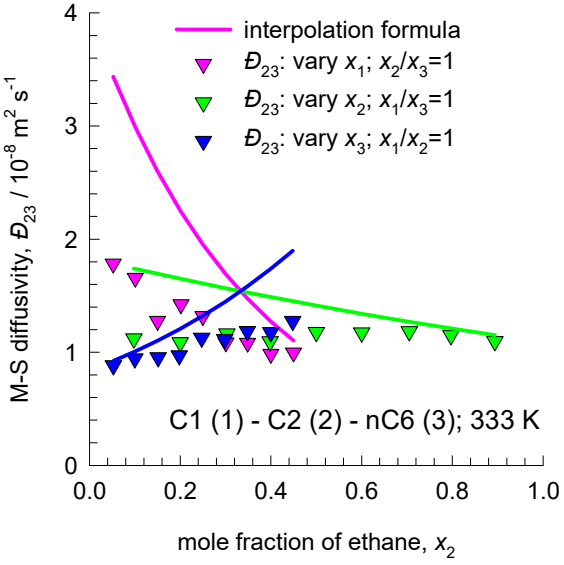

These parity plots are obtained using the Vignes interpolation formula

$$Đ_{ij} = \left(Đ_{ij}^{x_i \to 1}\right)^{x_i} \left(Đ_{ij}^{x_j \to 1}\right)^{x_j} \left(Đ_{ij}^{x_k \to 1}\right)^{x_k}$$

combined with the Wesselingh Bollen interpolation

$$Đ_{12}^{x_3 \to 1} = \sqrt{\left(Đ_{13}^{x_3 \to 1} Đ_{23}^{x_3 \to 1}\right)}$$

$$Đ_{13}^{x_2 \to 1} = \sqrt{\left(Đ_{12}^{x_2 \to 1} Đ_{23}^{x_2 \to 1}\right)}$$

$$Đ_{23}^{x_3 \to 1} = \sqrt{\left(Đ_{12}^{x_1 \to 1} Đ_{13}^{x_1 \to 1}\right)}$$

$$Đ_{12}^{x_1 \to 1} = 5.3; \quad Đ_{12}^{x_2 \to 1} = 2.5; \quad Đ_{13}^{x_1 \to 1} = 3; \quad Đ_{13}^{x_3 \to 1} = 1.05; \quad Đ_{23}^{x_2 \to 1} = 1.09; \quad Đ_{23}^{x_3 \to 1} = 0.84.$$

Fig. S22

C1/C2/C3 system: interpolation ternaries

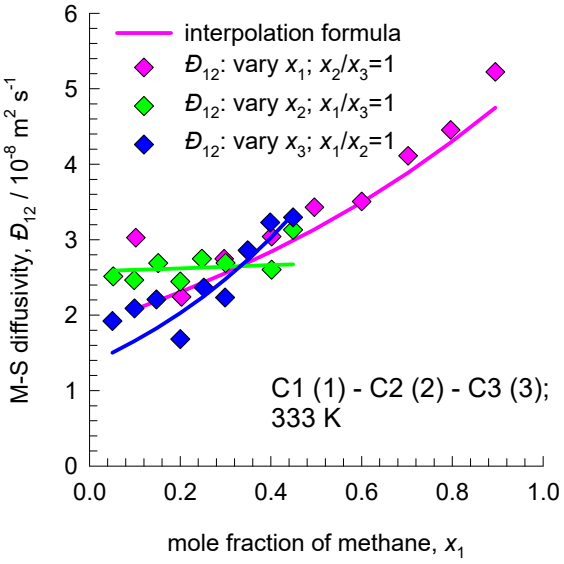

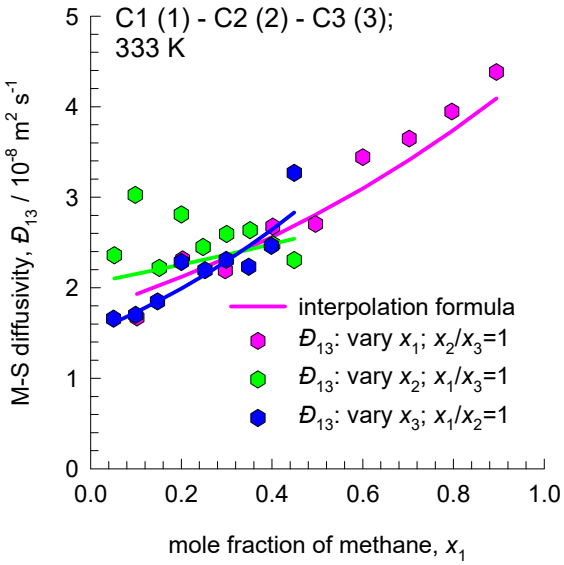

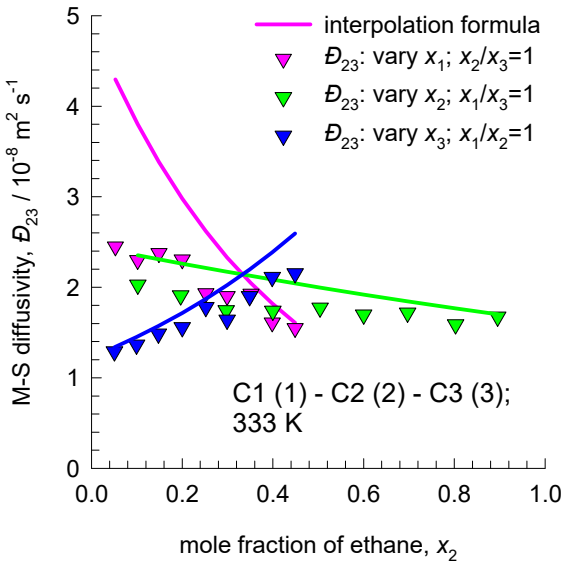

These parity plots are obtained using the Vignes interpolation formula

$$Đ_{ij} = \left(Đ_{ij}^{x_i \to 1}\right)^{x_i} \left(Đ_{ij}^{x_j \to 1}\right)^{x_j} \left(Đ_{ij}^{x_k \to 1}\right)^{x_k}$$

combined with the Wesselingh Bollen interpolation

$$Đ_{12}^{x_3 \to 1} = \sqrt{\left(Đ_{13}^{x_3 \to 1} Đ_{23}^{x_3 \to 1}\right)}$$

$$Đ_{13}^{x_2 \to 1} = \sqrt{\left(Đ_{12}^{x_2 \to 1} Đ_{23}^{x_2 \to 1}\right)}$$

$$Đ_{23}^{x_3 \to 1} = \sqrt{\left(Đ_{12}^{x_1 \to 1} Đ_{13}^{x_1 \to 1}\right)}$$

$$Đ_{12}^{x_1 \to 1} = 5.3; \quad Đ_{12}^{x_2 \to 1} = 2.5; \quad Đ_{13}^{x_1 \to 1} = 4.52; \quad Đ_{13}^{x_3 \to 1} = 1.5; \quad Đ_{23}^{x_2 \to 1} = 1.63; \quad Đ_{23}^{x_3 \to 1} = 1.23.$$

Fig. S23

C1/C3/nC6 system: interpolation ternaries

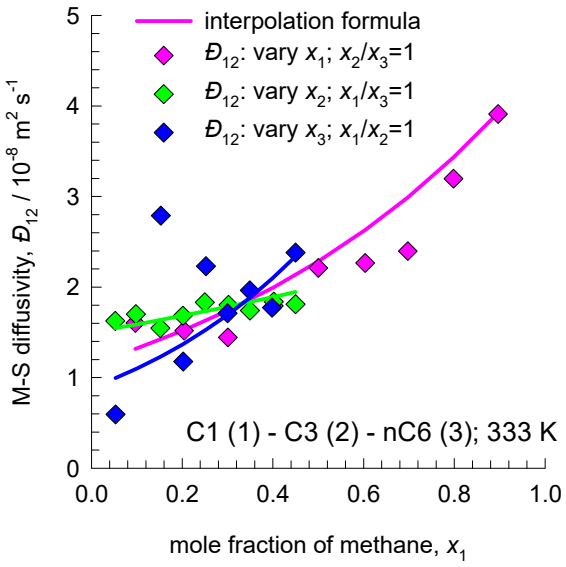

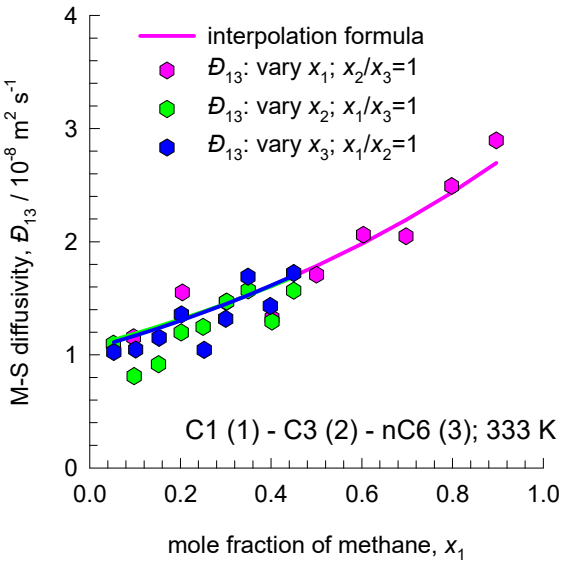

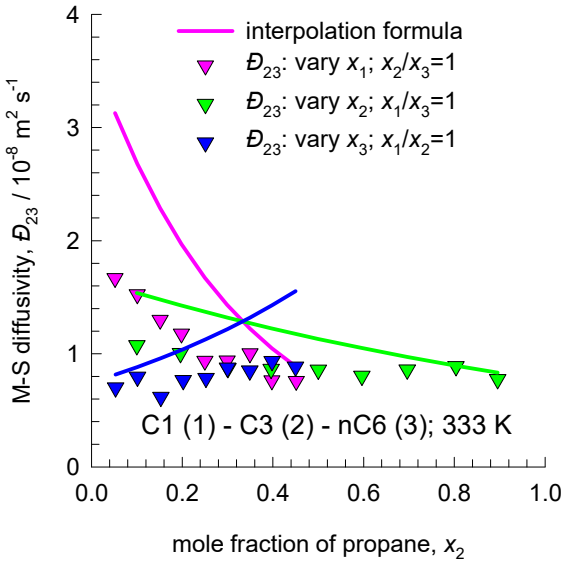

These parity plots are obtained using the Vignes interpolation formula

$$Đ_{ij} = \left(Đ_{ij}^{x_i \to 1}\right)^{x_i} \left(Đ_{ij}^{x_j \to 1}\right)^{x_j} \left(Đ_{ij}^{x_k \to 1}\right)^{x_k}$$

combined with the Wesselingh Bollen interpolation

$$Đ_{12}^{x_3 \to 1} = \sqrt{\left(Đ_{13}^{x_3 \to 1} Đ_{23}^{x_3 \to 1}\right)}$$

$$Đ_{13}^{x_2 \to 1} = \sqrt{\left(Đ_{12}^{x_2 \to 1} Đ_{23}^{x_2 \to 1}\right)}$$

$$Đ_{23}^{x_3 \to 1} = \sqrt{\left(Đ_{12}^{x_1 \to 1} Đ_{13}^{x_1 \to 1}\right)}$$

$$Đ_{12}^{x_1 \to 1} = 4.52; \quad Đ_{12}^{x_2 \to 1} = 1.5; \quad Đ_{13}^{x_1 \to 1} = 3; \quad Đ_{13}^{x_3 \to 1} = 1.05; \quad Đ_{23}^{x_2 \to 1} = 0.77; \quad Đ_{23}^{x_3 \to 1} = 0.75.$$

Fig. S24

C2/C3/nC4 system: interpolation ternaries

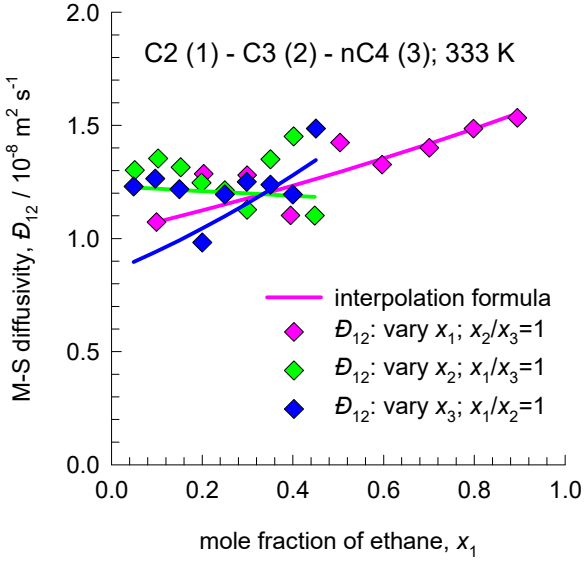

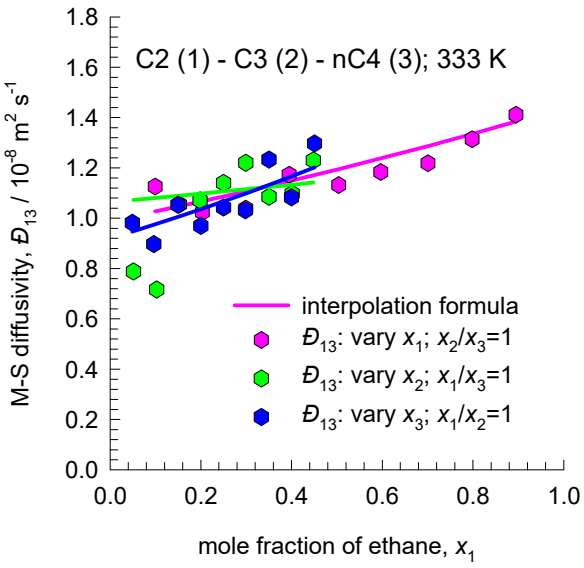

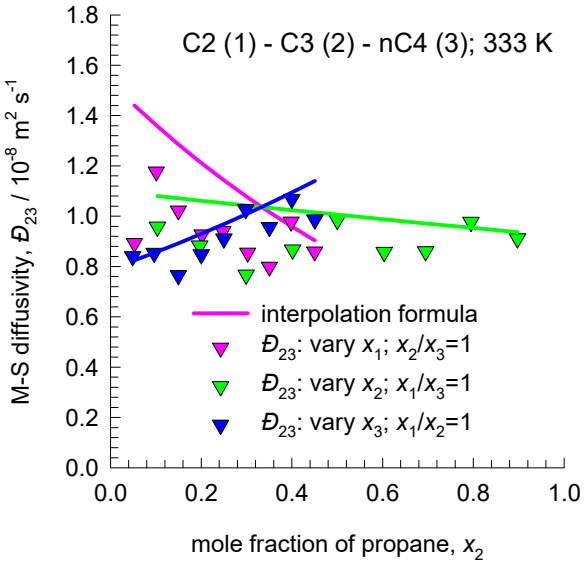

These parity plots are obtained using the Vignes interpolation formula

$$Đ_{ij} = \left(Đ_{ij}^{x_i \to 1}\right)^{x_i} \left(Đ_{ij}^{x_j \to 1}\right)^{x_j} \left(Đ_{ij}^{x_k \to 1}\right)^{x_k}$$

combined with the Wesselingh Bollen interpolation

$$Đ_{12}^{x_3 \to 1} = \sqrt{\left(Đ_{13}^{x_3 \to 1} Đ_{23}^{x_3 \to 1}\right)}$$

$$Đ_{13}^{x_2 \to 1} = \sqrt{\left(Đ_{12}^{x_2 \to 1} Đ_{23}^{x_2 \to 1}\right)}$$

$$Đ_{23}^{x_3 \to 1} = \sqrt{\left(Đ_{12}^{x_1 \to 1} Đ_{13}^{x_1 \to 1}\right)}$$

$$Đ_{12}^{x_1 \to 1} = 1.63; \quad Đ_{12}^{x_2 \to 1} = 1.23; \quad Đ_{13}^{x_1 \to 1} = 1.44; \quad Đ_{13}^{x_3 \to 1} = 0.92; \quad Đ_{23}^{x_2 \to 1} = 0.92; \quad Đ_{23}^{x_3 \to 1} = 0.79.$$

Fig. S25

C3/nC4/nC5 system: interpolation ternaries

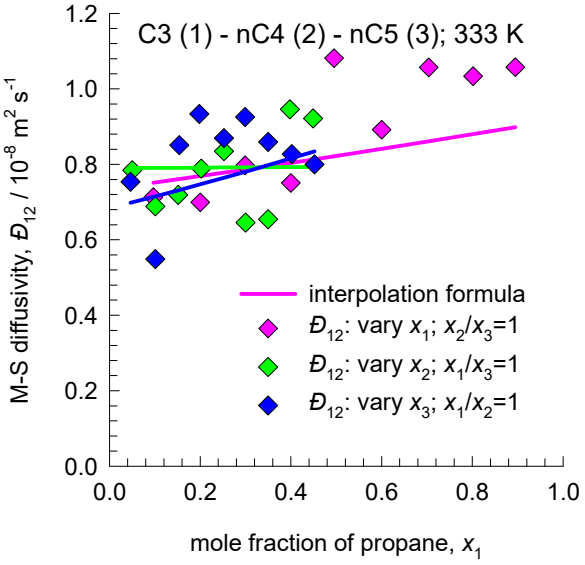

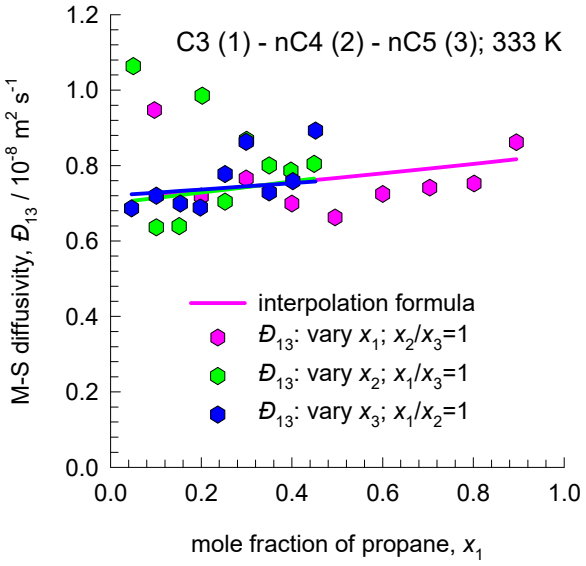

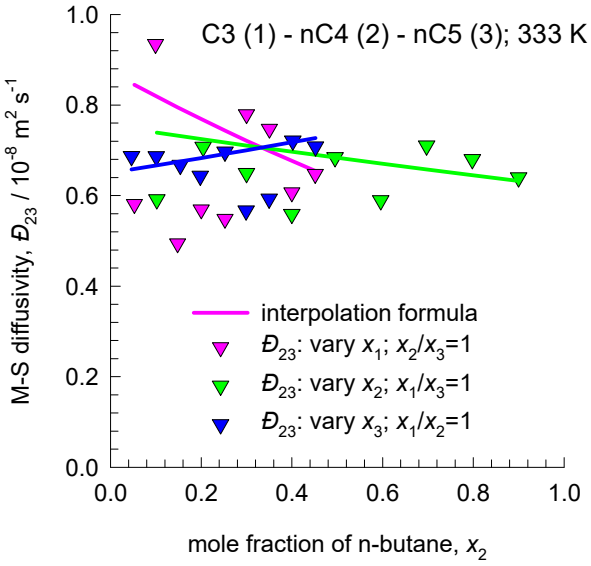

These parity plots are obtained using the Vignes interpolation formula

$$Đ_{ij} = \left(Đ_{ij}^{x_i \to 1}\right)^{x_i} \left(Đ_{ij}^{x_j \to 1}\right)^{x_j} \left(Đ_{ij}^{x_k \to 1}\right)^{x_k}$$

combined with the Wesselingh Bollen interpolation

$$Đ_{12}^{x_3 \to 1} = \sqrt{\left(Đ_{13}^{x_3 \to 1} Đ_{23}^{x_3 \to 1}\right)}$$

$$Đ_{13}^{x_2 \to 1} = \sqrt{\left(Đ_{12}^{x_2 \to 1} Đ_{23}^{x_2 \to 1}\right)}$$

$$Đ_{23}^{x_3 \to 1} = \sqrt{\left(Đ_{12}^{x_1 \to 1} Đ_{13}^{x_1 \to 1}\right)}$$

$$Đ_{12}^{x_1 \to 1} = 0.92; \quad Đ_{12}^{x_2 \to 1} = 0.79; \quad Đ_{13}^{x_1 \to 1} = 0.83; \quad Đ_{13}^{x_3 \to 1} = 0.72; \quad Đ_{23}^{x_2 \to 1} = 0.62; \quad Đ_{23}^{x_3 \to 1} = 0.65.$$

$|\Lambda|^{1/2}$: MD vs interpolation

Fig. S26

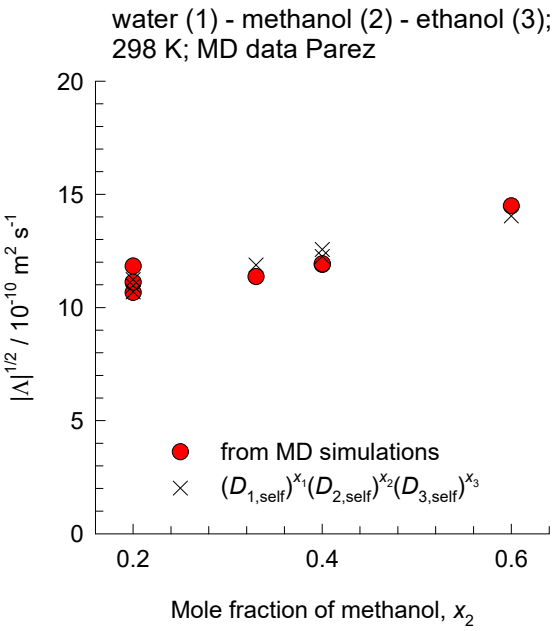

The interpolation formula is

$$|\Lambda|^{1/2} = \left(D_{1,self}\right)^{x_1}\left(D_{2,self}\right)^{x_2}\left(D_{3,self}\right)^{x_3}$$

where the fitted self-diffusivity values are

$D_{1,self}$ = 10.3
$D_{2,self}$ = 18
$D_{3,self}$ = 9.1
Units: 10^{-10} m^2 s^{-1}

Binaries: Acetone/Benzene/CCl_4

Fig. S27

(a)

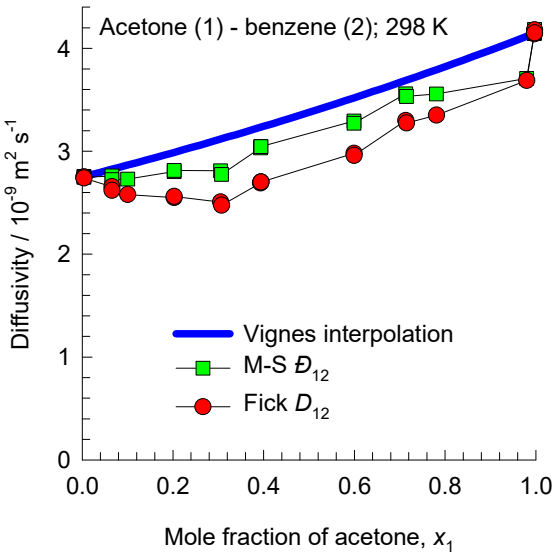

$$Đ_{12}^{x_1\to 1} = 4.15; \quad Đ_{12}^{x_2\to 1} = 2.75; \quad \text{for acetone(1)/benzene(2) binary mixture}$$

$$Đ_{13}^{x_1\to 1} = 3.57; \quad Đ_{13}^{x_3\to 1} = 1.7; \quad \text{for acetone(1)/}CCl_4\text{(3) binary mixture}$$

$$Đ_{23}^{x_2\to 1} = 1.91; \quad Đ_{23}^{x_3\to 1} = 1.42 \quad \text{for benzene(2)/}CCl_4\text{(3) binary mixture}$$

(b)

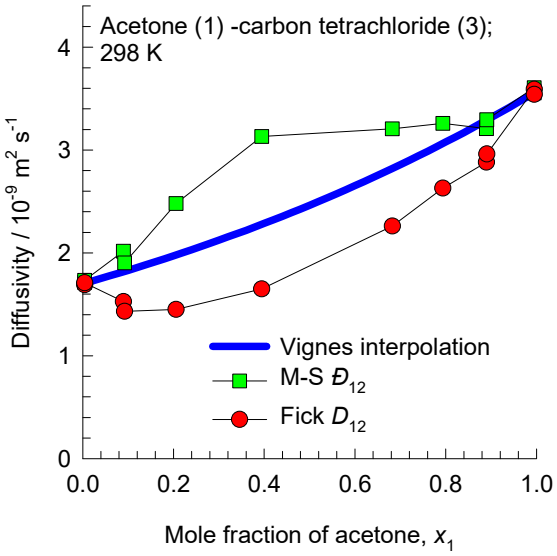

(c)

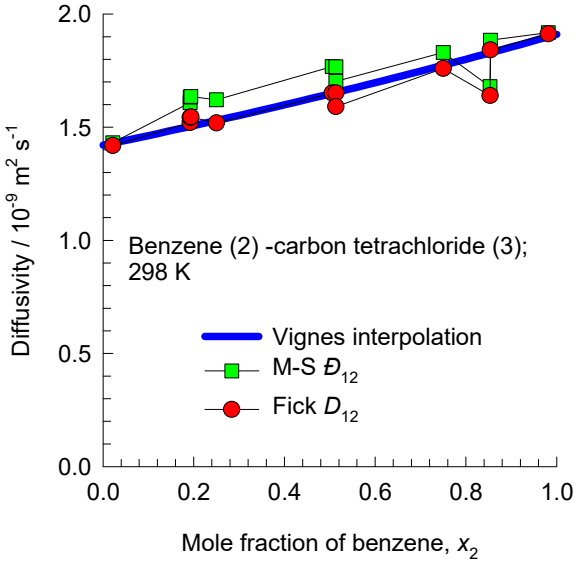

Fick matrix: Acetone/Benzene/CCl_4

Fig. S28

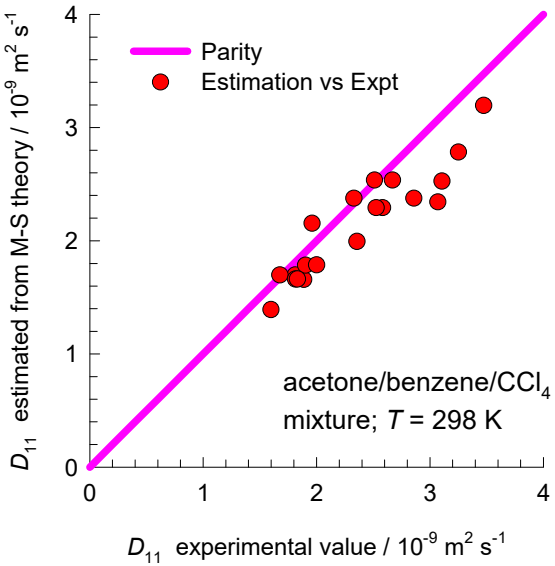

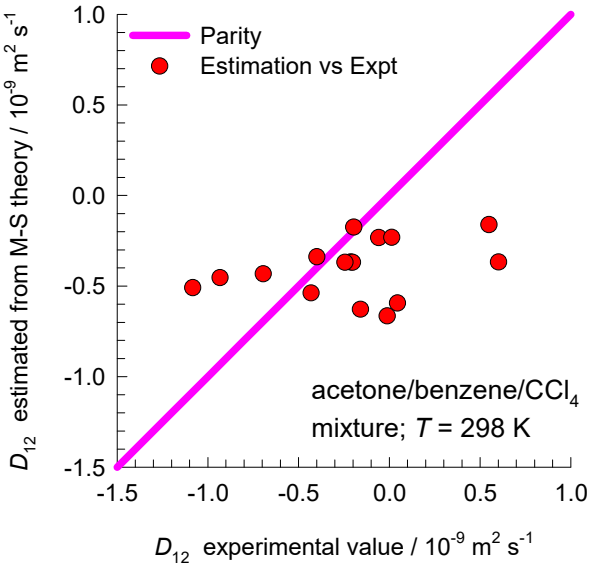

The Fick matrix is estimated using

$$[D]=[B]^{-1}[\Gamma]=[\Lambda][\Gamma]$$

The elements of [B] are estimated using the Vignes interpolation formula

$$Đ_{ij}=\left(Đ_{ij}^{x_i\to 1}\right)^{x_i}\left(Đ_{ij}^{x_j\to 1}\right)^{x_j}\left(Đ_{ij}^{x_k\to 1}\right)^{x_k}$$

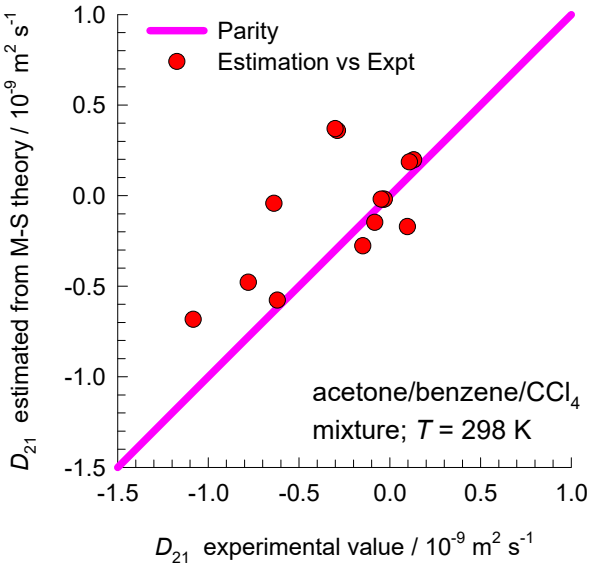

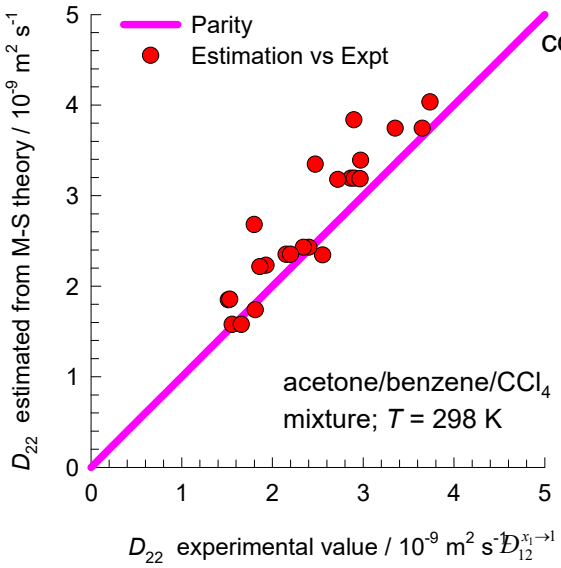

combined with the Wesselingh Bollen interpolation

$$Đ_{12}^{x_3\to 1}=\sqrt{\left(Đ_{13}^{x_3\to 1}Đ_{23}^{x_3\to 1}\right)}$$

$$Đ_{13}^{x_2\to 1}=\sqrt{\left(Đ_{12}^{x_2\to 1}Đ_{23}^{x_2\to 1}\right)}$$

$$Đ_{23}^{x_3\to 1}=\sqrt{\left(Đ_{12}^{x_1\to 1}Đ_{13}^{x_1\to 1}\right)}$$

$Đ_{12}^{x_1\to 1}=4.15$; $Đ_{12}^{x_2\to 1}=2.75$; for acetone(1)/benzene(2) binary mixture

$Đ_{13}^{x_1\to 1}=3.57$; $Đ_{13}^{x_3\to 1}=1.7$; for acetone(1)/CCl_4(3) binary mixture

$Đ_{23}^{x_2\to 1}=1.91$; $Đ_{23}^{x_3\to 1}=1.42$ for benzene(2)/CCl_4(3) binary mixture

$|\Lambda|^{1/2} = |D|^{1/2} / |\Gamma|^{1/2}$

Fig. S29

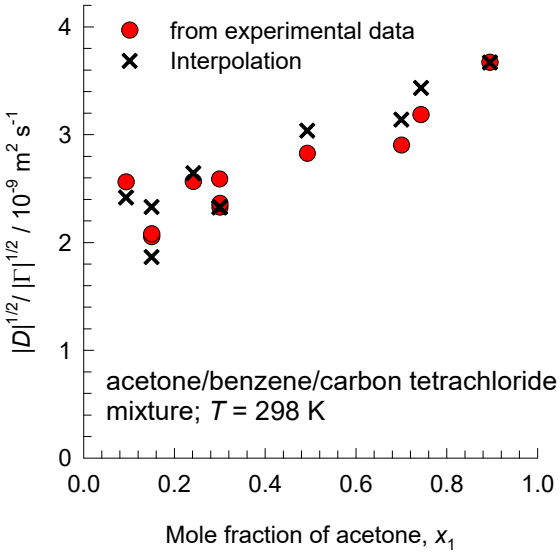

The values of $|\Lambda|^{1/2} = \dfrac{|D|^{1/2}}{|\Gamma|^{1/2}}$

obtained from experimental data are compared with $|\Lambda|^{1/2}$ calculations using

$$|\Lambda|^{1/2} = \sqrt{\frac{Đ_{12}Đ_{13}Đ_{23}}{x_1Đ_{23}+x_2Đ_{13}+x_3Đ_{12}}}$$

along with the Vignes interpolation formula

$$Đ_{ij} = \left(Đ_{ij}^{x_i \to 1}\right)^{x_i} \left(Đ_{ij}^{x_j \to 1}\right)^{x_j} \left(Đ_{ij}^{x_k \to 1}\right)^{x_k}$$

combined with the Wesselingh Bollen interpolation

$$Đ_{12}^{x_3 \to 1} = \sqrt{\left(Đ_{13}^{x_3 \to 1} Đ_{23}^{x_3 \to 1}\right)}$$

$$Đ_{13}^{x_2 \to 1} = \sqrt{\left(Đ_{12}^{x_2 \to 1} Đ_{23}^{x_2 \to 1}\right)}$$

$$Đ_{23}^{x_3 \to 1} = \sqrt{\left(Đ_{12}^{x_1 \to 1} Đ_{13}^{x_1 \to 1}\right)}$$

$Đ_{12}^{x_1 \to 1} = 4.15$; $Đ_{12}^{x_2 \to 1} = 2.75$; for acetone(1)/benzene(2) binary mixture

$Đ_{13}^{x_1 \to 1} = 3.57$; $Đ_{13}^{x_3 \to 1} = 1.7$; for acetone(1)/CCl_4(3) binary mixture

$Đ_{23}^{x_2 \to 1} = 1.91$; $Đ_{23}^{x_3 \to 1} = 1.42$ for benzene(2)/CCl_4(3) binary mixture

Fick matrix: Acetone/Benzene/CCl_4

Fig. S30

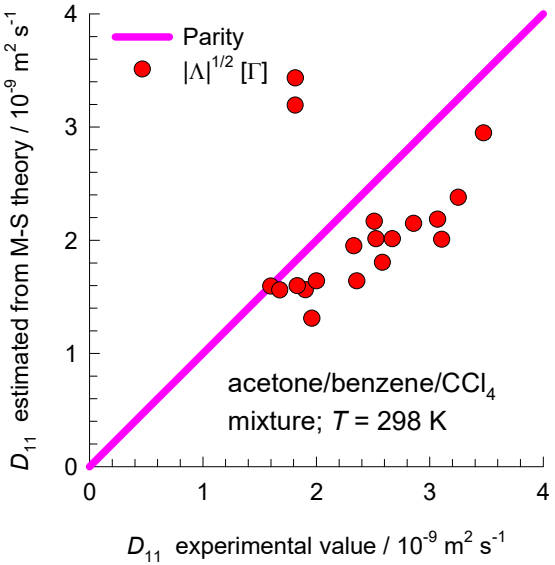

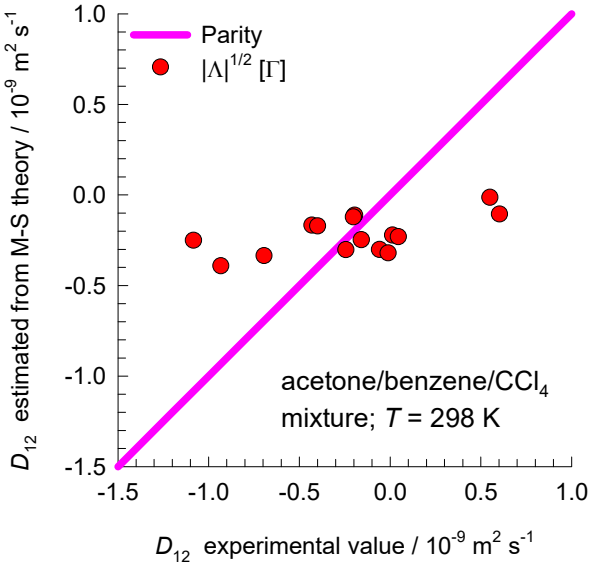

The Fick matrix is estimated using

$$[D]=|\Lambda|^{1/2}[\Gamma]$$

$$|\Lambda|^{1/2}=\sqrt{\frac{Đ_{12}Đ_{13}Đ_{23}}{x_1Đ_{23}+x_2Đ_{13}+x_3Đ_{12}}}$$

along with the Vignes interpolation formula

$$Đ_{ij}=\left(Đ_{ij}^{x_i\to 1}\right)^{x_i}\left(Đ_{ij}^{x_j\to 1}\right)^{x_j}\left(Đ_{ij}^{x_k\to 1}\right)^{x_k}$$

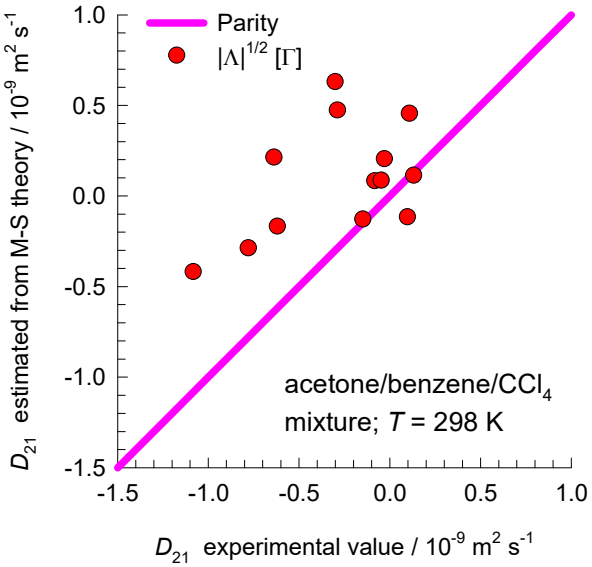

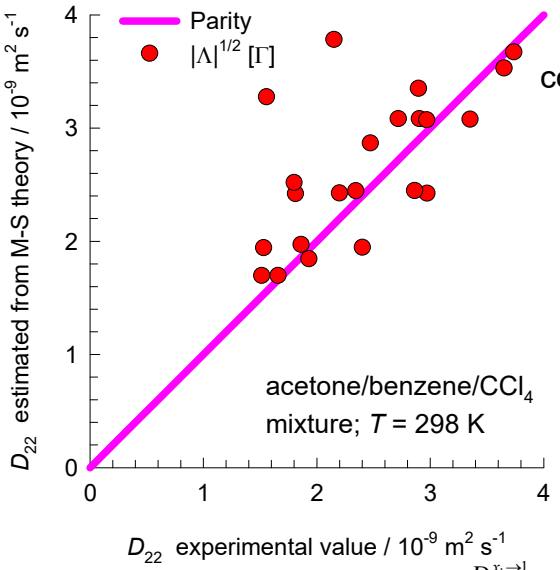

combined with the Wesselingh Bollen interpolation

$$Đ_{12}^{x_3\to 1}=\sqrt{\left(Đ_{13}^{x_3\to 1}Đ_{23}^{x_3\to 1}\right)}$$

$$Đ_{13}^{x_2\to 1}=\sqrt{\left(Đ_{12}^{x_2\to 1}Đ_{23}^{x_2\to 1}\right)}$$

$$Đ_{23}^{x_3\to 1}=\sqrt{\left(Đ_{12}^{x_1\to 1}Đ_{13}^{x_1\to 1}\right)}$$

$Đ_{12}^{x_1\to 1}=4.15$; $Đ_{12}^{x_2\to 1}=2.75$; for acetone(1)/benzene(2) binary mixture

$Đ_{13}^{x_1\to 1}=3.57$; $Đ_{13}^{x_3\to 1}=1.7$; for acetone(1)/CCl_4(3) binary mixture

$Đ_{23}^{x_2\to 1}=1.91$; $Đ_{23}^{x_3\to 1}=1.42$ for benzene(2)/CCl_4(3) binary mixture

Binaries: Acetone/Benzene/Methanol

Fig. S31

(a)

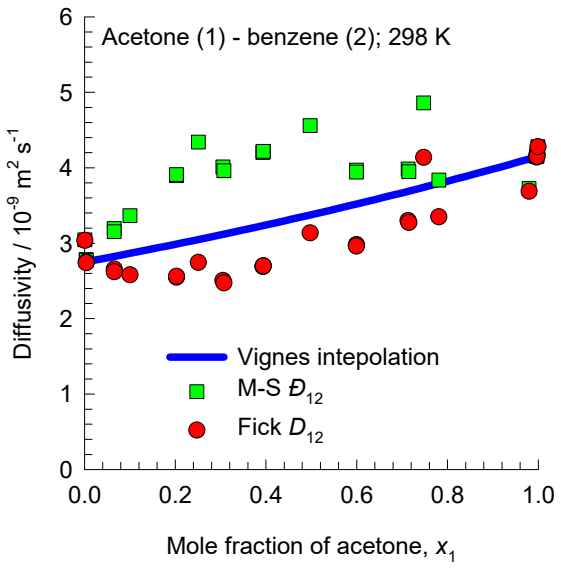

$Đ_{12}^{x_1 \to 1} = 4.15$; $Đ_{12}^{x_2 \to 1} = 2.75$; for acetone(1)/benzene(2) binary mixture

$Đ_{13}^{x_1 \to 1} = 5.3$; $Đ_{13}^{x_3 \to 1} = 2.7$; for acetone(1)/methanol(3) binary mixture

$Đ_{23}^{x_2 \to 1} = 4.3$; $Đ_{23}^{x_3 \to 1} = 3$ for benzene(2)/methanol(3) binary mixture

(b)

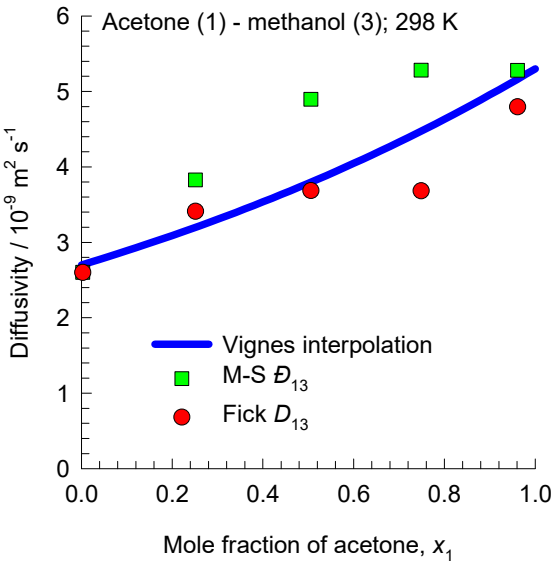

(c)

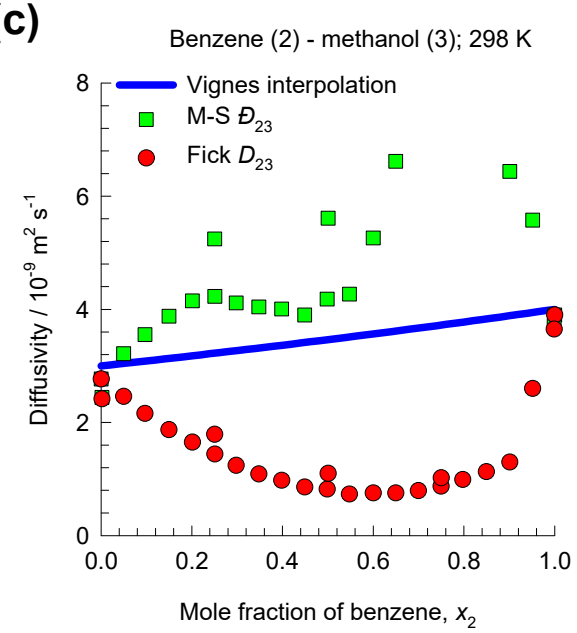

$|\Lambda|^{1/2} = |D|^{1/2} / |\Gamma|^{1/2}$

Fig. S32

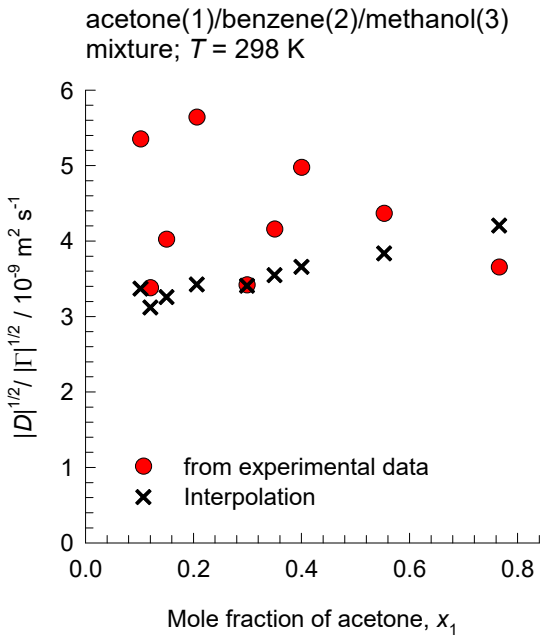

The values of $|\Lambda|^{1/2} = \dfrac{|D|^{1/2}}{|\Gamma|^{1/2}}$

obtained from experimental data are compared with $|\Lambda|^{1/2}$ calculations using

$$|\Lambda|^{1/2} = \sqrt{\frac{Đ_{12}Đ_{13}Đ_{23}}{x_1Đ_{23}+x_2Đ_{13}+x_3Đ_{12}}}$$

combined with the Vignes interpolation formula

$$Đ_{ij} = \left(Đ_{ij}^{x_i\to 1}\right)^{x_i}\left(Đ_{ij}^{x_j\to 1}\right)^{x_j}\left(Đ_{ij}^{x_k\to 1}\right)^{x_k}$$

combined with the Wesselingh Bollen interpolation

$$Đ_{12}^{x_3\to 1} = \sqrt{\left(Đ_{13}^{x_3\to 1}Đ_{23}^{x_3\to 1}\right)}$$

$$Đ_{13}^{x_2\to 1} = \sqrt{\left(Đ_{12}^{x_2\to 1}Đ_{23}^{x_2\to 1}\right)}$$

$$Đ_{23}^{x_3\to 1} = \sqrt{\left(Đ_{12}^{x_1\to 1}Đ_{13}^{x_1\to 1}\right)}$$

$Đ_{12}^{x_1\to 1} = 4.15$; $Đ_{12}^{x_2\to 1} = 2.75$; for acetone(1)/benzene(2) binary mixture

$Đ_{13}^{x_1\to 1} = 5.3$; $Đ_{13}^{x_3\to 1} = 2.7$; for acetone(1)/methanol(3) binary mixture

$Đ_{23}^{x_2\to 1} = 4.3$; $Đ_{23}^{x_3\to 1} = 3$ for benzene(2)/methanol(3) binary mixture

Fick matrix for Acetone-Benzene-Methanol

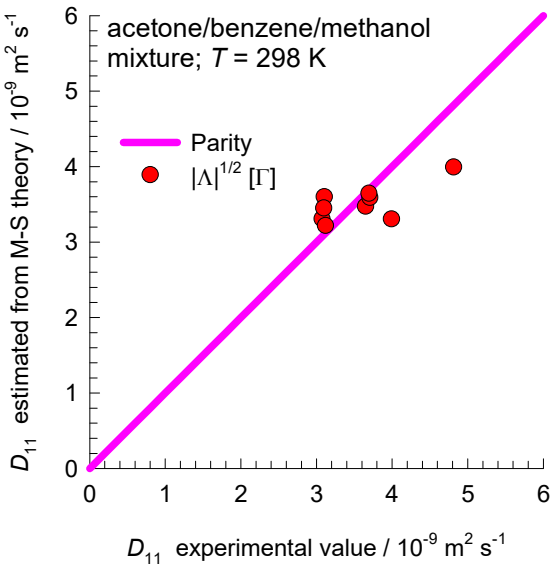

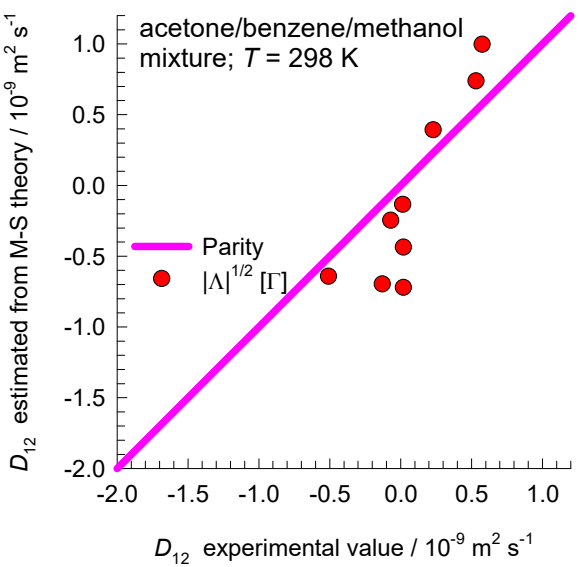

The Fick matrix is estimated using

$$[D] = |\Lambda|^{1/2}[\Gamma]$$

$$|\Lambda|^{1/2} = \sqrt{\frac{Đ_{12}Đ_{13}Đ_{23}}{x_1Đ_{23}+x_2Đ_{13}+x_3Đ_{12}}}$$

along with the Vignes interpolation formula

$$Đ_{ij} = \left(Đ_{ij}^{x_i\to 1}\right)^{x_i}\left(Đ_{ij}^{x_j\to 1}\right)^{x_j}\left(Đ_{ij}^{x_k\to 1}\right)^{x_k}$$

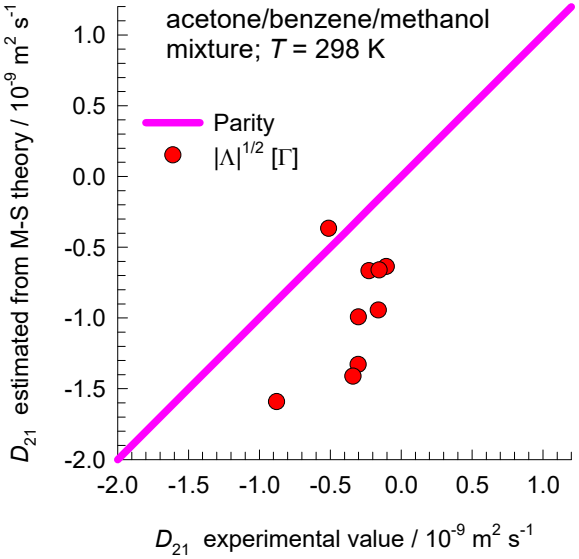

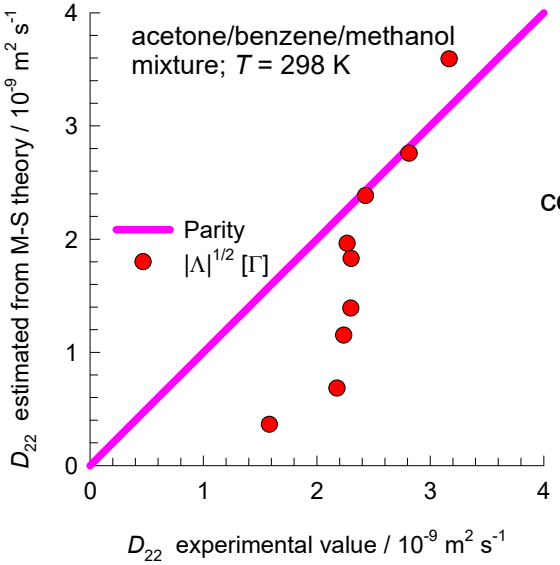

combined with the Wesselingh Bollen interpolation

$$Đ_{12}^{x_3\to 1} = \sqrt{\left(Đ_{13}^{x_3\to 1}Đ_{23}^{x_3\to 1}\right)}$$

$$Đ_{13}^{x_2\to 1} = \sqrt{\left(Đ_{12}^{x_2\to 1}Đ_{23}^{x_2\to 1}\right)}$$

$$Đ_{23}^{x_3\to 1} = \sqrt{\left(Đ_{12}^{x_1\to 1}Đ_{13}^{x_1\to 1}\right)}$$

$Đ_{12}^{x_1\to 1} = 4.15$; $Đ_{12}^{x_2\to 1} = 2.75$; for acetone(1)/benzene(2) binary mixture

$Đ_{13}^{x_1\to 1} = 5.3$; $Đ_{13}^{x_3\to 1} = 2.7$; for acetone(1)/methanol(3) binary mixture

$Đ_{23}^{x_2\to 1} = 4.3$; $Đ_{23}^{x_3\to 1} = 3$ for benzene(2)/methanol(3) binary mixture

Coupling effects: Acetone/Benzene/Methanol

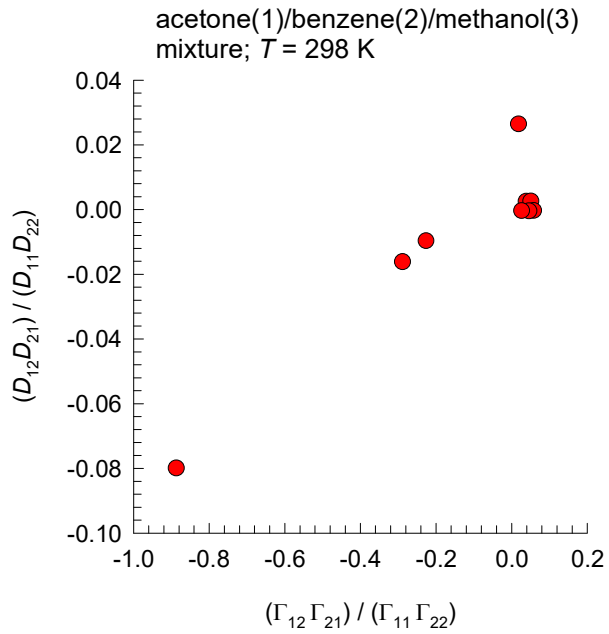

$|\Lambda|^{1/2} = |D|^{1/2} / |\Gamma|^{1/2}$

Fig. S35

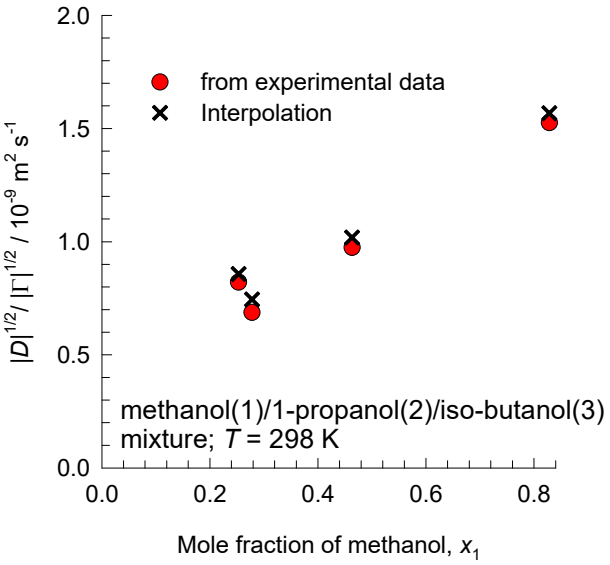

The values of $|\Lambda|^{1/2} = \dfrac{|D|^{1/2}}{|\Gamma|^{1/2}}$

obtained from experimental data are compared with $|\Lambda|^{1/2}$ calculations using

$$|\Lambda|^{1/2} = \sqrt{\frac{Đ_{12} Đ_{13} Đ_{23}}{x_1 Đ_{23} + x_2 Đ_{13} + x_3 Đ_{12}}}$$

combined with the Vignes interpolation formula

$$Đ_{ij} = \left(Đ_{ij}^{x_i \to 1}\right)^{x_i} \left(Đ_{ij}^{x_j \to 1}\right)^{x_j} \left(Đ_{ij}^{x_k \to 1}\right)^{x_k}$$

combined with the Wesselingh Bollen interpolation

$$Đ_{12}^{x_3 \to 1} = \sqrt{\left(Đ_{13}^{x_3 \to 1} Đ_{23}^{x_3 \to 1}\right)}$$
$$Đ_{13}^{x_2 \to 1} = \sqrt{\left(Đ_{12}^{x_2 \to 1} Đ_{23}^{x_2 \to 1}\right)}$$
$$Đ_{23}^{x_3 \to 1} = \sqrt{\left(Đ_{12}^{x_1 \to 1} Đ_{13}^{x_1 \to 1}\right)}$$

$$Đ_{12}^{x_1 \to 1} = 1.966; \quad Đ_{12}^{x_2 \to 1} = 0.804;$$
$$Đ_{13}^{x_1 \to 1} = 1.83; \quad Đ_{13}^{x_3 \to 1} = 0587;$$
$$Đ_{23}^{x_2 \to 1} = 0.584; \quad Đ_{23}^{x_3 \to 1} = 0.398.$$

Fick matrix for Methanol-1-Propanol-Iso-butanol

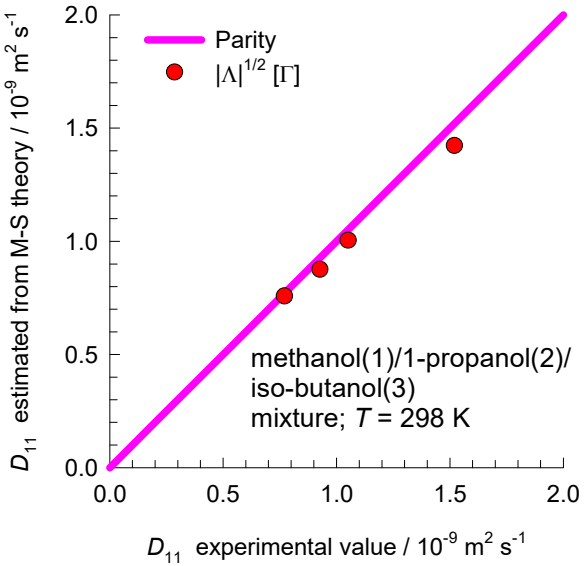

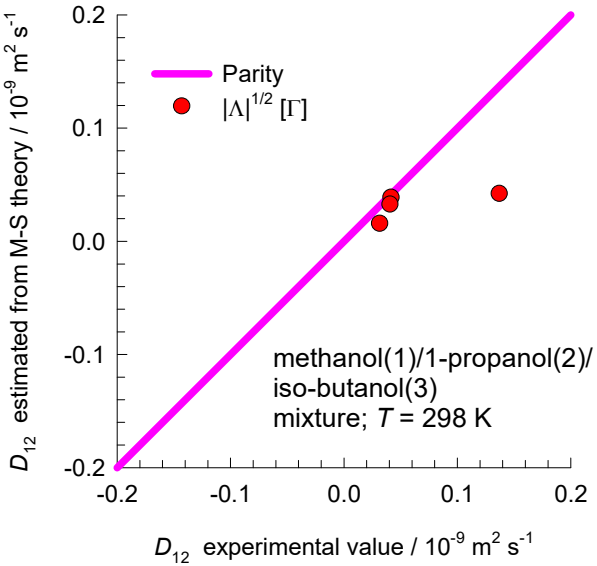

The Fick matrix is estimated using

$$[D]=|\Lambda|^{1/2}[\Gamma]$$

$$|\Lambda|^{1/2}=\sqrt{\frac{Đ_{12}Đ_{13}Đ_{23}}{x_1Đ_{23}+x_2Đ_{13}+x_3Đ_{12}}}$$

along with the Vignes interpolation formula

$$Đ_{ij}=\left(Đ_{ij}^{x_i\to 1}\right)^{x_i}\left(Đ_{ij}^{x_j\to 1}\right)^{x_j}\left(Đ_{ij}^{x_k\to 1}\right)^{x_k}$$

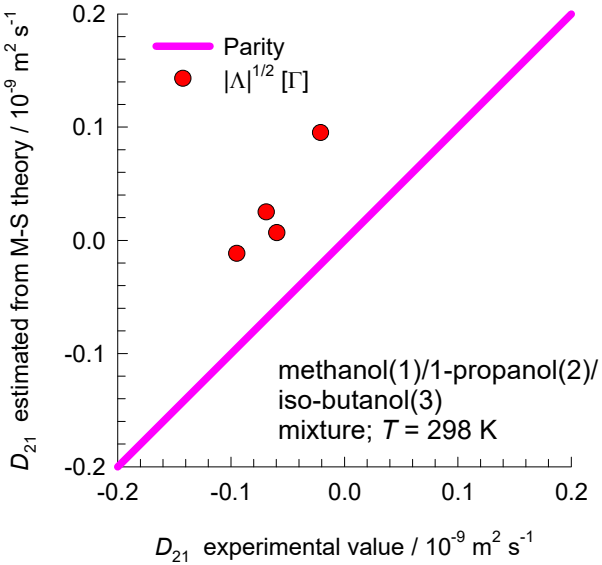

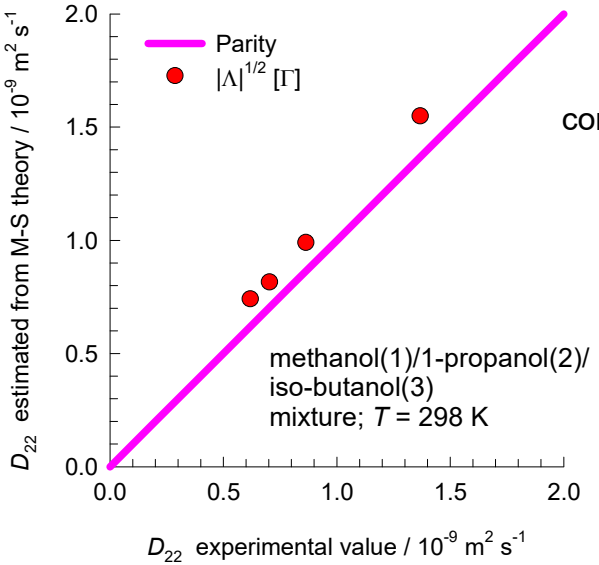

combined with the Wesselingh Bollen interpolation

$$Đ_{12}^{x_3\to 1}=\sqrt{\left(Đ_{13}^{x_3\to 1}Đ_{23}^{x_3\to 1}\right)}$$
$$Đ_{13}^{x_2\to 1}=\sqrt{\left(Đ_{12}^{x_2\to 1}Đ_{23}^{x_2\to 1}\right)}$$
$$Đ_{23}^{x_3\to 1}=\sqrt{\left(Đ_{12}^{x_1\to 1}Đ_{13}^{x_1\to 1}\right)}$$

$$Đ_{12}^{x_1\to 1}=1.966;\quad Đ_{12}^{x_2\to 1}=0.804;$$
$$Đ_{13}^{x_1\to 1}=1.83;\quad Đ_{13}^{x_3\to 1}=0587;$$
$$Đ_{23}^{x_2\to 1}=0.584;\quad Đ_{23}^{x_3\to 1}=0.398.$$

Fig. S37

Coupling effects: Methanol-1-Propanol-Iso-butanol

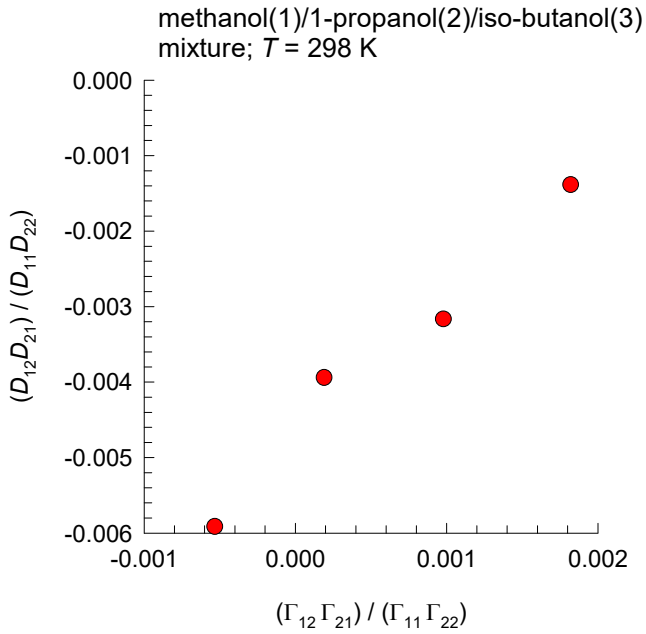

Fig. S38

2-Propanol/Glycerol/Water mixture

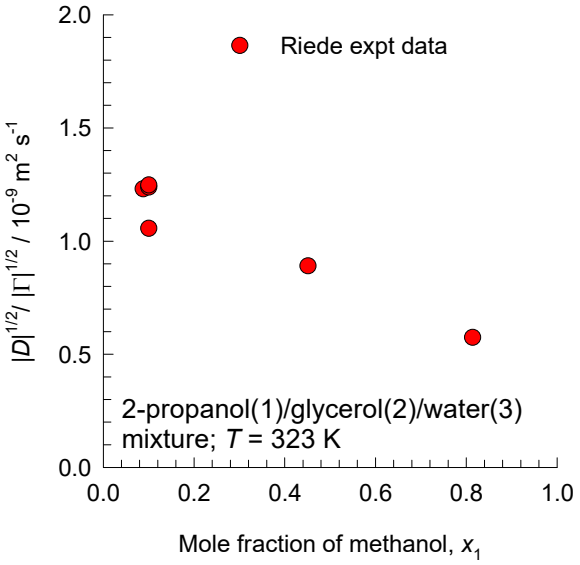

Binary pairs: methanol/1-butanol/1-propanol

Fig. S39

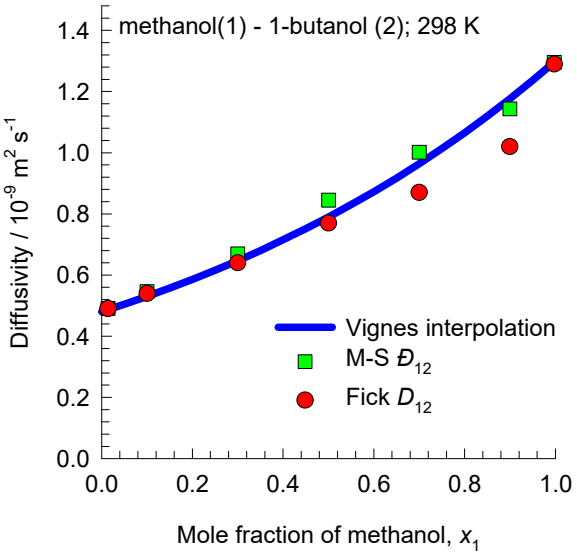

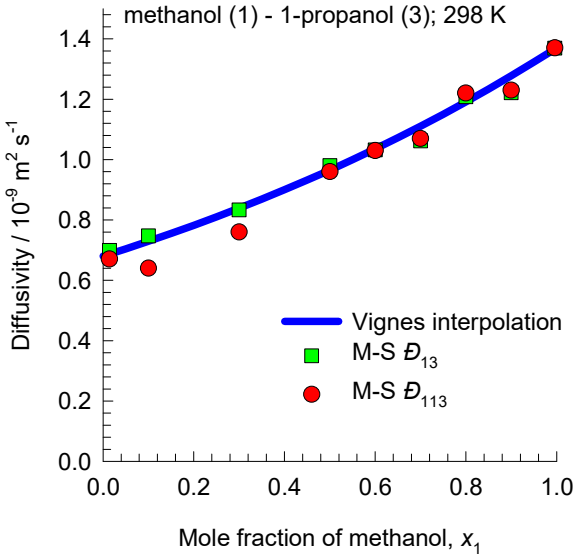

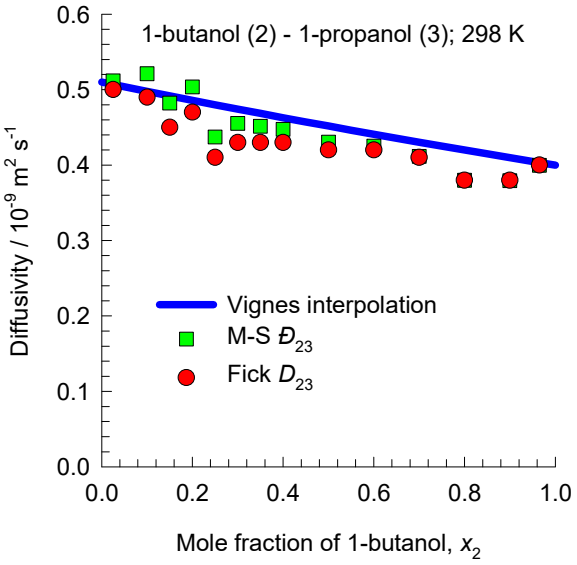

$$Đ_{12}^{x_1\to 1}=1.3;\quad Đ_{12}^{x_2\to 1}=0.48;\quad Đ_{13}^{x_1\to 1}=1.37;\quad Đ_{13}^{x_3\to 1}=0.68;\quad Đ_{23}^{x_2\to 1}=0.4;\quad Đ_{23}^{x_3\to 1}=0.51$$

Binary pairs: acetone/water/1-propanol

Fig. S40

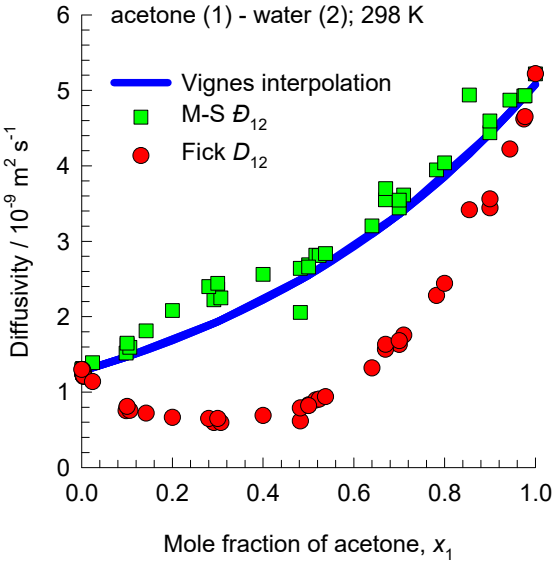

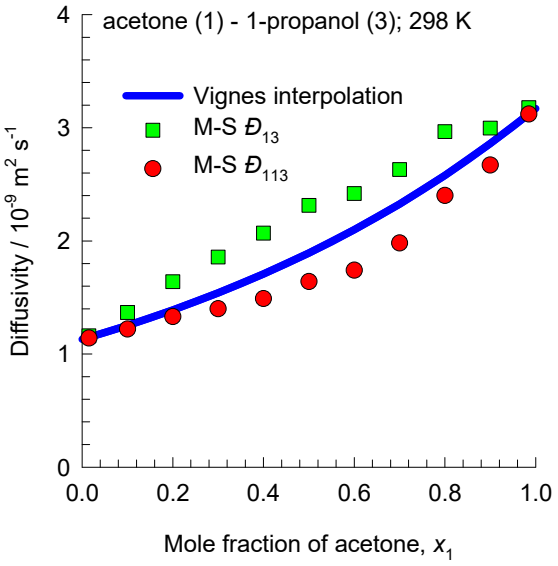

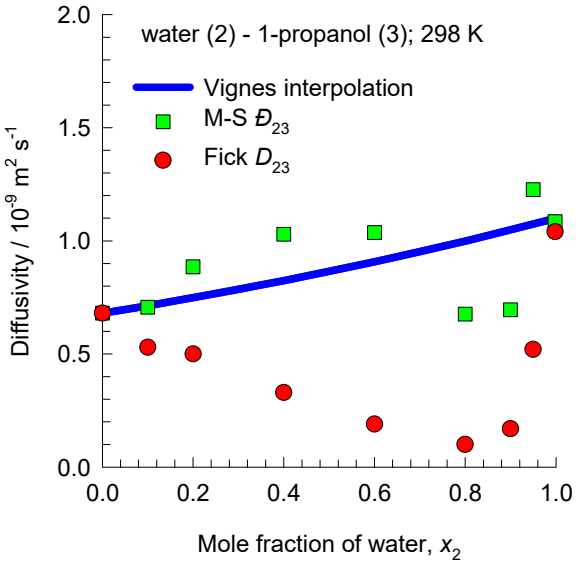

$$Đ_{12}^{x_1\to 1} = 5.08; \quad Đ_{12}^{x_2\to 1} = 1.28; \quad Đ_{13}^{x_1\to 1} = 3.17; \quad Đ_{13}^{x_3\to 1} = 1.13; \quad Đ_{23}^{x_2\to 1} = 1.1; \quad Đ_{23}^{x_3\to 1} = 0.68$$

Binary pairs: acetone/1-butanol/1-propanol

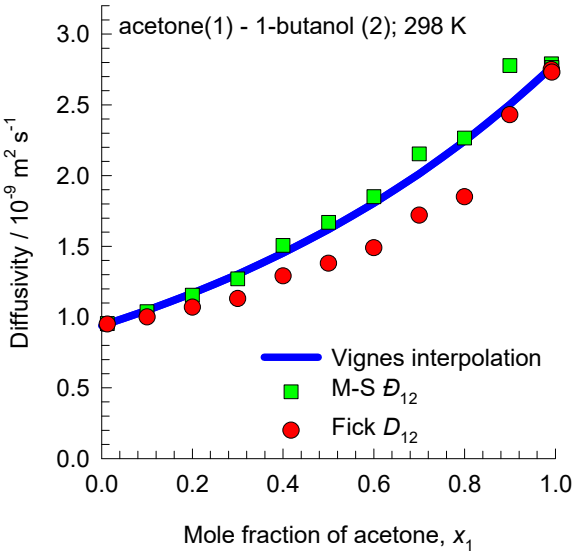

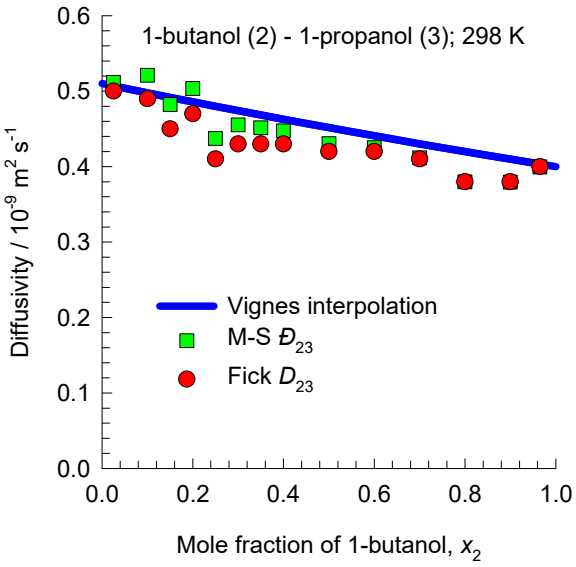

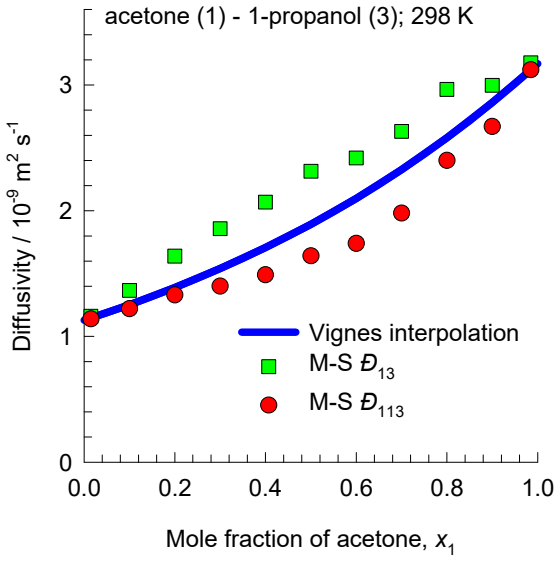

$$Đ_{12}^{x_1\to 1} = 2.79; \quad Đ_{12}^{x_2\to 1} = 0.94; \quad Đ_{13}^{x_1\to 1} = 3.17; \quad Đ_{13}^{x_3\to 1} = 1.13; \quad Đ_{23}^{x_2\to 1} = 0.4; \quad Đ_{23}^{x_3\to 1} = 0.51$$

Binary pairs: 1-propanol/1-chlorobutane/n-heptane

Fig. S42

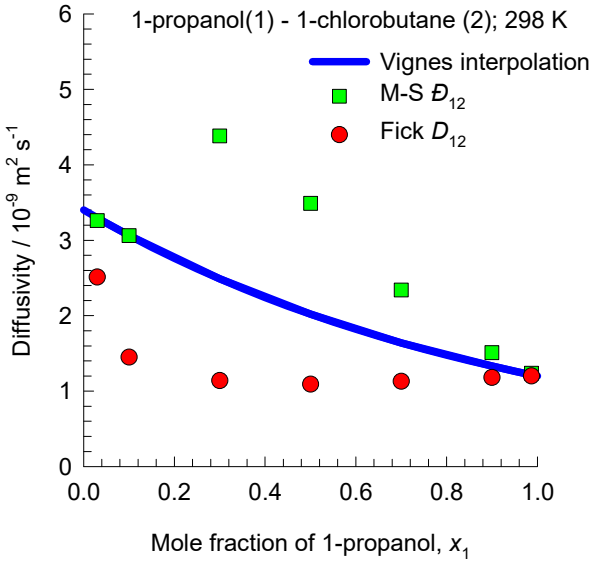

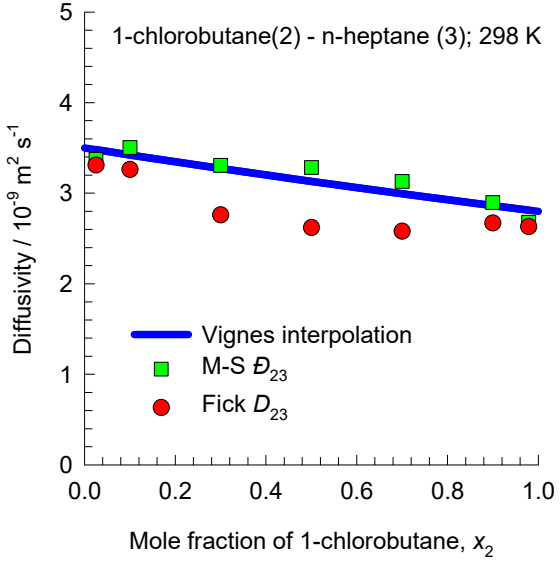

$$Đ_{12}^{x_1\to 1}=1.2;\quad Đ_{12}^{x_2\to 1}=3.4;\quad Đ_{13}^{x_1\to 1}=1.5;\quad Đ_{13}^{x_3\to 1}=6;\quad Đ_{23}^{x_2\to 1}=2.8;\quad Đ_{23}^{x_3\to 1}=3.5$$

Rehfeldt: methanol/1-butanol/1-propanol

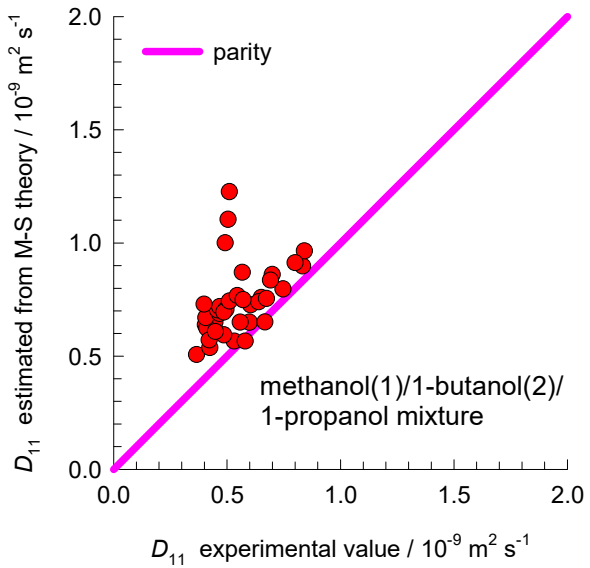

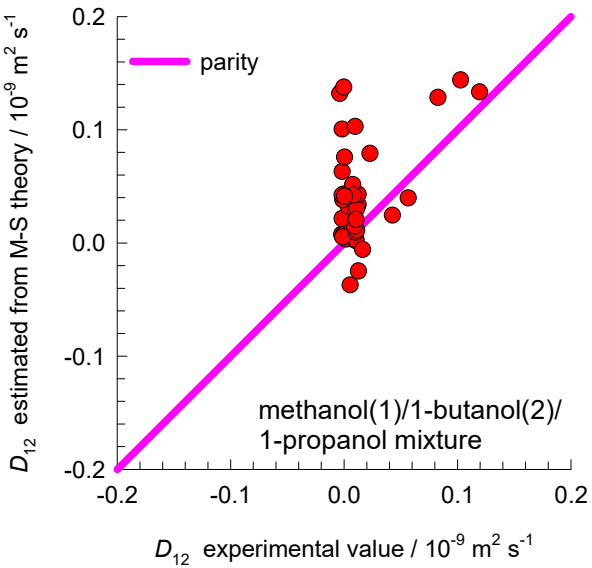

The Fick matrix is estimated using

$$[D] = [B]^{-1}[\Gamma] = [R][\Gamma]$$

The elements of [B] are estimated using the Vignes interpolation formula

$$Đ_{ij} = \left(Đ_{ij}^{x_i \to 1}\right)^{x_i} \left(Đ_{ij}^{x_j \to 1}\right)^{x_j} \left(Đ_{ij}^{x_k \to 1}\right)^{x_k}$$

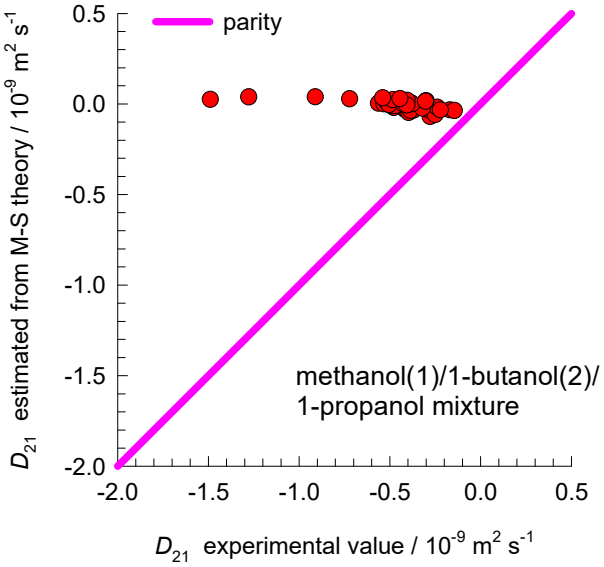

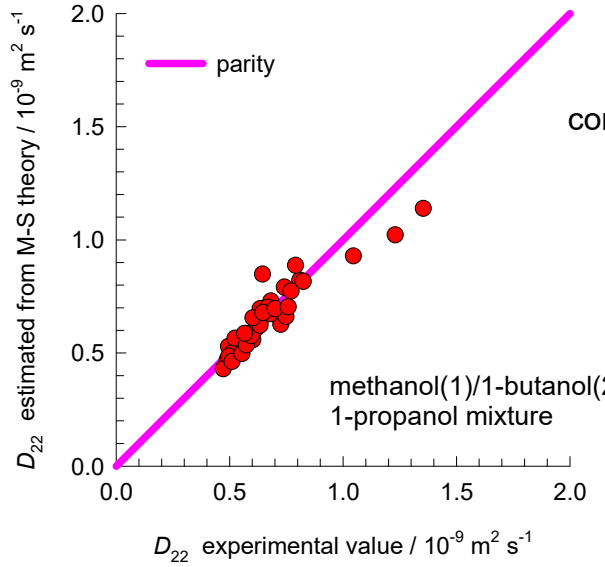

combined with the Wesselingh Bollen interpolation

$$Đ_{12}^{x_3 \to 1} = \sqrt{\left(Đ_{13}^{x_3 \to 1} Đ_{23}^{x_3 \to 1}\right)}$$
$$Đ_{13}^{x_2 \to 1} = \sqrt{\left(Đ_{12}^{x_2 \to 1} Đ_{23}^{x_2 \to 1}\right)}$$
$$Đ_{23}^{x_3 \to 1} = \sqrt{\left(Đ_{12}^{x_1 \to 1} Đ_{13}^{x_1 \to 1}\right)}$$

$$Đ_{12}^{x_1 \to 1} = 1.3; \quad Đ_{12}^{x_2 \to 1} = 0.48; \quad Đ_{13}^{x_1 \to 1} = 1.37; \quad Đ_{13}^{x_3 \to 1} = 0.68; \quad Đ_{23}^{x_2 \to 1} = 0.4; \quad Đ_{23}^{x_3 \to 1} = 0.51$$

Rehfeldt: acetone/water/1-propanol

Fig. S44

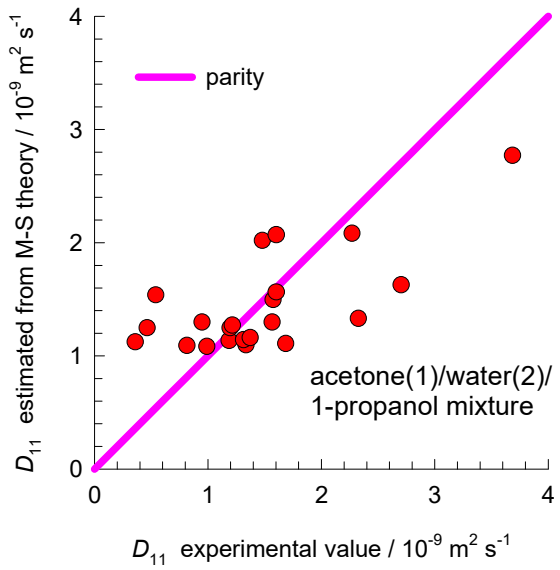

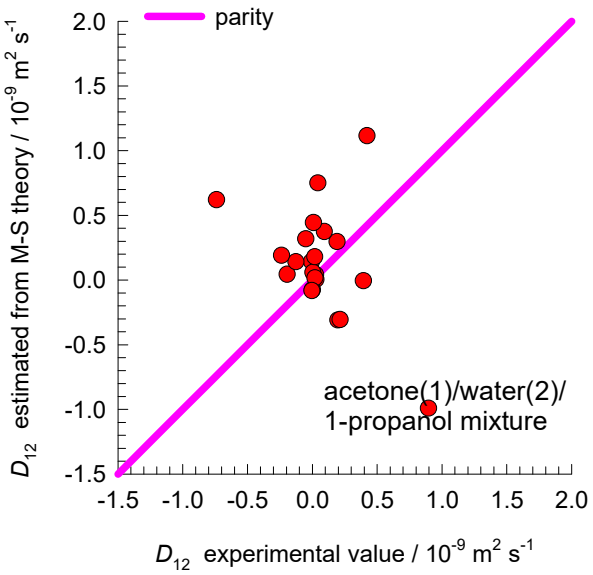

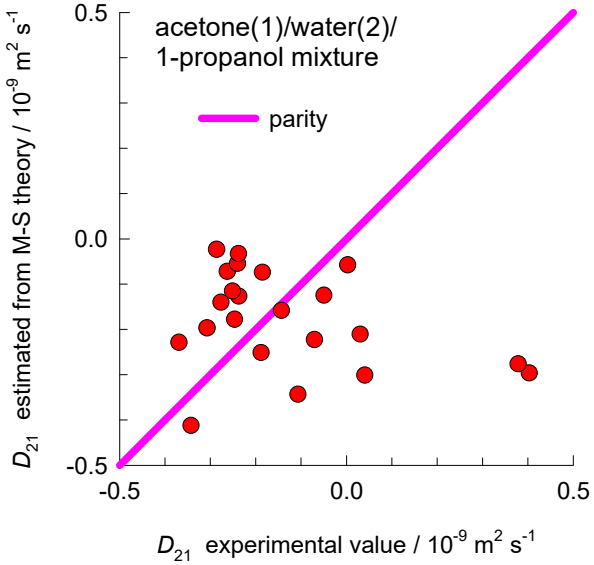

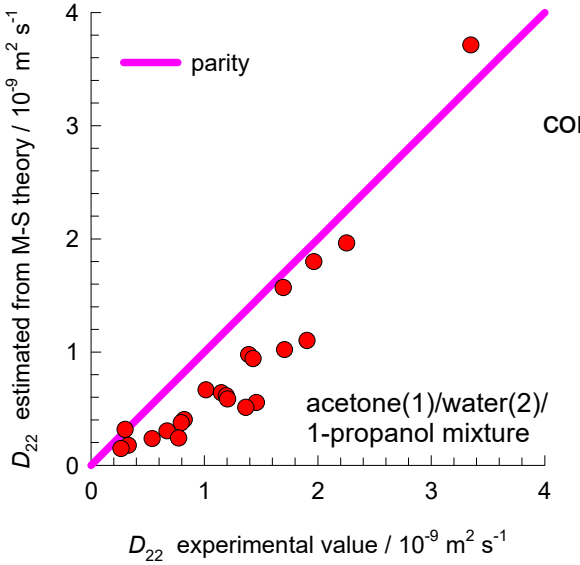

The Fick matrix is estimated using

$$[D] = [B]^{-1}[\Gamma] = [R][\Gamma]$$

The elements of [B] are estimated using the Vignes interpolation formula

$$Đ_{ij} = \left(Đ_{ij}^{x_i \to 1}\right)^{x_i} \left(Đ_{ij}^{x_j \to 1}\right)^{x_j} \left(Đ_{ij}^{x_k \to 1}\right)^{x_k}$$

combined with the Wesselingh Bollen interpolation

$$Đ_{12}^{x_3 \to 1} = \sqrt{\left(Đ_{13}^{x_3 \to 1} Đ_{23}^{x_3 \to 1}\right)}$$
$$Đ_{13}^{x_2 \to 1} = \sqrt{\left(Đ_{12}^{x_2 \to 1} Đ_{23}^{x_2 \to 1}\right)}$$
$$Đ_{23}^{x_3 \to 1} = \sqrt{\left(Đ_{12}^{x_1 \to 1} Đ_{13}^{x_1 \to 1}\right)}$$

$$Đ_{12}^{x_1 \to 1} = 5.08; \quad Đ_{12}^{x_2 \to 1} = 1.28; \quad Đ_{13}^{x_1 \to 1} = 3.17; \quad Đ_{13}^{x_3 \to 1} = 1.13; \quad Đ_{23}^{x_2 \to 1} = 1.1; \quad Đ_{23}^{x_3 \to 1} = 0.68$$

Rehfeldt: acetone/1-butanol/1-propanol

Fig. S45

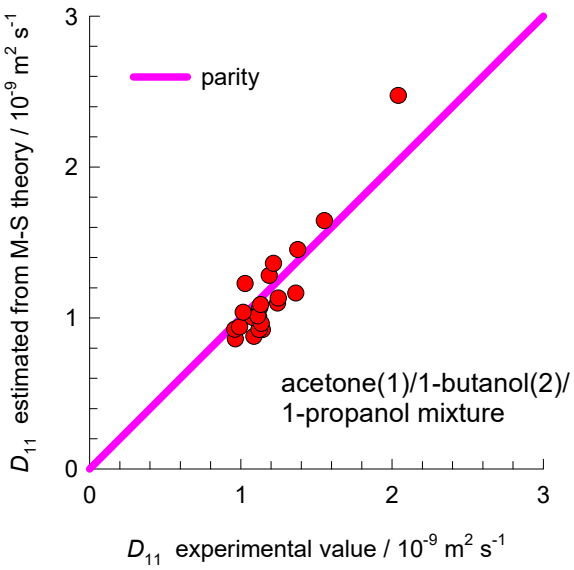

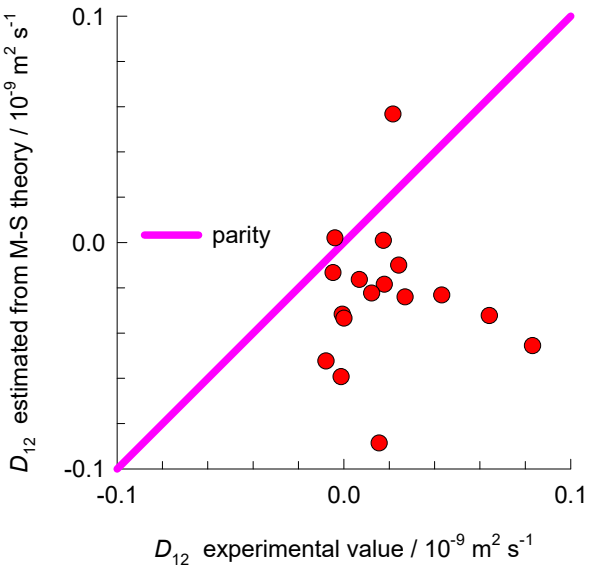

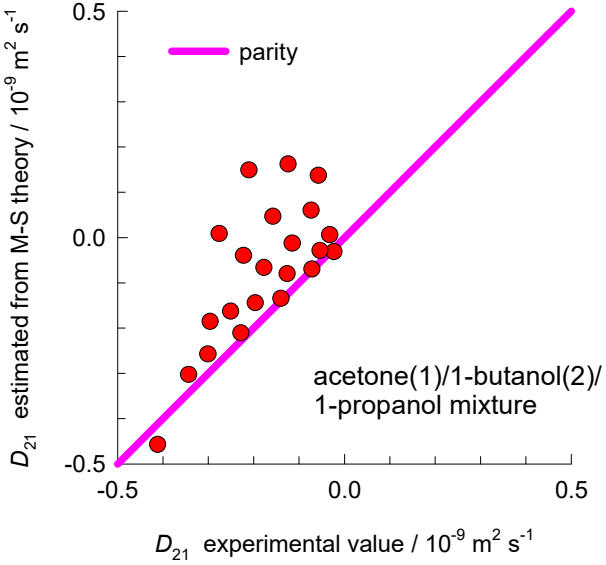

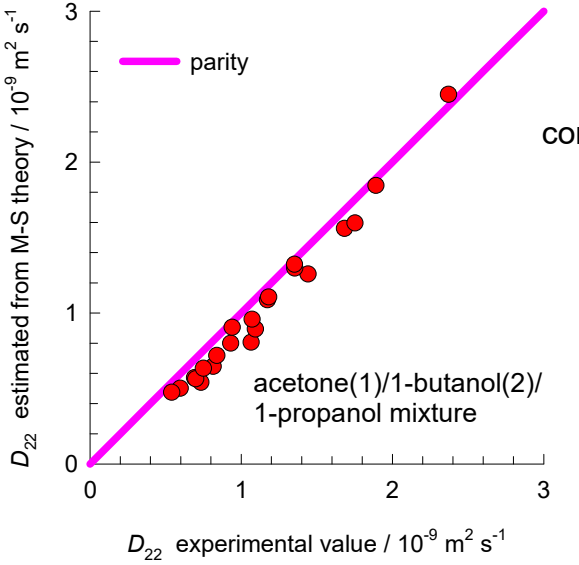

The Fick matrix is estimated using

$$[D] = [B]^{-1}[\Gamma] = [R][\Gamma]$$

The elements of [B] are estimated using the Vignes interpolation formula

$$Đ_{ij} = \left(Đ_{ij}^{x_i \to 1}\right)^{x_i} \left(Đ_{ij}^{x_j \to 1}\right)^{x_j} \left(Đ_{ij}^{x_k \to 1}\right)^{x_k}$$

combined with the Wesselingh Bollen interpolation

$$Đ_{12}^{x_3 \to 1} = \sqrt{\left(Đ_{13}^{x_3 \to 1} Đ_{23}^{x_3 \to 1}\right)}$$
$$Đ_{13}^{x_2 \to 1} = \sqrt{\left(Đ_{12}^{x_2 \to 1} Đ_{23}^{x_2 \to 1}\right)}$$
$$Đ_{23}^{x_3 \to 1} = \sqrt{\left(Đ_{12}^{x_1 \to 1} Đ_{13}^{x_1 \to 1}\right)}$$

$$Đ_{12}^{x_1 \to 1} = 2.79; \quad Đ_{12}^{x_2 \to 1} = 0.94; \quad Đ_{13}^{x_1 \to 1} = 3.17; \quad Đ_{13}^{x_3 \to 1} = 1.13; \quad Đ_{23}^{x_2 \to 1} = 0.4; \quad Đ_{23}^{x_3 \to 1} = 0.51$$

Fig. S46

Rehfeldt: 1-propanol/1-chlorobutane/n-heptane

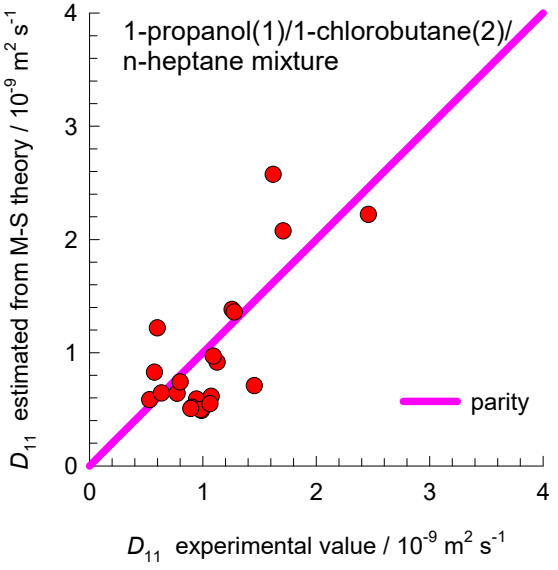

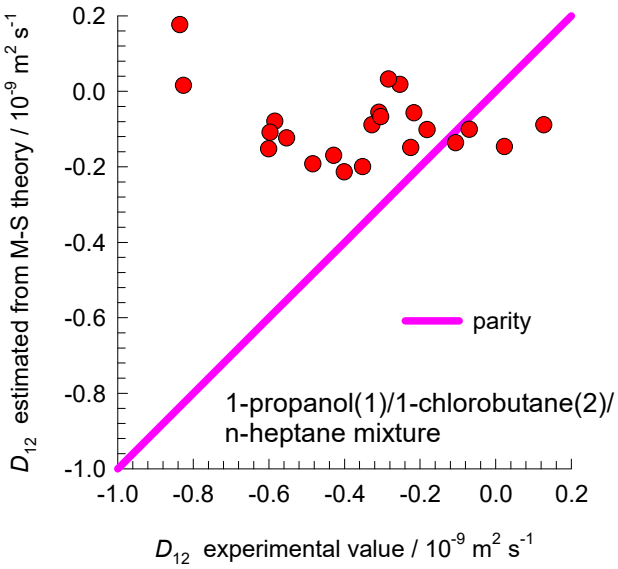

The Fick matrix is estimated using

$$[D] = [B]^{-1}[\Gamma] = [R][\Gamma]$$

The elements of [B] are estimated using the Vignes interpolation formula

$$Đ_{ij} = \left(Đ_{ij}^{x_i \to 1}\right)^{x_i} \left(Đ_{ij}^{x_j \to 1}\right)^{x_j} \left(Đ_{ij}^{x_k \to 1}\right)^{x_k}$$

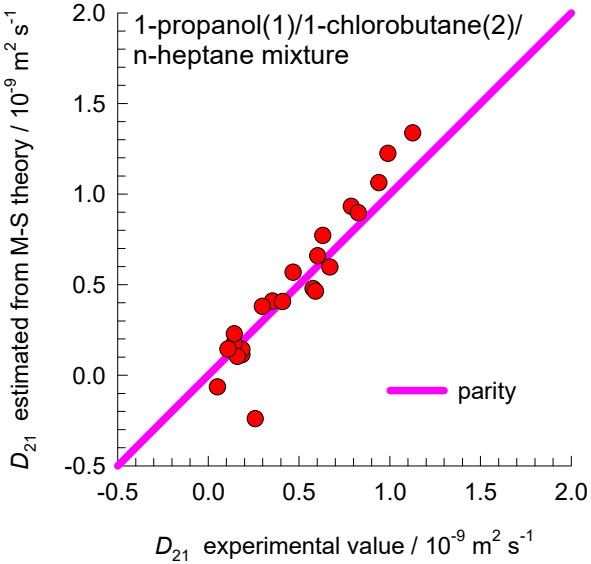

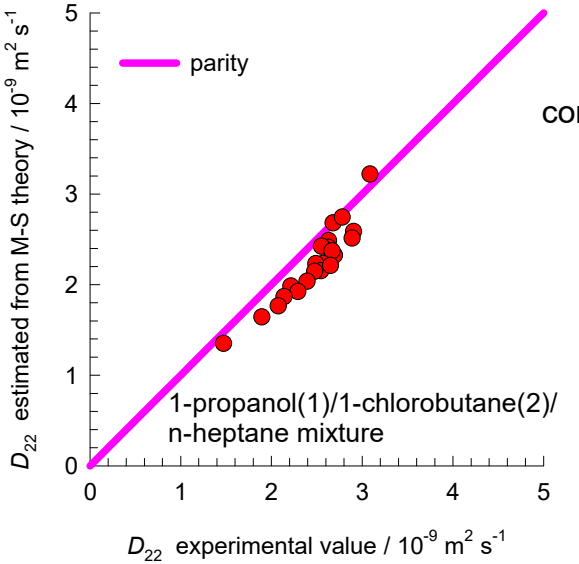

combined with the Wesselingh Bollen interpolation

$$Đ_{12}^{x_3 \to 1} = \sqrt{\left(Đ_{13}^{x_3 \to 1} Đ_{23}^{x_3 \to 1}\right)}$$
$$Đ_{13}^{x_2 \to 1} = \sqrt{\left(Đ_{12}^{x_2 \to 1} Đ_{23}^{x_2 \to 1}\right)}$$
$$Đ_{23}^{x_3 \to 1} = \sqrt{\left(Đ_{12}^{x_1 \to 1} Đ_{13}^{x_1 \to 1}\right)}$$

$$Đ_{12}^{x_1 \to 1} = 1.2; \quad Đ_{12}^{x_2 \to 1} = 3.4; \quad Đ_{13}^{x_1 \to 1} = 1.5; \quad Đ_{13}^{x_3 \to 1} = 6; \quad Đ_{23}^{x_2 \to 1} = 2.8; \quad Đ_{23}^{x_3 \to 1} = 3.5$$

Fig. S47

Rehfeldt: 1-propanol/1-chlorobutane/n-heptane

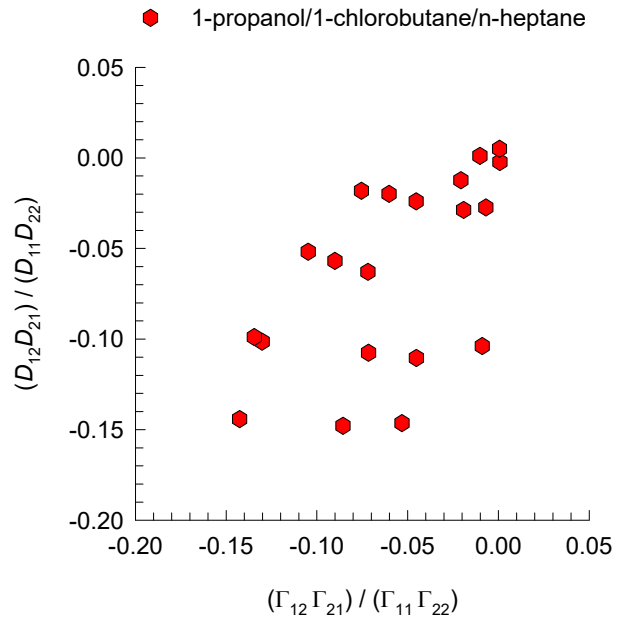

Rehfeldt: Ratio $|D|^{1/2}/|\Gamma|^{1/2}$

Fig. S48

(a)

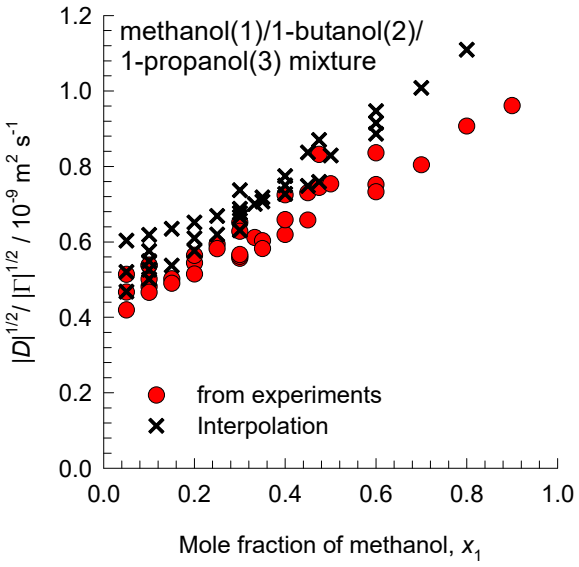

(b)

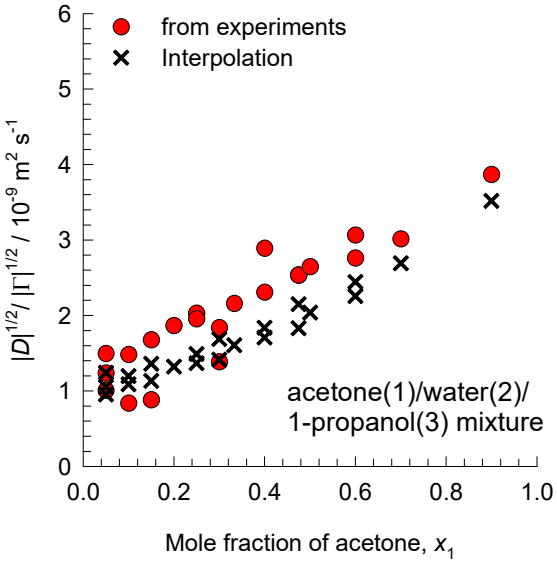

The values of $|\Lambda|^{1/2} = \dfrac{|D|^{1/2}}{|\Gamma|^{1/2}}$ obtained from experimental data are compared with $|\Lambda|^{1/2}$ calculations using

$$|\Lambda|^{1/2} = \sqrt{\frac{Đ_{12}Đ_{13}Đ_{23}}{x_1Đ_{23}+x_2Đ_{13}+x_3Đ_{12}}}$$

along with the Vignes interpolation formula

$$Đ_{ij} = \left(Đ_{ij}^{x_i\to 1}\right)^{x_i}\left(Đ_{ij}^{x_j\to 1}\right)^{x_j}\left(Đ_{ij}^{x_k\to 1}\right)^{x_k}$$

(c)

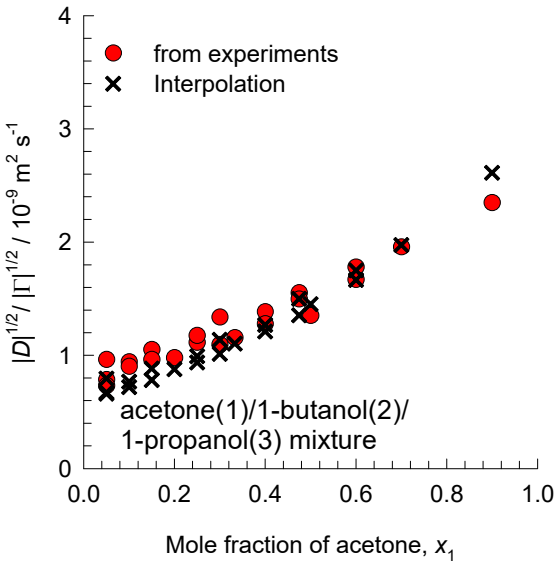

(d)

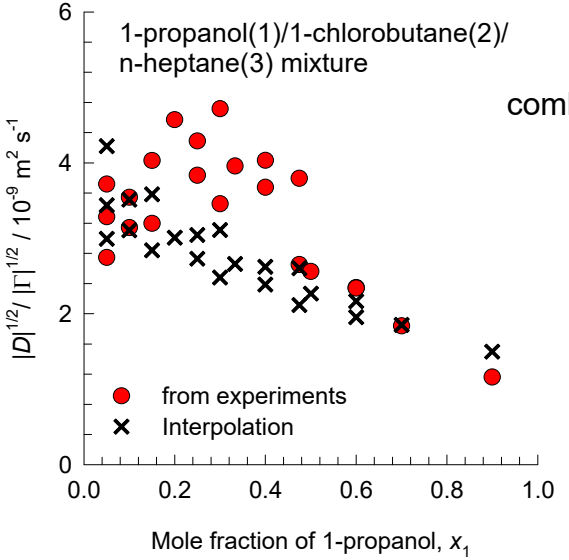

combined with the Wesselingh Bollen interpolation

$$Đ_{12}^{x_3\to 1} = \sqrt{\left(Đ_{13}^{x_3\to 1}Đ_{23}^{x_3\to 1}\right)}$$
$$Đ_{13}^{x_2\to 1} = \sqrt{\left(Đ_{12}^{x_2\to 1}Đ_{23}^{x_2\to 1}\right)}$$
$$Đ_{23}^{x_3\to 1} = \sqrt{\left(Đ_{12}^{x_1\to 1}Đ_{13}^{x_1\to 1}\right)}$$

Rehfeldt: methanol/1-butanol/1-propanol

Fig. S49

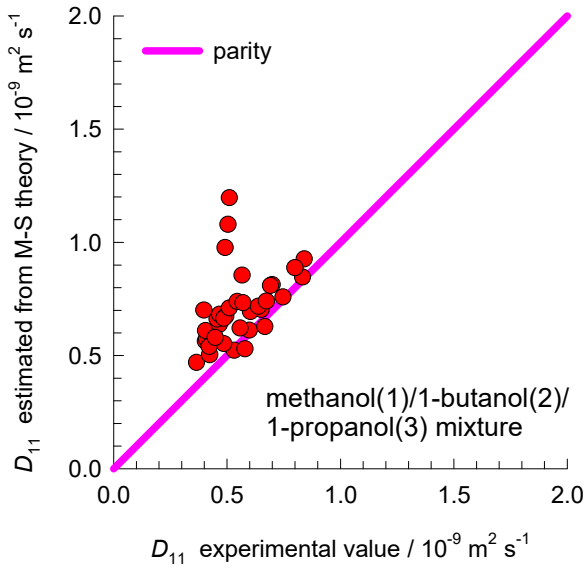

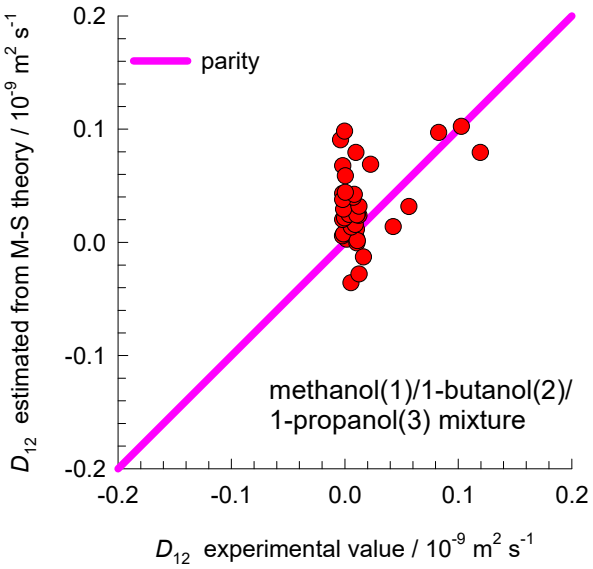

The Fick matrix is estimated using

$$[D] = |\Lambda|^{1/2}[\Gamma]$$

$$|\Lambda|^{1/2} = \sqrt{\frac{Đ_{12}Đ_{13}Đ_{23}}{x_1Đ_{23}+x_2Đ_{13}+x_3Đ_{12}}}$$

along with the Vignes interpolation formula

$$Đ_{ij} = \left(Đ_{ij}^{x_i \to 1}\right)^{x_i}\left(Đ_{ij}^{x_j \to 1}\right)^{x_j}\left(Đ_{ij}^{x_k \to 1}\right)^{x_k}$$

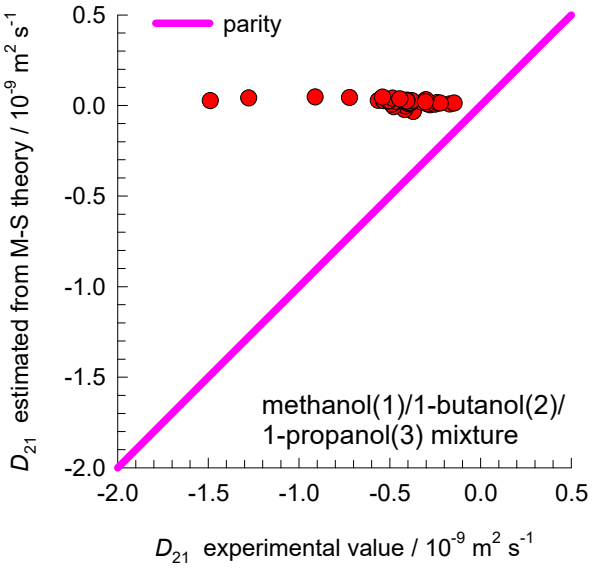

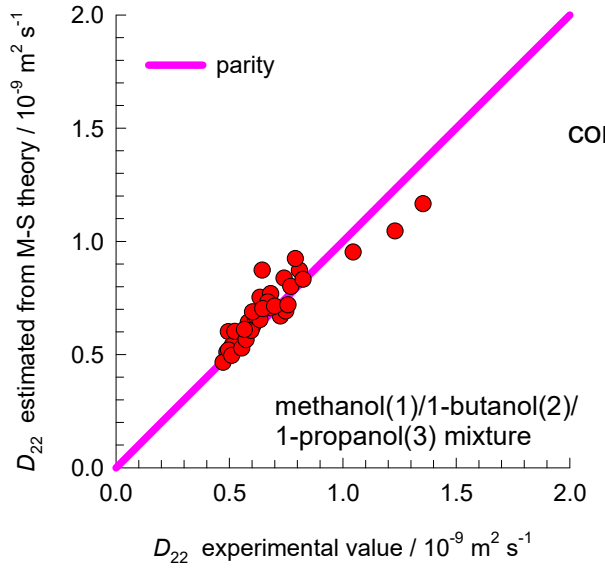

combined with the Wesselingh Bollen interpolation

$$Đ_{12}^{x_3 \to 1} = \sqrt{\left(Đ_{13}^{x_3 \to 1}Đ_{23}^{x_3 \to 1}\right)}$$
$$Đ_{13}^{x_2 \to 1} = \sqrt{\left(Đ_{12}^{x_2 \to 1}Đ_{23}^{x_2 \to 1}\right)}$$
$$Đ_{23}^{x_3 \to 1} = \sqrt{\left(Đ_{12}^{x_1 \to 1}Đ_{13}^{x_1 \to 1}\right)}$$

$$Đ_{12}^{x_1 \to 1} = 1.3; \quad Đ_{12}^{x_2 \to 1} = 0.48; \quad Đ_{13}^{x_1 \to 1} = 1.37; \quad Đ_{13}^{x_3 \to 1} = 0.68; \quad Đ_{23}^{x_2 \to 1} = 0.4; \quad Đ_{23}^{x_3 \to 1} = 0.51$$

Rehfeldt: acetone/water/1-propanol

Fig. S50

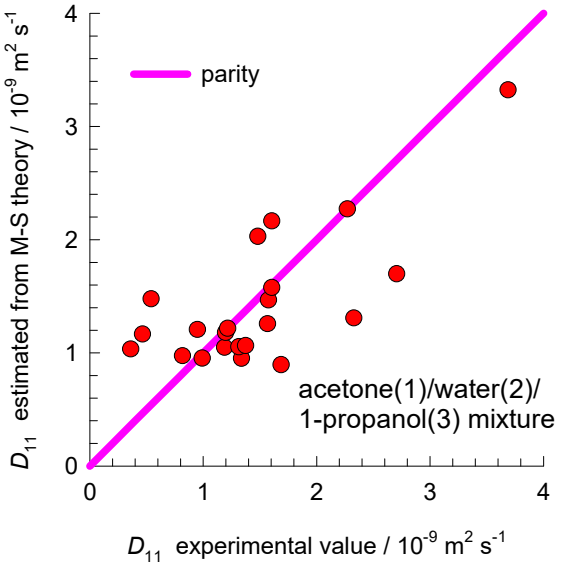

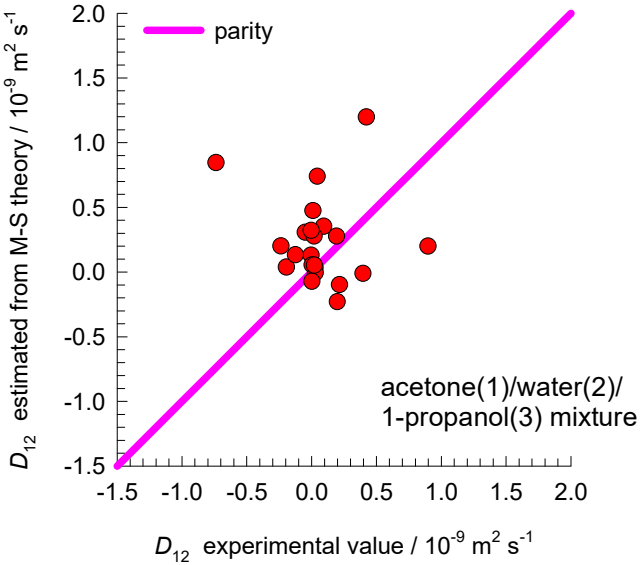

The Fick matrix is estimated using

$$[D] = |\Lambda|^{1/2}[\Gamma]$$

$$|\Lambda|^{1/2} = \sqrt{\frac{Đ_{12}Đ_{13}Đ_{23}}{x_1Đ_{23}+x_2Đ_{13}+x_3Đ_{12}}}$$

along with the Vignes interpolation formula

$$Đ_{ij} = \left(Đ_{ij}^{x_i\to 1}\right)^{x_i}\left(Đ_{ij}^{x_j\to 1}\right)^{x_j}\left(Đ_{ij}^{x_k\to 1}\right)^{x_k}$$

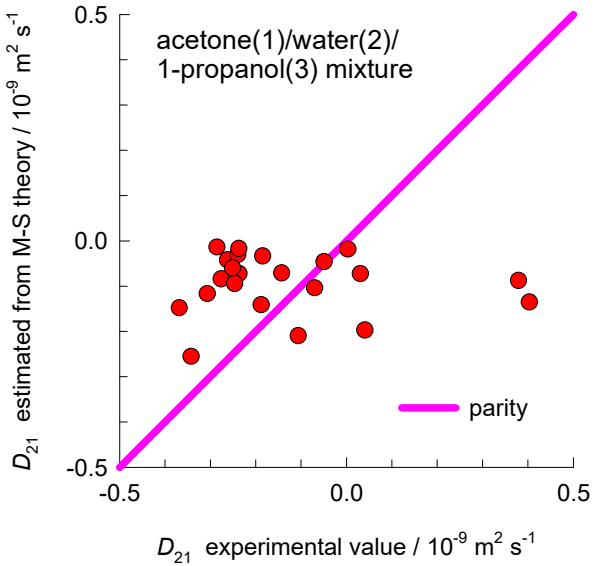

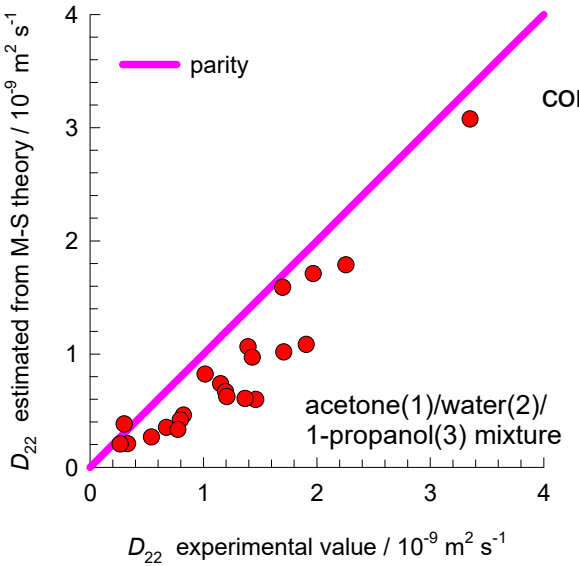

combined with the Wesselingh Bollen interpolation

$$Đ_{12}^{x_3\to 1} = \sqrt{\left(Đ_{13}^{x_3\to 1}Đ_{23}^{x_3\to 1}\right)}$$

$$Đ_{13}^{x_2\to 1} = \sqrt{\left(Đ_{12}^{x_2\to 1}Đ_{23}^{x_2\to 1}\right)}$$

$$Đ_{23}^{x_3\to 1} = \sqrt{\left(Đ_{12}^{x_1\to 1}Đ_{13}^{x_1\to 1}\right)}$$

$Đ_{12}^{x_1\to 1} = 5.08;\quad Đ_{12}^{x_2\to 1} = 1.28;\quad Đ_{13}^{x_1\to 1} = 3.17;\quad Đ_{13}^{x_3\to 1} = 1.13;\quad Đ_{23}^{x_2\to 1} = 1.1;\quad Đ_{23}^{x_3\to 1} = 0.68$

Rehfeldt: acetone/1-butanol/1-propanol

Fig. S51

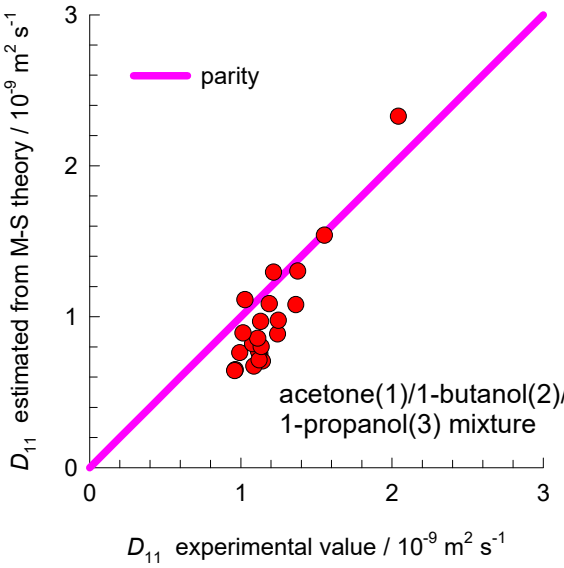

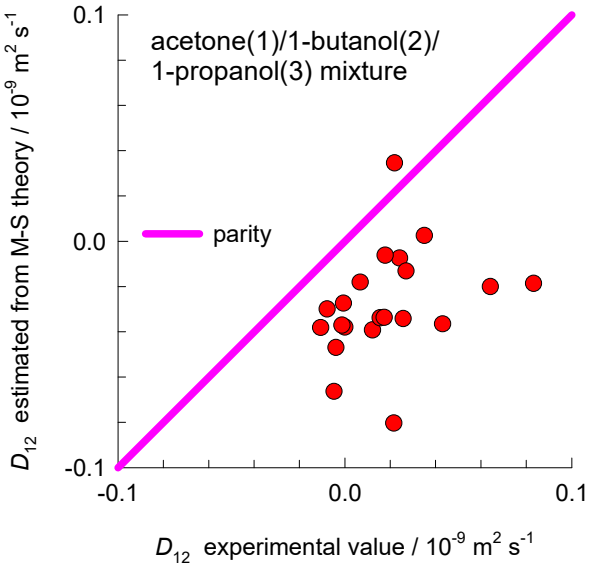

The Fick matrix is estimated using

$$[D] = |\Lambda|^{1/2}[\Gamma]$$

$$|\Lambda|^{1/2} = \sqrt{\frac{Đ_{12}Đ_{13}Đ_{23}}{x_1Đ_{23}+x_2Đ_{13}+x_3Đ_{12}}}$$

along with the Vignes interpolation formula

$$Đ_{ij} = \left(Đ_{ij}^{x_i\to 1}\right)^{x_i}\left(Đ_{ij}^{x_j\to 1}\right)^{x_j}\left(Đ_{ij}^{x_k\to 1}\right)^{x_k}$$

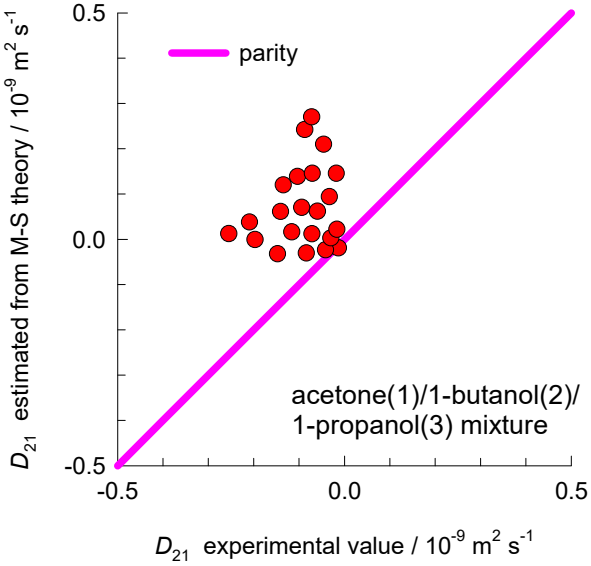

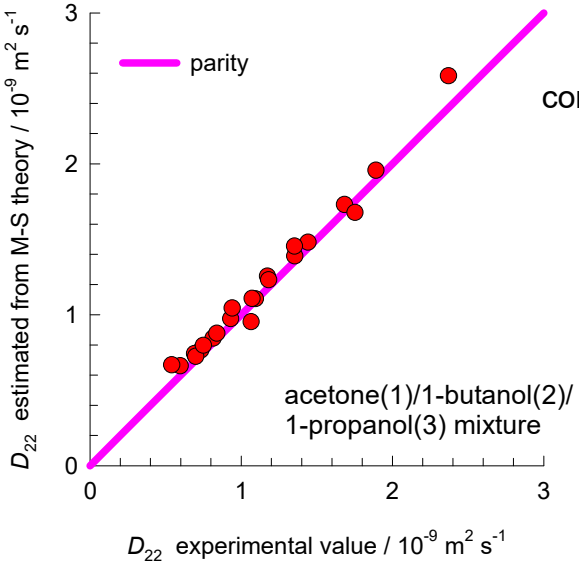

combined with the Wesselingh Bollen interpolation

$$Đ_{12}^{x_3\to 1} = \sqrt{\left(Đ_{13}^{x_3\to 1}Đ_{23}^{x_3\to 1}\right)}$$
$$Đ_{13}^{x_2\to 1} = \sqrt{\left(Đ_{12}^{x_2\to 1}Đ_{23}^{x_2\to 1}\right)}$$
$$Đ_{23}^{x_3\to 1} = \sqrt{\left(Đ_{12}^{x_1\to 1}Đ_{13}^{x_1\to 1}\right)}$$

$$Đ_{12}^{x_1\to 1} = 2.79; \quad Đ_{12}^{x_2\to 1} = 0.94; \quad Đ_{13}^{x_1\to 1} = 3.17; \quad Đ_{13}^{x_3\to 1} = 1.13; \quad Đ_{23}^{x_2\to 1} = 0.4; \quad Đ_{23}^{x_3\to 1} = 0.51$$

Fig. S52

Rehfeldt: 1-propanol/1-chlorobutane/n-heptane

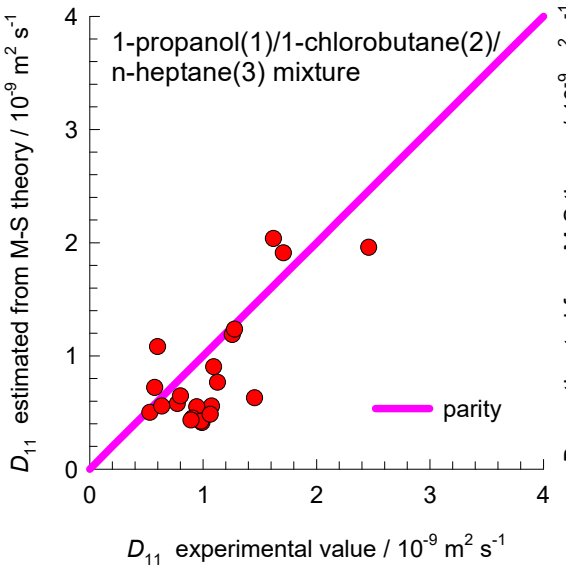

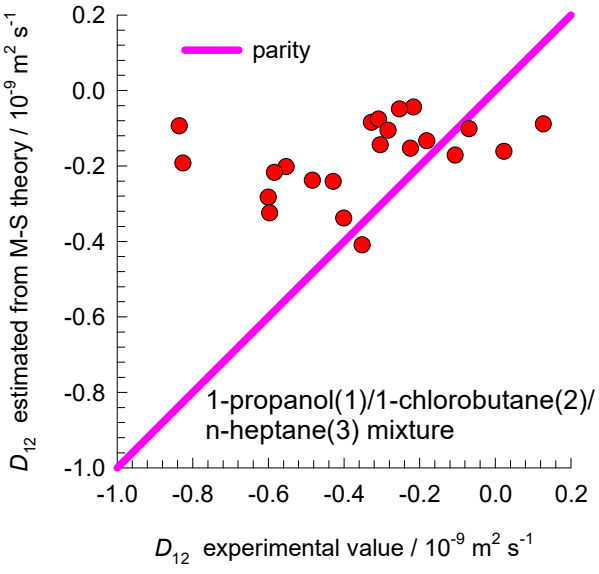

The Fick matrix is estimated using

$$[D] = |\Lambda|^{1/2}[\Gamma]$$

$$|\Lambda|^{1/2} = \sqrt{\frac{Đ_{12}Đ_{13}Đ_{23}}{x_1Đ_{23}+x_2Đ_{13}+x_3Đ_{12}}}$$

along with the Vignes interpolation formula

$$Đ_{ij} = \left(Đ_{ij}^{x_i\to 1}\right)^{x_i}\left(Đ_{ij}^{x_j\to 1}\right)^{x_j}\left(Đ_{ij}^{x_k\to 1}\right)^{x_k}$$

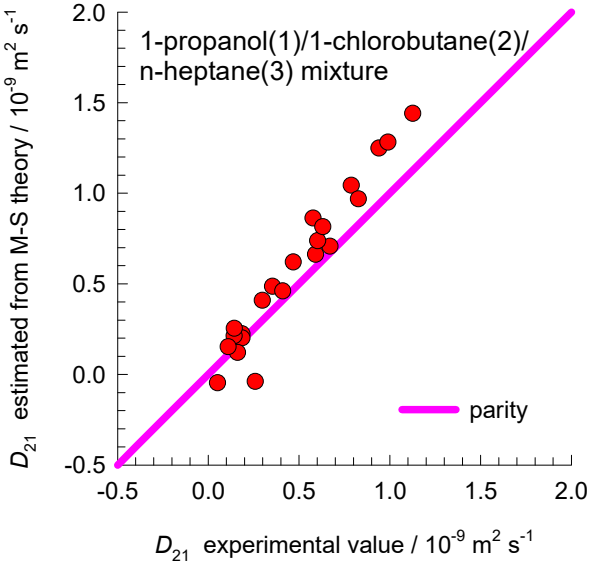

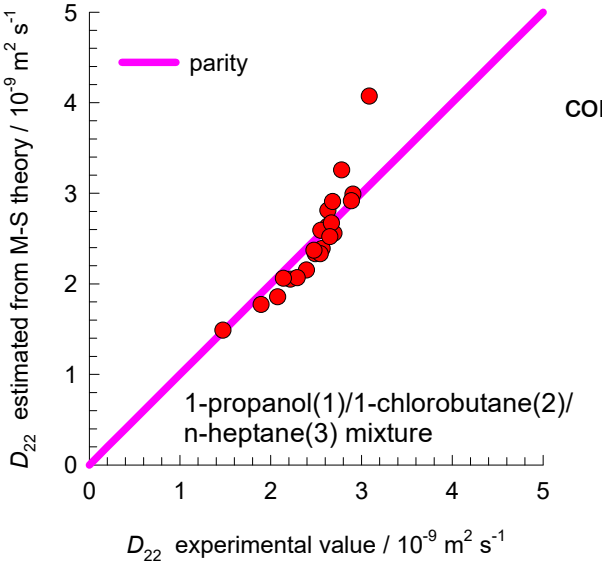

combined with the Wesselingh Bollen interpolation

$$Đ_{12}^{x_3\to 1} = \sqrt{\left(Đ_{13}^{x_3\to 1}Đ_{23}^{x_3\to 1}\right)}$$
$$Đ_{13}^{x_2\to 1} = \sqrt{\left(Đ_{12}^{x_2\to 1}Đ_{23}^{x_2\to 1}\right)}$$
$$Đ_{23}^{x_3\to 1} = \sqrt{\left(Đ_{12}^{x_1\to 1}Đ_{13}^{x_1\to 1}\right)}$$

$Đ_{12}^{x_1\to 1} = 1.2;\quad Đ_{12}^{x_2\to 1} = 3.4;\quad Đ_{13}^{x_1\to 1} = 1.5;\quad Đ_{13}^{x_3\to 1} = 6;\quad Đ_{23}^{x_2\to 1} = 2.8;\quad Đ_{23}^{x_3\to 1} = 3.5$

Fe/Cr binary mixture

Fig. S53

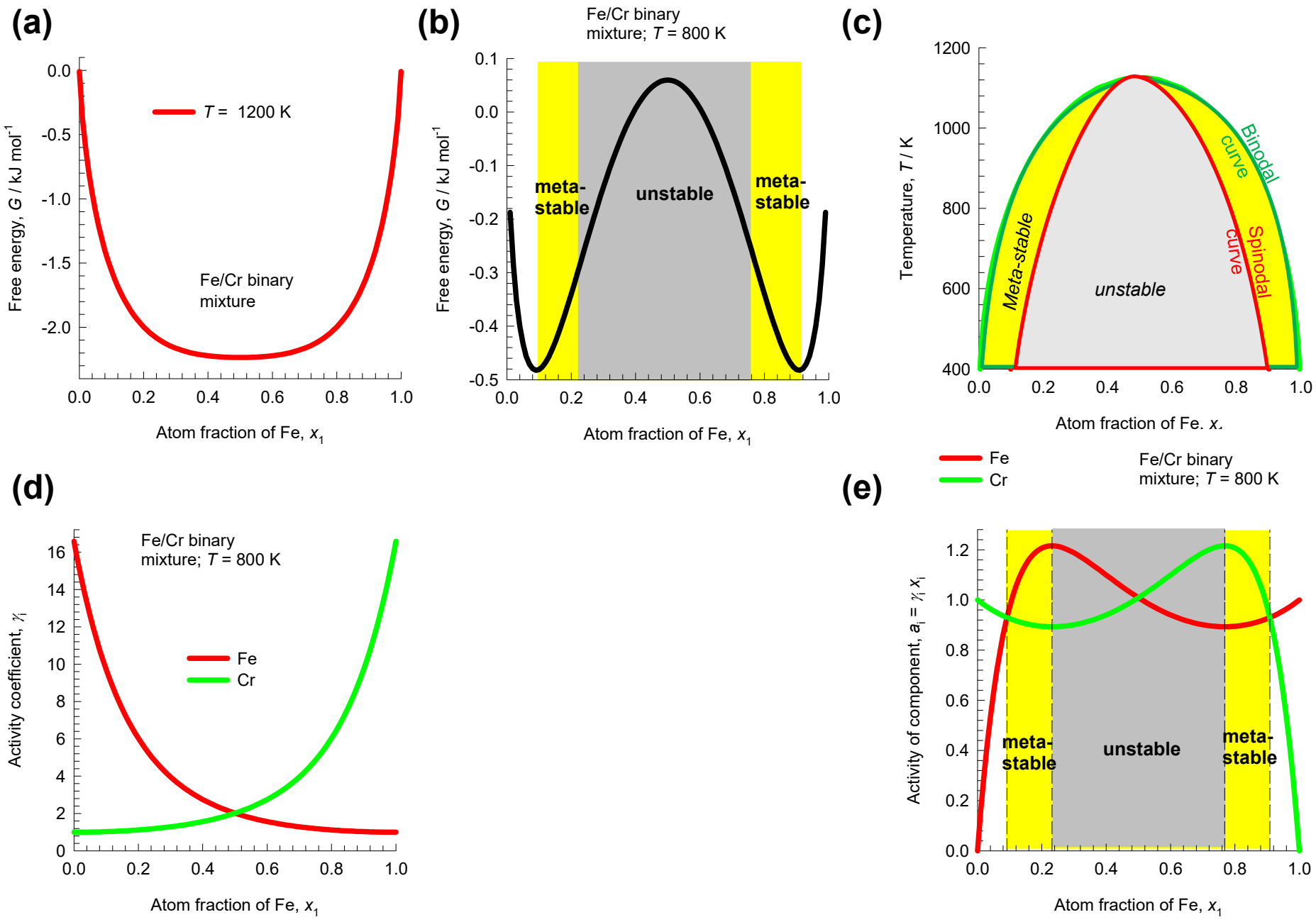

Tri-ethylamine/water mixture diffusion

Fig. S54

(a)

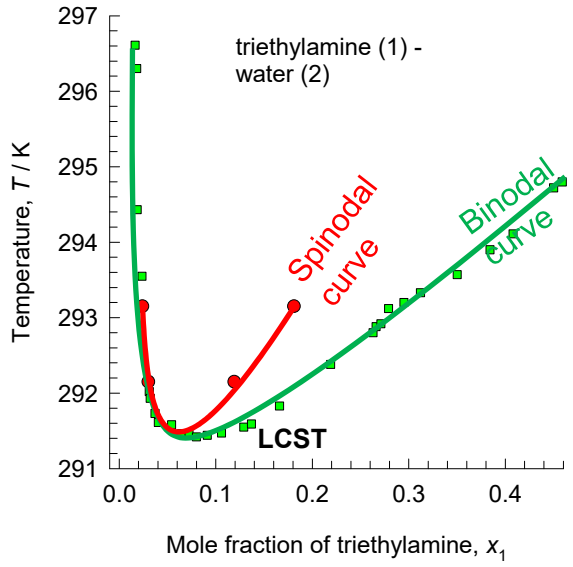

(b)

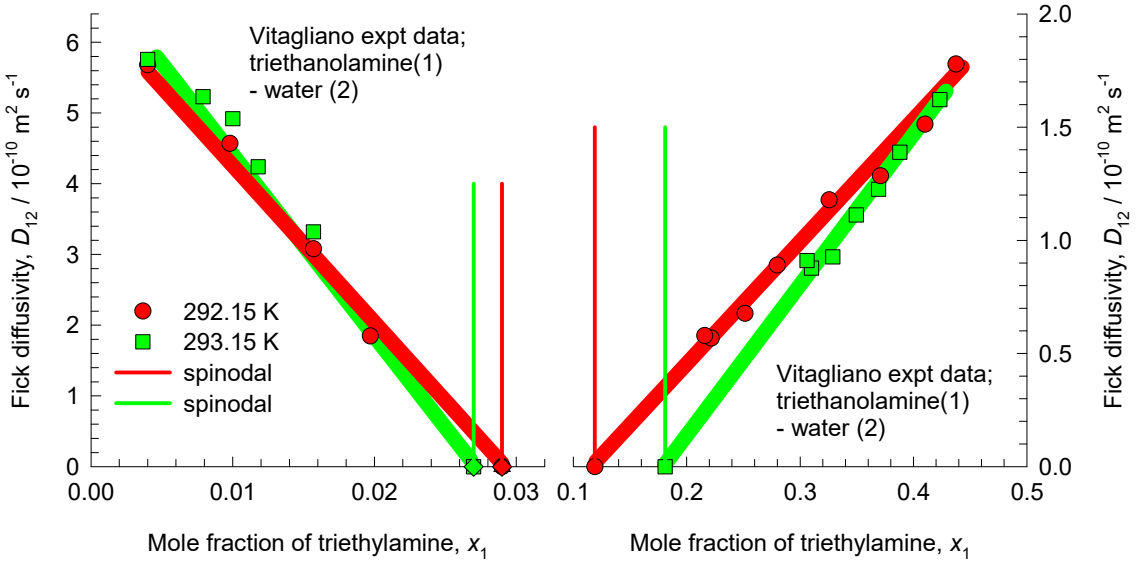

1-butanol/water mixture diffusion

Fig. S55

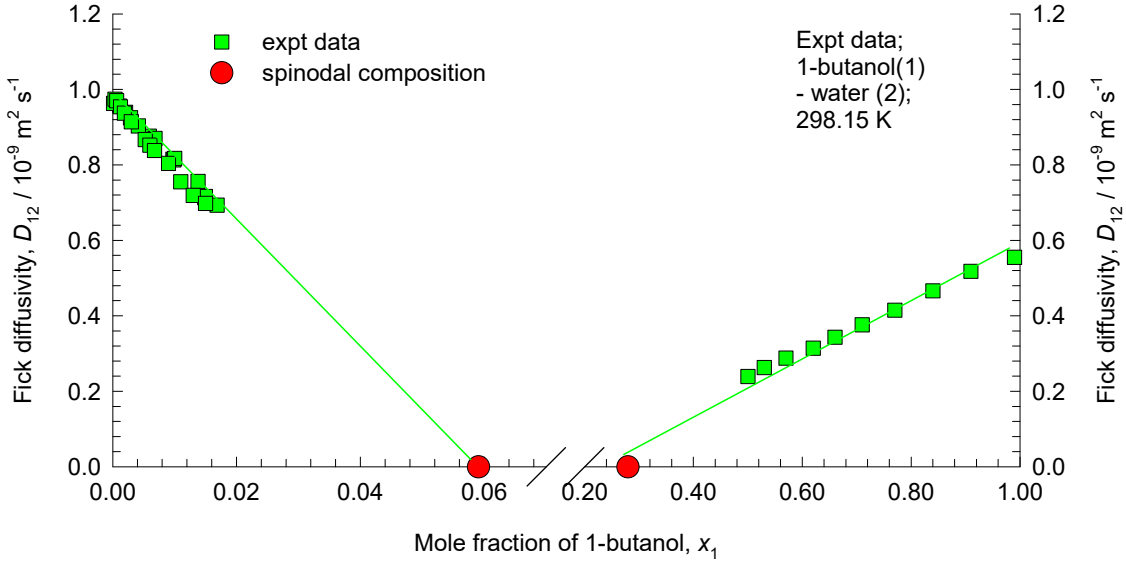

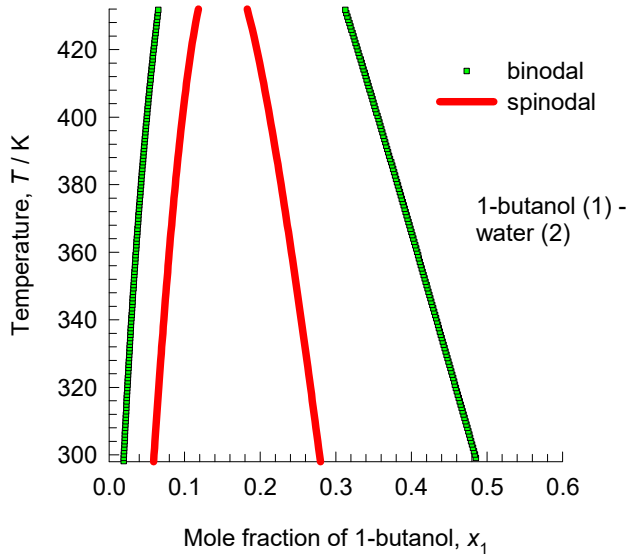

MIPK/water mixture diffusion

Fig. S56

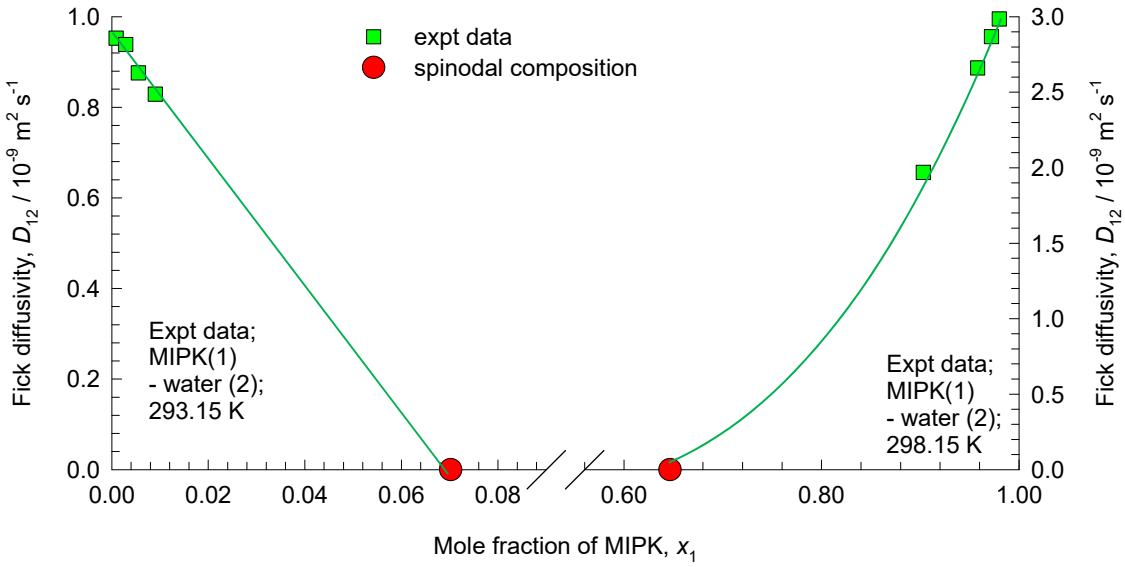

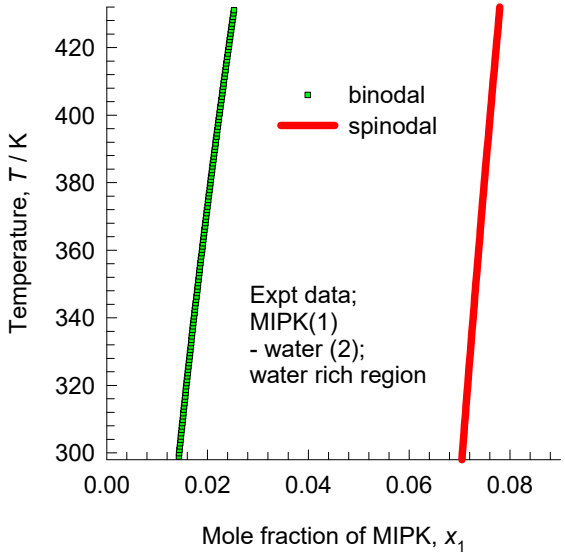

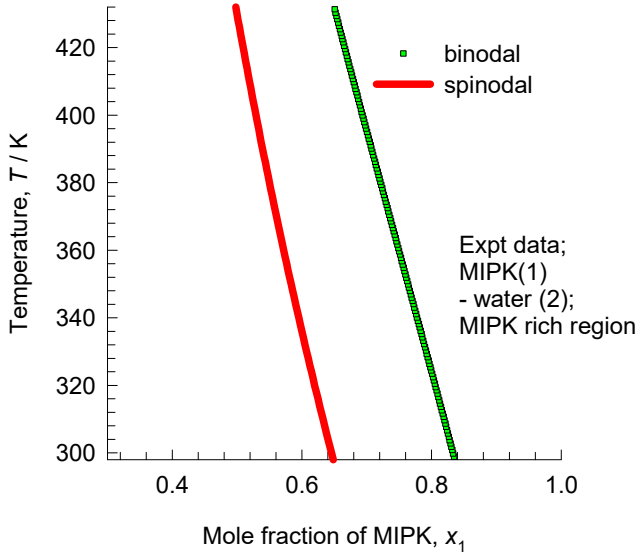

glycerol/acetone mixture diffusion

Fig. S57

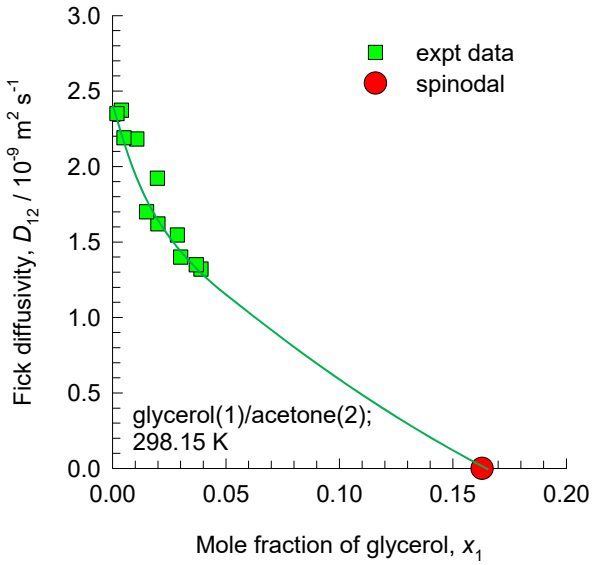

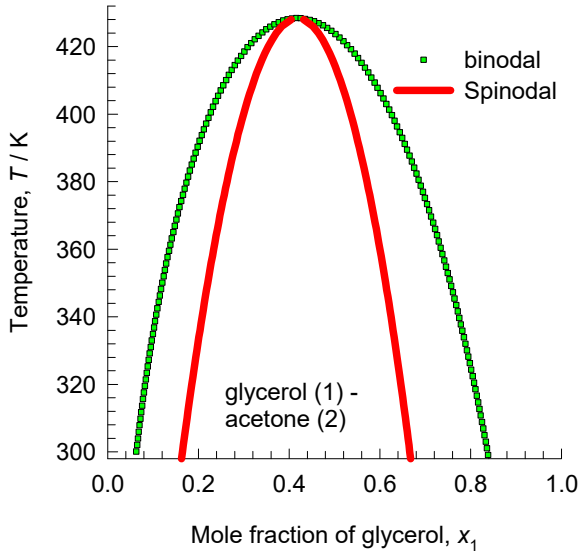

Methanol/CS_2 mixture diffusion

Fig. S58

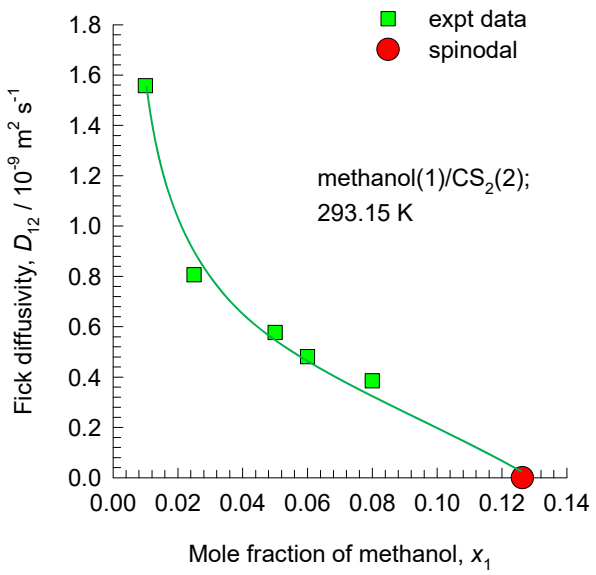

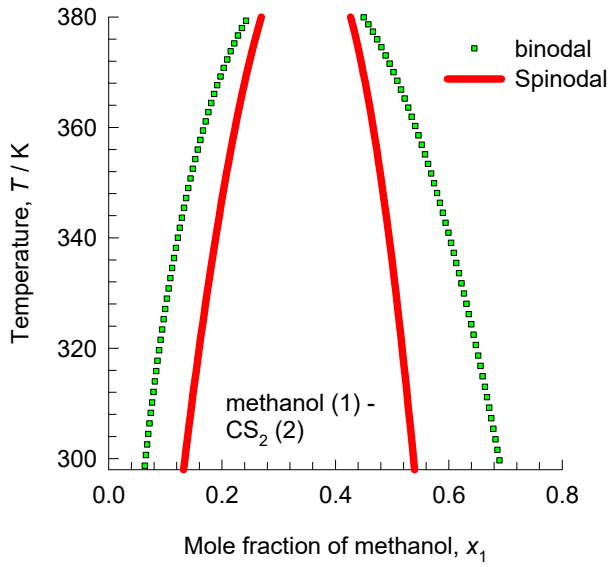

Vapor/liquid phase transitions

Fig. S59

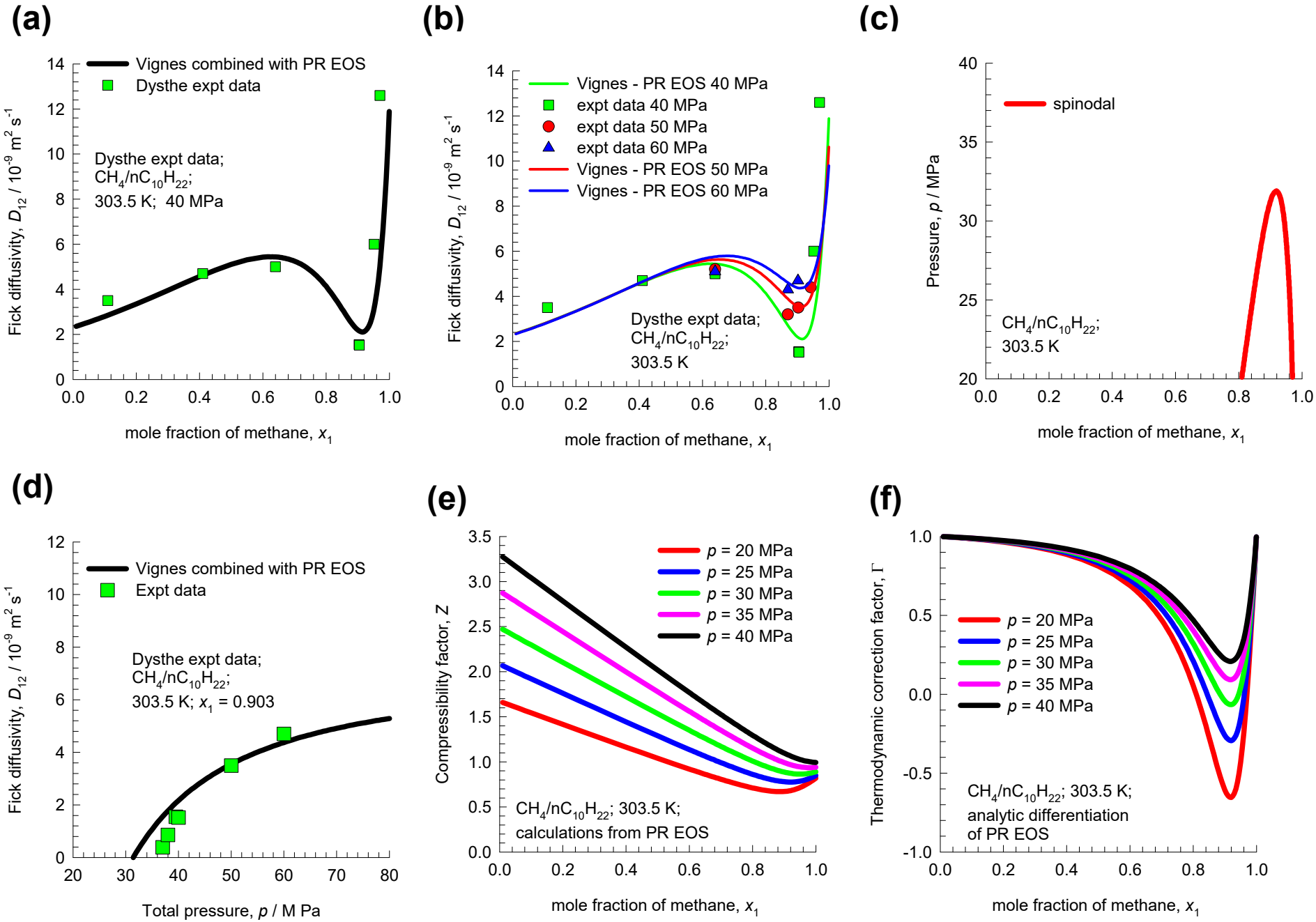

Diffusion in benzene/CO_2 mixtures

Fig. S60

(a)

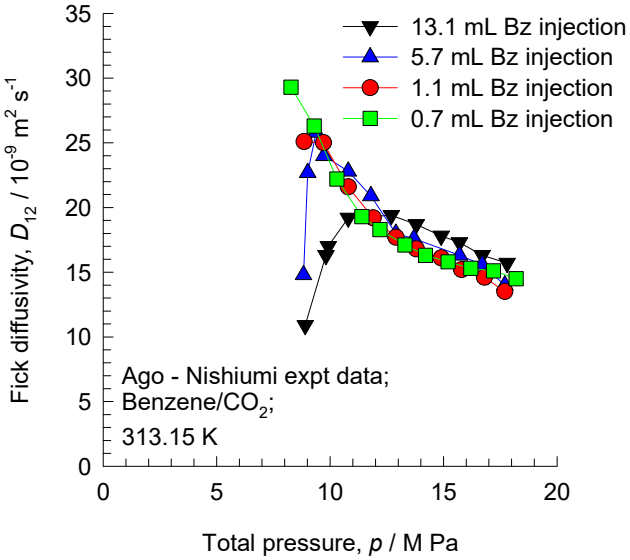

(b)

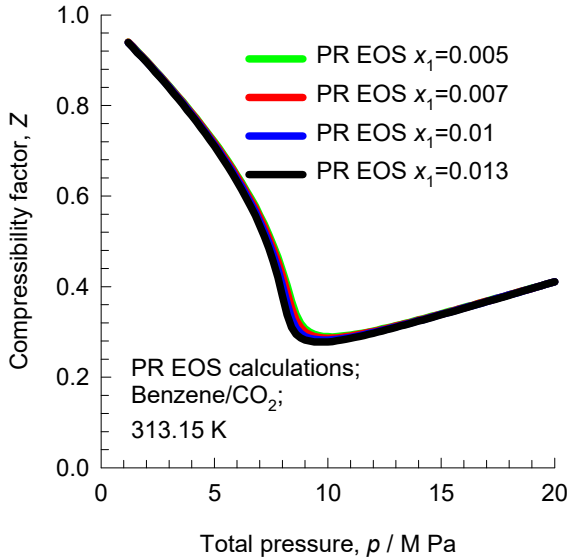

(c)

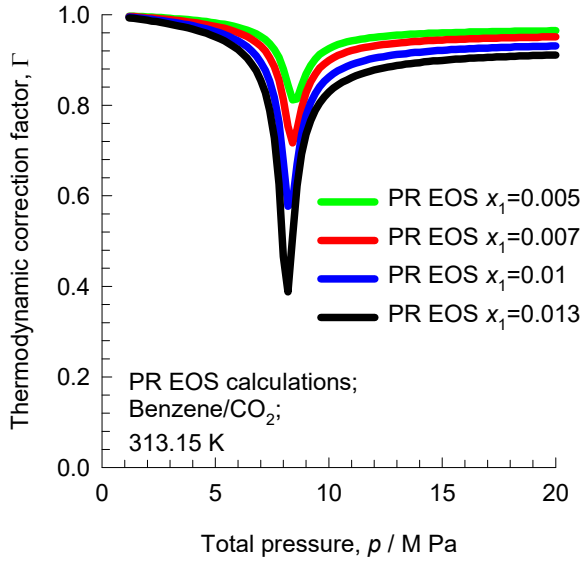

(d)

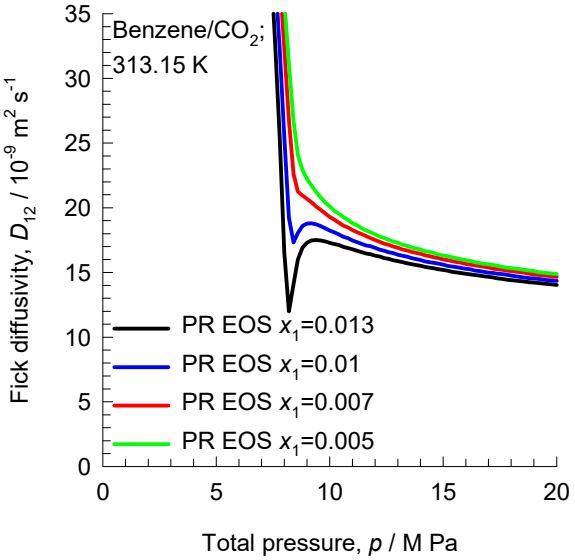

Ternary Liquid/Liquid System

Fig. S61

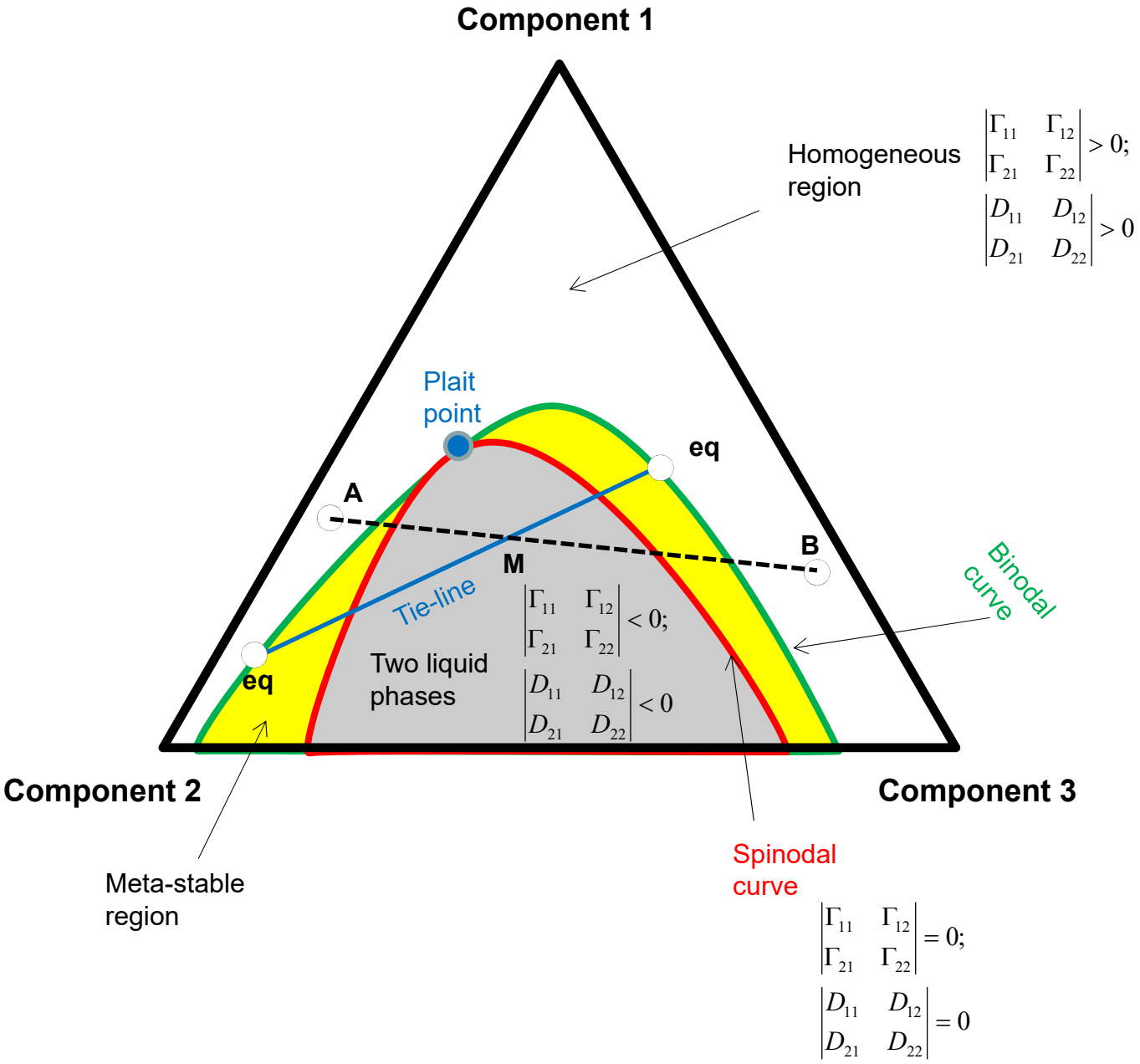

Fick diffusivities in Glycerol/Acetone/Water

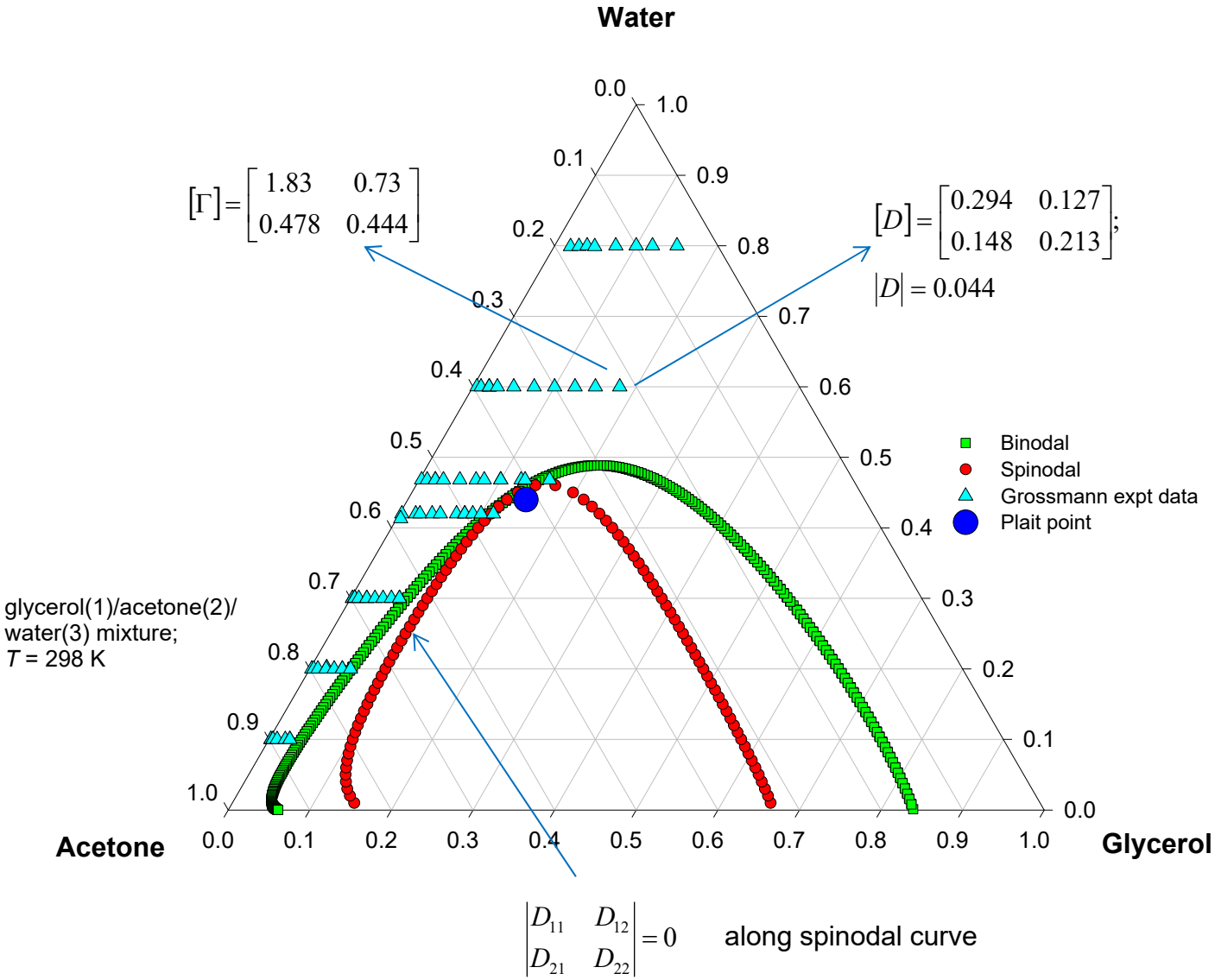

Magnitude of Fick matrix

Fig. S63

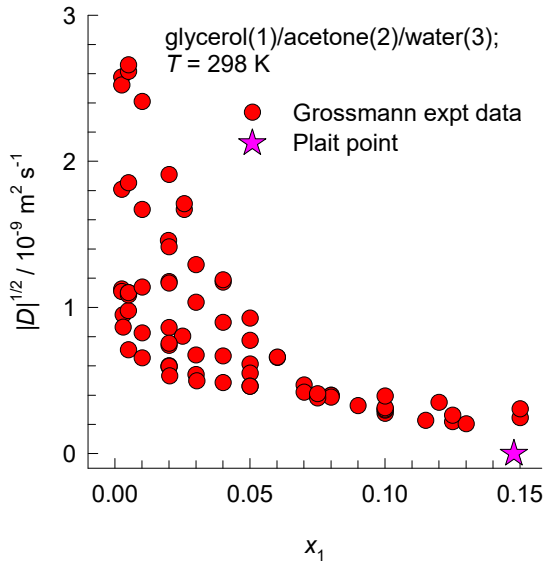

Coupling effects: Glycerol/Acetone/Water

Fig. S64

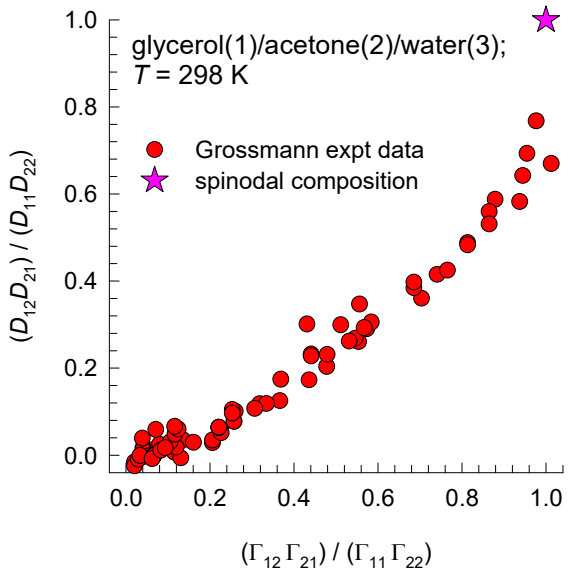

Factoring out thermodynamic influences

(a)

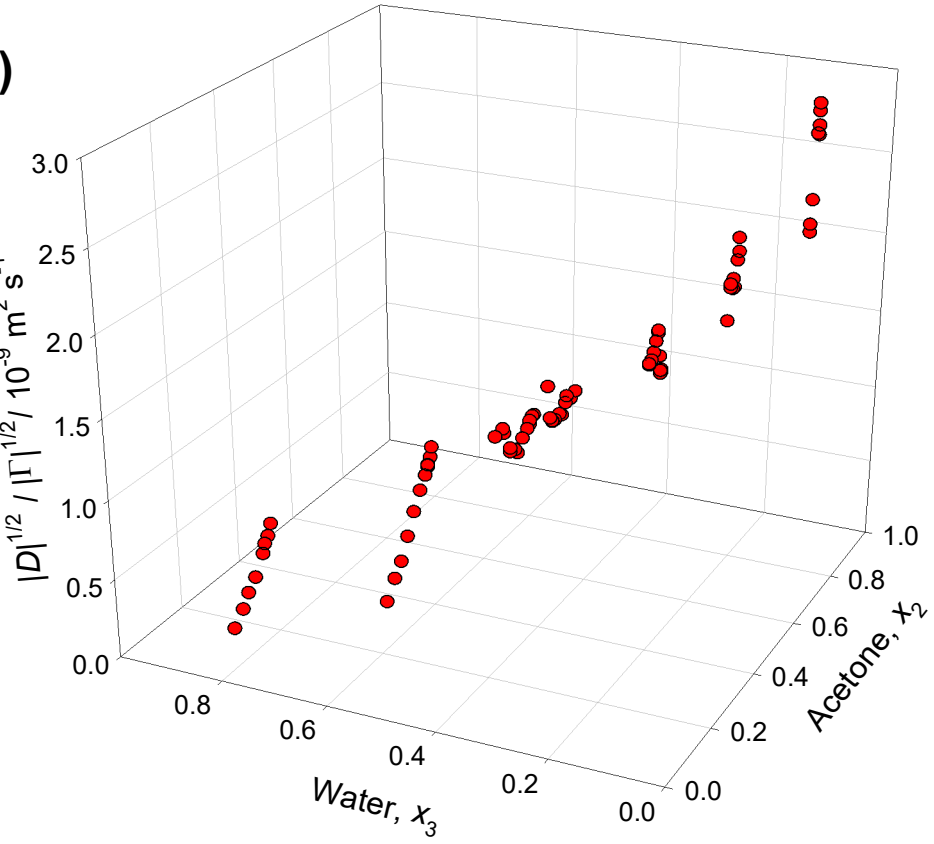

(b)

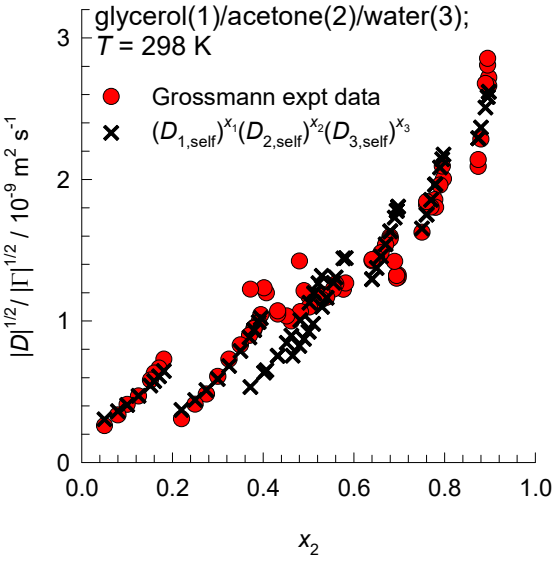

The fitted values of the self-diffusivities are

$D_{1,self}$ = 0.01
$D_{2,self}$ = 3.2
$D_{3,self}$ = 0.5
Units: 10^{-9} m^2 s^{-1}

Fick matrix: parity plots

Fig. S66

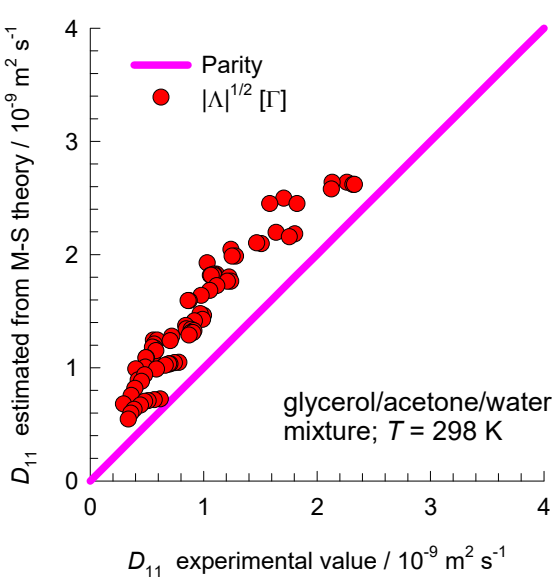

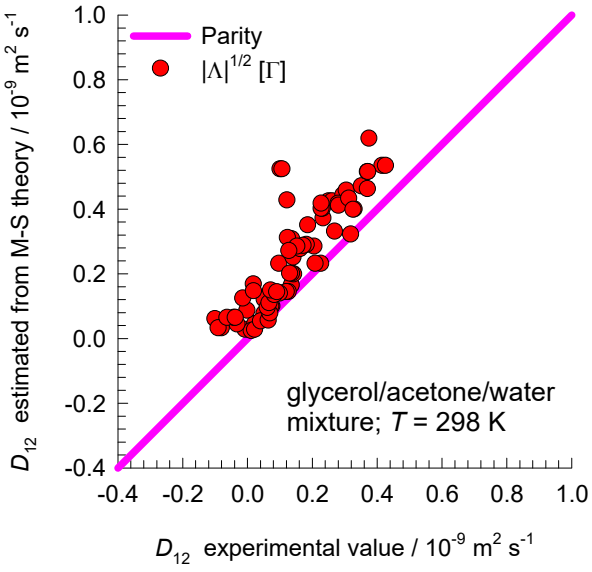

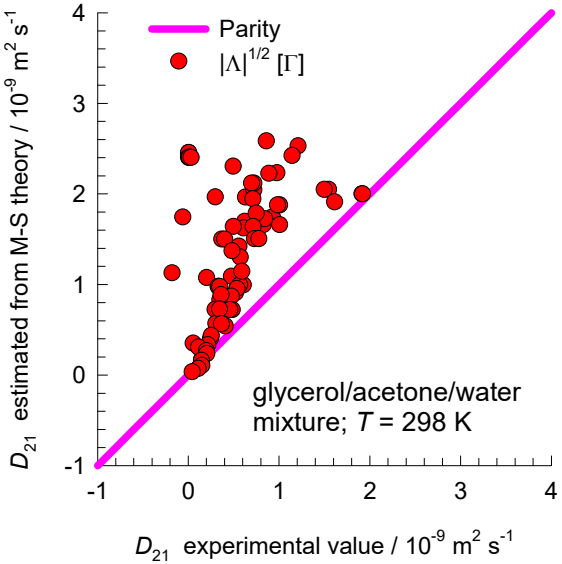

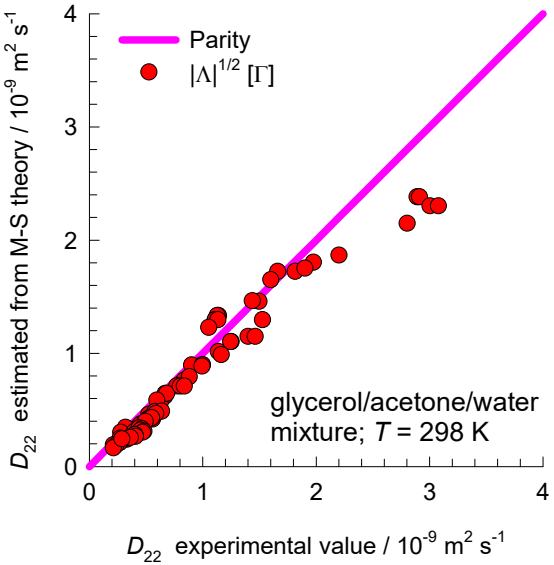

The Fick matrix is estimated using

$$[D] = |\Lambda|^{1/2}[\Gamma]$$

$$|\Lambda|^{1/2} = \left(D_{1,self}\right)^{x_1}\left(D_{2,self}\right)^{x_2}\left(D_{3,self}\right)^{x_3}$$

where the fitted self-diffusivity values are

$D_{1,self}$ = 0.01
$D_{2,self}$ = 3.2
$D_{3,self}$ = 0.5
Units: 10^{-9} m^2 s^{-1}

Water/Chloroform/Acetic Acid Diffusion

Fig. S67

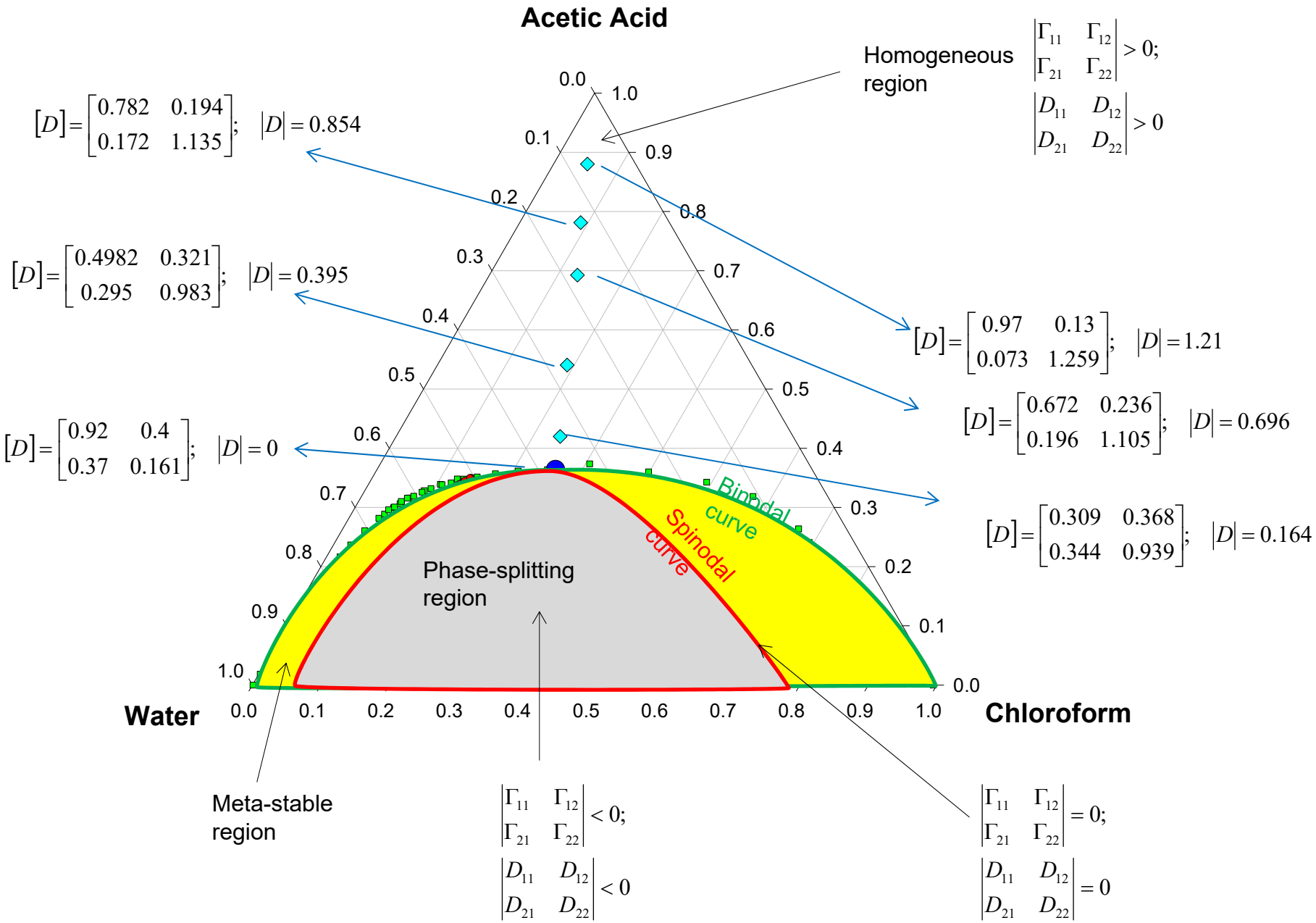

Water/Chloroform/Acetic Acid Diffusion

Fig. S68

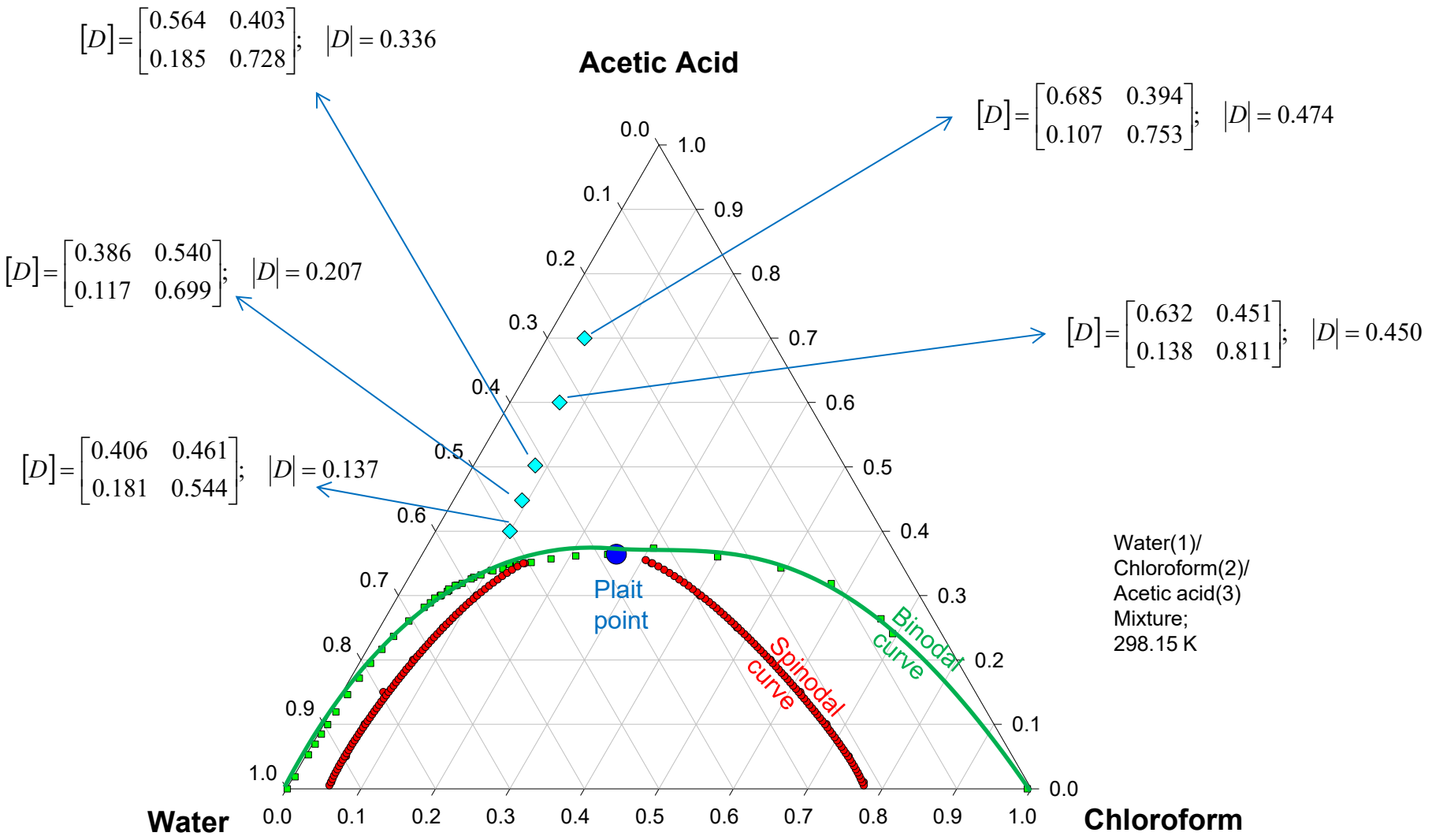

Magnitude of Fick matrix

Fig. S69

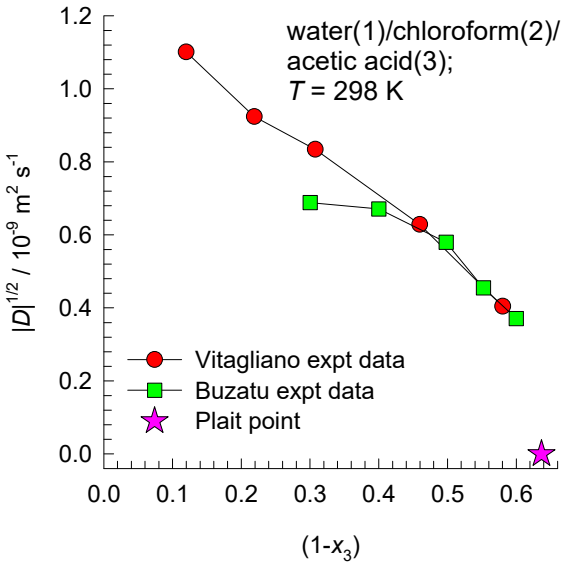

Fig. S70

Coupling effects

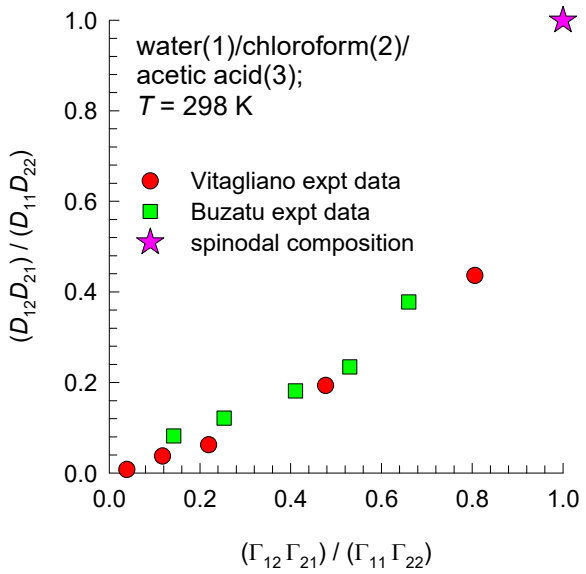

Fig. S71

Factoring out thermodynamic influences

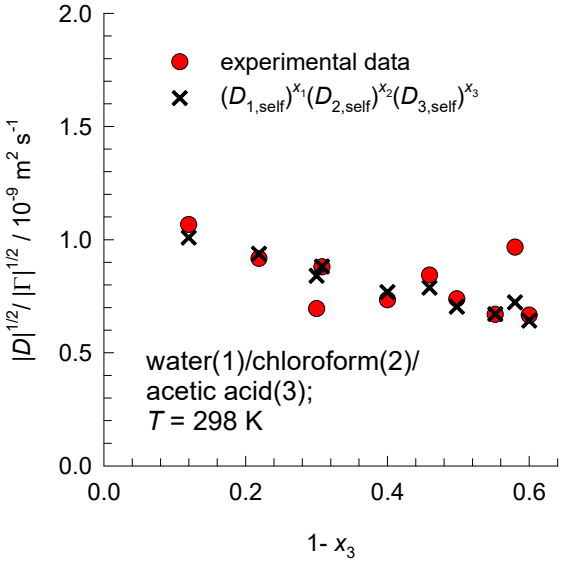

The fitted values of the self-diffusivities
are

$D_{1,self}$ = 0.4
$D_{2,self}$ = 0.8
$D_{3,self}$ = 1.1
Units: 10^{-9} m^2 s^{-1}

Fick matrix: parity plots

Fig. S72

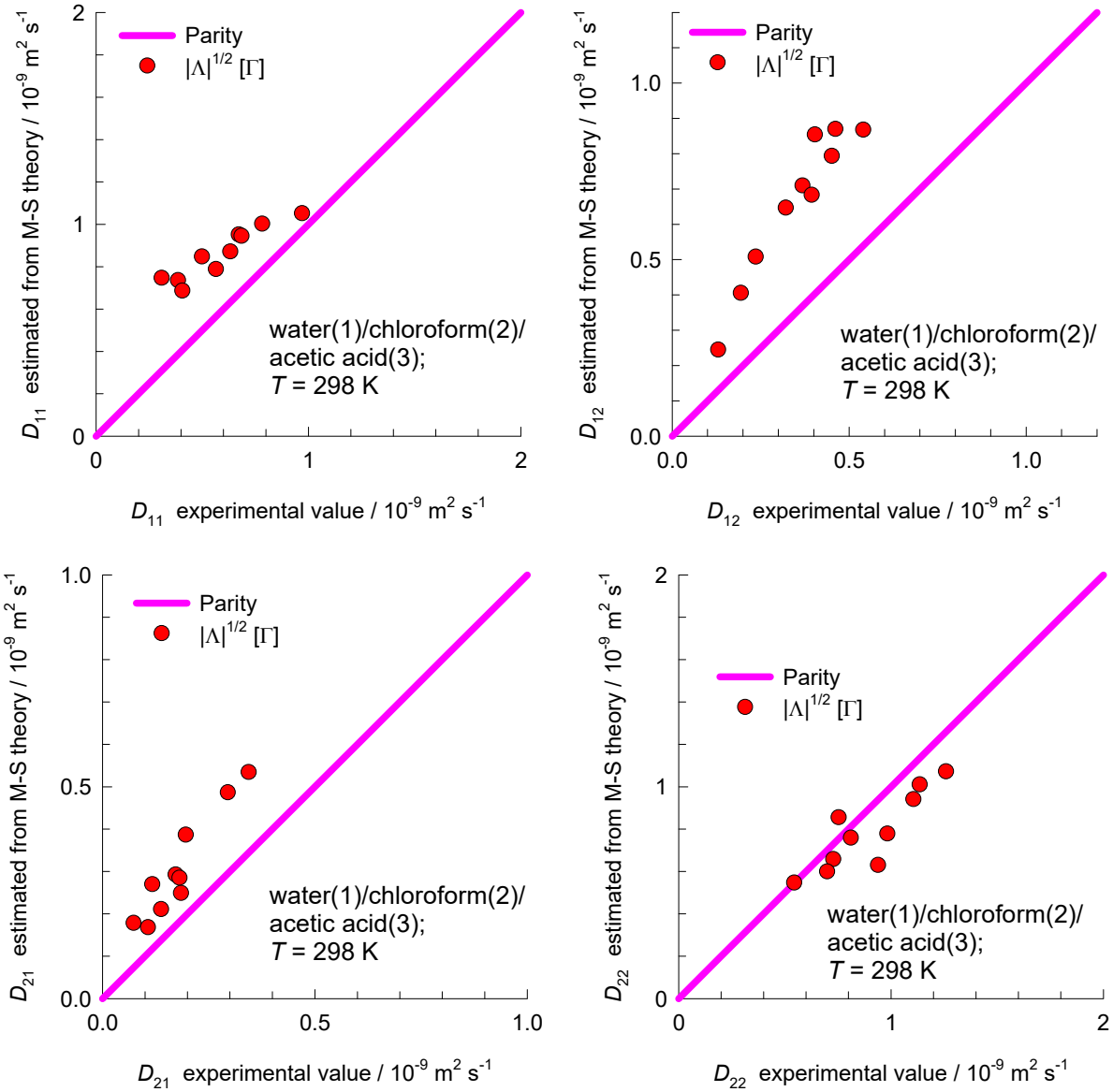

The Fick matrix is estimated using

$$[D] = |\Lambda|^{1/2}[\Gamma]$$

$$|\Lambda|^{1/2} = (D_{1,self})^{x_1}(D_{2,self})^{x_2}(D_{3,self})^{x_3}$$

where the fitted self-diffusivity values are

$D_{1,\text{self}}$ = 0.4
$D_{2,\text{self}}$ = 0.8
$D_{3,\text{self}}$ = 1.1
Units: 10^{-9} m^2 s^{-1}

Water/2-propanol/cyclohexane mixture diffusion

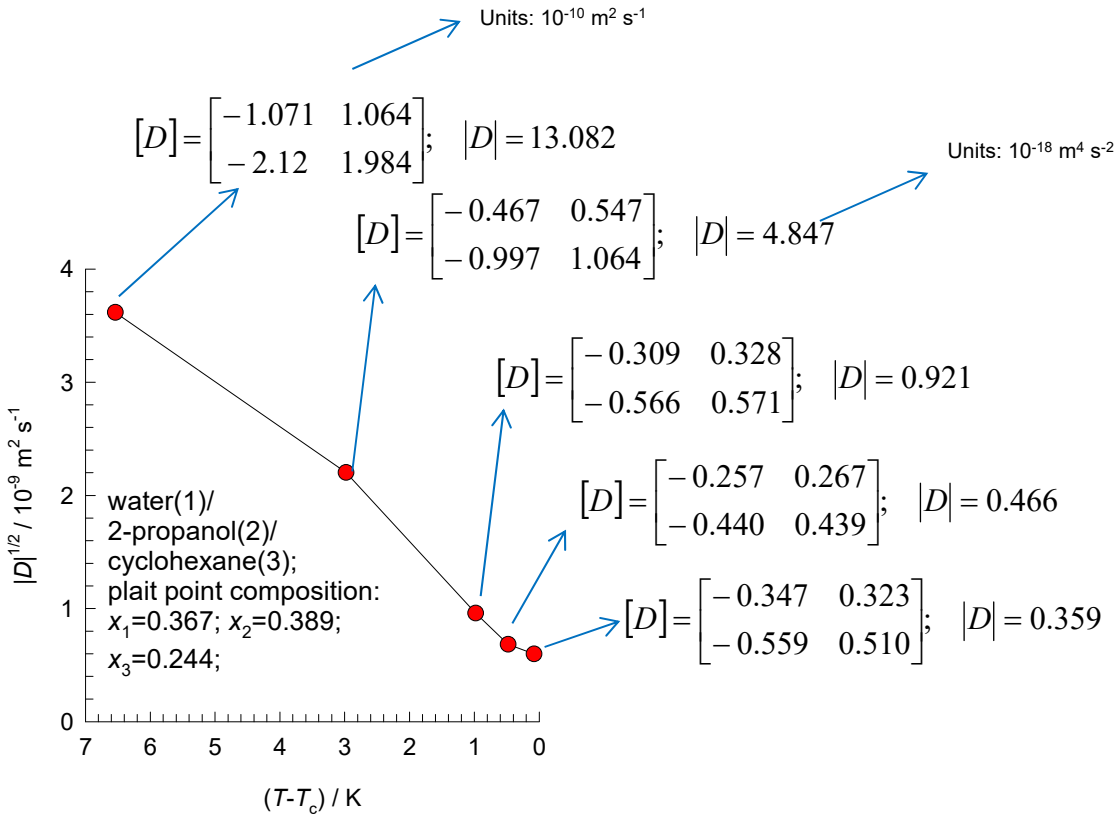

Glycerol/Acetone/Water Equilibration

Fig. S74

	Left	Right
Initial compositions:	$x_1 = 0.08$ $x_2 = 0.55$ $x_3 = 0.37$	$x_1 = 0.12$ $x_2 = 0.314$ $x_3 = 0.566$

Equilibrated compositions:

$x_1 = 0.1$;
$x_2 = 0.432$;
$x_3 = 0.468$;

Expt Fick diffusivity matrix at equilibrated composition

$$[D] = \begin{bmatrix} 0.4901 & 0.2267 \\ 0.4585 & 0.3991 \end{bmatrix} \times 10^{-9} \quad \mathrm{m^2\ s^{-1}}$$

Magnitude of M-S diffusivity at equilibrated composition

$$|\Lambda|^{1/2} = 0.754 \times 10^{-9} \quad \mathrm{m^2\ s^{-1}}$$

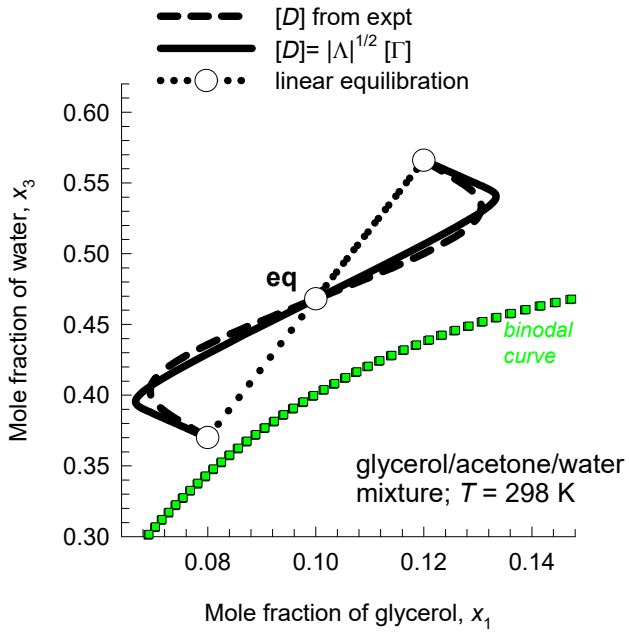

Glycerol/Acetone/Water Equilibration

Fig. S75

	Left	Right
Initial compositions:	$x_1 = 0.05$; $x_2 = 0.28$; $x_3 = 0.67$	$x_1 = 0.31$; $x_2 = 0.16$; $x_3 = 0.53$

Equilibrated compositions:

$x_1 = 0.18$;
$x_2 = 0.22$;
$x_3 = 0.6$;

Expt Fick diffusivity matrix at equilibrated composition

$$[D] = \begin{bmatrix} 0.2938 & 0.1271 \\ 0.1483 & 0.2127 \end{bmatrix} \times 10^{-9} \quad \mathrm{m^2\ s^{-1}}$$

Magnitude of M-S diffusivity at equilibrated composition

$$|\Lambda|^{1/2} = 0.372 \times 10^{-9} \quad \mathrm{m^2\ s^{-1}}$$

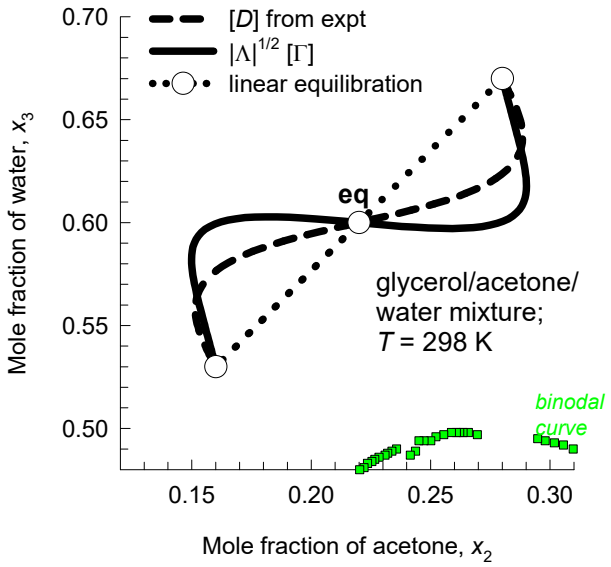

Water/Chloroform/Acetic Acid equilibration

Fig. S76

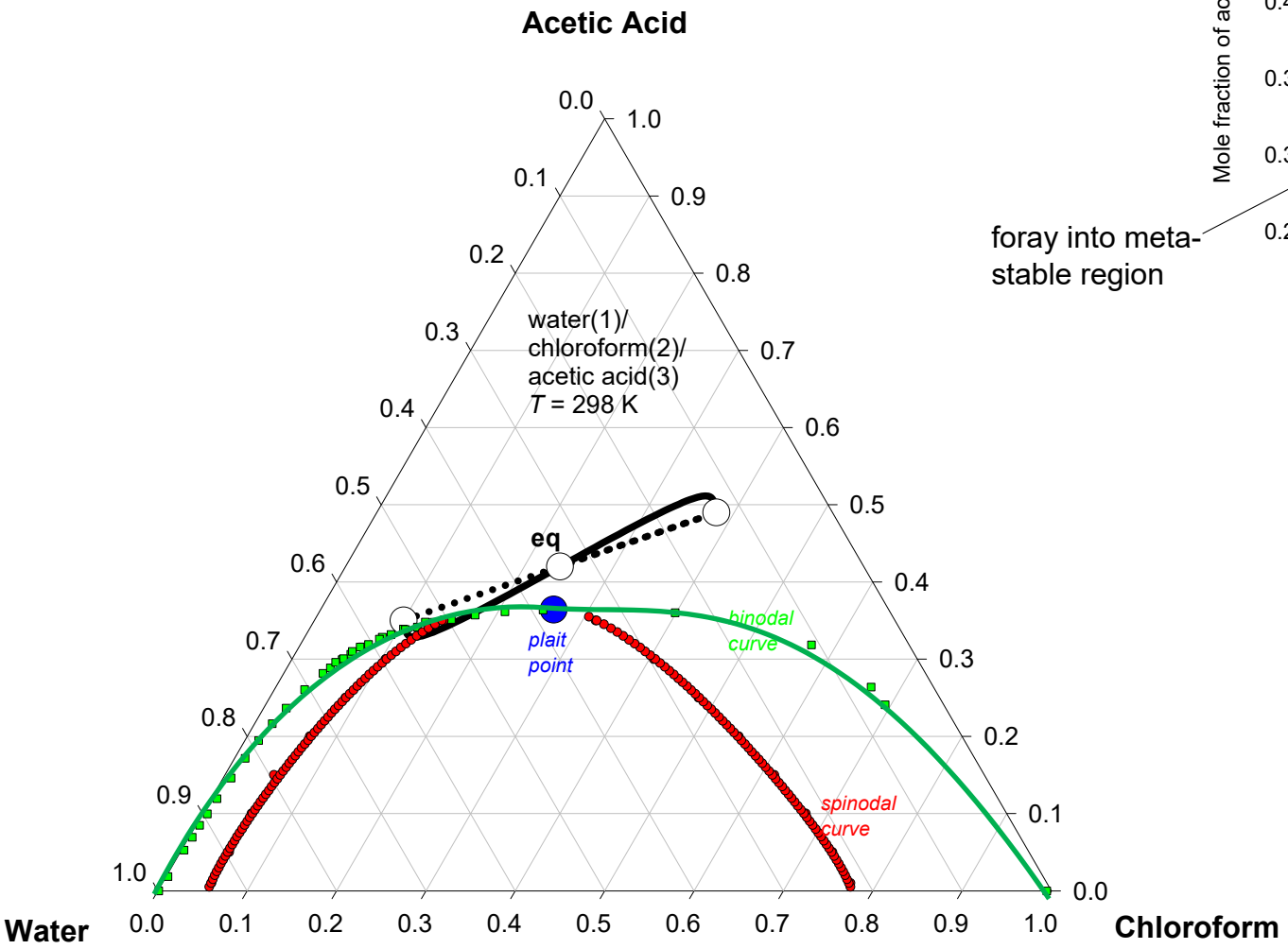

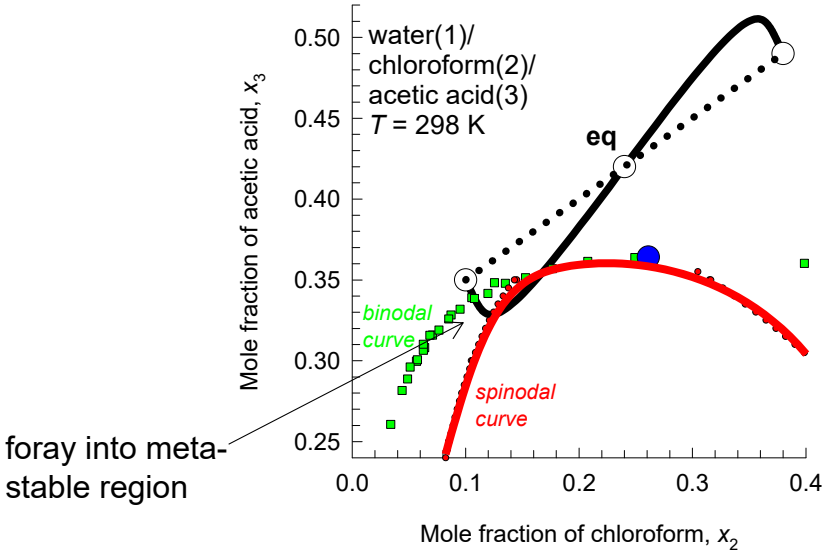

foray into meta-stable region

Serpentine trajectory obtained with

$$[D] = \begin{bmatrix} 0.309 & 0.368 \\ 0.344 & 0.939 \end{bmatrix}; \quad |D| = 0.164$$

predicts possibility of emulsification

Linear equilibration trajectory: *no emulsification*

Glycerol/Acetone/Water equilibration

Fig. S77

	Left	Right
glycerol	$x_1 = 0.30$	$x_1 = 0.70$
acetone	$x_2 = 0.22$	$x_2 = 0.12$
water	$x_3 = 0.48$	$x_3 = 0.33$

foray into meta-stable region

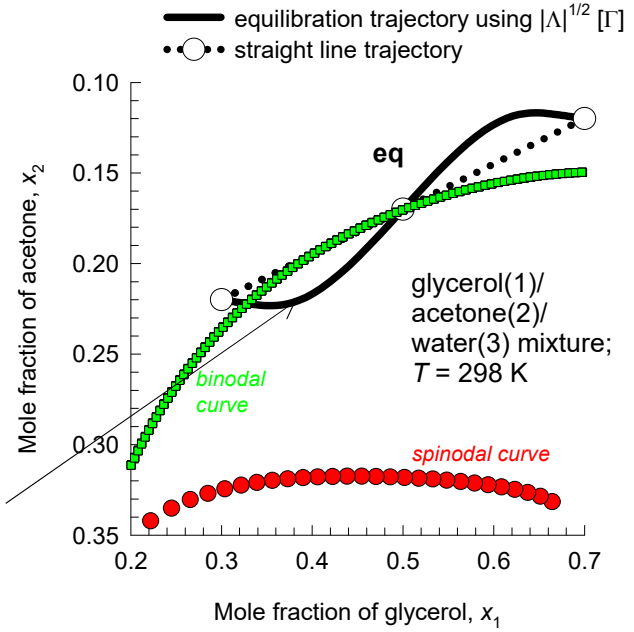

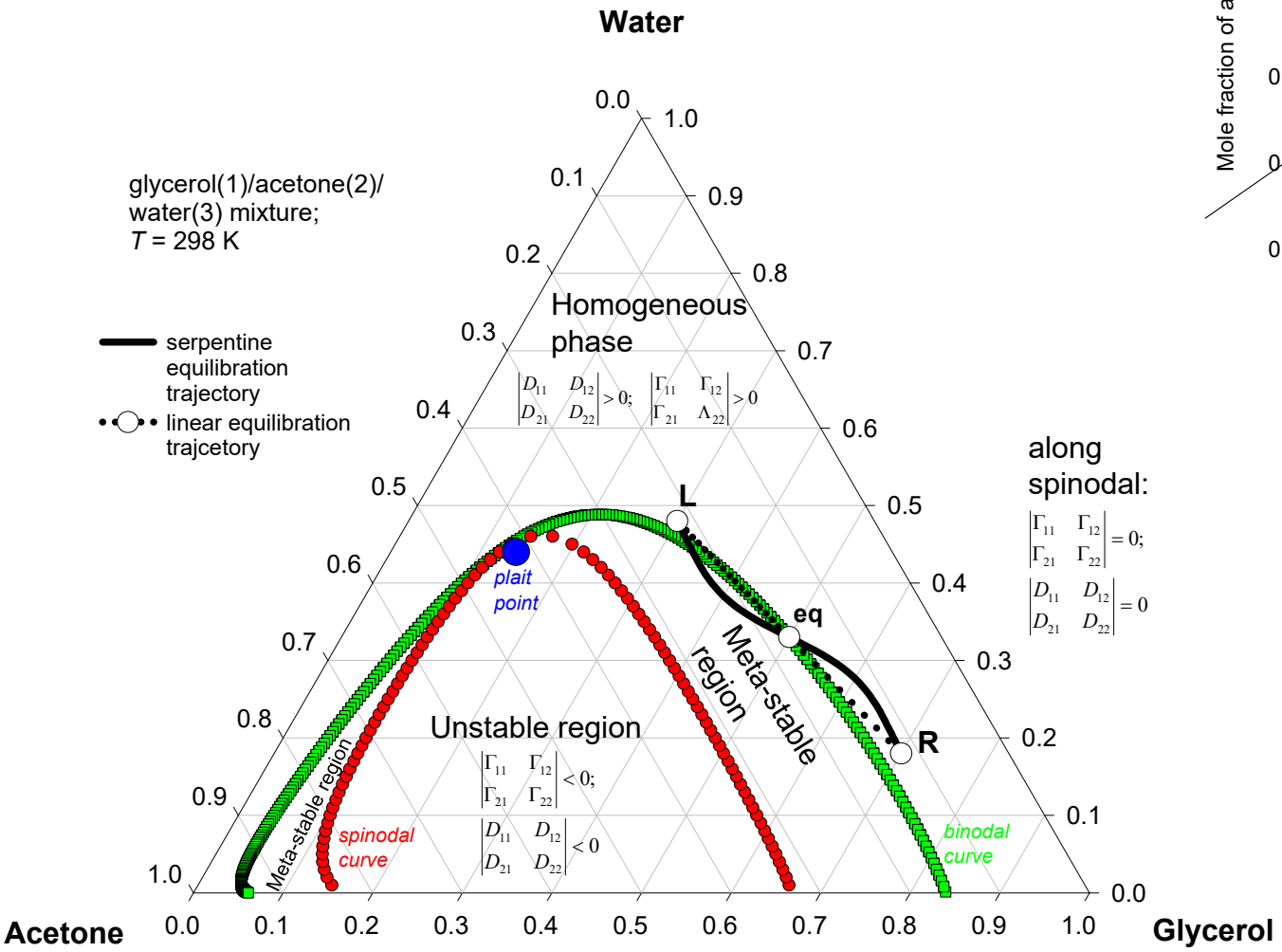

along spinodal:

$$\left|\begin{matrix} \Gamma_{11} & \Gamma_{12} \\ \Gamma_{21} & \Gamma_{22} \end{matrix}\right| = 0;$$

$$\left|\begin{matrix} D_{11} & D_{12} \\ D_{21} & D_{22} \end{matrix}\right| = 0$$

Serpentine trajectory obtained with

$$[D] = \begin{bmatrix} 0.223 & 0.133 \\ 0.0144 & 0.045 \end{bmatrix} \times 10^{-9} \quad \mathrm{m^2\ s^{-1}}$$

predicts possibility of emulsification

Linear equilibration trajectory (dotted line): *no emulsification*

Water/DMSO/THF equilibration

Fig. S78

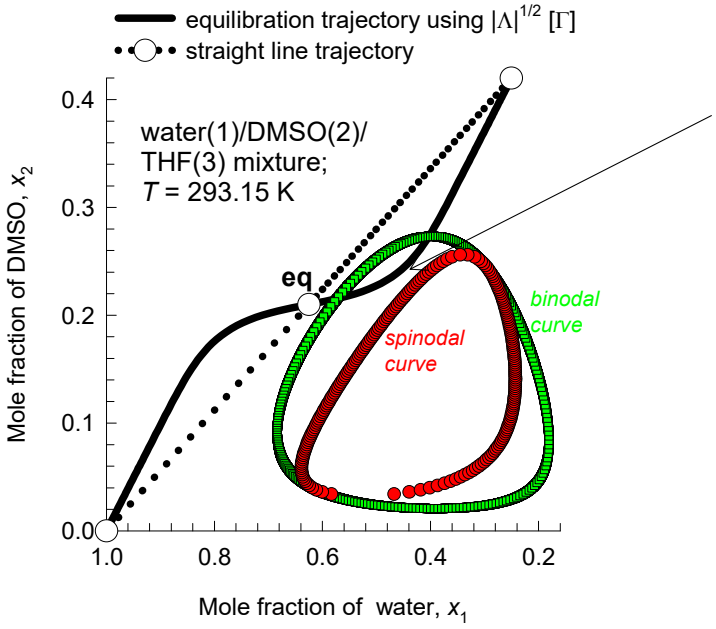

foray into meta-stable region

	Left	Right
Initial mole fractions	$x_1 = 1$ $x_2 = 0$ $x_3 = 0$	$x_1 = 0.25$ $x_2 = 0.42$ $x_3 = 0.33$

Serpentine trajectory obtained with

$$[D] = \begin{bmatrix} 1.614 & -3.535 \\ -1.2974 & 3.766 \end{bmatrix} \times 10^{-9} \quad \mathrm{m^2\ s^{-1}}$$

predicts possibility of emulsification

Linear equilibration trajectory (dotted line): *no emulsification*

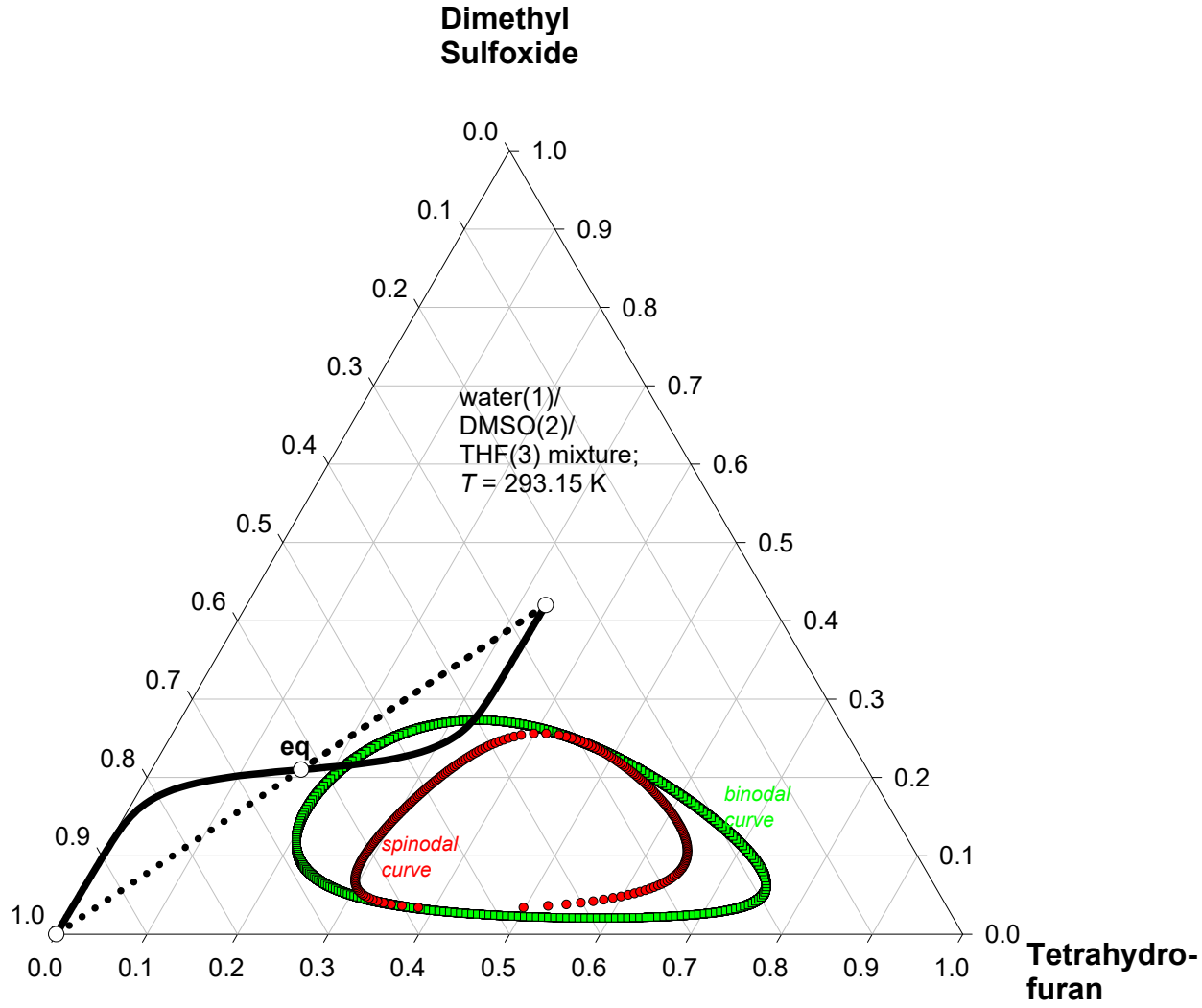

Water/DMSO/THF equilibration

Fig. S79

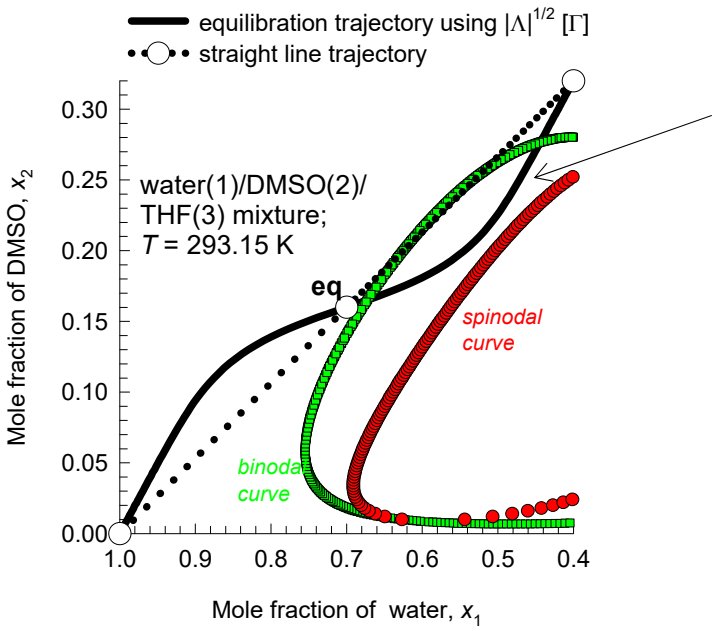

foray into meta-stable region

	Left	Right
Initial mole fractions	$x_1 = 1$ $x_2 = 0$ $x_3 = 0$	$x_1 = 0.4$ $x_2 = 0.32$ $x_3 = 0.28$

Serpentine trajectory obtained with

$$[D] = \begin{bmatrix} 0.948 & -2.458 \\ -0.6091 & 2.756 \end{bmatrix} \times 10^{-9} \quad \mathrm{m^2\ s^{-1}}$$

predicts possibility of emulsification

Linear equilibration trajectory (dotted line): *no emulsification*

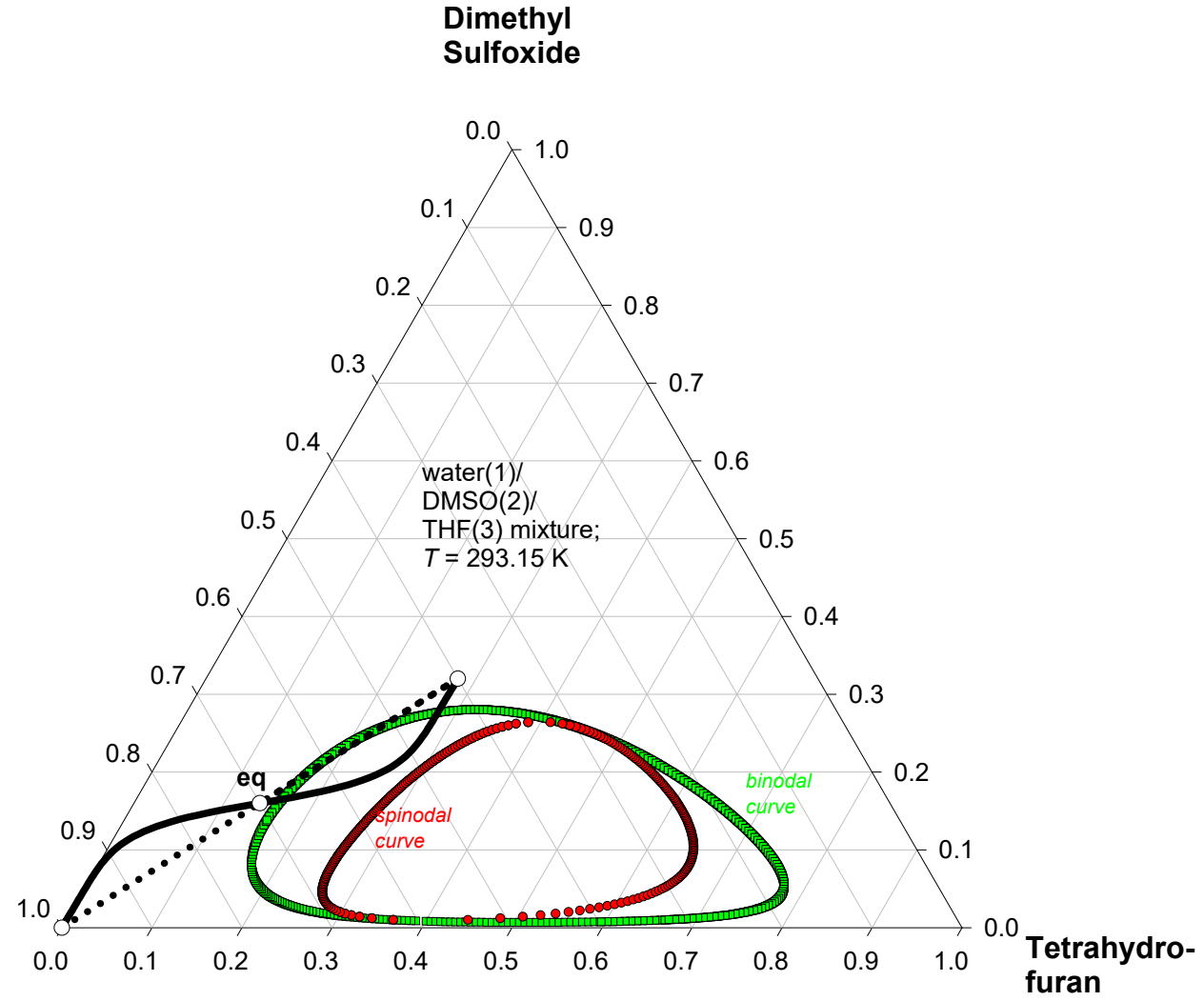

Water/acetone/phenol equilibration

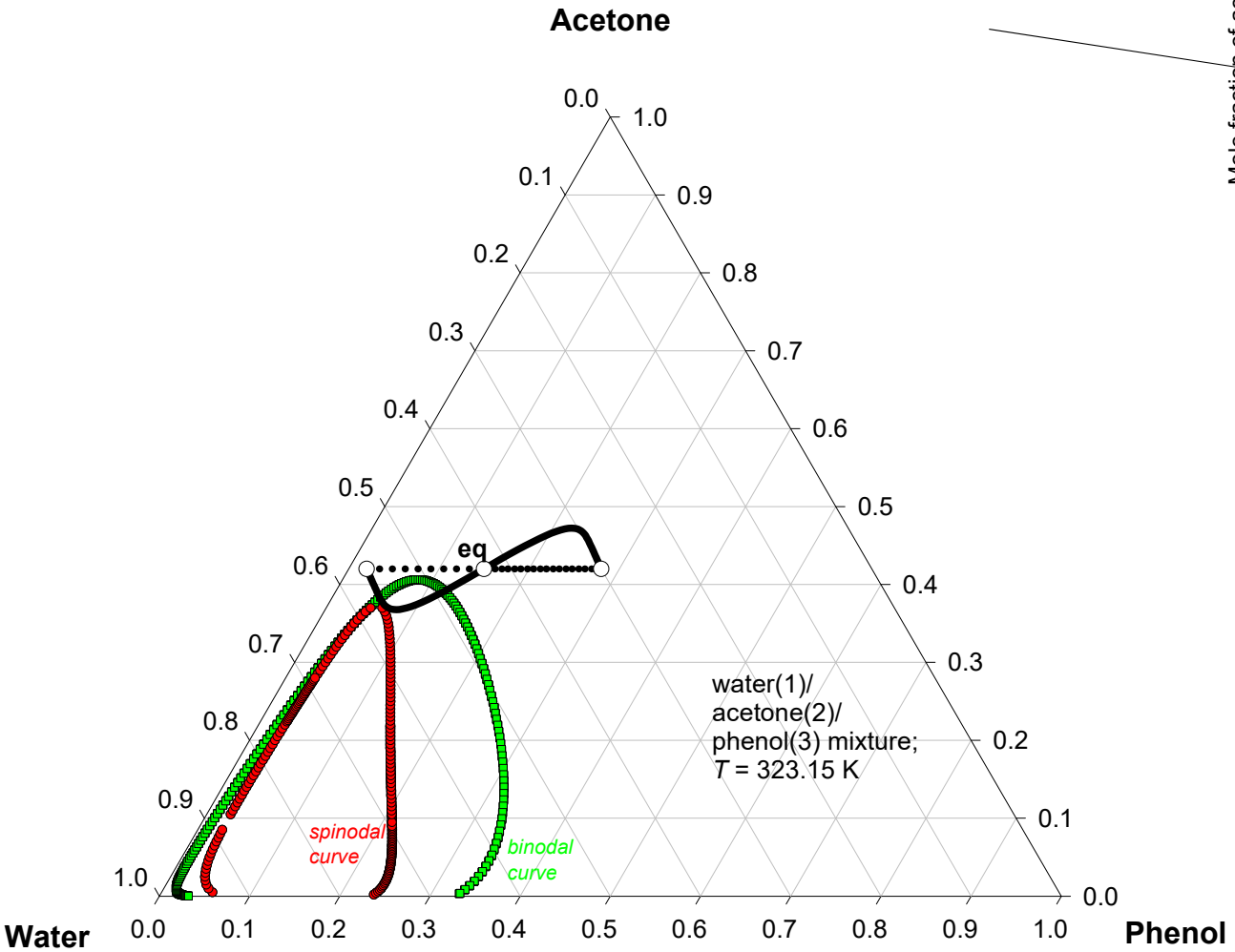

foray into meta-stable region

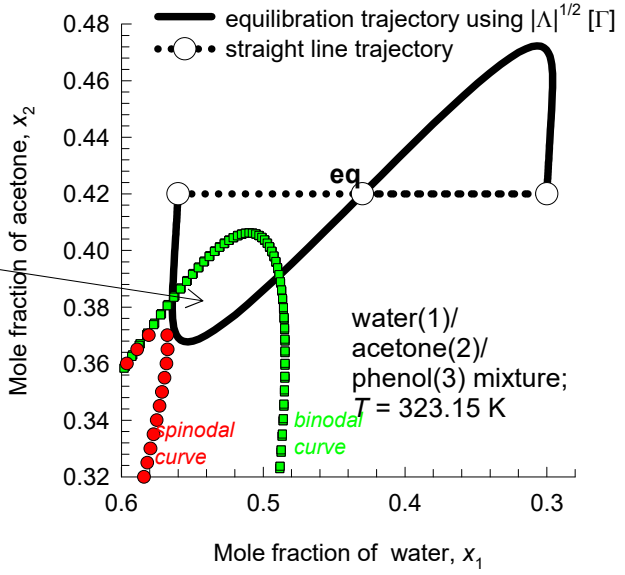

Serpentine trajectory obtained with

$$[D] = \begin{bmatrix} 1.648\times10^{-3} & -0.3437 \\ 2.013 & 3.1942 \end{bmatrix} \times 10^{-9} \quad \mathrm{m^2\ s^{-1}}$$

predicts possibility of emulsification

Linear equilibration trajectory (dotted line): *no emulsification*

Fig. S81

Water/acetone/TCE equilibration

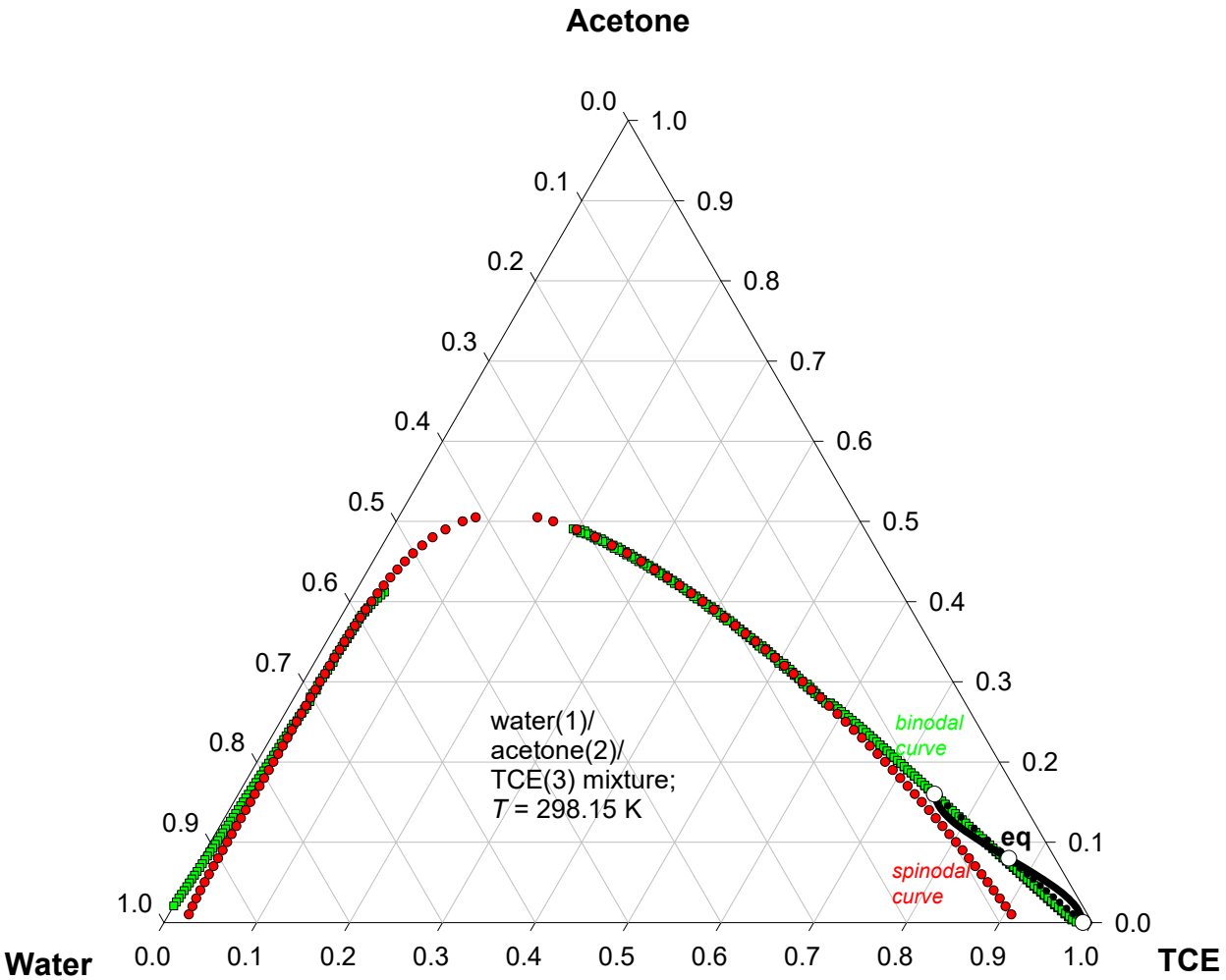

foray into meta-stable region

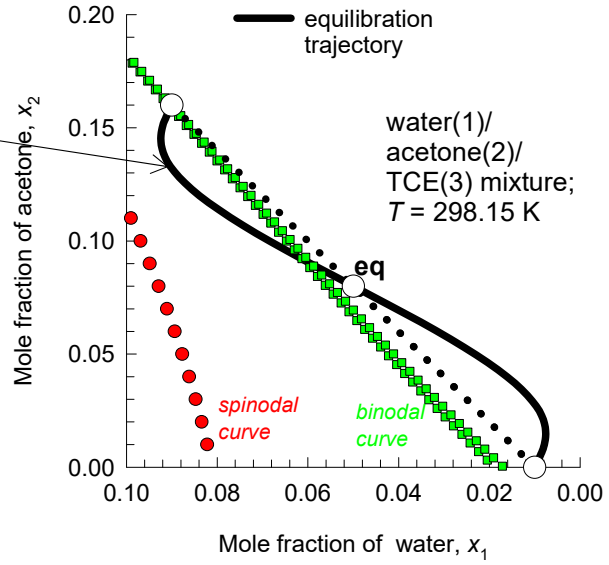

Serpentine trajectory obtained with

$$[D]=\begin{bmatrix}0.3792 & -0.1983\\ -0.246 & 1.106\end{bmatrix}\times 10^{-9}\ \ \mathrm{m^2\ s^{-1}}$$

predicts possibility of emulsification

Linear equilibration trajectory (dotted line): *no emulsification*

Fig. S82

Water/2-propanol/phenol equilibration

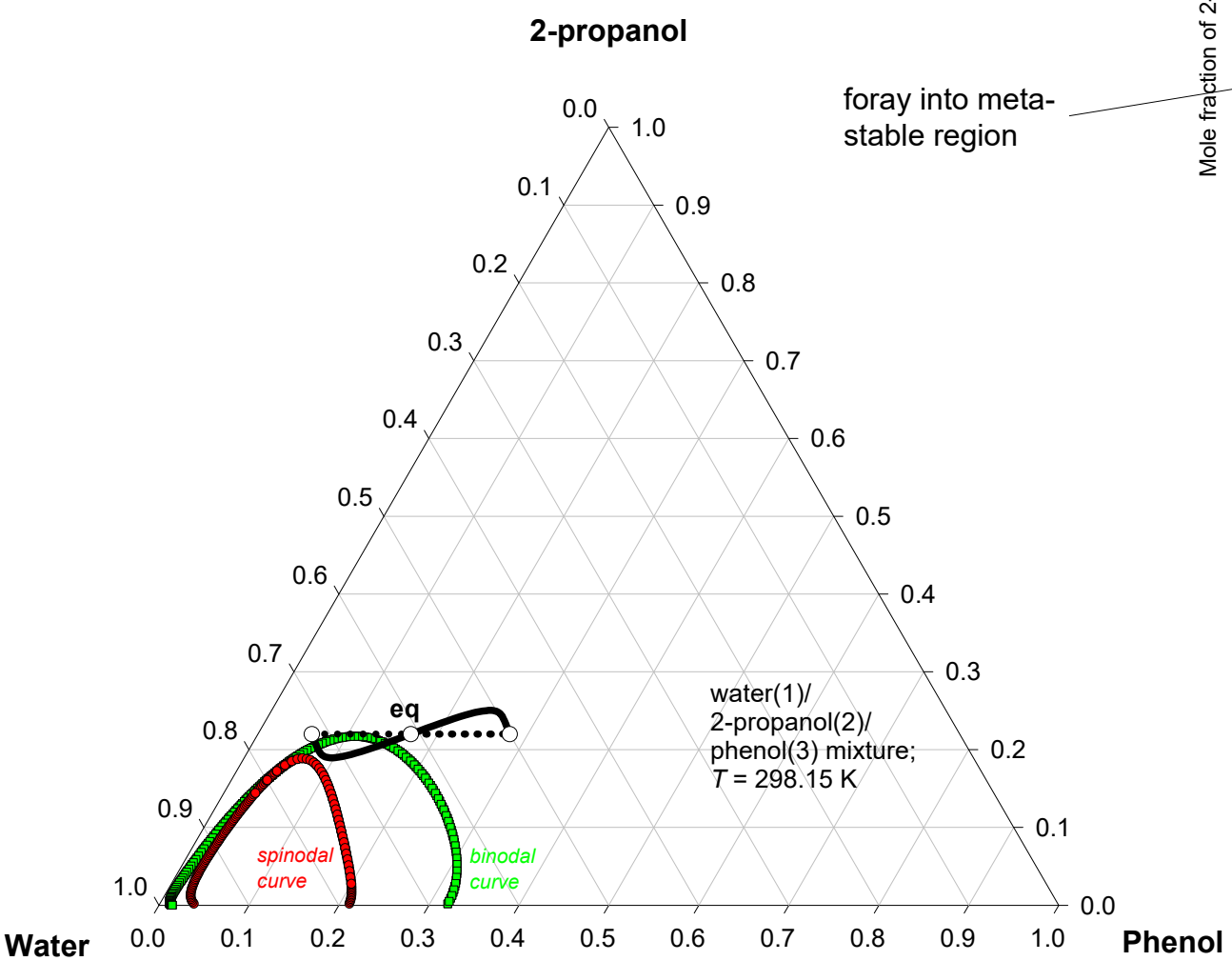

foray into meta-stable region

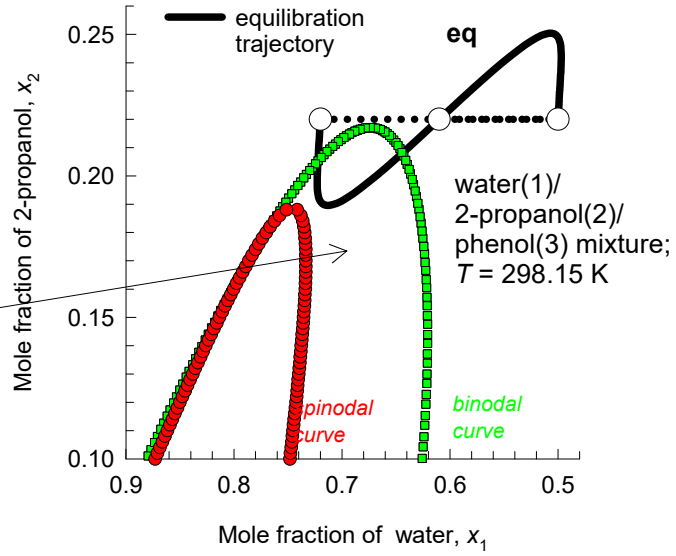

Serpentine trajectory obtained with

$$[D] = \begin{bmatrix} 0.049 & -0.4195 \\ 1.342 & 2.964 \end{bmatrix} \times 10^{-9} \quad \mathrm{m^2\ s^{-1}}$$

predicts possibility of emulsification

Linear equilibration trajectory (dotted line): *no emulsification*

Fig. S83

Water/trichloroacetic acid/antipyrine equilibration

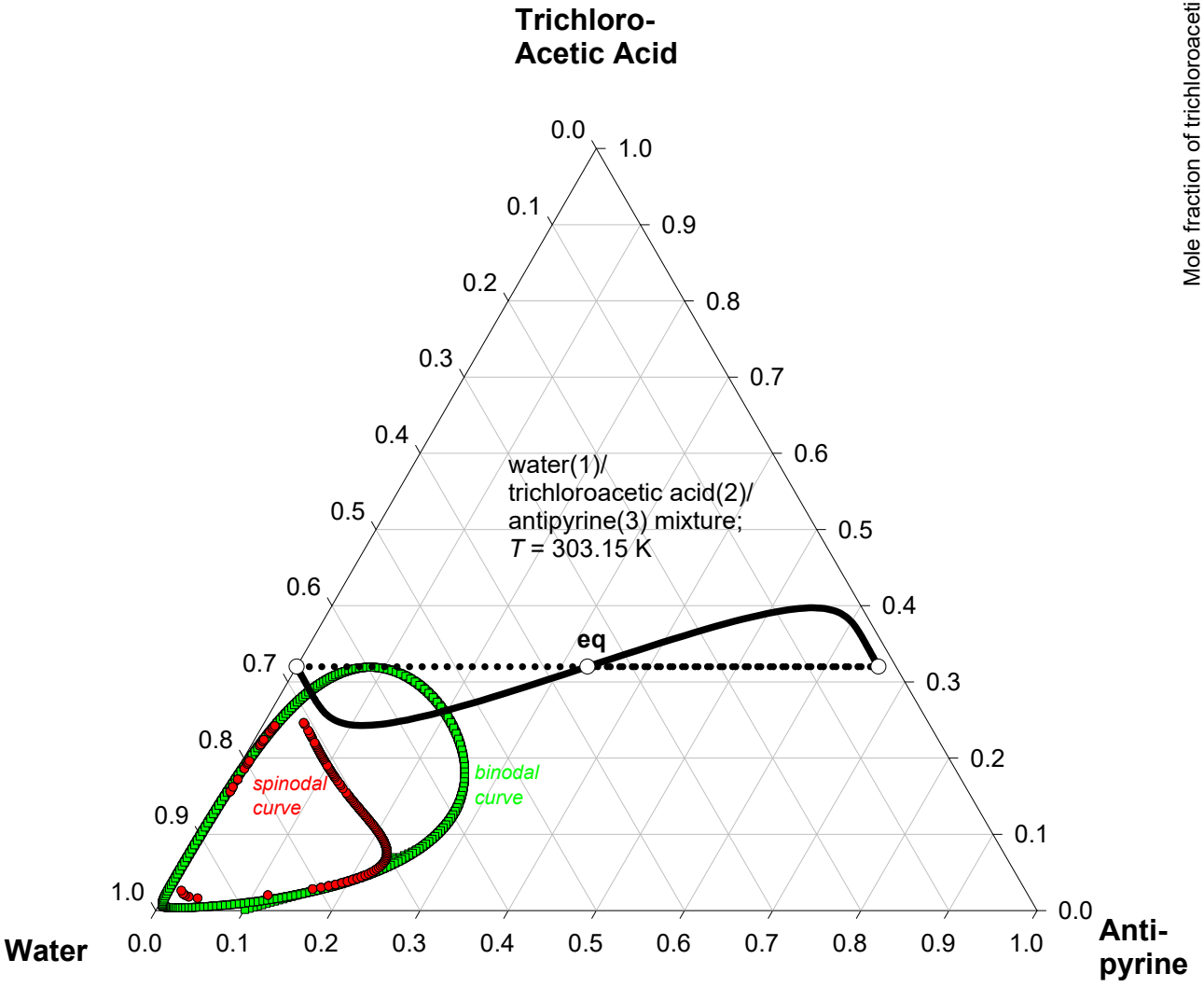

foray into meta-stable region

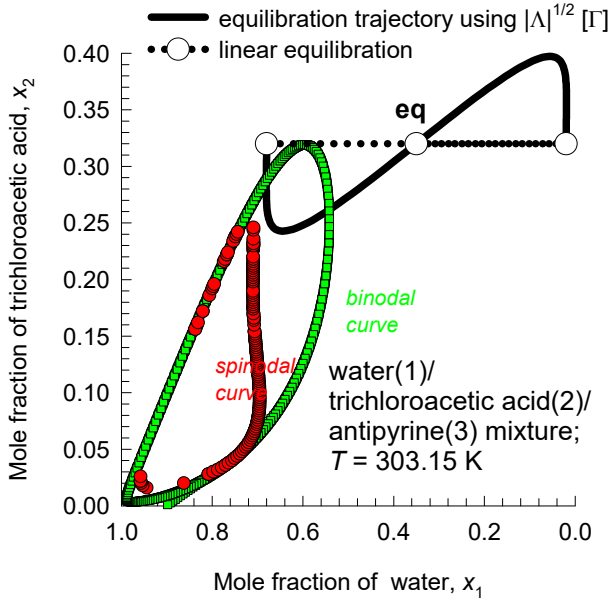

Serpentine trajectory obtained with

$$[D] = \begin{bmatrix} 0.7169 & -0.1595 \\ 3.094 & 7.312 \end{bmatrix} \times 10^{-9} \quad \mathrm{m^2\ s^{-1}}$$

predicts possibility of emulsification

Linear equilibration trajectory (dotted line): *no emulsification*

Acetone/Ethylacetate/Water equilibration

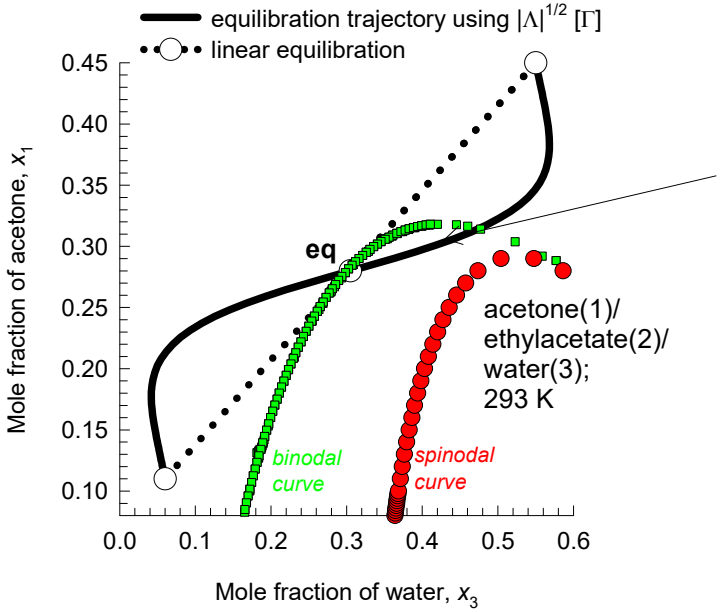

foray into meta-stable region

Serpentine trajectory obtained with

$$[D] = \begin{bmatrix} 1.18 & -0.097 \\ -0.649 & 0.2257 \end{bmatrix} \times 10^{-9} \quad \mathrm{m^2\ s^{-1}}$$

predicts possibility of emulsification

Linear equilibration trajectory (dotted line): *no emulsification*

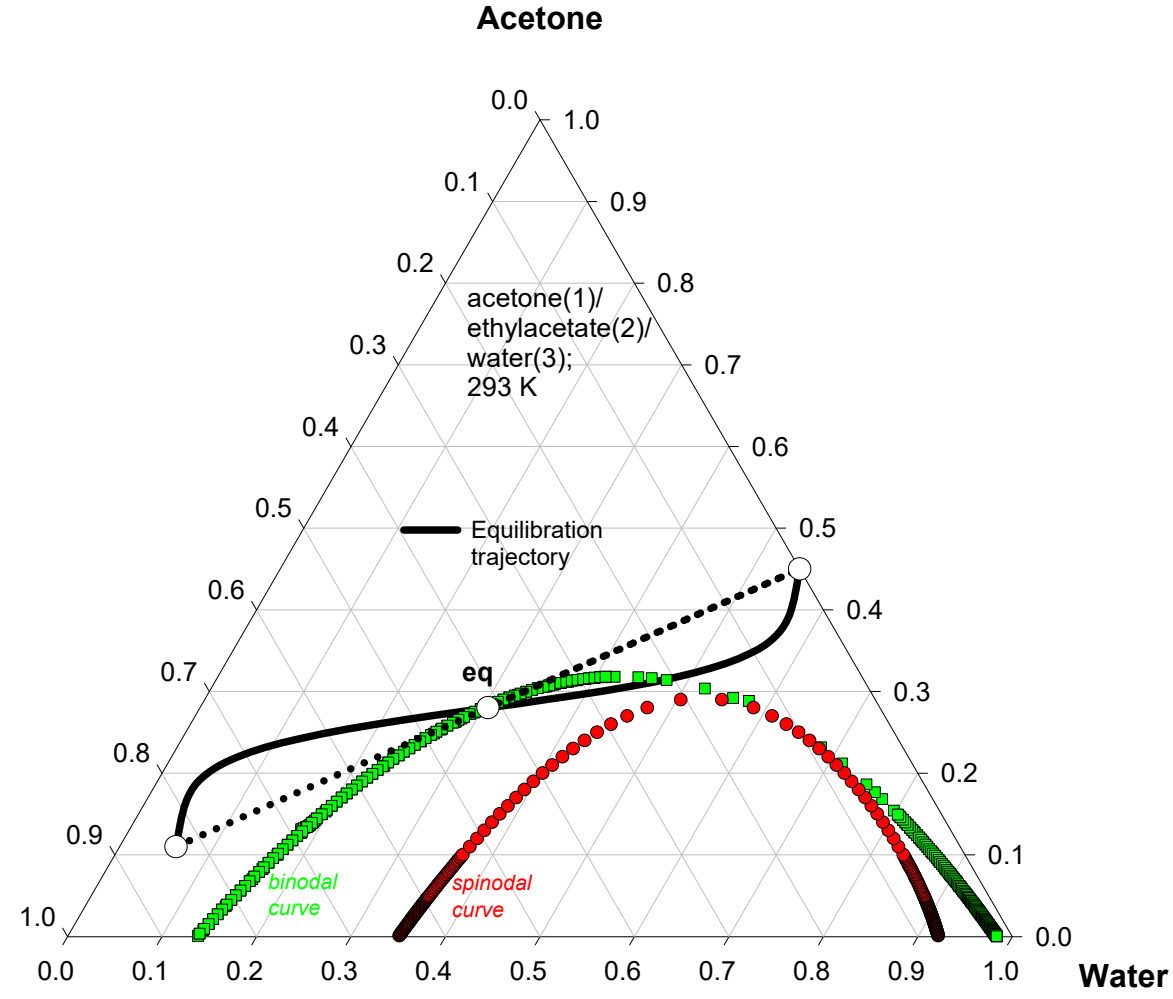

Propyl acetate/formic acid/water equilibration

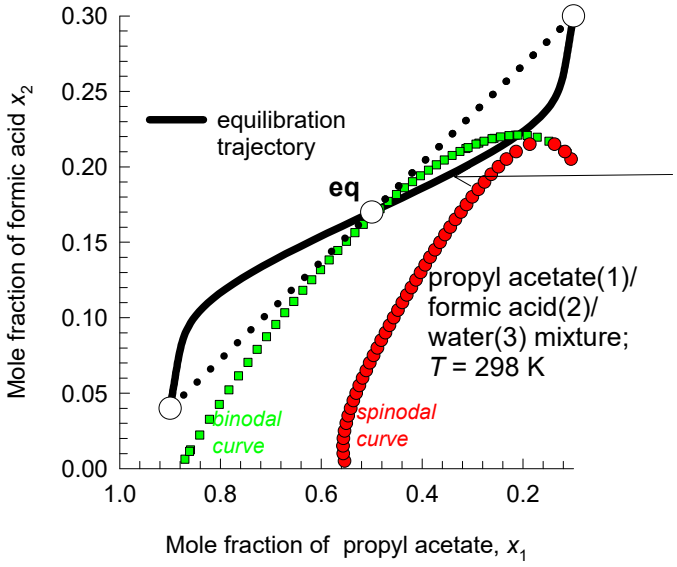

foray into meta-stable region

Serpentine trajectory obtained with

$$[D] = \begin{bmatrix} 0.1786 & -1.561 \\ 0.243 & 3.485 \end{bmatrix} \times 10^{-9} \quad \mathrm{m^2\ s^{-1}}$$

predicts possibility of emulsification

Linear equilibration trajectory (dotted line): *no emulsification*

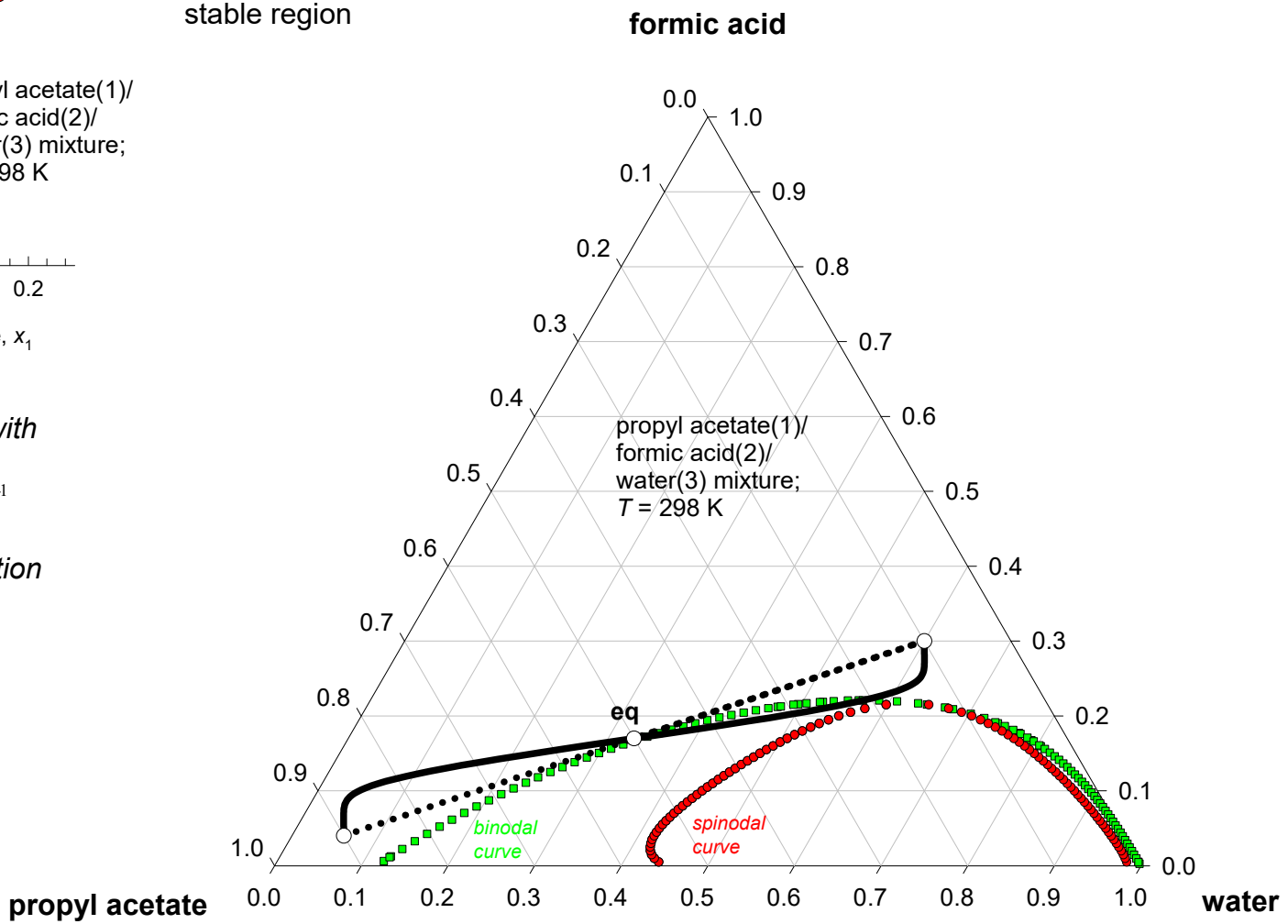

Furfural/formic acid/water equilibration

Fig. S86

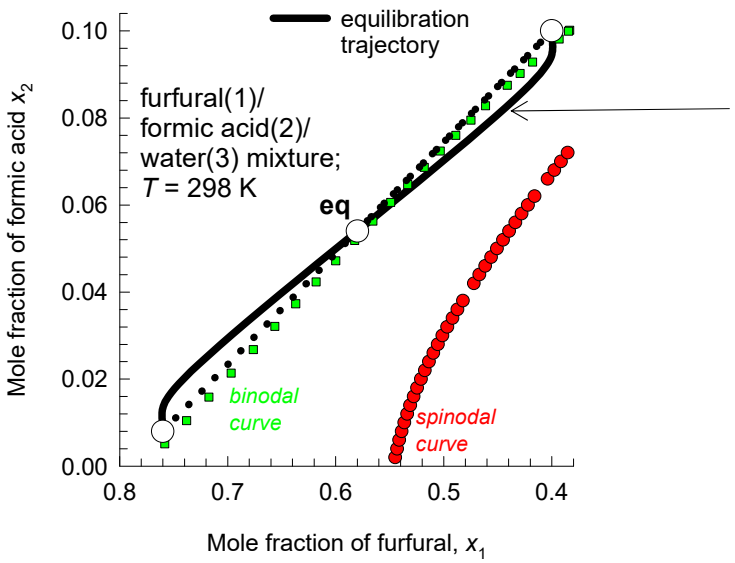

foray into meta-stable region

Serpentine trajectory obtained with

$$[D]=\begin{bmatrix}0.2602 & 0.392\\ 0.271 & 1.72\end{bmatrix}\times 10^{-9}\quad \mathrm{m^2\ s^{-1}}$$

predicts possibility of emulsification

Linear equilibration trajectory (dotted line): *no emulsification*

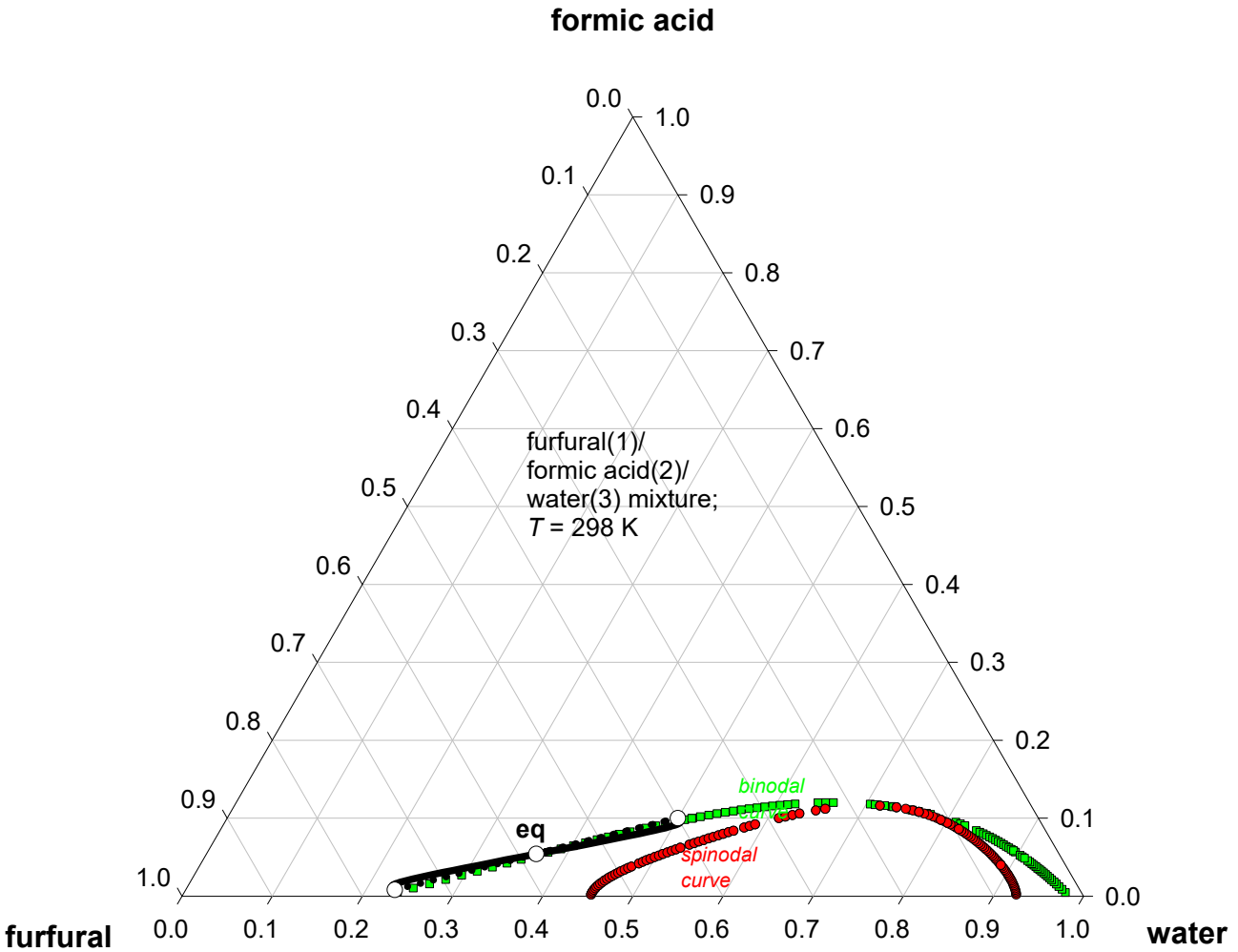

1-butanol/methanol/water equilibration

Fig. S87

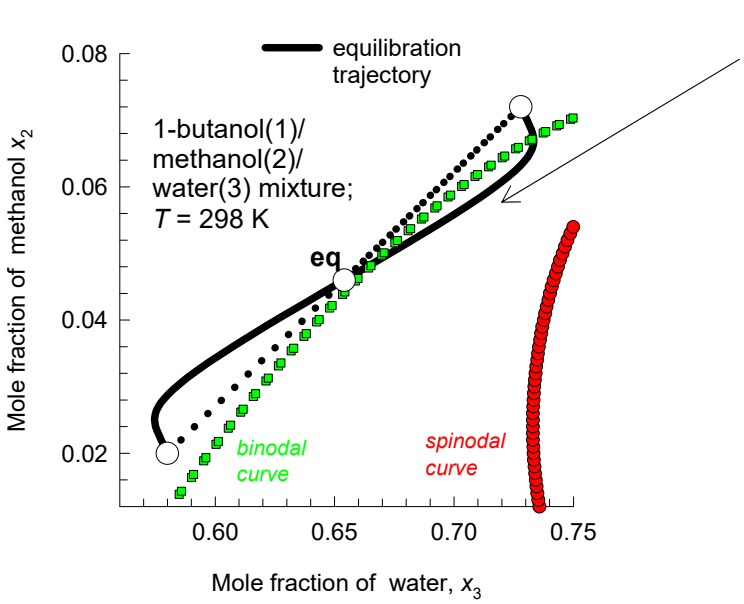

foray into meta-stable region

Serpentine trajectory obtained with

$$[D] = \begin{bmatrix} 0.273 & 0.484 \\ 0.198 & 1.74 \end{bmatrix} \times 10^{-9} \quad \mathrm{m^2\ s^{-1}}$$

predicts possibility of emulsification

Linear equilibration trajectory (dotted line): *no emulsification*

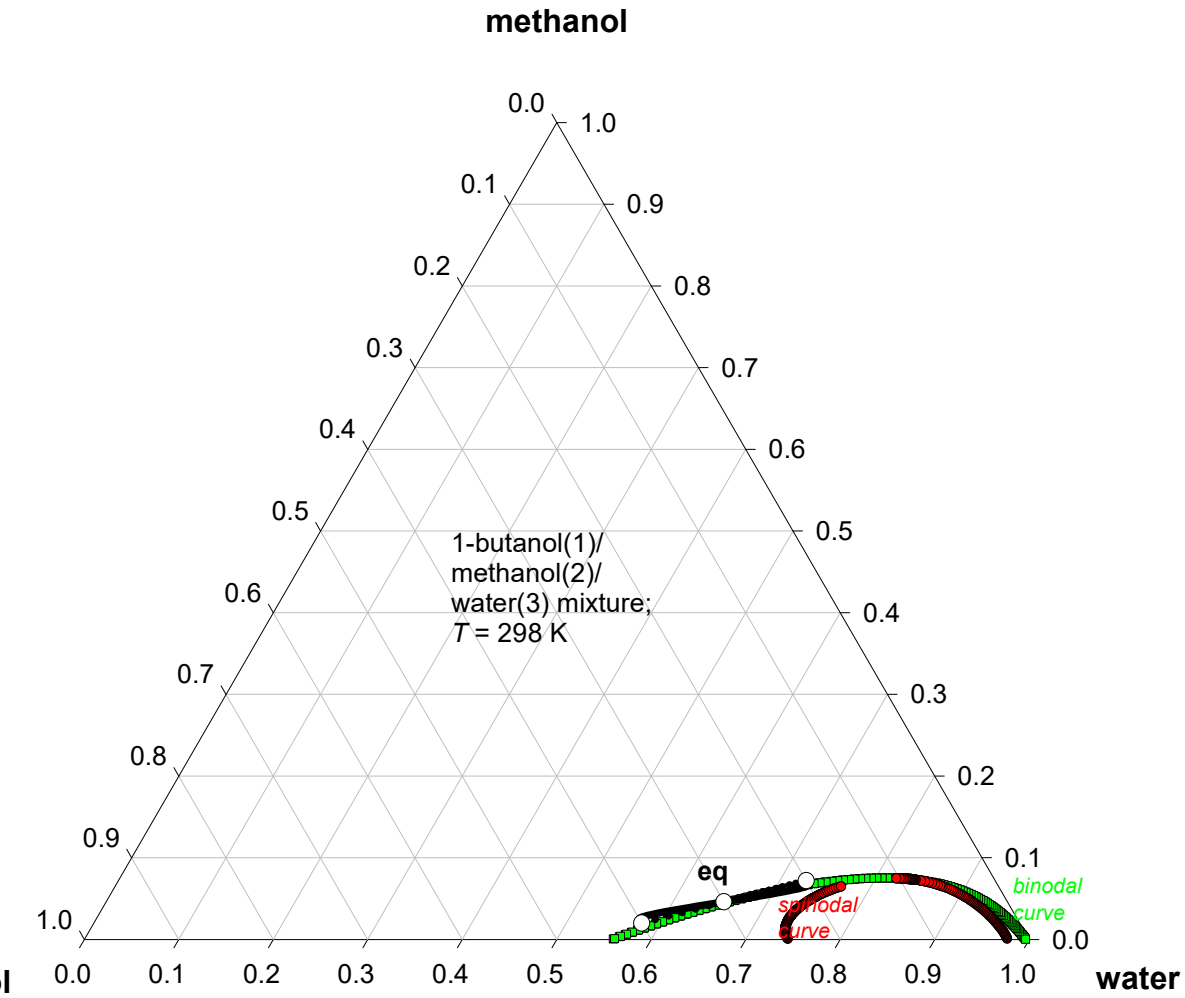

Water/Acetic Acid/Dichloromethane equilibration

Fig. S88

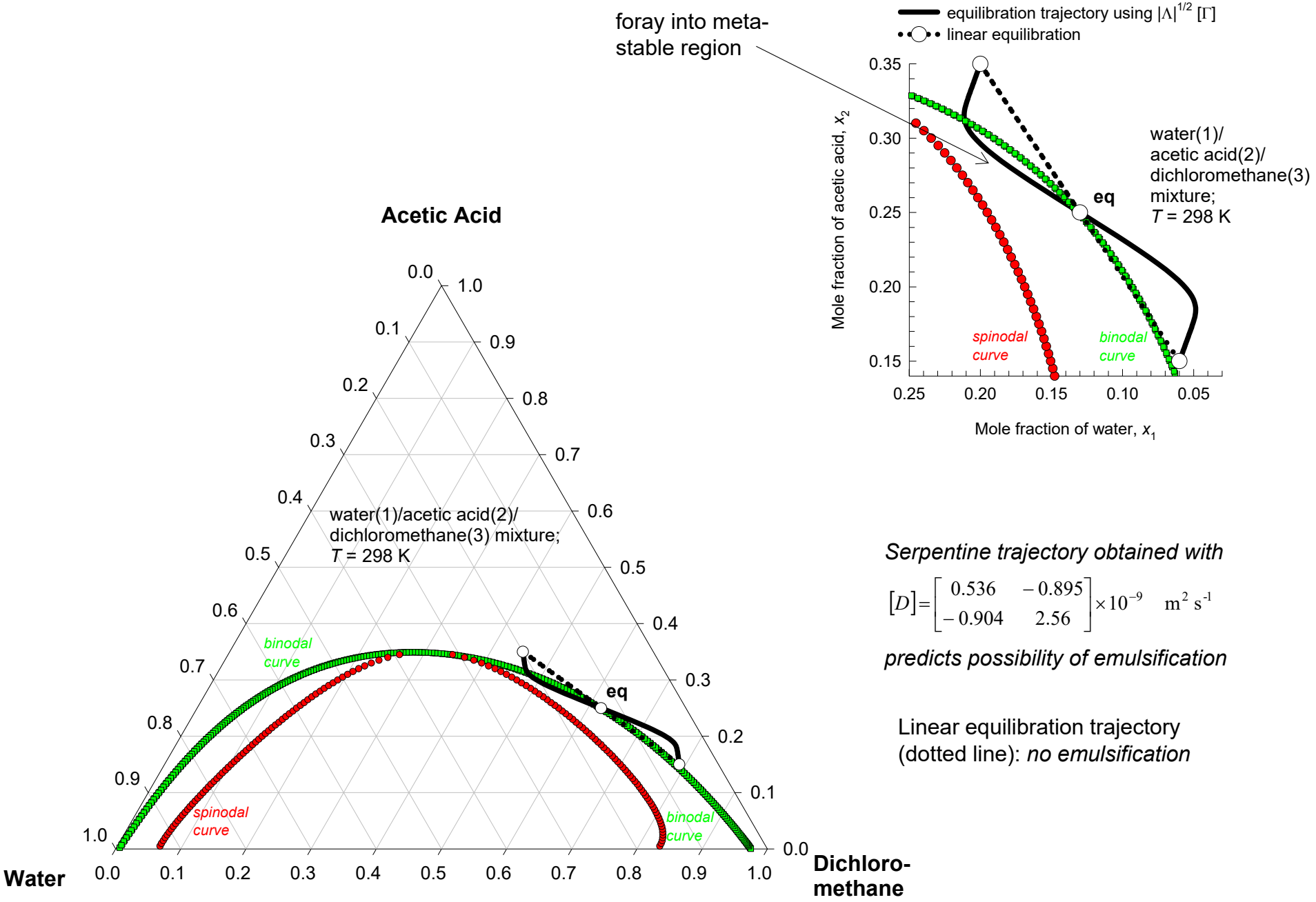

Serpentine trajectory obtained with

$$[D] = \begin{bmatrix} 0.536 & -0.895 \\ -0.904 & 2.56 \end{bmatrix} \times 10^{-9} \quad \mathrm{m^2\ s^{-1}}$$

predicts possibility of emulsification

Linear equilibration trajectory (dotted line): *no emulsification*

Water/Acetic Acid/1-hexanol equilibration

Fig. S89

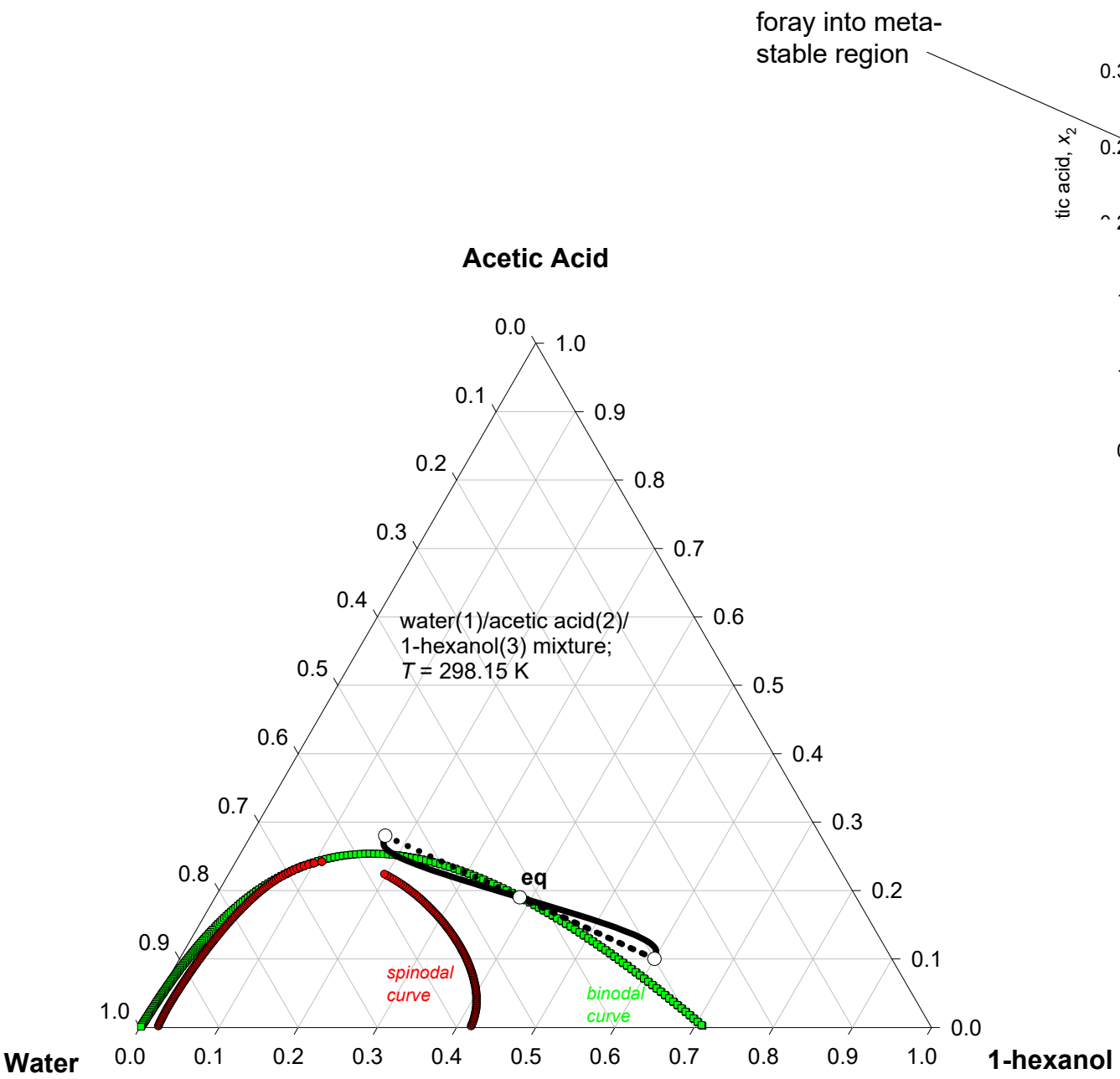

foray into meta-stable region

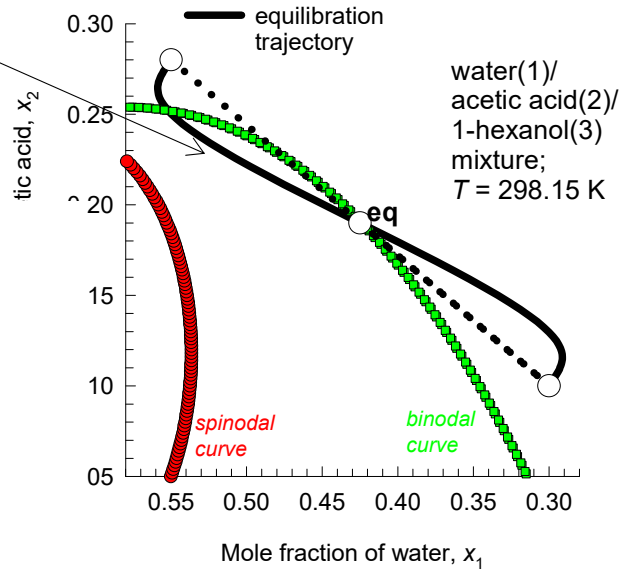

Serpentine trajectory obtained with

$$[D] = \begin{bmatrix} 0.4158 & -0.6816 \\ -0.1967 & 1.1194 \end{bmatrix} \times 10^{-9} \quad \mathrm{m^2\ s^{-1}}$$

predicts possibility of emulsification

Linear equilibration trajectory (dotted line): *no emulsification*

Toluene/Acetaldehyde/Water equilibration

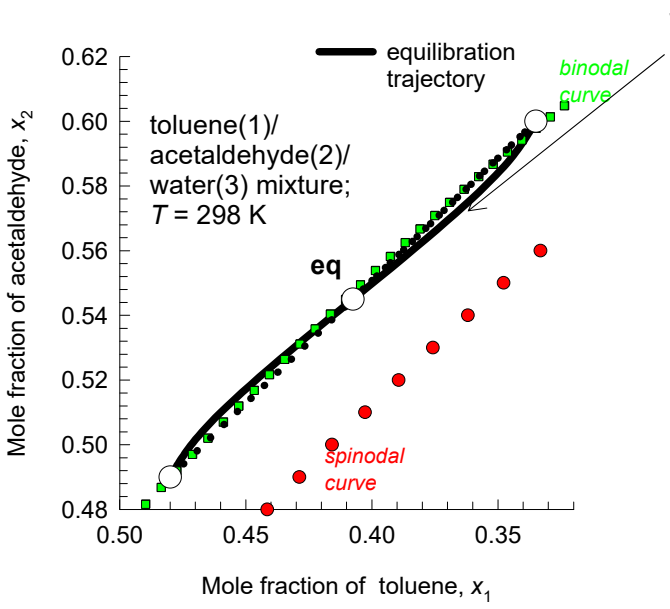

Serpentine trajectory obtained with

$$[D] = \begin{bmatrix} -0.236 & -1.095 \\ 0.674 & 1.72 \end{bmatrix} \times 10^{-9} \quad \mathrm{m^2\ s^{-1}}$$

predicts possibility of emulsification

Linear equilibration trajectory (dotted line): *no emulsification*

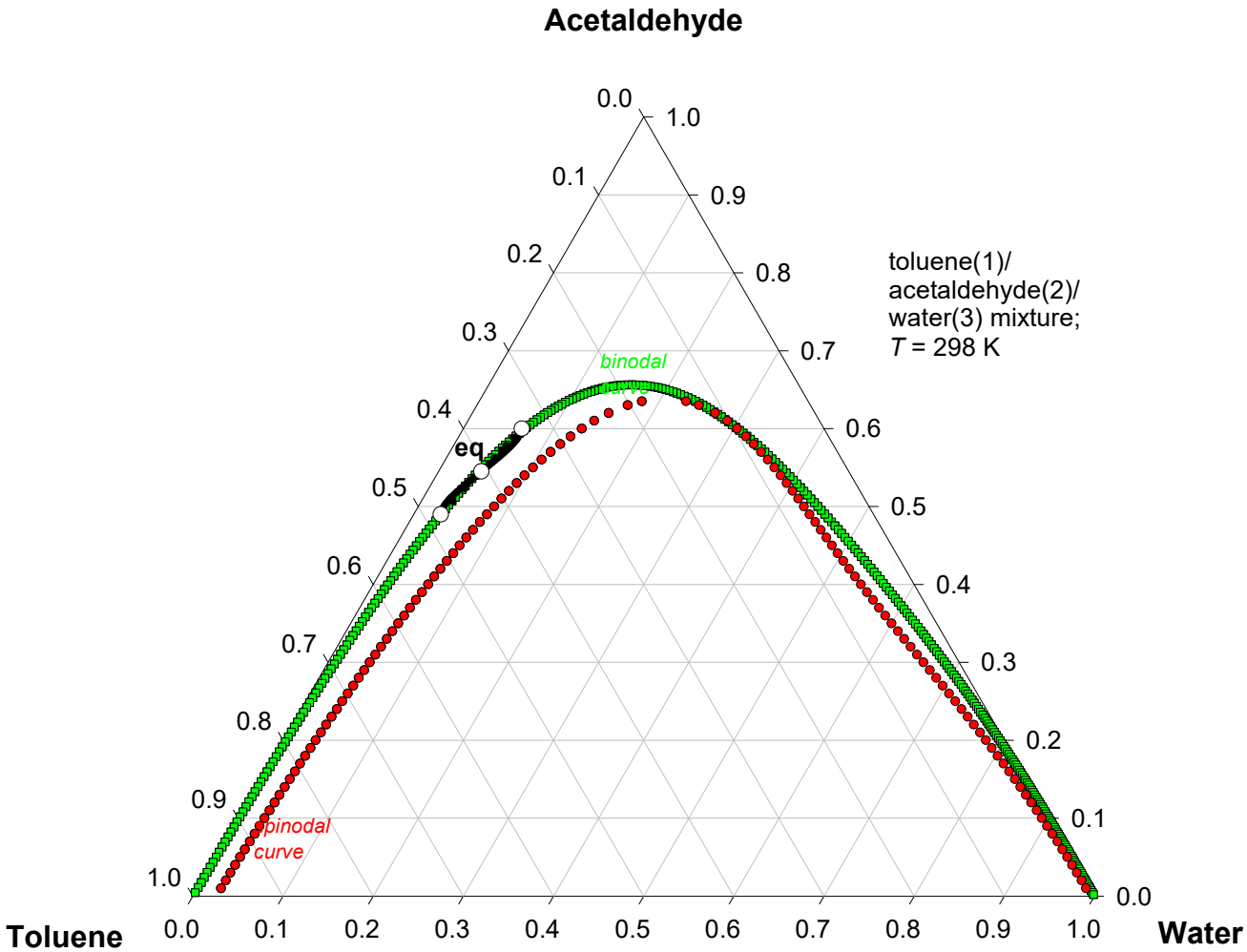

1-hexanol/nitromethane/water equilibration

Fig. S91

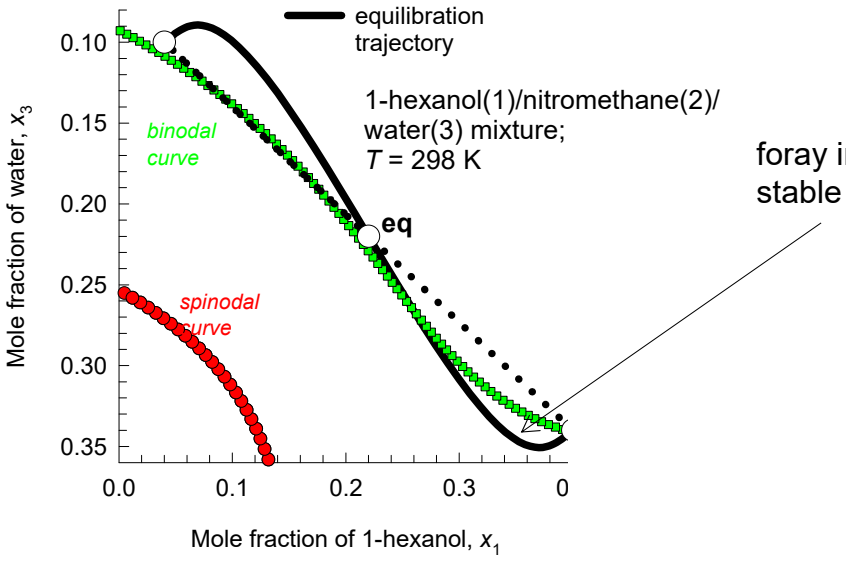

Serpentine trajectory obtained with

$$[D] = \begin{bmatrix} 0.854 & 0.1733 \\ -0.2546 & 0.1526 \end{bmatrix} \times 10^{-9} \quad \mathrm{m^2\ s^{-1}}$$

predicts possibility of emulsification

Linear equilibration trajectory (dotted line): *no emulsification*

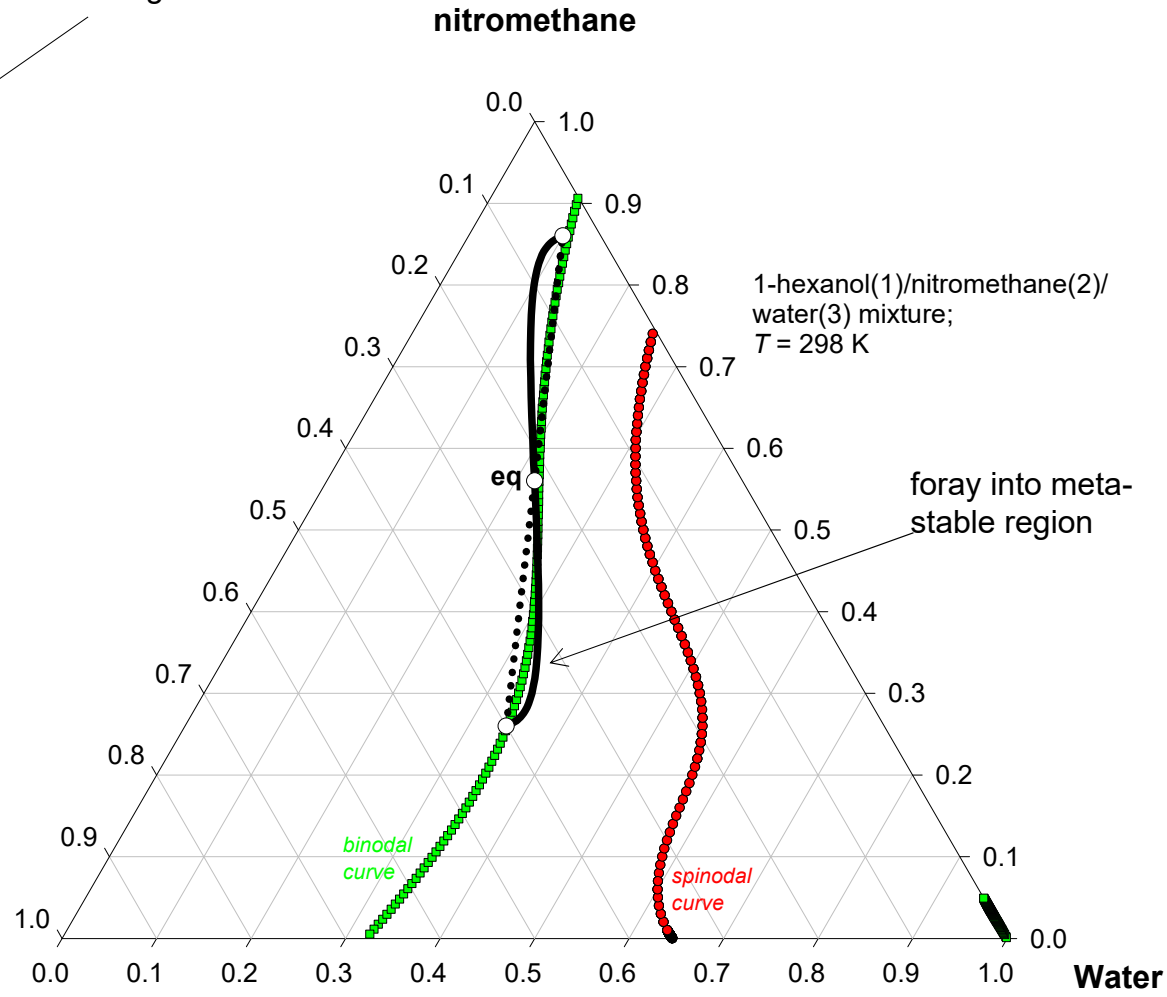

4M2P/acetonitrile/water equilibration

Fig. S92

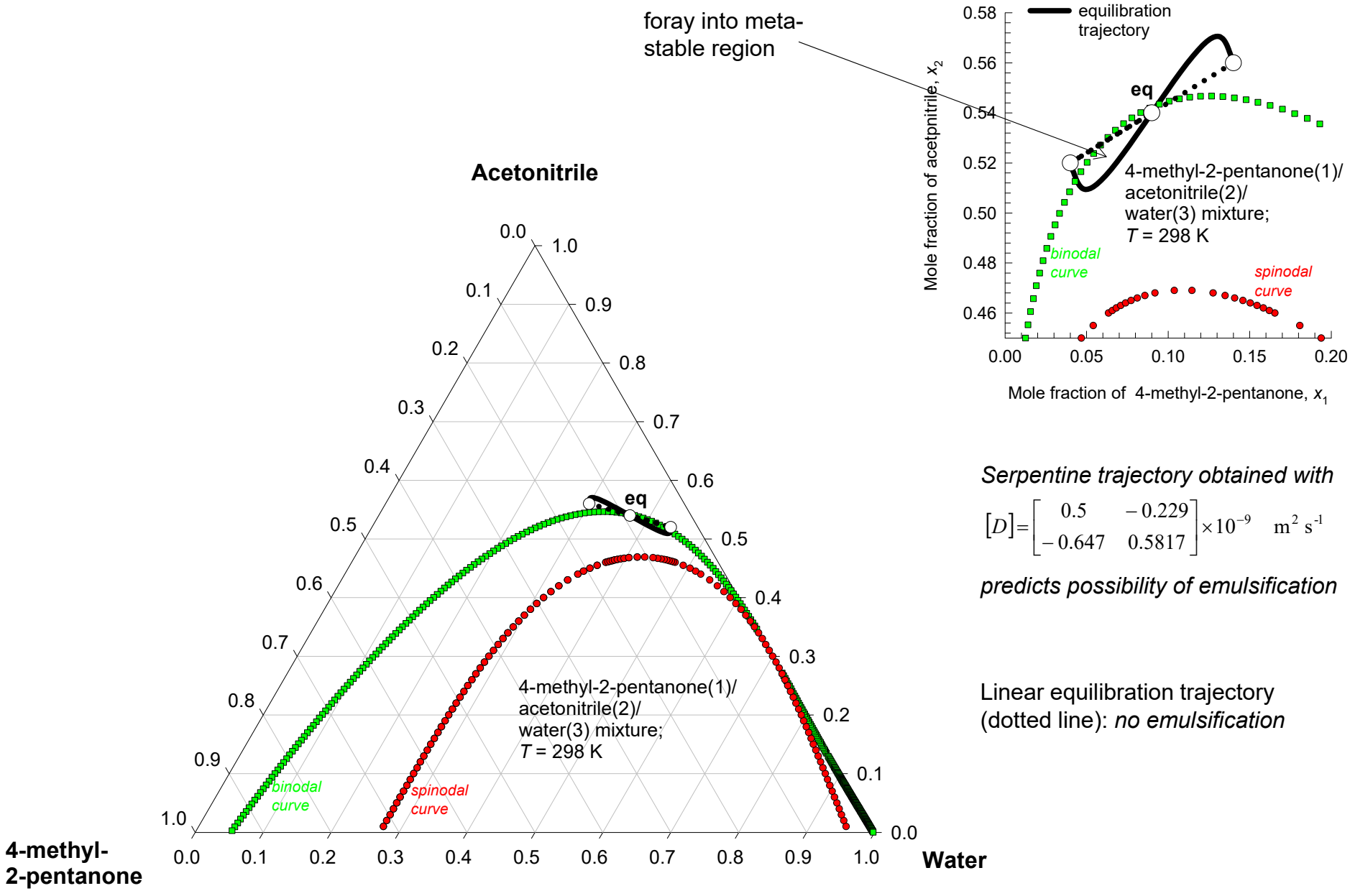

Serpentine trajectory obtained with

$$[D] = \begin{bmatrix} 0.5 & -0.229 \\ -0.647 & 0.5817 \end{bmatrix} \times 10^{-9} \quad \mathrm{m^2\ s^{-1}}$$

predicts possibility of emulsification

Linear equilibration trajectory (dotted line): *no emulsification*

Acetonitrile/1-propanol/hexane equilibration

Fig. S93

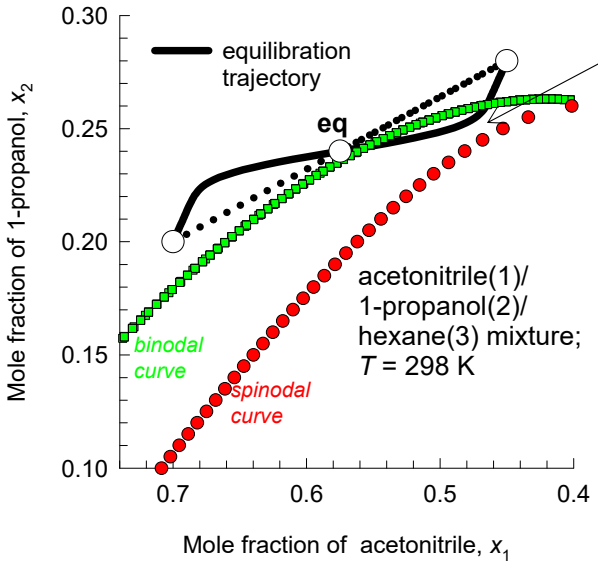

foray into meta-stable region

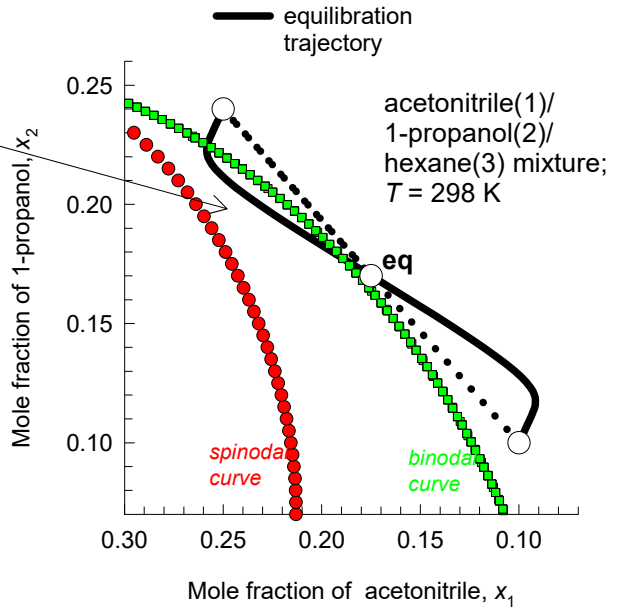

Serpentine trajectory obtained with

$$[D]=\begin{bmatrix}0.133 & -1.79\\ 0.017 & 2.53\end{bmatrix}\times 10^{-9}\quad \mathrm{m^2\ s^{-1}}$$

predicts possibility of emulsification

Linear equilibration trajectory(dotted line): *no emulsification*

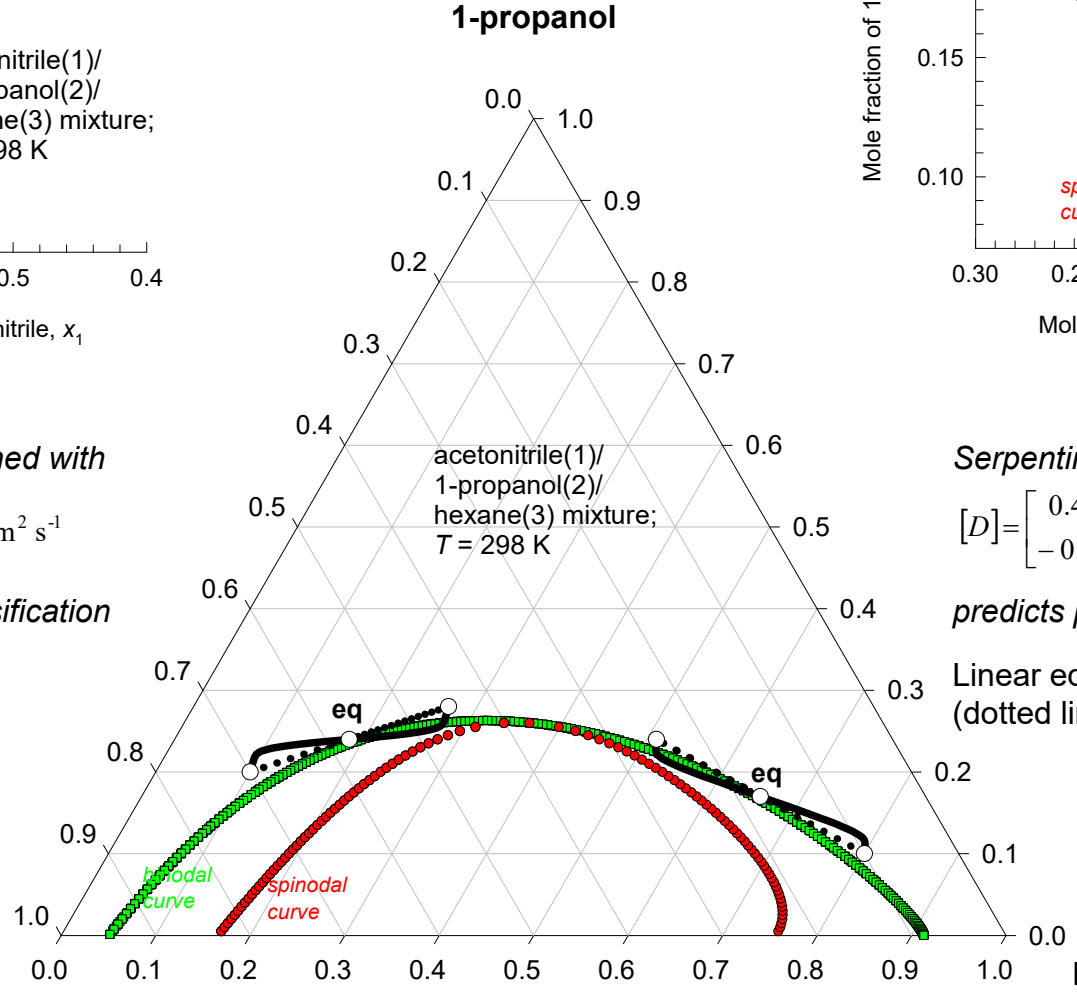

Serpentine trajectory obtained with

$$[D]=\begin{bmatrix}0.452 & -0.819\\ -0.565 & 1.6\end{bmatrix}\times 10^{-9}\quad \mathrm{m^2\ s^{-1}}$$

predicts possibility of emulsification

Linear equilibration trajectory (dotted line): *no emulsification*

Water/Caprolactam/Toluene equilibration

Fig. S94

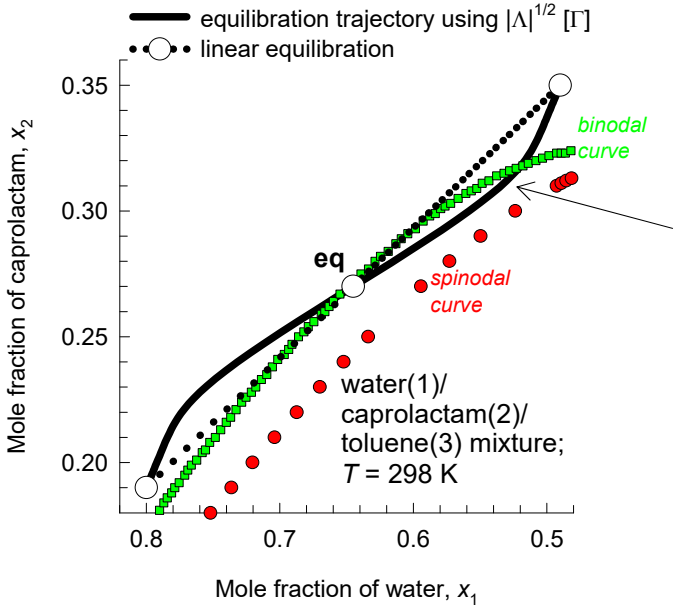

foray into meta-stable region

Serpentine trajectory obtained with

$$[D]=\begin{bmatrix} -0.187 & -1.524 \\ 0.44 & 2.12 \end{bmatrix}\times 10^{-9} \quad \mathrm{m^2\ s^{-1}}$$

predicts possibility of emulsification

Linear equilibration trajectory (dotted line): *no emulsification*

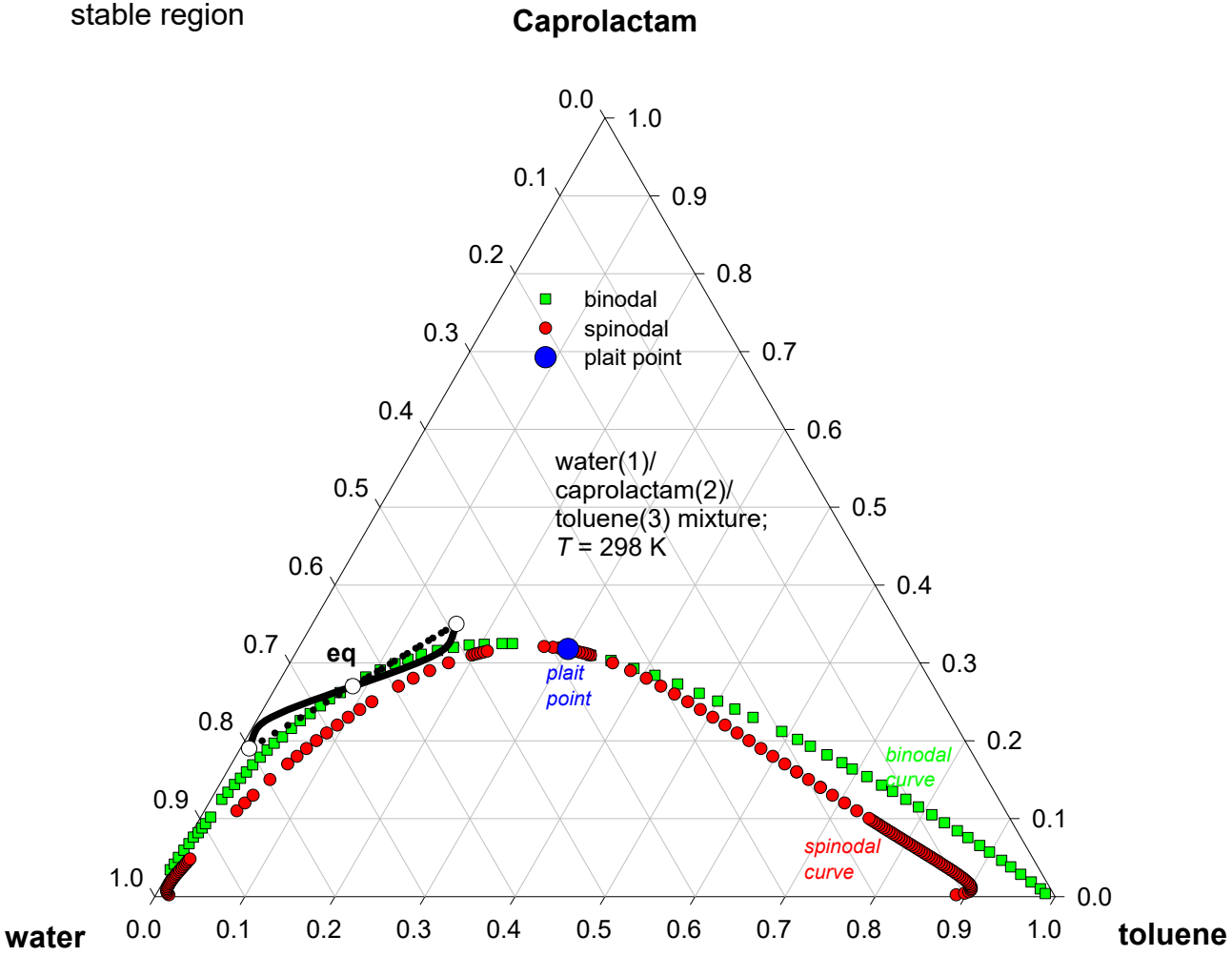

Water/Caprolactam/Benzene equilibration

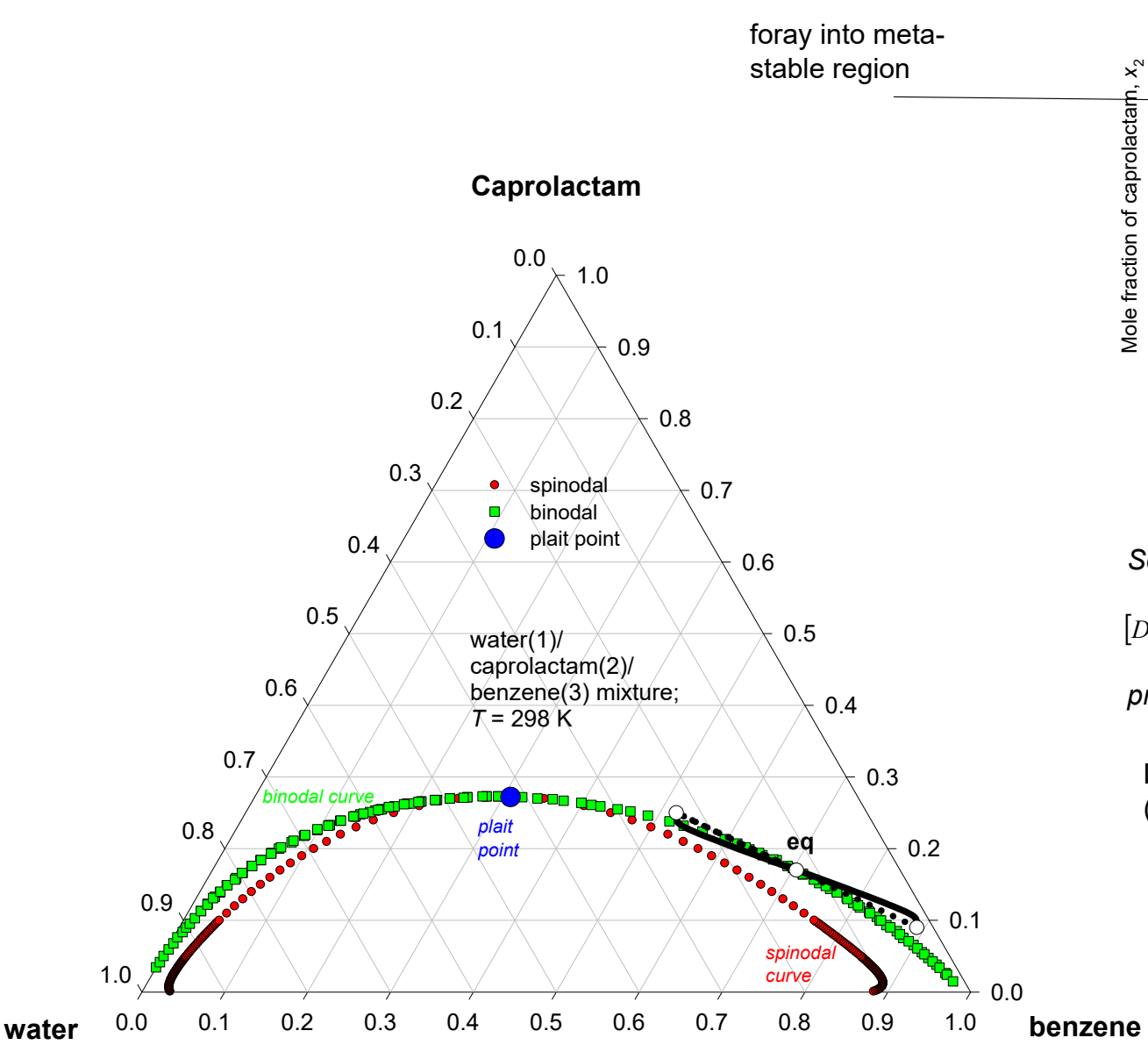

foray into meta-stable region

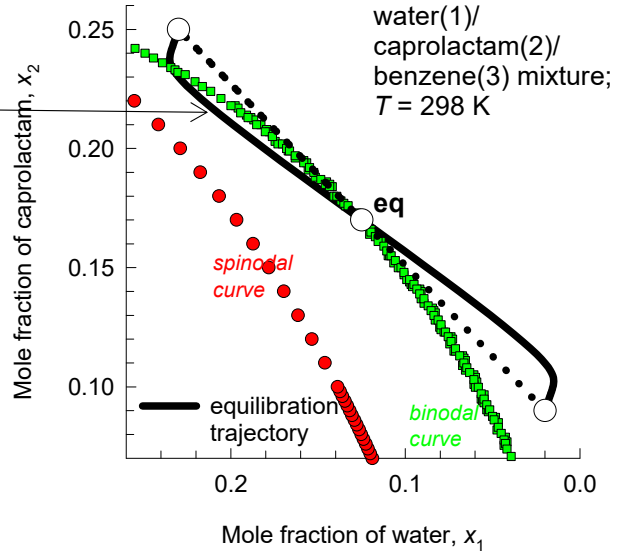

Serpentine trajectory obtained with

$$[D] = \begin{bmatrix} 0.598 & -0.911 \\ -0.882 & 2.11 \end{bmatrix} \times 10^{-9} \quad \mathrm{m^2\ s^{-1}}$$

predicts possibility of emulsification

Linear equilibration trajectory (dotted line): *no emulsification*

Toluene//Propionic acid/Water equilibration

Fig. S96

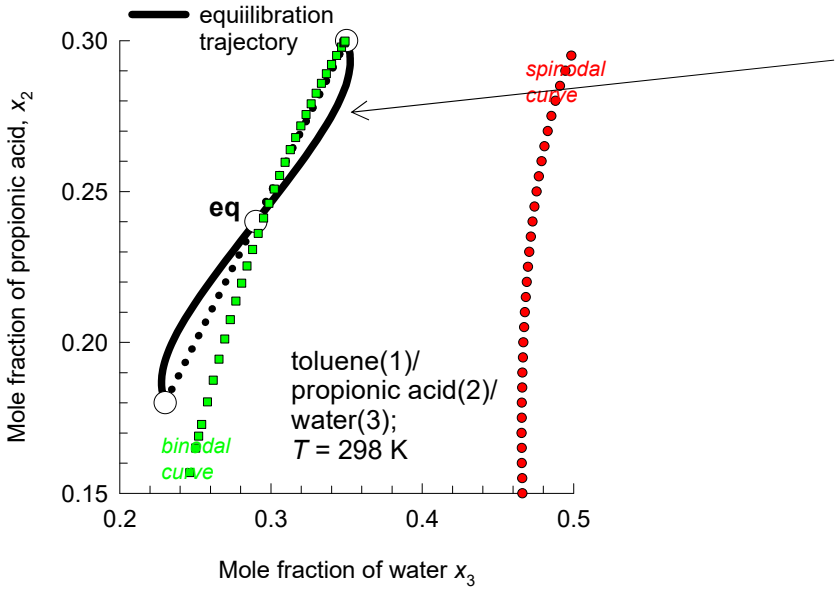

Serpentine trajectory obtained with

$$[D]=\begin{bmatrix} 0.318 & -0.3 \\ 0.178 & 1.196 \end{bmatrix}\times 10^{-9} \quad \mathrm{m^2\ s^{-1}}$$

predicts possibility of emulsification

Linear equilibration trajectory (dotted line): *no emulsification*

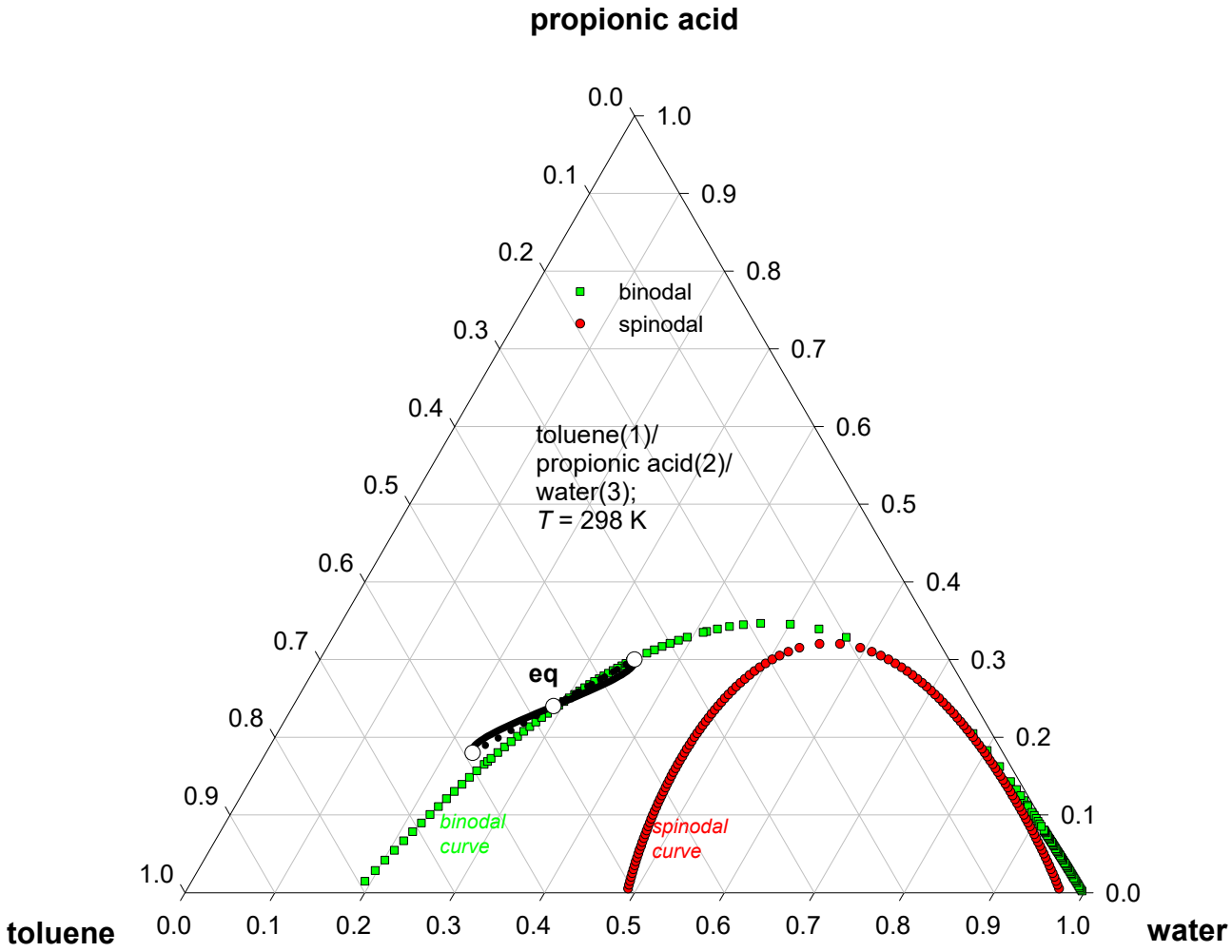

Ethylacetate/Propionic acid/Water equilibration

Fig. S97

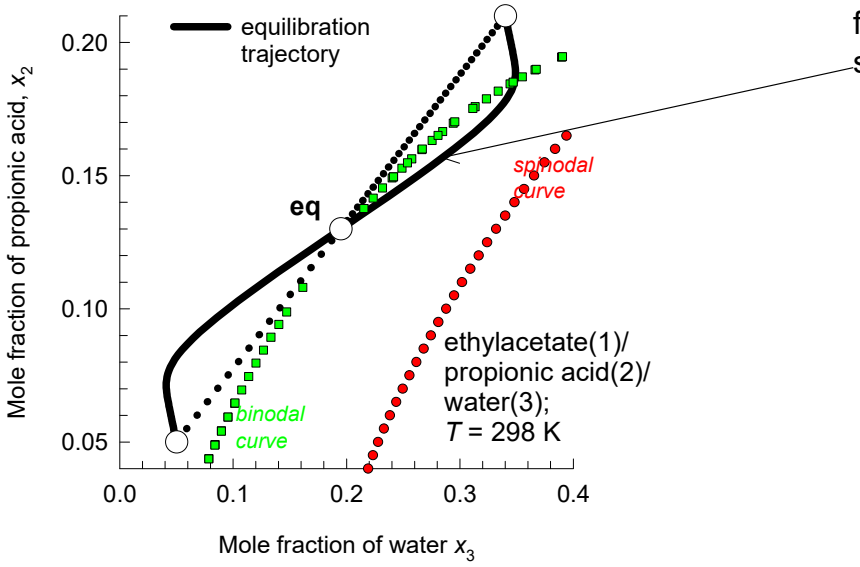

Serpentine trajectory obtained with

$$[D] = \begin{bmatrix} -0.0358 & -1.7447 \\ 0.5700 & 3.6379 \end{bmatrix} \times 10^{-9} \quad \mathrm{m^2\ s^{-1}}$$

predicts possibility of emulsification

Linear equilibration trajectory (dotted line): *no emulsification*

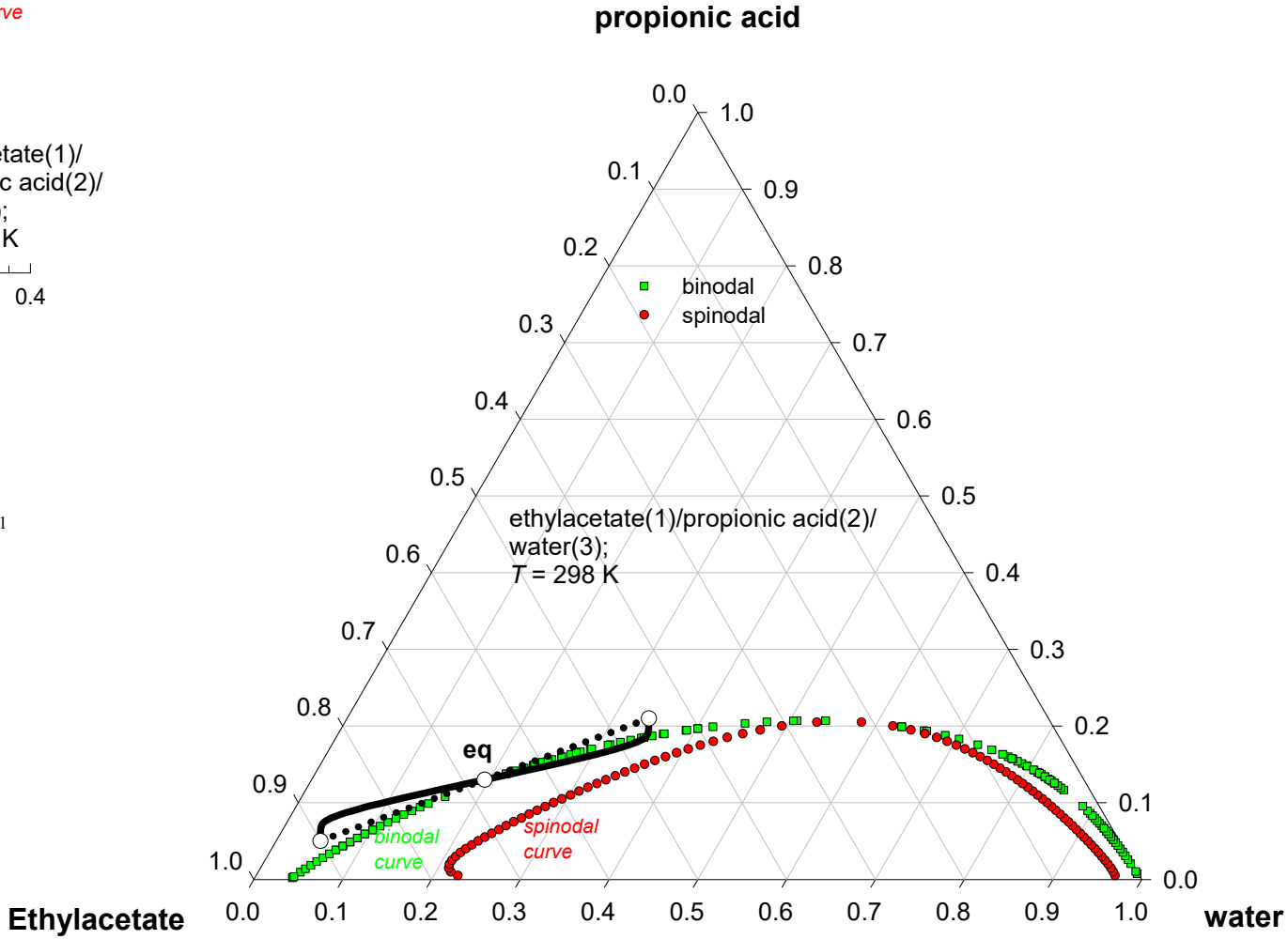

Fig. S98

Water/acetic acid/isophorone equilibration

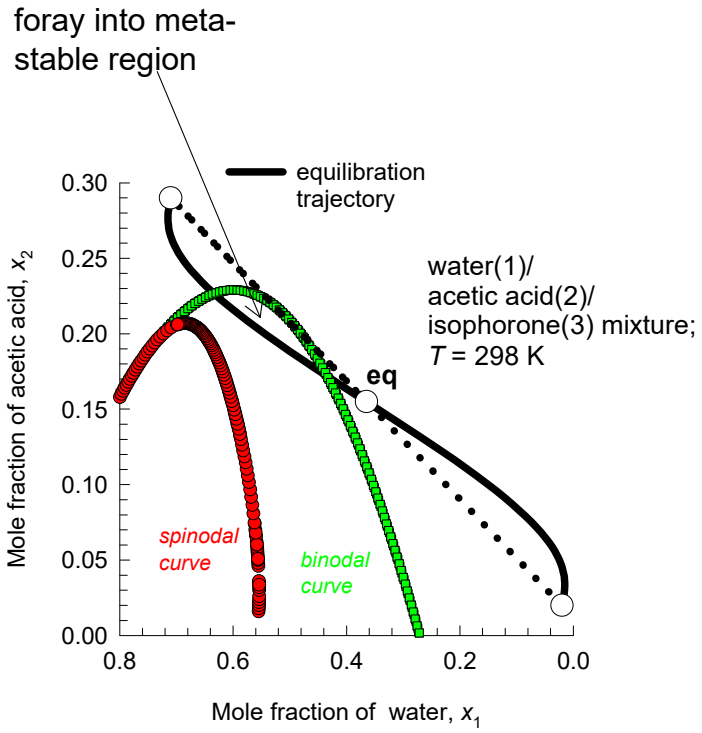

Serpentine trajectory obtained with

$$[D] = \begin{bmatrix} 0.5558 & -0.6106 \\ -0.0923 & 1.591 \end{bmatrix} \times 10^{-9} \quad \mathrm{m^2\ s^{-1}}$$

predicts possibility of emulsification

Linear equilibration trajectory
(dotted line): *no emulsification*

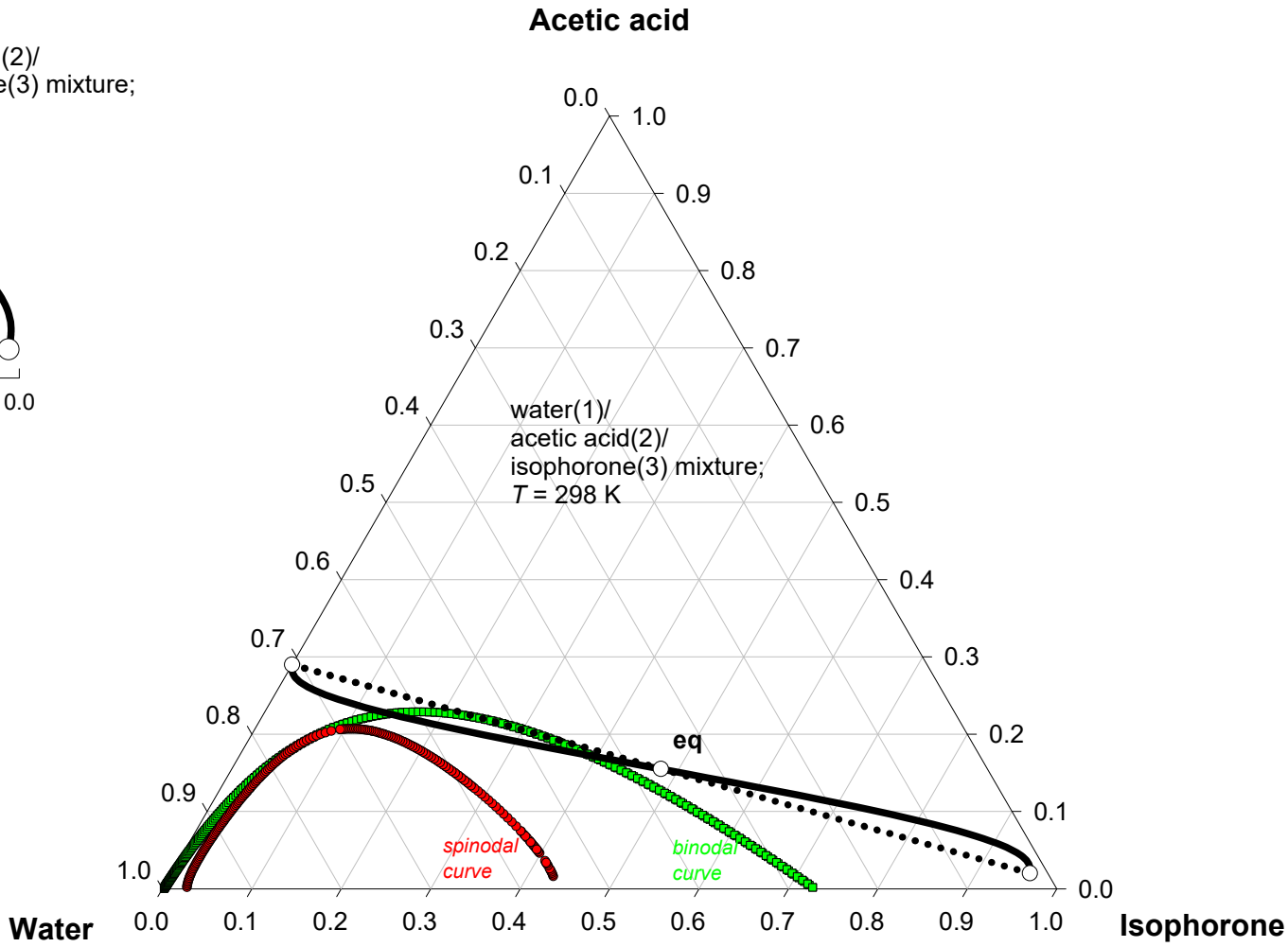

Fig. S99

Water/acetic acid/ethyl acetate equilibration

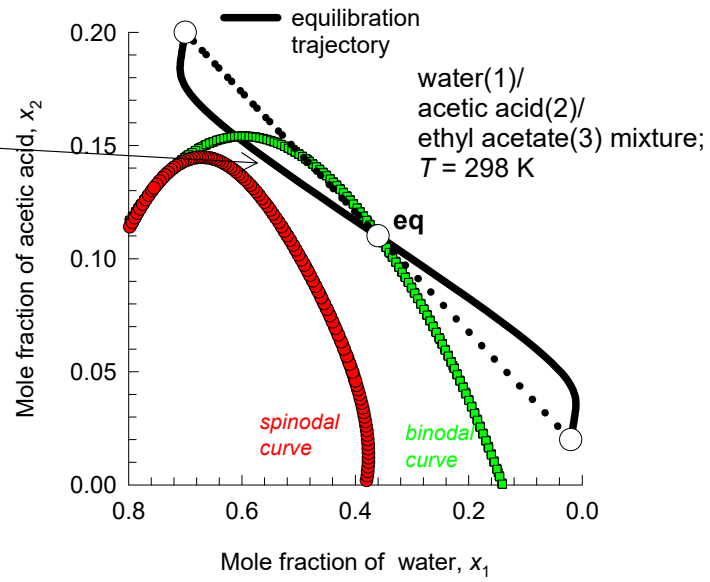

foray into meta-stable region

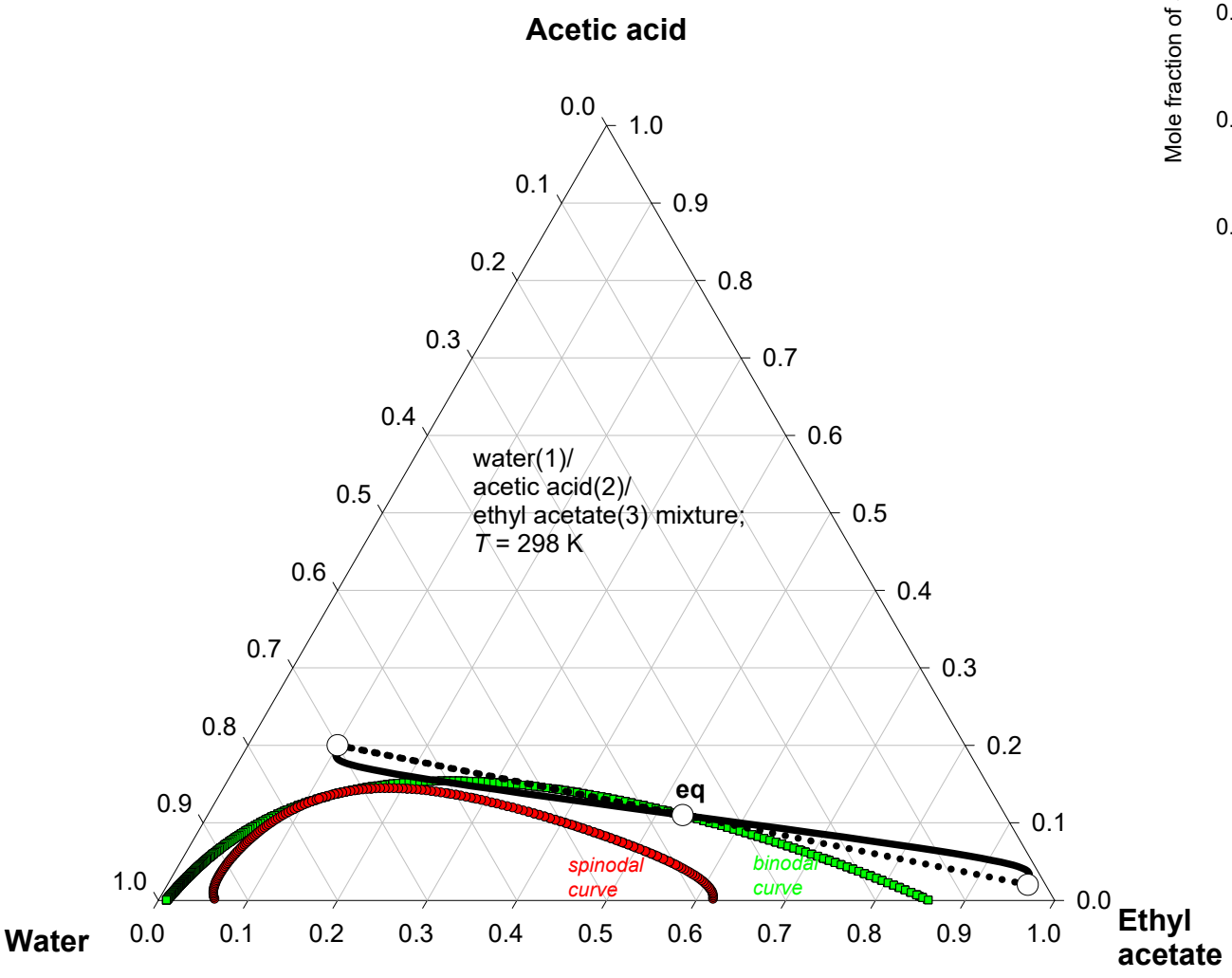

Serpentine trajectory obtained with

$$[D] = \begin{bmatrix} 0.3748 & -1.23 \\ -0.2363 & 2.041 \end{bmatrix} \times 10^{-9} \quad \mathrm{m^2\ s^{-1}}$$

predicts possibility of emulsification

Linear equilibration trajectory (dotted line): *no emulsification*

Water/acetic acid/MTBE equilibration

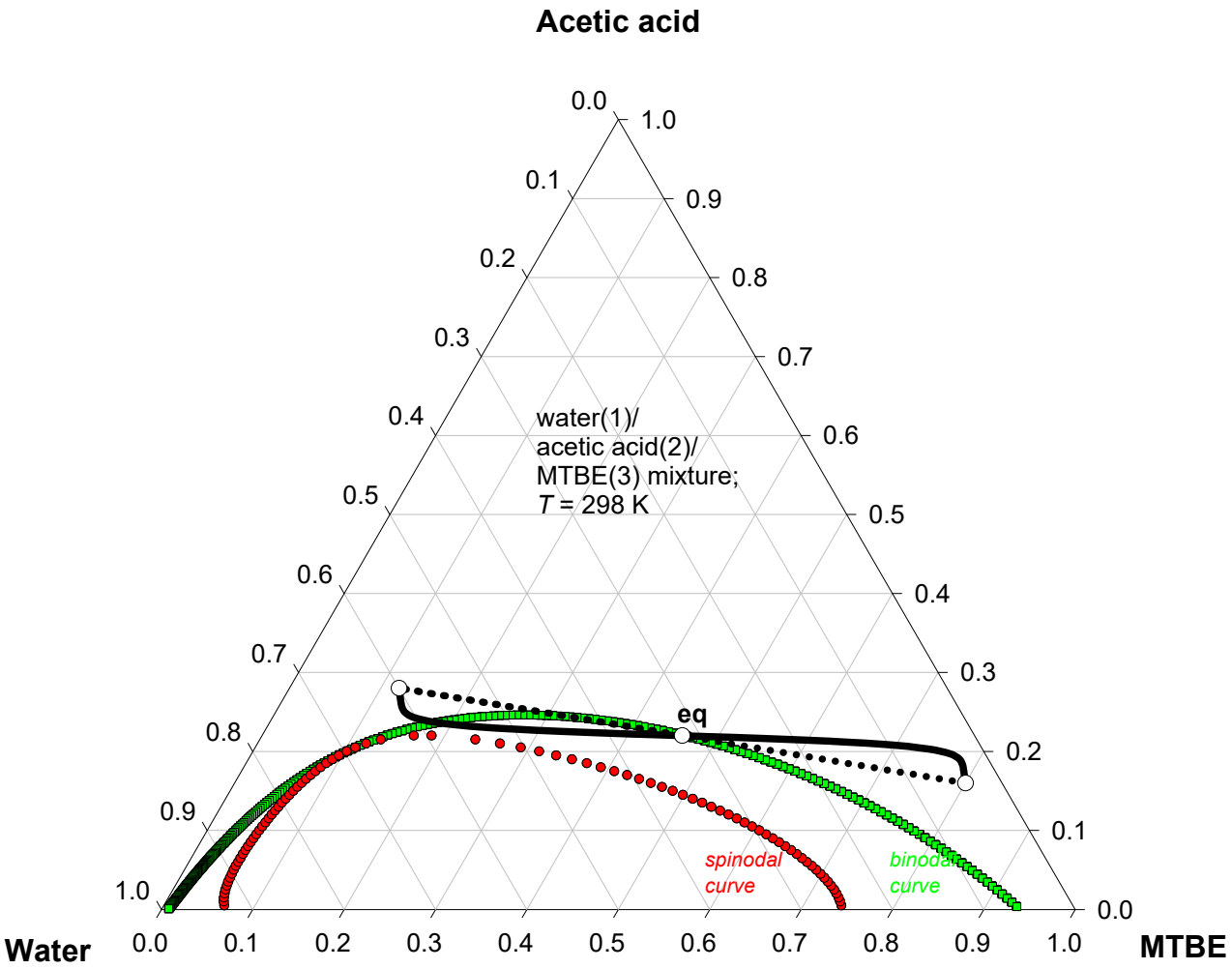

foray into meta-stable region

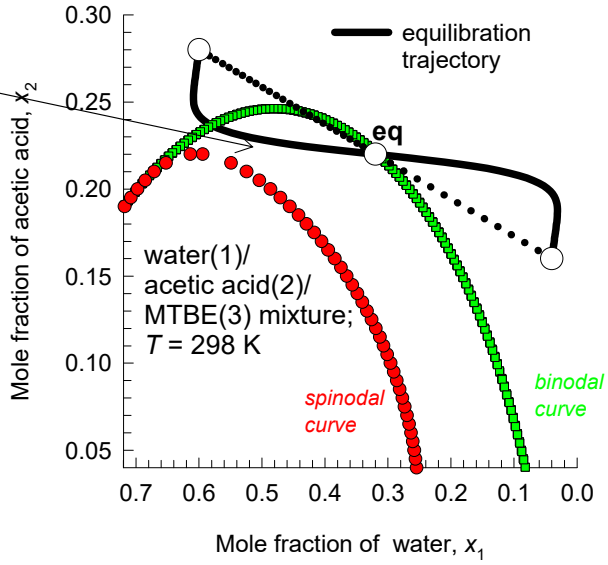

Serpentine trajectory obtained with

$$[D] = \begin{bmatrix} 0.1986 & -0.8834 \\ 0.0689 & 2.565 \end{bmatrix} \times 10^{-9} \quad \mathrm{m^2\ s^{-1}}$$

predicts possibility of emulsification

Linear equilibration trajectory (dotted line): *no emulsification*

Ethanol/Toluene/n-decane equilibration

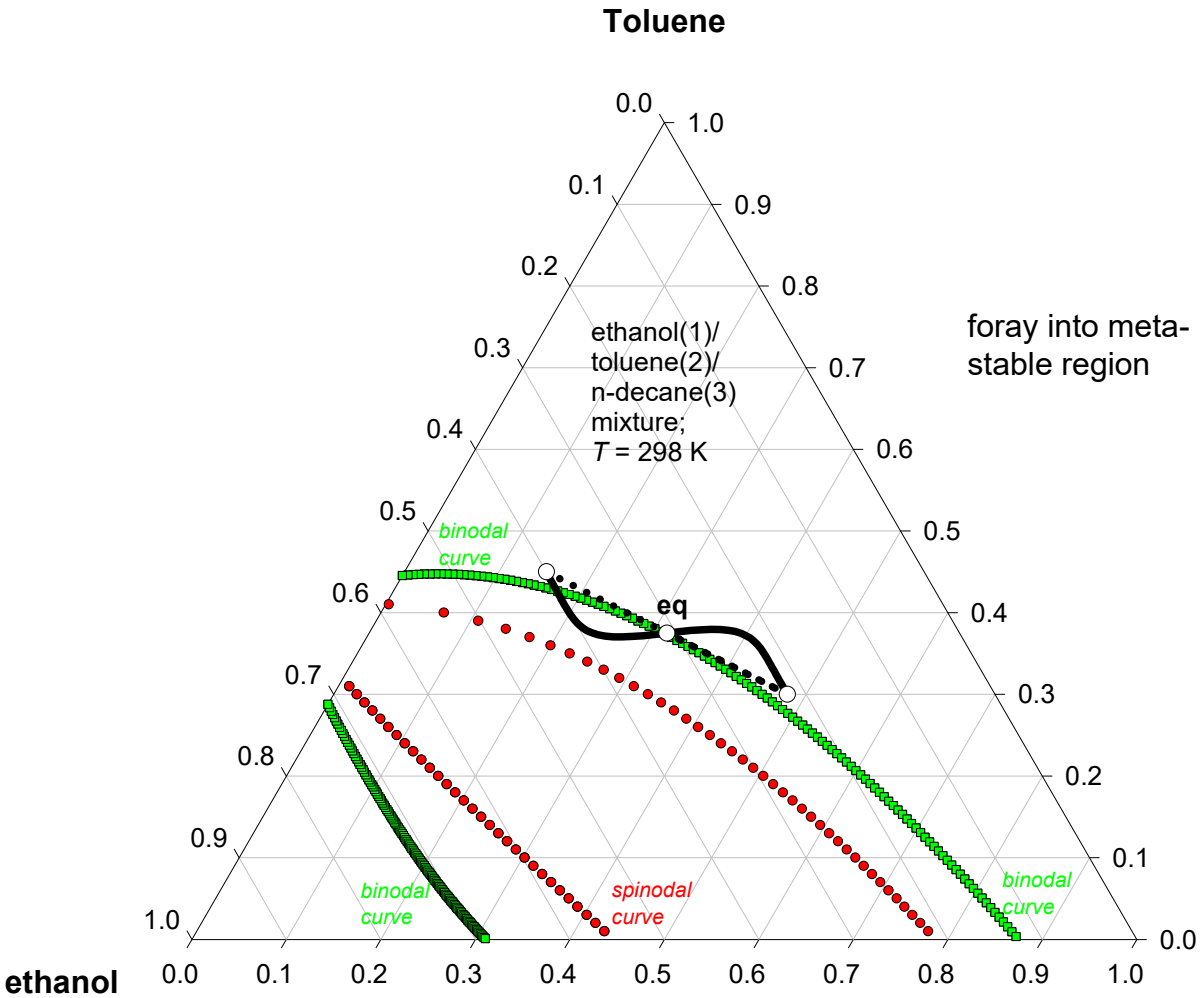

foray into meta-stable region

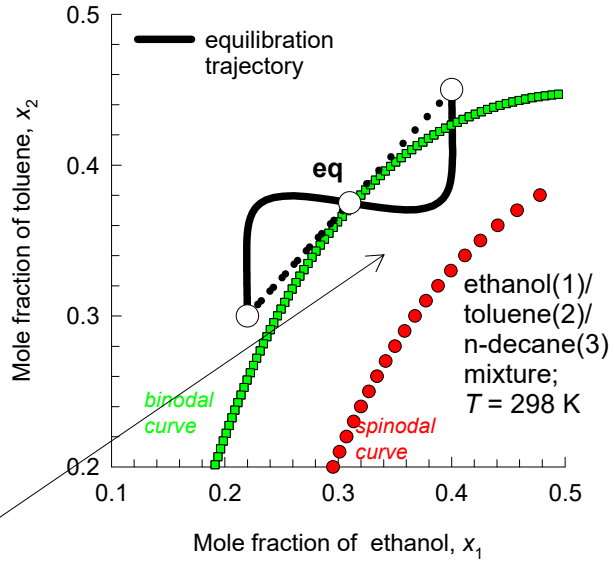

Serpentine trajectory obtained with

$$[D] = \begin{bmatrix} 0.083 & -0.0209 \\ 0.5102 & 1.065 \end{bmatrix} \times 10^{-9} \quad \mathrm{m^2\ s^{-1}}$$

predicts possibility of emulsification

Linear equilibration trajectory (dotted line): *no emulsification*

Water/ethanol/benzene equilibration

Fig. S102

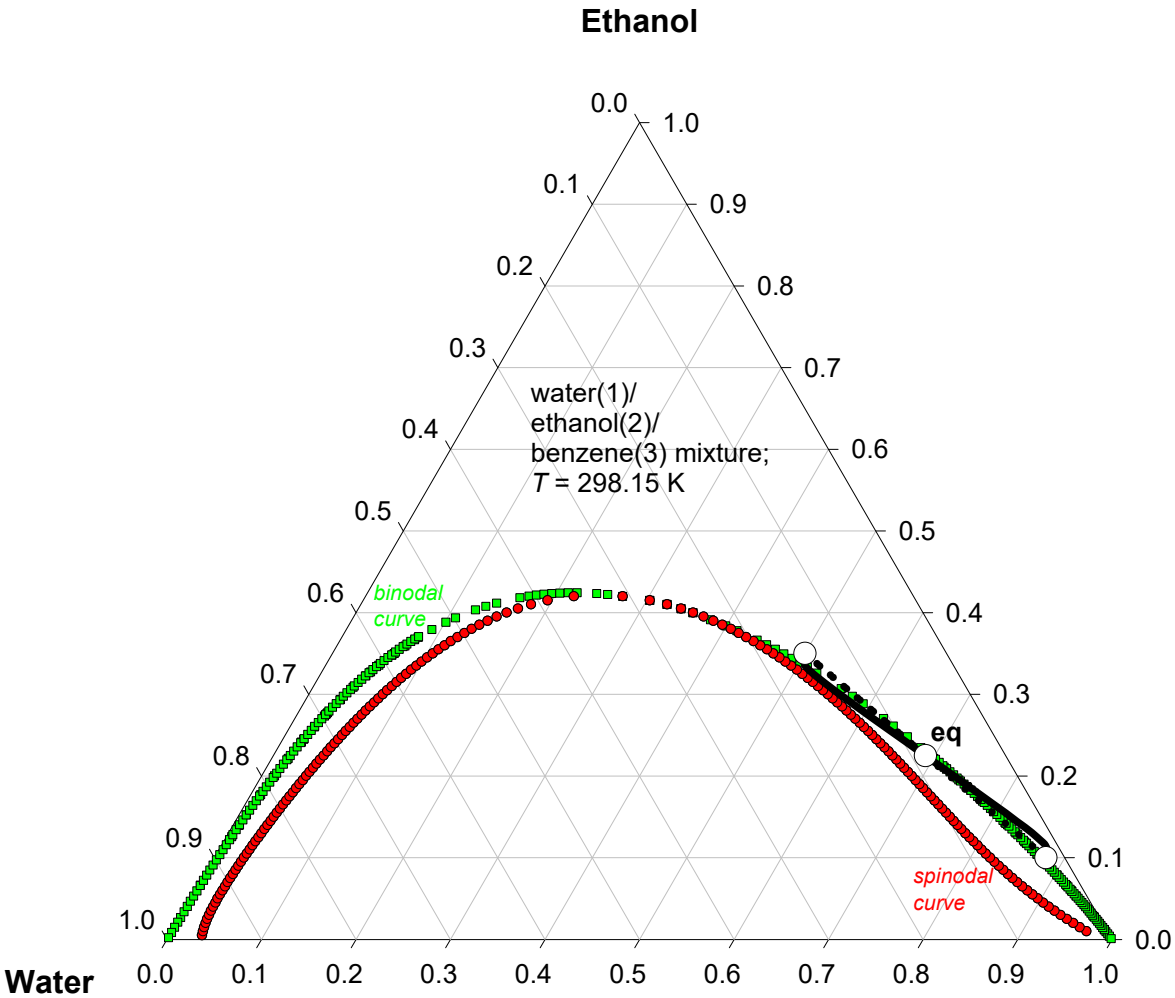

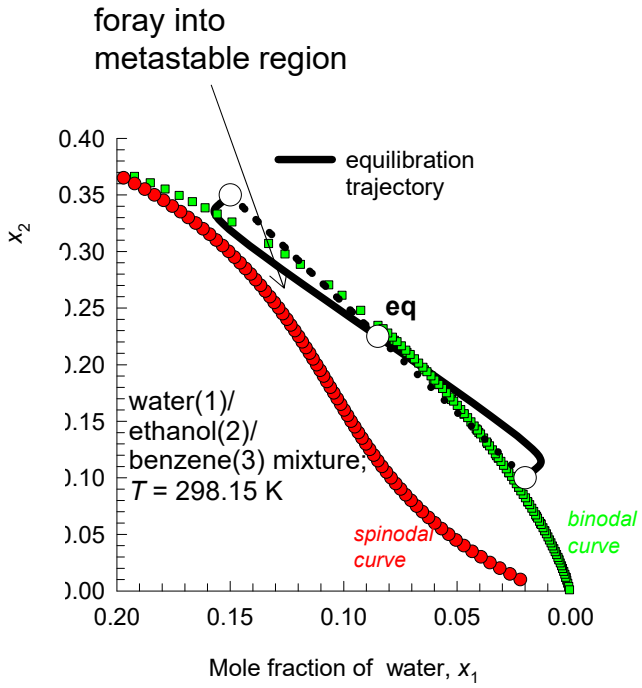

Serpentine trajectory obtained with

$$[D] = \begin{bmatrix} 0.6809 & -0.4738 \\ -1.01 & 0.8943 \end{bmatrix} \times 10^{-9} \quad \mathrm{m^2\ s^{-1}}$$

predicts possibility of emulsification

Linear equilibration trajectory (dotted line): *no emulsification*

NMP/propylbenzene/dodecane equilibration

Fig. S103

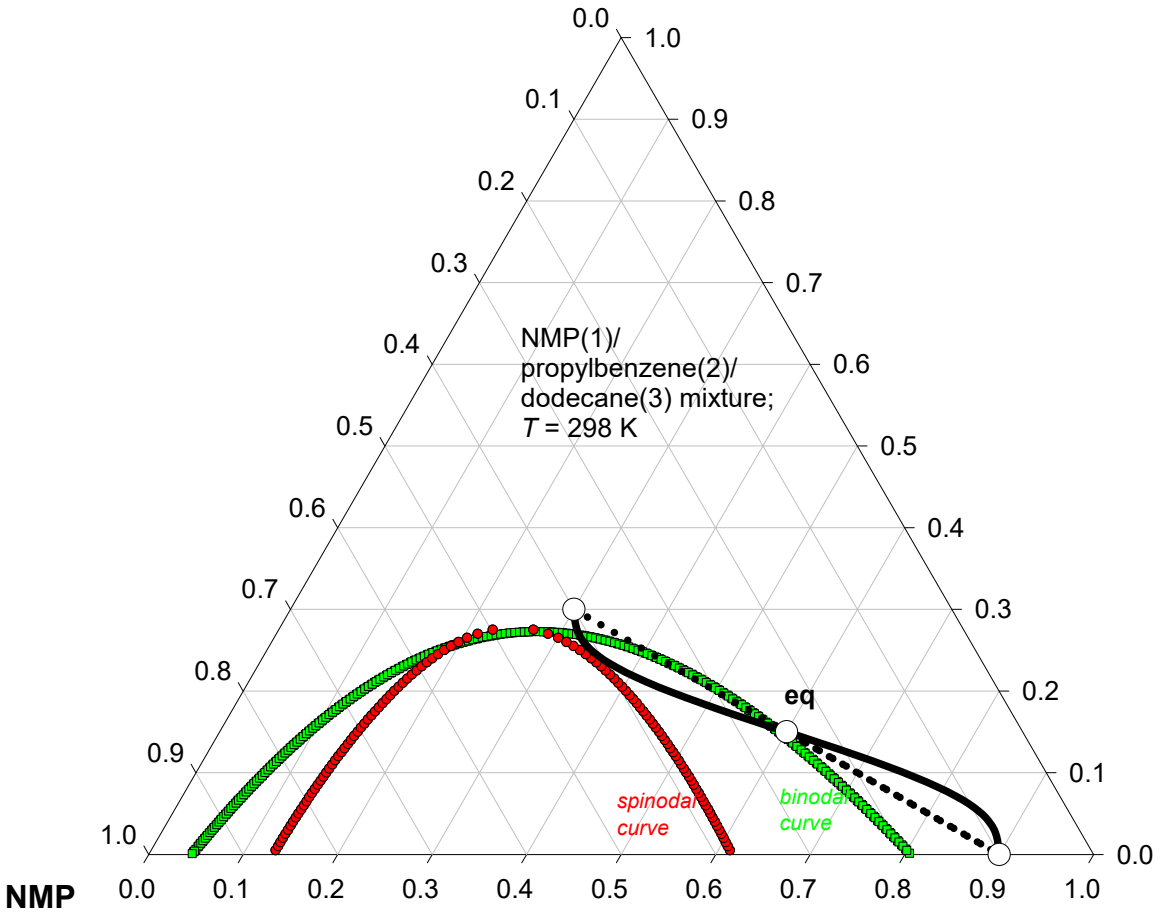

foray into metastable region

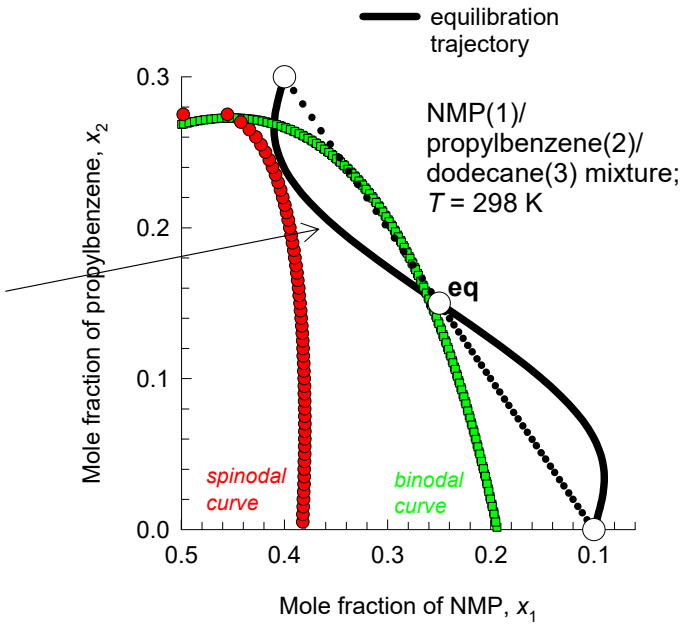

Serpentine trajectory obtained with

$$[D] = \begin{bmatrix} 0.3081 & -0.3568 \\ -0.0821 & 1.1072 \end{bmatrix} \times 10^{-9} \quad \mathrm{m^2\ s^{-1}}$$

predicts possibility of emulsification

Linear equilibration trajectory (dotted line): *no emulsification*

NMP/propylbenzene/tetradecane equilibration

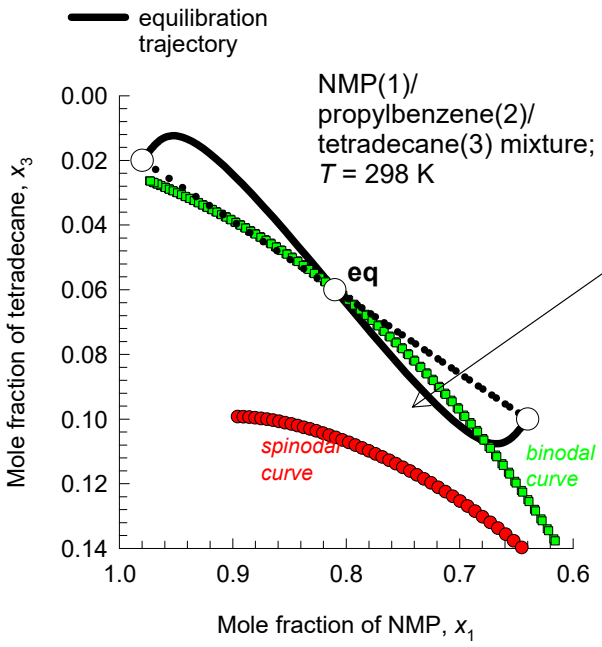

foray into metastable region

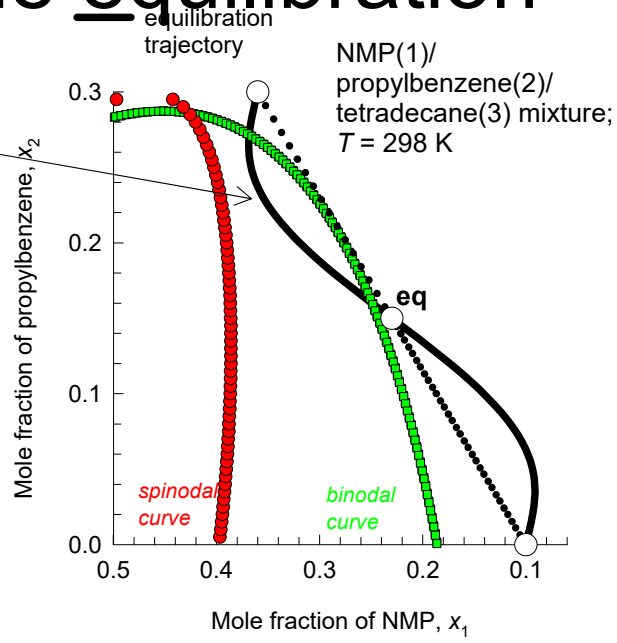

Serpentine trajectory obtained with

$$[D] = \begin{bmatrix} -0.0524 & -1.038 \\ 0.5064 & 1.803 \end{bmatrix} \times 10^{-9} \quad \mathrm{m^2\ s^{-1}}$$

predicts possibility of emulsification

Linear equilibration trajectory (dotted line): *no emulsification*

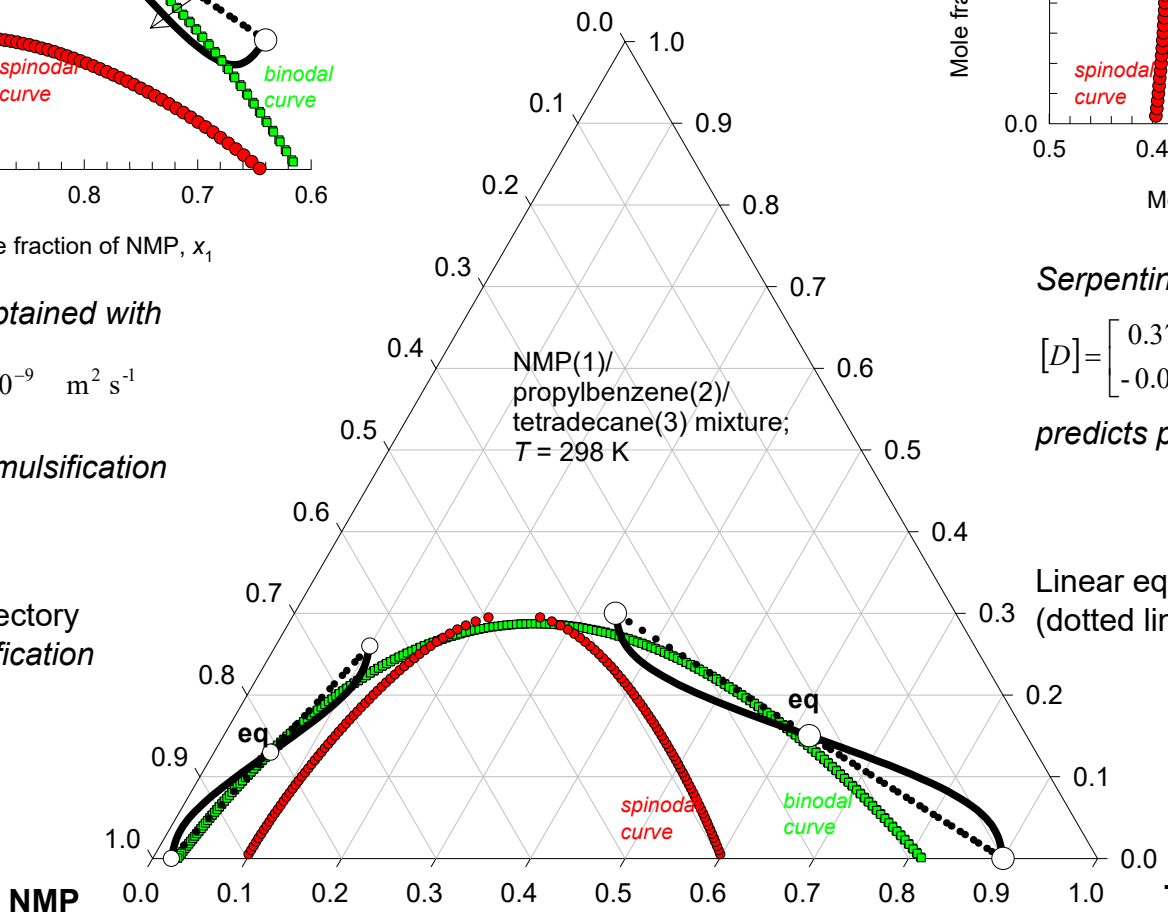

Serpentine trajectory obtained with

$$[D] = \begin{bmatrix} 0.3773 & -0.3802 \\ -0.0713 & 1.416 \end{bmatrix} \times 10^{-9} \quad \mathrm{m^2\ s^{-1}}$$

predicts possibility of emulsification

Linear equilibration trajectory (dotted line): *no emulsification*

Heptane/toluene/sulpholane equilibration

Fig. S105

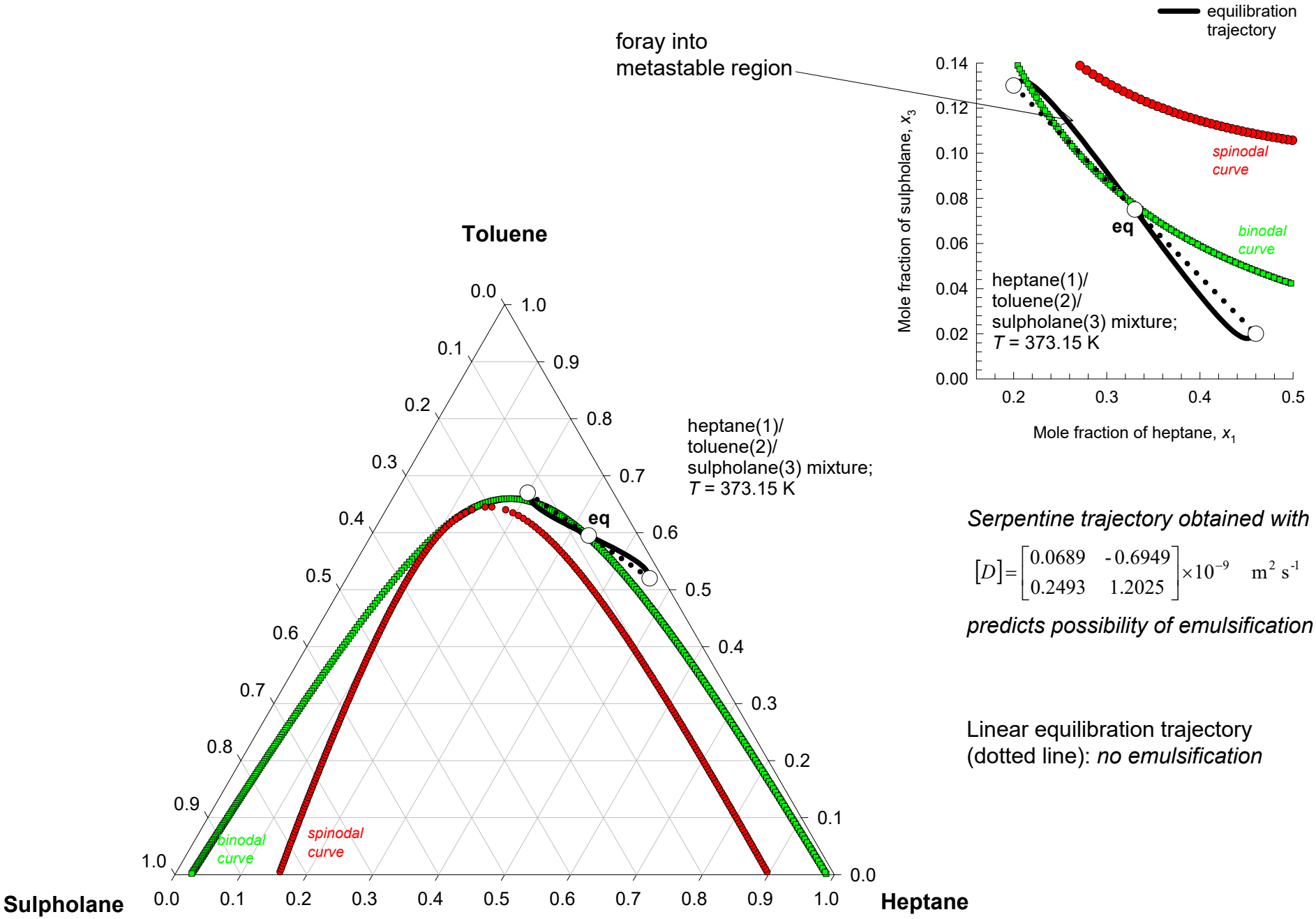

Serpentine trajectory obtained with

$$[D] = \begin{bmatrix} 0.0689 & -0.6949 \\ 0.2493 & 1.2025 \end{bmatrix} \times 10^{-9} \quad \mathrm{m^2\ s^{-1}}$$

predicts possibility of emulsification

Linear equilibration trajectory (dotted line): *no emulsification*

[omim][Cl]/ethanol/TAEE equilibration

Fig. S106

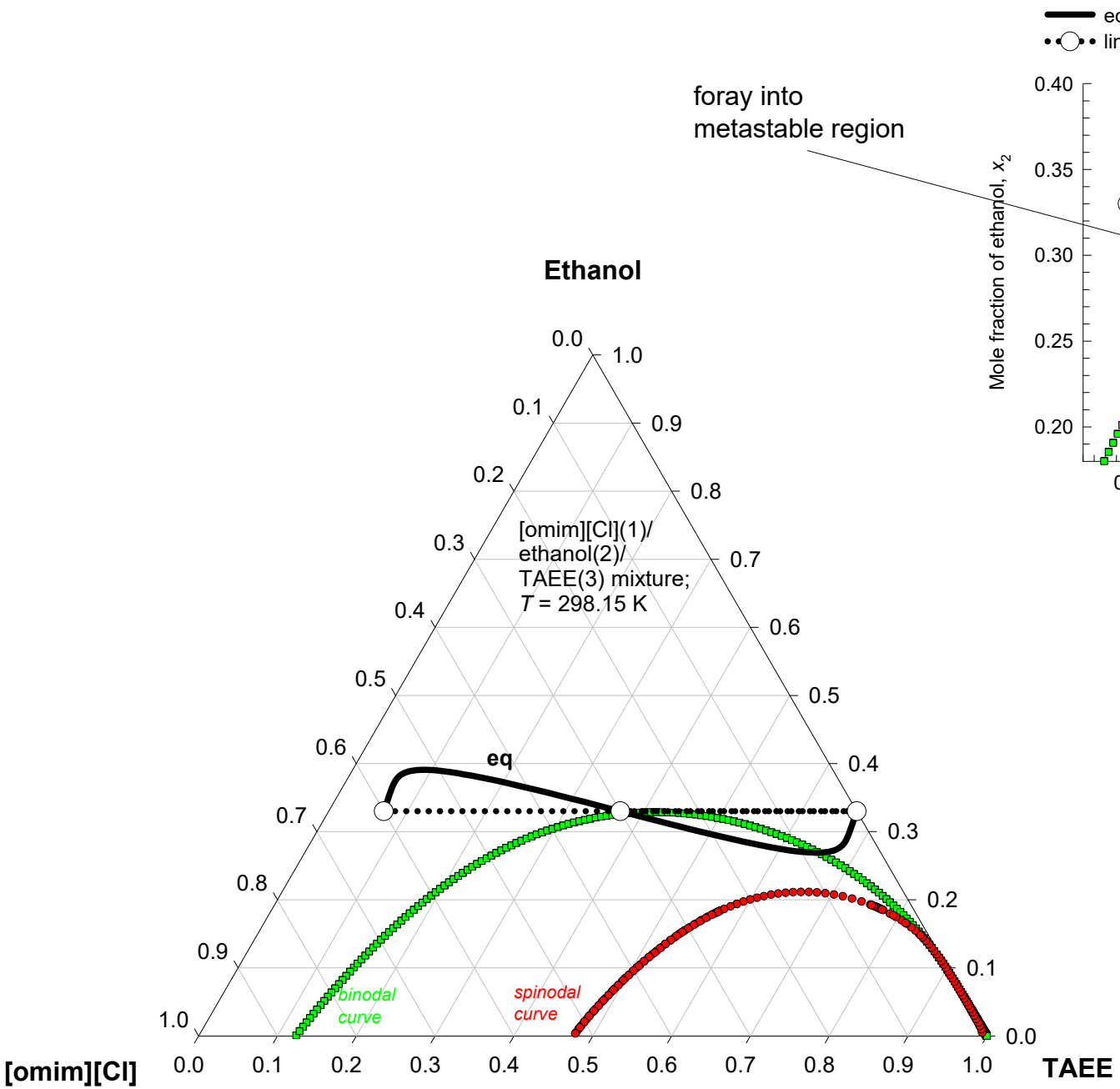

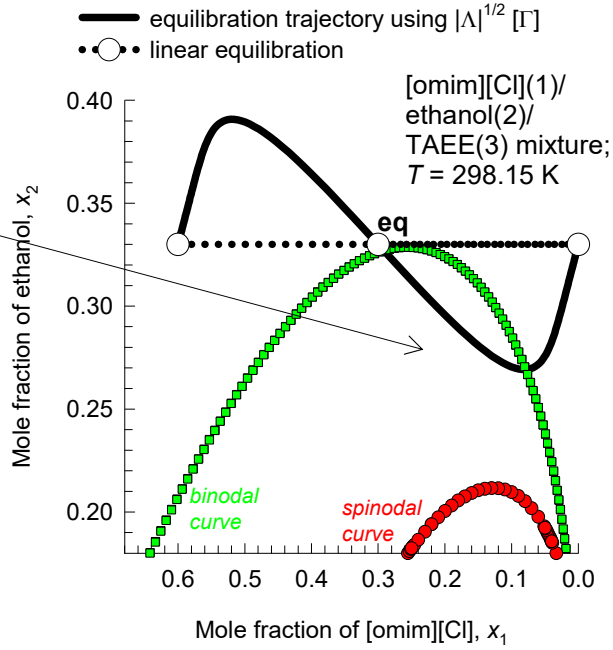

Serpentine trajectory obtained with

$$[D] = \begin{bmatrix} 2.498 & -3.1605 \\ -2.3352 & 4.603 \end{bmatrix} \times 10^{-9} \quad \mathrm{m^2\ s^{-1}}$$

predicts possibility of emulsification

Linear equilibration trajectory (dotted line): *no emulsification*

[omim][Cl]/ethanol/TAEE equilibration

Fig. S107

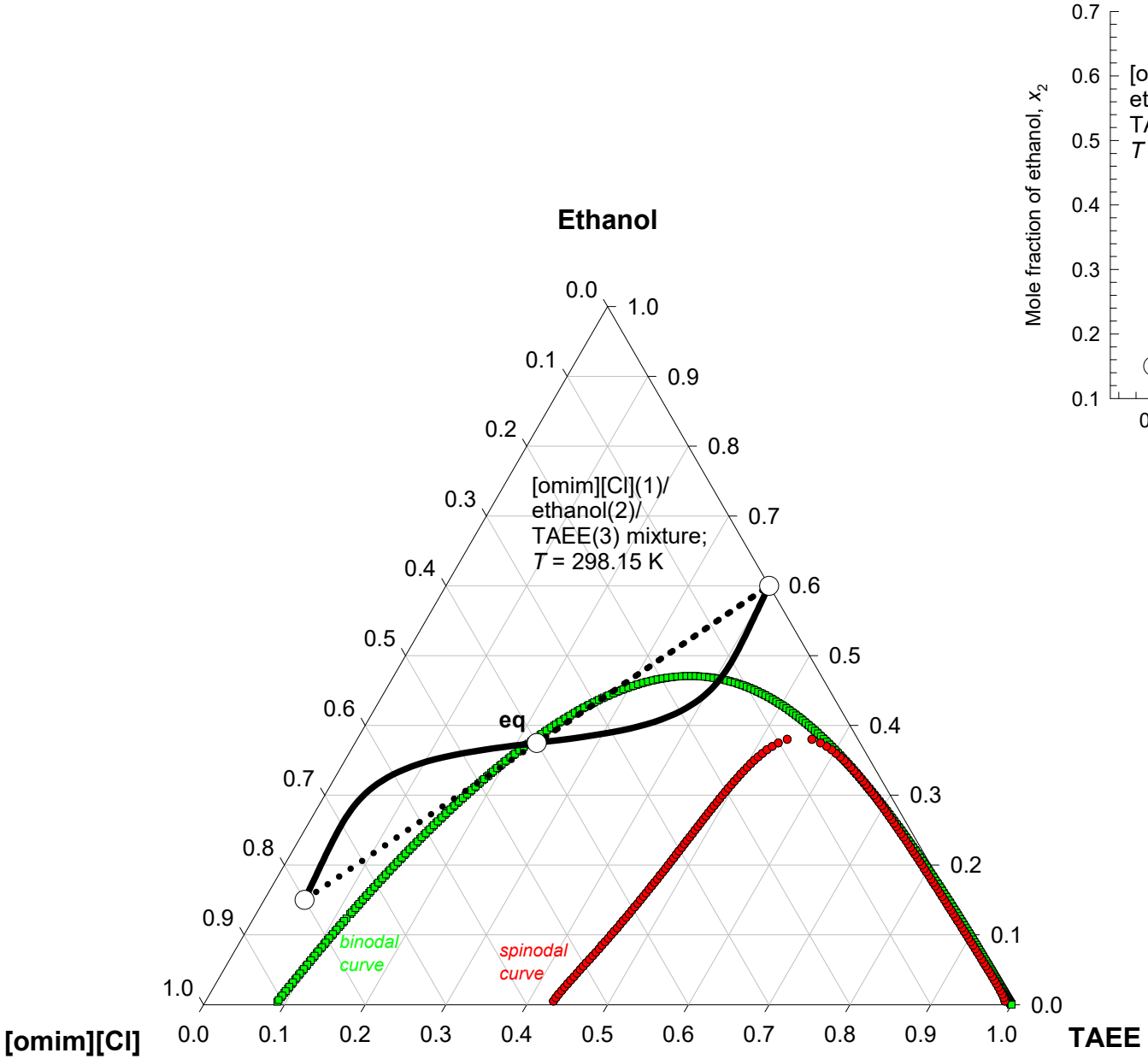

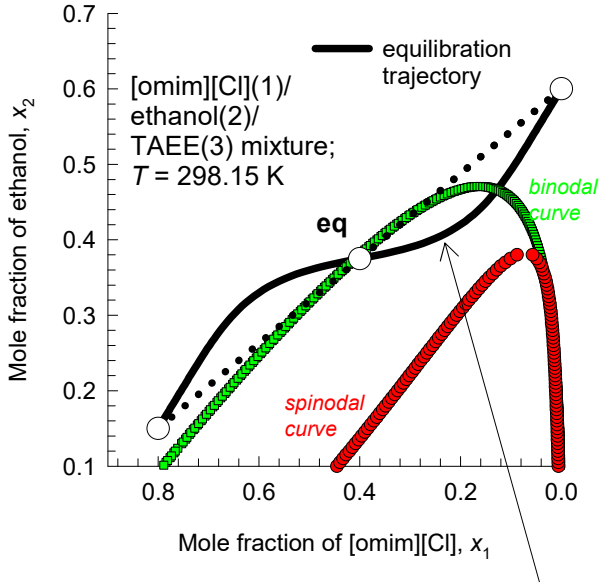

foray into
metastable region

Serpentine trajectory obtained with

$$[D] = \begin{bmatrix} 1.652 & -1.949 \\ -1.306 & 2.607 \end{bmatrix} \times 10^{-9} \quad \mathrm{m^2\ s^{-1}}$$

predicts possibility of emulsification

Linear equilibration trajectory
(dotted line): *no emulsification*

[bmim][TfO]/ethanol/TAEE equilibration

Fig. S108

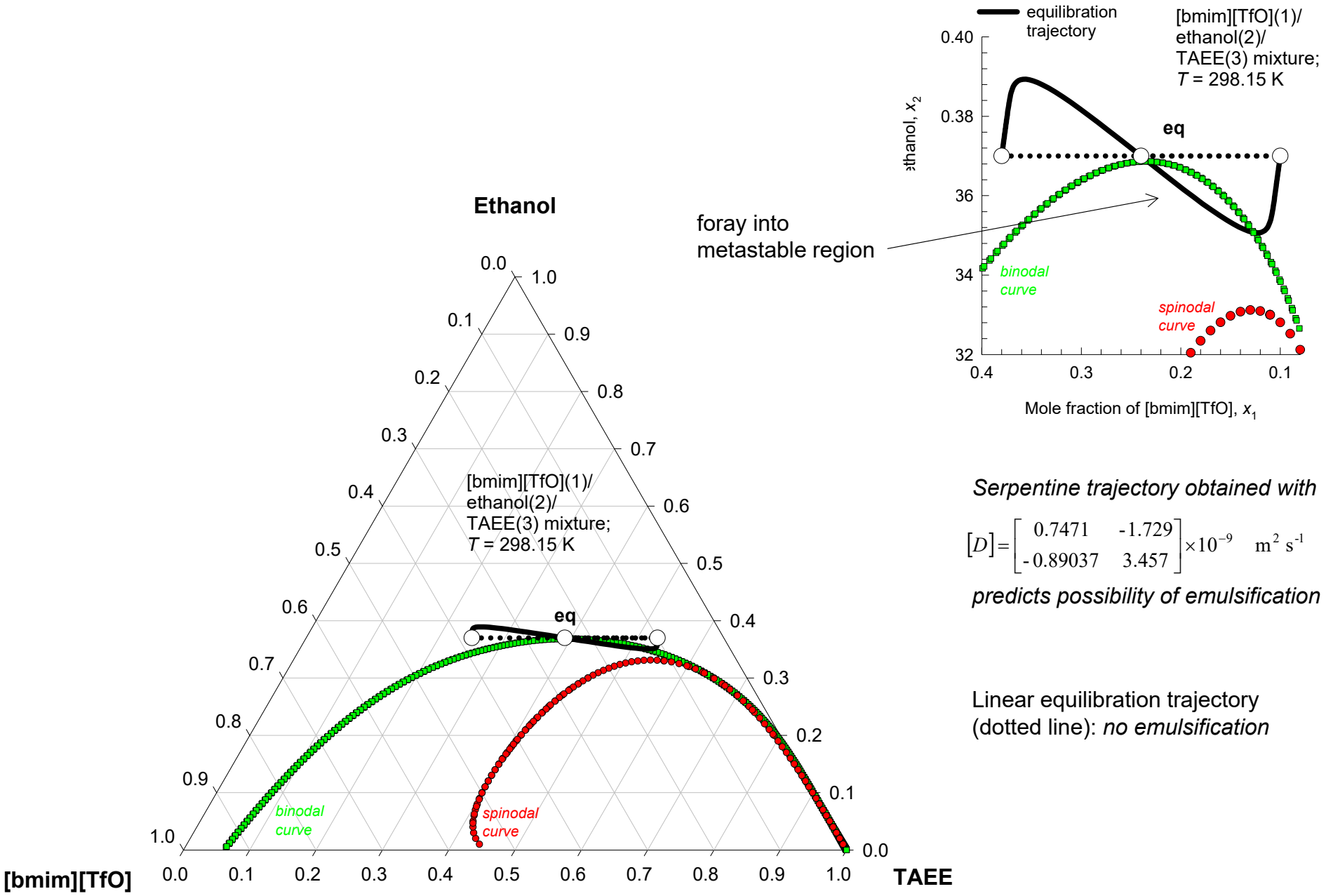

Serpentine trajectory obtained with

$$[D] = \begin{bmatrix} 0.7471 & -1.729 \\ -0.89037 & 3.457 \end{bmatrix} \times 10^{-9} \quad \mathrm{m^2\ s^{-1}}$$

predicts possibility of emulsification

Linear equilibration trajectory (dotted line): *no emulsification*

Water/Acetone/Toluene equilibration

Fig. S109

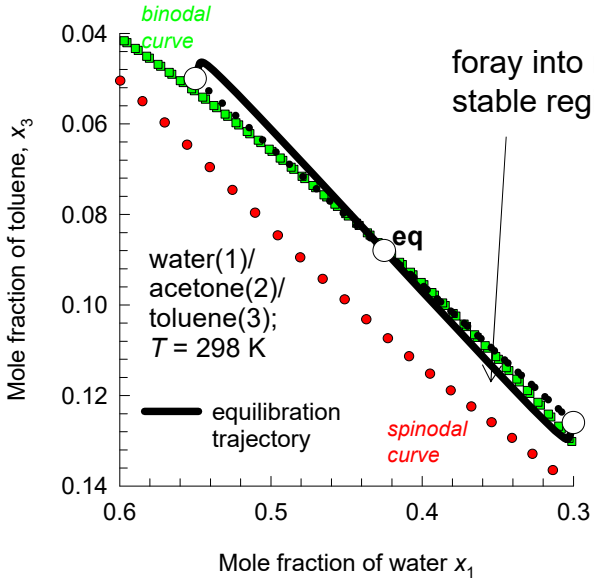

Serpentine trajectory obtained with

$$[D] = \begin{bmatrix} -0.3805 & -0.6848 \\ 0.9492 & 1.567 \end{bmatrix} \times 10^{-9} \quad \mathrm{m^2\ s^{-1}}$$

predicts possibility of emulsification.

Linear equilibration trajectory (dotted line): *no emulsification*

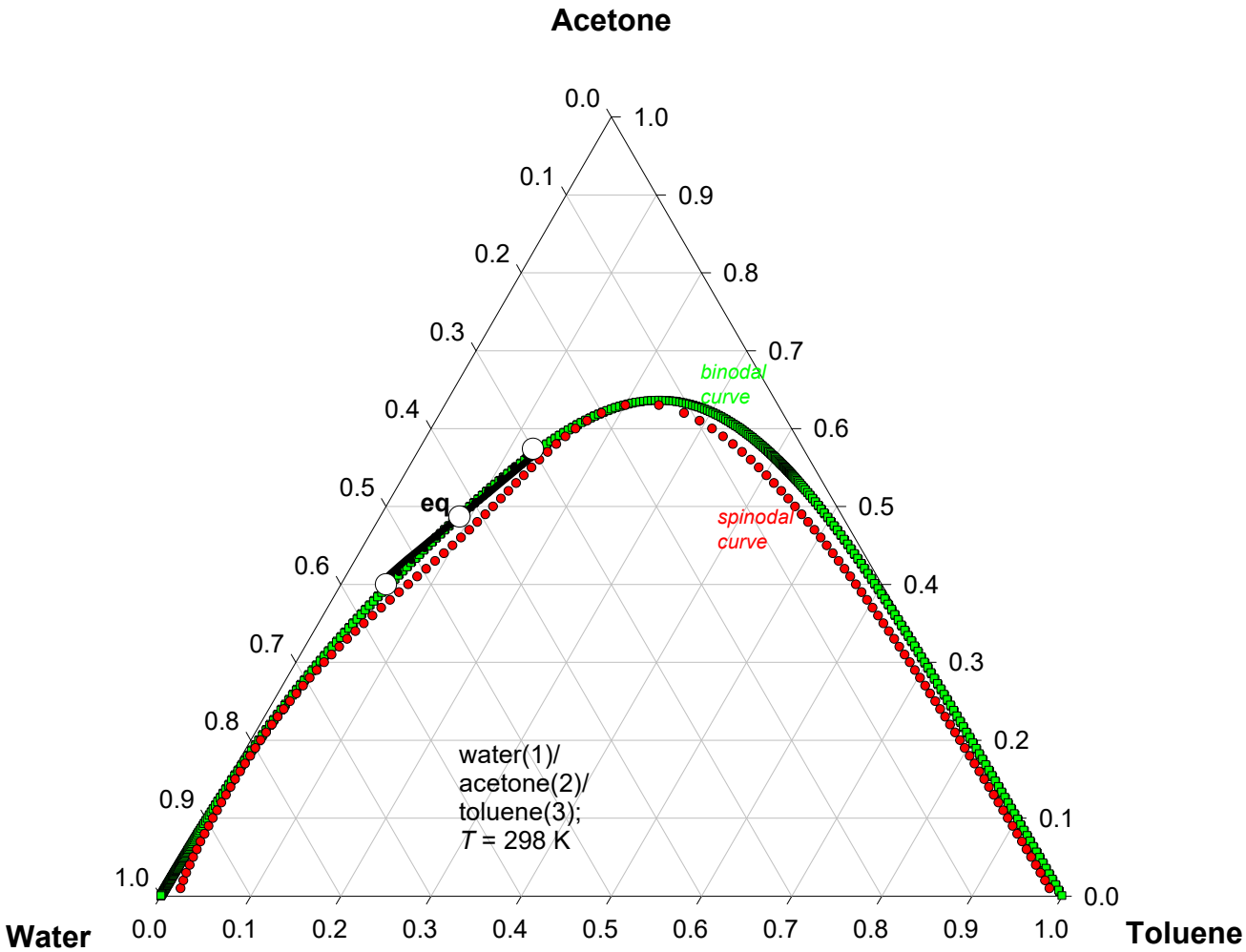

Water/Ethanol/Cyclohexane equilibration

Fig. S110

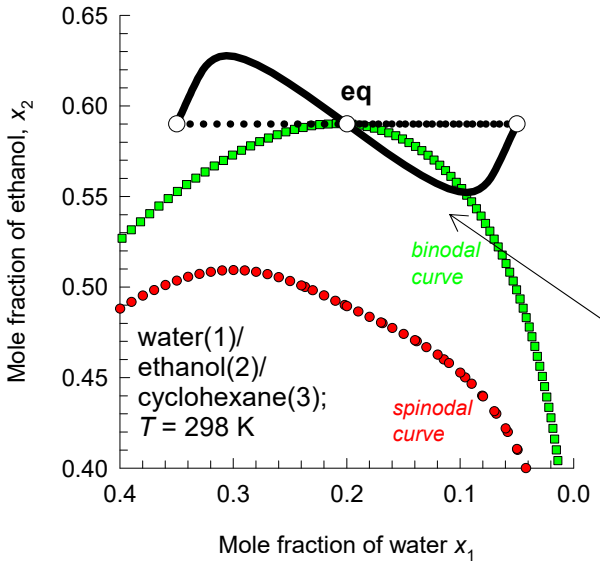

foray into meta-stable region

Serpentine trajectory obtained with

$$[D] = \begin{bmatrix} 0.335 & -0.3193 \\ -0.3493 & 0.5158 \end{bmatrix} \times 10^{-9} \quad \mathrm{m^2\ s^{-1}}$$

predicts possibility of emulsification.

Linear equilibration trajectory (dotted line): *no emulsification*

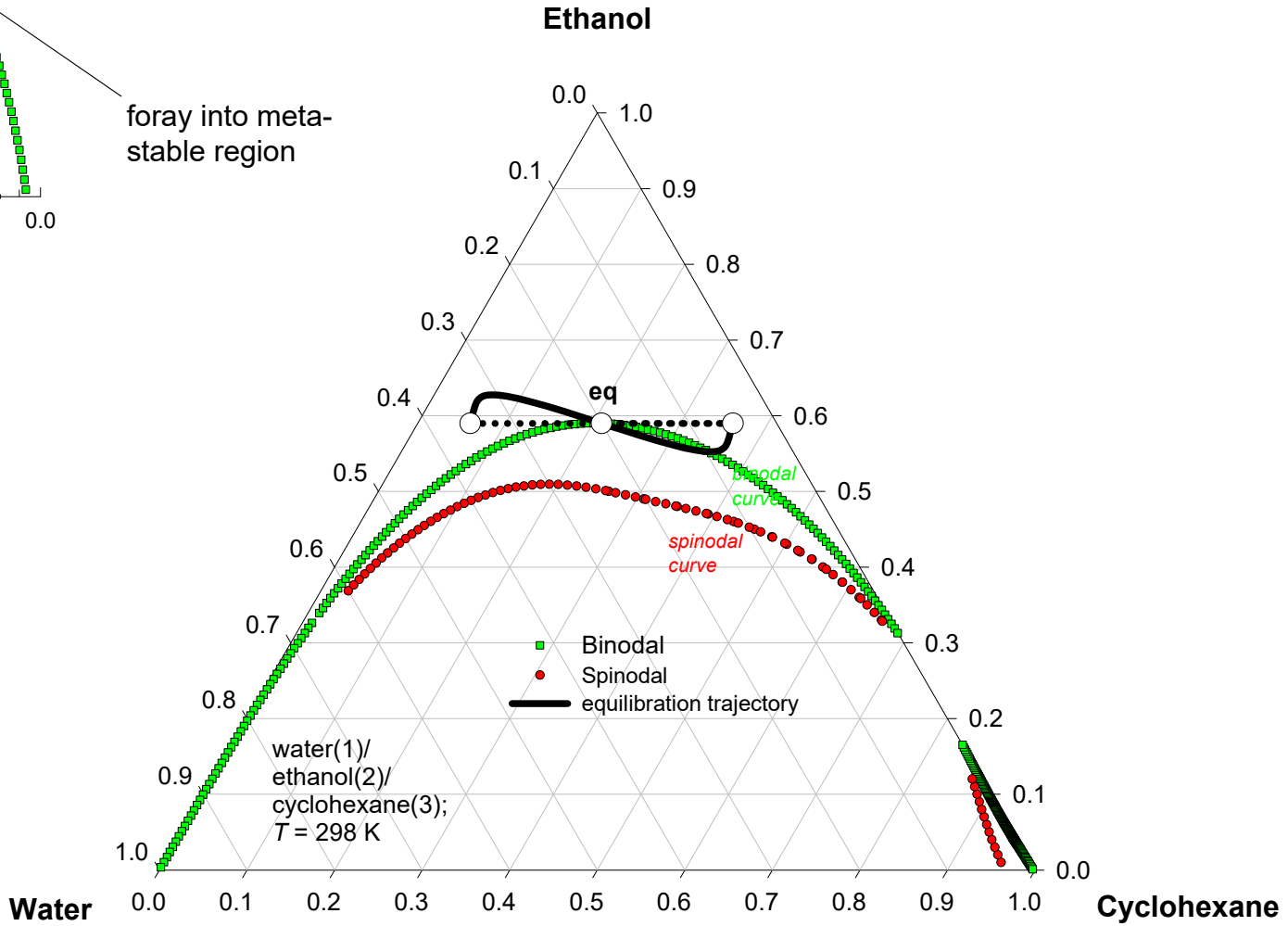

Toluene/ethanol/water equilibration

Fig. S111

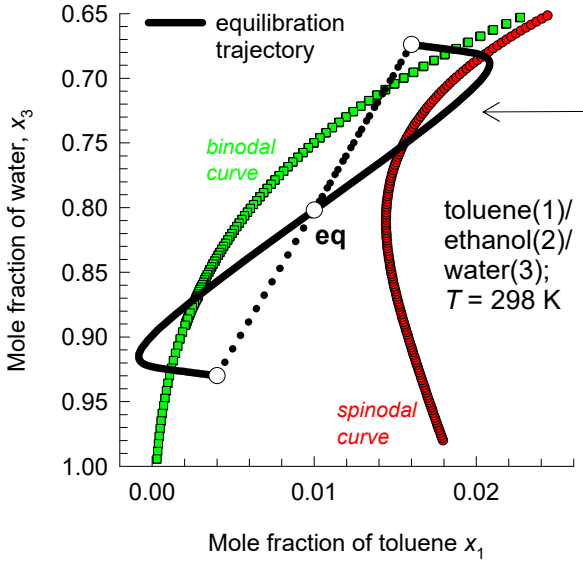

foray into unstable region

Serpentine trajectory obtained with

$$[D]=\begin{bmatrix} 0.715 & -0.1028 \\ -1.656 & 0.343 \end{bmatrix}\times 10^{-9} \quad \mathrm{m^2\ s^{-1}}$$

predicts possibility of spinodal decomposition.

Linear equilibration trajectory (dotted line): *no spinodal decomposition*